Beaufort Regional Environmental Assessment – Marine Fishes Program (BREA-MFP) Annual Report on the Physical System – 2014

Ryan Galley, Andrea Niemi, Jane Eert, Andrew Majewski, Matthew Friesen, William Williams

Fisheries and Oceans Canada
Freshwater Institute
501 University Crescent
Winnipeg, Manitoba
Canada, R3T 2N6

2026

Canadian Technical Report of Hydrography and Ocean Sciences 427

Fisheries and Oceans Canada | Pêches et Océans Canada

Canada

Canadian Technical Report of Hydrography and Ocean Sciences

Technical reports contain scientific and technical information of a type that represents a contribution to existing knowledge but which is not normally found in the primary literature. The subject matter is generally related to programs and interests of the Oceans and Science sectors of Fisheries and Oceans Canada.

Technical reports may be cited as full publications. The correct citation appears above the abstract of each report. Each report is abstracted in the data base *Aquatic Sciences and Fisheries Abstracts.*

Technical reports are produced regionally but are numbered nationally. Requests for individual reports will be filled by the issuing establishment listed on the front cover and title page.

Regional and headquarters establishments of Ocean Science and Surveys ceased publication of their various report series as of December 1981. A complete listing of these publications and the last number issued under each title are published in the *Canadian Journal of Fisheries and Aquatic Sciences*, Volume 38: Index to Publications 1981. The current series began with Report Number 1 in January 1982.

Rapport technique canadien sur l'hydrographie et les sciences océaniques

Les rapports techniques contiennent des renseignements scientifiques et techniques qui constituent une contribution aux connaissances actuelles mais que l'on ne trouve pas normalement dans les revues scientifiques. Le sujet est généralement rattaché aux programmes et intérêts des secteurs des Océans et des Sciences de Pêches et Océans Canada.

Les rapports techniques peuvent être cités comme des publications à part entière. Le titre exact figure au-dessus du résumé de chaque rapport. Les rapports techniques sont résumés dans la base de données *Résumés des sciences aquatiques et halieutiques*.

Les rapports techniques sont produits à l'échelon régional, mais numérotés à l'échelon national. Les demandes de rapports seront satisfaites par l'établissement auteur dont le nom figure sur la couverture et la page de titre.

Les établissements de l'ancien secteur des Sciences et Levés océaniques dans les régions et à l'administration centrale ont cessé de publier leurs diverses séries de rapports en décembre 1981. Vous trouverez dans l'index des publications du volume 38 du *Journal canadien des sciences halieutiques et aquatiques*, la liste de ces publications ainsi que le dernier numéro paru dans chaque catégorie. La nouvelle série a commencé avec la publication du rapport numéro 1 en janvier 1982.

Canadian Technical Report of
Hydrography and Ocean Sciences 427

2026

Beaufort Regional Environmental Assessment – Marine Fishes Program (BREA-MFP) Annual Report on the Physical System – 2014

by

Ryan Galley, Andrea Niemi, Jane Eert, Andrew Majewski, Matthew Friesen, William Williams

Fisheries and Oceans Canada
Freshwater Institute
501 University Crescent
Winnipeg, Manitoba
Canada, R3T 2N6

© His Majesty the King in Right of Canada, as represented by the Minister of the Department of Fisheries and Oceans, 2026

This work is licensed under the Open Government Licence

Cat. No. Fs.97-18/427E-PDF ISBN 978-1-100-01145-5 ISSN 1488-5417

https://doi.org/10.60825/rr62-cd74

Correct Citation for this publication:

Galley, R., Niemi, A., Eert, J., Majewski, A., Friesen, M., Williams, W. 2026. Beaufort Regional Environmental Assessment – Marine Fishes Program (BREA-MFP) Annual Report on the Physical System – 2014. Can. Tech. Rep. Hydrogr. Ocean Sci. 427: ix + 119 p.
https://doi.org/10.60825/rr62-cd74

TABLE OF CONTENTS

LIST OF FIGURES iv

LIST OF TABLES vii

ABSTRACT viii

RÉSUMÉ ix

1 Introduction 1

2 Data and Methods 4

2.1 Environmental Forcing 5

2.2 Sea Ice Concentration and Motion 5

2.3 Sea ice-adjusted Surface Solar Radiation Downwards 6

2.4 Sea Surface Temperature 7

2.5 BREA-Marine Fishes Project Sampling 7

3 Results and Discussion 8

3.1 Winter 9

3.2 Spring 10

3.3 Summer 12

3.3.1 Summer Ocean Conditions 14

3.4 Autumn 18

4 Conclusion 20

5 Acknowledgements 22

6 References 23

7 Figures 28

8 Tables 65

Appendix A – Profiles of salinity, temperature, potential density anomaly, and N^2, and T-S plots for each of the 59 stations sampled during BREA-MFP 2014. 66

LIST OF FIGURES

Figure 1. Monthly mean 2-m air temperature (°C) in 2014 over the Beaufort Sea and Amundsen Gulf.

Figure 2. Monthly mean 2-m air temperature anomalies (°C) in 2014 from the climatological average period 1983-2010 in the Beaufort Sea and Amundsen Gulf.

Figure 3. Monthly mean sea level pressure (kPa) over the Beaufort Sea and Amundsen Gulf in 2014.

Figure 4. Monthly mean sea level pressure anomalies (kPa) in 2014 from the climatological average period 1983-2010 in the Beaufort Sea and Amundsen Gulf.

Figure 5. Monthly mean 10-m wind speed (m s^{-1}) and direction in 2014 in the Beaufort Sea and Amundsen Gulf.

Figure 6. Monthly mean 10-m wind speed (m s^{-1}) and direction anomalies from the climatological average period 1983-2010 in the Beaufort Sea and Amundsen Gulf in 2014.

Figure 7. Monthly mean sea ice concentration (10^{ths}) for total sea ice and three stages of development (old, first-year, and young + new ice) for January, February, and March [winter] 2014.

Figure 8. Monthly mean sea ice concentration anomalies (10^{ths}) for total sea ice and three stages of development (old, first-year, and young + new ice) for January, February, and March [winter] 2014.

Figure 9. Monthly mean sea ice concentration (10^{ths}) for total sea ice and three stages of development (old, first-year, and young + new ice) for April, May, and June [spring] 2014.

Figure 10. Monthly mean sea ice concentration anomalies (10^{ths}) for total sea ice and three stages of development (old, first-year, and young + new ice) for April, May, and June [spring] 2014.

Figure 11. Monthly mean sea ice concentration (10^{ths}) for total sea ice and three stages of development (old, first-year, and young + new ice) for July, August, and September [summer] 2014.

Figure 12. Monthly mean sea ice concentration anomalies (10^{ths}) for total sea ice and three stages of development (old, first-year, and young + new ice) for July, August, and September [summer] 2014.

Figure 13. Monthly mean sea ice concentration (10^{ths}) for total sea ice and three stages of development (old, first-year, and young + new ice) for October, November, and December [autumn] 2014.

Figure 14. Monthly mean sea ice concentration anomalies (10^{ths}) for total sea ice and three stages of development (old, first-year, and young + new ice) for October, November, and December [autumn] 2014.

Figure 15. Monthly mean sea ice velocity (cm s^{-1}) and direction in 2014 in the Beaufort Sea and Amundsen Gulf.

Figure 16. Monthly mean sea ice velocity (cm s^{-1}) and direction anomalies in 2014 from the climatological mean period 1983-2010 in the Beaufort Sea and Amundsen Gulf.

Figure 17. Monthly mean sea ice-adjusted surface solar radiation downwards (J m^{-2}) in 2014 in the Beaufort Sea and Amundsen Gulf.

Figure 18. Monthly sea ice-adjusted surface solar radiation downwards anomalies (J m^{-2}) in 2014 compared to the climatological average period 1983-2010 in the Beaufort Sea and Amundsen Gulf.

Figure 19. Monthly mean sea surface temperature (°C) in 2014 in the Beaufort Sea and Amundsen Gulf.

Figure 20. Monthly mean sea surface temperature anomalies (°C) in 2014 compared to the mean period 1983-2010 in the Beaufort Sea and Amundsen Gulf.

Figure 21. (a) Mean accumulated sea ice-adjusted surface solar radiation downwards (J m^{-2}) between January and August in 2014 (inclusive), and (b) accumulated sea ice-adjusted surface solar radiation downwards anomaly (J m^{-2}) between January and August 2019 (inclusive) compared to the climatological average over the period 1983-2010.

Figure 22. (a) Mean accumulated sea ice-adjusted surface solar radiation downwards (J m^{-2}) between January and December in 2014 (inclusive), and (b) accumulated sea ice-adjusted surface solar radiation downwards anomaly (J m^{-2}) between January and December 2019 (inclusive) compared to the climatological average over the period 1983-2010.

Figure 23. CTD station and section locations in the Amundsen Gulf region in 2014, overlain on ETOPO1 bathymetry data.

Figure 23. (a) Surface temperature (°C), and (b) surface salinity at each station in the Amundsen Gulf region in 2014.

Figure 25. (a) Depth of the maximum N^2 in meters (b) Ocean heat content (kJ in a $1m^2$ column to a depth of the N^2 max), and (c) Freshwater anomaly relative to S = 34.8 (meters in a $1m^2$ column to the depth of the N^2 max) at each station in the Amundsen Gulf region in 2014.

Figure 26. Sections from west to east across Dolphin and Union Strait (DOL) in 2014: salinity (a, b) and temperature (c, d). Full depth (a, c) and enlarged to show only the top 50m (b, d). N^2-derived surface layer depths at each station are connoted by white dots.

Figure 27. Sections from west to east across Minto Inlet in 2014: salinity (a, b) and temperature (c, d). Full depth (a, c) and enlarged to show only the top 50m (b, d). N^2-derived surface layer depths at each station are connoted by white dots.

Figure 28. Sections from south to north across Minto Inlet (MNT) in 2014: salinity (a, b) and temperature (c, d). Full depth (a, c) and enlarged to show only the top 50m (b, d). N^2-derived surface layer depths at each station are connoted by white dots.

Figure 29. Sections from west to east across Walker Bay (WLK) in 2014: salinity (a) and temperature (b). N^2-derived surface layer depths at each station are connoted by white dots.

Figure 30. Sections from west to east across the south end of Prince of Wales Strait using the Alexander Milne Point (ALX) stations in 2014: salinity (a) and temperature (b). N^2-derived surface layer depths at each station are connoted by white dots.

Figure 31. Sections from south to north in eastern Amundsen Gulf using the AMN stations in 2014: salinity (a, b) and temperature (c, d). Full depth (a, c) and enlarged to show only the top 50 m (b, d). N^2-derived surface layer depths at each station are denoted by white dots.

Figure 32. Sections from west to east across Darnley Bay using the Bennett Point (BPT) stations in 2014: salinity (a) and temperature (b). N^2-derived surface layer depths at each station are denoted by white dots.

Figure 33. Sections from south to north along the Cape Parry (CPY) stations in 2014: salinity (a) and temperature (b). N^2-derived surface layer depths at each station are denoted by white dots.

Figure 34. Sections from west to east across Franklin Bay (FRK) in 2014: salinity (a, b) and temperature (c, d). Full depth (a, c) and enlarged to show only the top 50 m (b, d). N^2-derived surface layer depths at each station are denoted by white dots.

Figure 35. Sections from west to east along the Banks - North stations in 2014: salinity (a) and temperature (b). N^2-derived surface layer depths at each station are denoted by white dots.

Figure 36. Sections from west to east along the Banks - South stations in 2014: salinity (a, b) and temperature (c, d). Full depth (a, c) and enlarged to show only the top 50 m (b, d). N^2-derived surface layer depths at each station are denoted by white dots.

Figure 37. Sections from south to north along the Kugmallit (KUG) stations in 2014: salinity (a, b) and temperature (c, d). Full depth (a, c) and enlarged to show only the top 50 m (b, d). N^2-derived surface layer depths at each station are denoted by white dots.

LIST OF TABLES

Table 1. Surface and surface layer oceanographic parameters at each BREA-MFP station, August-September 2014. Freshwater content (FWC) and ocean heat content (OHC) is integrated over the surface layer (dbar) depth.

ABSTRACT

Galley, R., Niemi, A., Eert, J., Majewski, A., Friesen, M., Williams, W. 2026. Beaufort Regional Environmental Assessment – Marine Fishes Program (BREA-MFP) Annual Report on the Physical System – 2014. Can. Tech. Rep. Hydrogr. Ocean Sci. 427: ix + 119 p.
https://doi.org/10.60825/rr62-cd74

The Beaufort Regional Environmental Assessment – Marine Fishes Project (2012-2014) sought to establish diversity, abundance, and distributions of offshore marine fishes in the Beaufort Sea and Amundsen Gulf, and to collect data that would enable habitat characterization. These data were collected to establish a baseline from which changes might be elucidated over future annual physical, biological, and chemical oceanographic surveys. Conductivity-Temperature-Depth data in August and September 2014 reveal the end-of-summer physical oceanographic characteristics in the region using temperature, salinity, potential density, and N^2 profiles, temperature-salinity plots, temperature and salinity sections, as well as derived surface layer depth and ocean heat content and freshwater content in the surface layer at each station. Oceanographic results are set in the context of the annual evolution of air temperature, sea level pressure, winds, sea surface temperature, and sea ice concentration and motion in the region. Anomalously warm air temperatures and sea ice export-favorable winds created and maintained the Cape Bathurst flaw lead polynya in winter and spring (Jan-Jun) 2014. In summer (July, August, September) 2014, average air temperatures prevailed but sea ice was rotated clockwise through the region, importing old sea ice from the north and exporting sea ice to the west. This left the southern Beaufort Sea ice-free and maintained an ice-free Amundsen Gulf over summer after an early, dynamic breakup in June. Summer SST positive anomalies were extreme, likely the result of enhanced SSRD to open ocean and heat import from the terrestrial environment via the Mackenzie River. Anomalously warm air temperatures in October and positively anomalous sea ice-adjusted surface solar radiation downward between March-October 2014 delayed regional freeze-up, while export in October and November reduced regional sea ice thickness in autumn.

RÉSUMÉ

Galley, R., Niemi, A., Eert, J., Majewski, A., Friesen, M., Williams, W. 2026. Beaufort Regional Environmental Assessment – Marine Fishes Program (BREA-MFP) Annual Report on the Physical System – 2014. Can. Tech. Rep. Hydrogr. Ocean Sci. 427: ix + 119 p.
https://doi.org/10.60825/rr62-cd74

Le projet d'évaluation environnementale régionale de Beaufort – Poissons marins (2012-2014) visait à déterminer la diversité, l'abondance et la répartition des poissons marins au large de la mer de Beaufort et du golfe d'Amundsen, ainsi qu'à collecter des données permettant de caractériser leur habitat. Ces données ont été recueillies afin d'établir une base de référence à partir de laquelle les changements pourraient être mis en évidence lors de futures campagnes océanographiques annuelles portant sur les aspects physiques, biologiques et chimiques. Les données de conductivité, de température et de profondeur recueillies en août et septembre 2014 révèlent les caractéristiques océanographiques physiques de fin d'été dans la région, à l'aide de profils de température, de salinité, de densité potentielle et de N_2, de graphiques température-salinité, de coupes de température et de salinité, ainsi que de la profondeur de la couche superficielle, du contenu thermique de l'océan et de la teneur en eau douce de la couche superficielle à chaque station. Les résultats océanographiques s'inscrivent dans le contexte de l'évolution annuelle de la température de l'air, de la pression au niveau de la mer, des vents, de la température de surface de la mer, ainsi que de la concentration et du mouvement de la glace de mer dans la région. Des températures de l'air anormalement élevées et des vents favorables à l'exportation de la glace de mer ont favorisé la formation et le maintien de la polynie de Cape Bathurst Flaw Lead durant l'hiver et le printemps (janvier-juin) 2014. Au cours de l'été (juillet, août, septembre) 2014, les températures de l'air sont restées dans la moyenne, mais la banquise a effectué une rotation dans le sens des aiguilles d'une montre à travers la région, important de la vieille banquise depuis le nord et exportant de la banquise vers l'ouest. Cela a laissé le sud de la mer de Beaufort libre de glace et a maintenu le golfe d'Amundsen libre de glace tout au long de l'été, après une rupture précoce et dynamique en juin. Les anomalies positives de la température de surface de la mer (SST) en été ont été extrêmes, probablement en raison d'un renforcement du SSRD vers l'océan ouvert et d'un apport de chaleur provenant de l'environnement terrestre via le fleuve Mackenzie. Des températures de l'air anormalement chaudes en octobre et un rayonnement solaire de surface vers le bas, corrigé de la présence de glace de mer, présentant des anomalies positives entre mars et octobre 2014 ont retardé le gel régional, tandis que l'exportation en octobre et novembre a réduit l'épaisseur régionale de la glace de mer à l'automne.

1 Introduction

Late in 2013 the offshore northeast Pacific Ocean began to experience unusually warm sea surface temperatures (SST) (Freeland, 2014) and these high SST anomalies continued through the winter. By February 2014, SST warm anomalies in the northeast Pacific were most noticeable in the Gulf of Alaska and extended to the shelf near-shore (Bond et al., 2015) and in June warm SST anomalies had reached the Bering Sea (Freeland, 2015). These warm SST anomalies were greater than three standard deviations from the climatological mean, and maybe the largest ever since 1900 (Bond et al. (2015). The pool of warm water in the upper 100 m of the northeast Pacific was greater than 4 standard deviations from its mean temperature, and evidence of reduced salinity in the surface layer has been presented (Chandler et al., 2015). Warm surface layer temperatures and decreased salinity reduced the surface layer water density, substantially increasing the strength of stratification in the upper ocean (Freeland and Ross, 2019), reducing vertical mixing of nutrients from depth to the surface, and all but halting the warm surface water from mixing with cooler, deeper water (Chandler et al., 2015). Bond et al. (2015) outline the physical processes which may have enabled this anomalous warming in the northeast Pacific in 2013-2014, including anomalous, sustained high atmospheric pressure over the northeast Pacific, which nearly eliminated wind-forced processes (currents and mixing), and reduced surface heat loss mainly due to retarded turbulent fluxes via anomalous low surface wind speeds. “The Blob” (first named that by Nick Bond), warm anomalous SSTs in the Pacific, formed three identifiable zones by September 2014: one small zone off the coast of Mexico and southern California, one off the coast of North America from northern California to Canada and the Gulf of Alaska, and one in the Bering Sea. Belkin and Short (2023) indicate that ‘The Blob’ propagated northward along the Gulf of Alaska shelf toward the Aleutian Islands and into the Bering Sea via the Polar Front Current. Advance of ‘The Blob’ into the Bering Sea in 2014 abruptly and substantially shrank the bottom water cold pool in the region (Thorson, 2019).

The biological impacts of the 2013-2015 warm water anomaly in the Pacific have been relatively well studied (e.g. Danielson et al., 2020). The lowlights include substantially decreased phytoplankton production in the north Pacific Ocean (Whitney, 2015, Belkin and Short, 2023), reduced silica supply instigating a switch in community composition from diatoms to dinoflagellates (Arteaga and Rousseaux, 2023), a large negative anomaly in copepod species richness in 2014 (Peterson et al., 2016), and limited large (>2 mm) copepod production and promotion of small (<2 mm) copepod and jellyfish production combining to lower the food chains’ ability to transfer energy to high trophic levels (von Biela et al., 2019). von Biela et al. (2019) found substantially decreased energy content in sand lance, a key forage species

for Pacific salmon, groundfish (halibut), seabirds (common murres, black-legged kittiwakes), and marine mammals (humpback whales), and Stevenson and Lauth (2019) observed dramatically reduced arctic cod abundance in the northern Bering Sea. In 2014-2016 reduced recruitment and increased mortality of Pacific salmon and pollock (Cavole et al., 2016) occurred, and Pacific halibut in the Bering Sea underwent decline following entry of 'The Blob' to the region in 2014 (Belkin and Short, 2023). Unusual baleen (fin and humpback) whale mortality in British Columbia and Alaska was observed (Savage, 2017), as was mass mortality of cassin's auklets from California to the Gulf of Alaska due to changes in prey abundance and quality (more specifically a reduction in the energy content of mesoplankton coincident with the loss of cold water foraging habitat (Jones et al., 2018)), and mass mortality of more than a million piscivorous common murres due to starvation (Piatt et al., 2020, Renner et al., 2024). These changes were observed across trophic levels, demonstrating ecosystem-level impacts of this warm water anomaly.

Stabeno et al. (2012) indicated the Bering Sea should be split roughly in half around 60 °N into northern and southern regions due to the presence or absence of sea ice in March and April playing a large role in the ocean temperature south of 60 °N averaged for the whole depth for spring, summer, and fall. Years where the southern Bering Sea is without sea ice in March/April possessed strong association to warm (>3.5 °C) average annual ocean temperatures (Stabeno et al., 2017). Substantial commercial fisheries exist in the southern half of the Bering Sea, which are sensitive to sea ice-free periods of two or more years (Stabeno et al., 2012). The north Pacific is intrinsically linked with the Canadian Beaufort Sea so ecological and physical effects of the blob were expected to manifest themselves in the Arctic as well. The Bering Sea and Chukchi Sea shelves, separated by the narrow (~ 80 km) and shallow (55 m) Bering Strait, are the Pacific gateway to the Arctic Ocean via the Bering Shelf Currents, the Alaska Coastal Current, the Anadyr Current, and the Chukchi Shelf Currents (see for e.g. Danielson et al., 2020). About half of the upper Arctic Ocean is Pacific Water, and long-standing evidence of heat and freshwater transport north across the Bering Strait into the Arctic exists (Aagaard and Carmack, 1989, Serreze et al., 2006, Woodgate et al., 2010, Woodgate et al., 2012, Woodgate, 2018). About a third of the freshwater in the Arctic Ocean can be traced to Bering Strait throughflow (Aagaard and Carmack, 1989), which contributes to the cold halocline (a layer at 50-100 m depth where the salinity increases substantially), insulating the Arctic surface from warm Atlantic Water at depth. The equivalent of one-third of the heat input to the Arctic Ocean through Fram Strait is supplied to the Arctic through the Bering Strait (3-6 $x10^{20}$ J $year^{-1}$ relative to freezing) (Woodgate, 2018). Flow from the Bering Sea through the Bering Strait has been increasing; a long-term increase in the Pacific-Arctic pressure head between 1990-2015 that may have accounted for two-thirds of the observed Bering Strait through-flow during that time (Woodgate et al., 2012, Woodgate, 2018). Interestingly, 2014

was a very average year for bottom water temperature in the Bering Strait (Woodgate, 2018) but that did not stop the SST anomalies from being large in the Bering Strait and Chukchi Sea in summer 2014 (Timmermans and Proshutinsky, 2014). In summer 2014, the Chukchi and Beaufort Seas experienced some of the highest SST anomalies recorded up to that time, with temperatures reaching as much as 4 °C above the 1982–2010 climatology (Jeffries et al., 2014). Combined with the marine heat wave that began in 2014, a step-wise increase in mean annual air temperature and mean annual ground temperatures occurred in in Alaska in 2014 (Swanson et al., 2021). Positive air temperature anomalies of up to 10 °C were observed in January in Alaska in 2014 as a consequence of the position of the jet stream, breaking a streak of seven years of cooler temperatures over Alaska and extensive sea ice cover in the Bering Sea (Overland et al., 2014).

Concomitant with the 2013-2015 warm water anomaly in the Pacific, 2014 was an ecological anomaly in the Beaufort Sea (Niemi et al., 2019). In 2012 and 2013, the zooplankton collected were predominantly crustaceans, calanoid copepods and amphipods, while in 2014 the zooplankton collected were mainly pteropods and amphipods associated with a matrix of jelly-like organisms (Majewski et al., 2016). In 2014 there was the dearth of arctic cod in the Beaufort Sea, both in young-of-the-year and adult life stages following on from general decline in 2011, 2012, and 2013 (Niemi et al., 2019), which were years that experienced anomalously high sea surface temperatures in the Beaufort Sea (Wood et al., 2013). These arctic cod, small forage fish of extremely high energetic value, are typically found under sea ice seeking refuge and/or feeding, and/or in cold (<4 °C) waters (Bluhm and Gradinger, 2008, Crawford and Jorgenson, 1993). In 2011 and 2012, the Mackenzie River plume was associated with surface layer stratification in the Beaufort Sea that was 6-8 m thick, and up to 12 °C (Wood et al. 2013). Arctic cod are a pillar of the marine food web in the Beaufort Sea as a forage species, accounting for 95% of the pelagic fish assemblage in the region (Geoffroy et al., 2016), providing a food source for fish, seals, whales, and birds (Mueter et al., 2016). The highly unusual presence and distribution of beluga whales (*Delphinapterus leucas*) in the region in 2014 was also of interest; more than 30 belugas were harvested at Uluhaktok at the mouth of Prince Albert Sound in 2014 (Loseto et al., 2018) having travelled much further east than usual. Belugas in the region in 2014 also showed impaired body condition (Choy et al., 2017) and uncharacteristic gut contents, including sand lance, squid, and other fish species instead of arctic cod (Loseto et al., 2018, Niemi et al., 2019). Gray whales make their way from feeding grounds in the North Pacific Ocean north into the Bering and Chukchi seas over an annual round trip of more than 15 000 km (Rugh et al., 2001) feeding mainly on benthic organisms in shallow seas (Rice and Wolman, 1971). Three gray whales (one pair, one individual) were sighted in the Beaufort Sea in 2014 near Cape Bathurst, more than 900 km east

of their usual end range at Point Barrow, after only two gray whales were sighted in the area since 1980 (one in 2007, and one in 2009) (Iwahara et al., 2016). Studies published to this point indicate 2014 and the years leading up to it were not only physically anomalous in the Pacific, Bering, Chukchi and Beaufort Seas, but also experienced substantial ecosystem changes, which may be due to incredible warmth in the ocean and terrestrially.

Beaufort Regional Environmental Assessment (BREA) research projects were undertaken to enhance regional knowledge, and thereby increase evidence-based support for informed decision-making regarding potential resource development in the western Arctic. Specifically, BREA projects aimed to inform and support the management of potential oil and gas activities in the region, including the Inuvialuit Settlement Area, by Inuvialuit, by industry, and by governments. Following on from the Department of Fisheries and Oceans Northern Coastal Marine Studies program (2003-2009), and ArcticNet work in the region (2003-2011), the BREA – Marine Fishes Project (MFP, 2012-2014) was an exploratory assessment of the diversity and distribution of marine fishes in the Canadian Beaufort Sea and Amundsen Gulf. The BREA-MFP also sought to provide habitat parameters and food web connections to increase understanding of regional ecosystem structure and function. This accumulation of knowledge in the region points to pronounced variability in parts of the ecosystem between years. Accumulated baseline understanding is necessary to disentangle interannual variability from longer-term systemic changes. Using baseline ecology of the region, stressors and the effects of climate change might be teased apart from natural variability (Majewski et al., 2016).

In this report, a monthly overview of the physical system of the Beaufort Sea region in 2014 is presented and compared with the long-term climatological standard normal period (1983-2010). Monthly anomalies in 2014 in the regional physical system are identified and discussed. Physical oceanographic data collected in 2014 is presented; those data are discussed in the context of the environmental and sea ice information. This report endeavors to inform ecological discussion of linkages between the physical and biological components of the Beaufort Sea ecosystem in 2014 by increasing understanding of the physical drivers of the Beaufort Sea ecosystem.

2 Data and Methods

This assessment of physical conditions and drivers in the study region during 2014 includes air temperature, sea level pressure, winds, and solar radiation at the ocean surface reanalysis products, sea surface temperature data, sea ice concentration data, and ship-based oceanographic sampling.

Climatological averages (1983-2010) have been calculated to determine how anomalous the conditions were in 2014. CTD data are used to identify the surface salinity and temperature, the thickness of the ocean surface layer at sampling stations, and then the corresponding freshwater content and ocean heat content in the surface layer is calculated. Finally, cross-sectional oceanographic plots are presented in areas of the study region using the CTD data.

2.1 Environmental Forcing

European Centre for Medium-range Weather Forecasts (ECMWF) Reanalysis v5 (ERA5) 2-m air temperature, sea level pressure, 10-m U- and V- winds, and surface solar radiation downwards (SSRD) data at six-hourly intervals from January 1, 1983 to December 31, 2021 (Hersbach et al., 2018) were obtained from the Copernicus Climate Change Service Climate Data Store (https://cds.climate.copernicus.eu/cdsapp#!/dataset/reanalysis-era5-pressure-levels?tab=overview)) on a ¼° grid. Monthly averaged 2-m air temperature, sea level pressure, and 10-m wind speed and direction were created for each of the 4089 grid cells in the study region for each month of 39 years (1983-2021). Monthly climatological standard normals (i.e., averages) for 2-m air temperature, sea level pressure, 10-m winds were produced from all the available data in each month in 1983-2010 (28 years; note we use 28 and not 30 years for this period ending in 2010 in order to maintain consistency with the sea ice data which begins in 1983). Monthly anomalies in 2018 were calculated using the monthly climatological standard normal, for example:

$$T_{a\ anomaly} = T_a - T_{a\ clim} \quad (1)$$

Where $T_{a\ anomaly}$ is the air temperature anomaly in a month in a year, T_a is the average air temperature in a month in 2014, and $T_{a\ clim}$ is the climatological average air temperature for the month in all the years in the climatological average period (1983-2010). Positive anomalies occur when the monthly average air temperature is greater than the climatological standard normal for that month, negative anomalies occur when the monthly average is less than the climatological standard normal for the month.

2.2 Sea Ice Concentration and Motion

Average sea ice concentration for each month between 1983 and 2021 were created by downloading and gridding regional Canadian Ice Service (CIS) digital archive data for the western Arctic (https://iceweb1.cis.ec.gc.ca/Archive/page1.xhtml?lang=en) at 1-km resolution on the CIS Lambert conformal conic projection. Analysis of the CIS data began in 1983 because the CIS data is broken down

by consistent source data and preparation method eras resulting in temporally distinct quality indices (please see Tivy et al., 2011 for detailed information). Using all the available CIS charts in each month in each year, the monthly mean total sea ice concentration (in tenths) and mean partial concentrations (in tenths) for old ice, first-year sea ice, and new-plus-young sea ice (new-plus-young contain all sea ice < 30cm thick) stages of development were computed on the 1-km grid. Monthly climatological averages for total sea ice concentration as well as old sea ice, first-year sea ice, and new-plus-young sea ice were calculated by averaging all the data in each month between 1983 and 2010 inclusive. Monthly anomalies in each year for total, old, first-year, and new-plus-young ice concentrations were created by subtracting the months' climatological (1983-2010) standard normal sea ice concentration from the corresponding monthly average concentration for each stage of development. Positive sea ice anomalies occur when the monthly average concentration is greater than the climatological standard normal (1983-2010) in that month.

Monthly average sea ice velocity and direction in the Beaufort Sea from 1983 to 2021 were calculated from the National Snow and Ice Data Centre Polar Pathfinder Daily 25 km EASE-grid sea ice motion vector data (Version 4) for the northern hemisphere, freely available at https://nsidc.org/data/NSIDC-0116 (Tschudi et al., 2019). Climatological monthly averages for each month were created using the u- and v-vector components for each month between 1983 and 2010 (inclusive). Monthly anomalies for 2014 were created by subtracting the monthly climatological standard normal u- and v- components of the sea ice motion from the monthly average sea ice motion u- and v- components each year.

2.3 Sea ice-adjusted Surface Solar Radiation Downwards

ECMWF ERA5 surface solar radiation downwards (SSRD, in J m^{-2}) data were also downloaded from the Copernicus Climate Change Service Climate Data Store at six-hourly intervals between 1983 and 2021 (inclusive). SSRD is the amount of shortwave radiation (including both diffuse and direct radiation) that reaches a horizontal plane at the surface of the earth; it is the model equivalent of the shortwave radiation a pyranometer would measure at the surface. For the purposes of this work, SSRD may be thought of as light energy from the sun that may be converted to heat energy if it is absorbed by the surface of the ocean, either melting surrounding sea ice or contributing to increased water temperatures. The SSRD must be adjusted for sea ice cover to approximate the amount of solar radiation incident on the ocean surface in the Arctic marine environment. In each month of each year between 1983-2021, the CIS monthly mean total sea ice concentration grid was downscaled to the ERA5 grid resolution, divided by 10 to obtain a fractional coverage, and then subtracted from unity to obtain the monthly fractional open

water area in each grid cell. The fractional open water area in a month was multiplied by the mean SSRD for the month in each SSRD grid cell to obtain the sea-ice adjusted SSRD (J m^{-2}) incident on the ocean surface in each grid cell. Monthly climatological averages over the period 1983-2010 were calculated using the sea ice-adjusted monthly SSRD means, and monthly anomalies of sea ice-adjusted SSRD were calculated for each month in each year between 1983 and 2021.

2.4 Sea Surface Temperature

National Oceanic and Atmospheric Administration (NOAA) optimal interpolation sea surface temperature (OISST v2) data on a ¼° global grid were obtained from the NOAA Physical Sciences Laboratory (https://downloads.psl.noaa.gov/Datasets/noaa.oisst.v2.highres/). Monthly mean sea surface temperature (SST) maps were created for 2014. Climatological monthly mean SSTs for each month were calculated using all the data for each month between 1983 and 2010. Monthly anomalies for 2014 were calculated by subtracting the monthly climatological average SST (1983-2010) from the monthly mean SST for each month in 2014.

2.5 BREA-Marine Fishes Project Sampling

Physical oceanographic sampling in the region was undertaken between 2 August and 9 September 2014 from *F/V Frosti* at 54 stations in eastern Amundsen Gulf, across Dolphin and Union Strait, in Minto Inlet, Walker Bay, at the mouth of Prince of Wales Strait and within it, west of Banks Island, north of Cape Parry in Amundsen Gulf, in Franklin Bay, in Darnley Bay, and across the Mackenzie shelf break north of Kugmallit Bay. Conductivity, temperature, and depth (CTD) measurements were made using a Seabird SBE 911plus on the *Frosti's* rosette. CTD salinity was calibrated using bottle data, and the resulting data is considered to be accurate within ±0.003. Average salinity (PSS-78) and temperature (ITS-90, °C) over 1 decibar increments were output after the data underwent quality control. An altimeter was employed for water depth measurements, and the noted depth at each station was the median of the deepest 2 meters recorded. In the absence of altimetric measurements at a station, the deepest depth measured by the CTD was used. At stations where more than one cast was undertaken, only the deepest cast was used in the present analysis.

Potential density referenced to the surface ((σ, θ), minus 1000 kg m^{-3}) and N^2, the square of the buoyancy frequency (N^2, in s^{-2}), were calculated for each CTD profile using the OCE package (Kelley, 2018) for R (R Core Team, 2022). Potential density referenced to the surface is the density of seawater with the compressive effect of pressure removed, allowing better comparison between water from different

depths. 1000 kg m^{-3} is subtracted as a way to highlight the small variations in seawater density that drive ocean dynamics. The buoyancy frequency squared (N^2) is a measure of the variation of density with depth, measuring the strength of the ocean's density stratification. It is calculated as:

$$\frac{g}{\rho} \times \frac{d\rho}{dz} \quad (2)$$

where g is gravity, ρ is density and z is depth. The topmost value of temperature and salinity at each of the 54 stations in 2014 were mapped (note that the depth of the topmost value in each cast is variable, Table 1). The depth of maximum N^2 was identified in each profile, and that value was used to connote the bottom of the surface layer of the ocean column. The surface layer depth derived by locating the maximum value of N^2 in each profile at each of the 54 stations was used to integrate the total freshwater content (FWC, meters) and the total ocean heat content (OHC, in kilojoules), in a 1-m^2 column of water to the depth of the surface layer using the FWC and OHC calculated for each depth interval in the surface layer. The FWC was calculated at each depth interval of the column specified by the maximum N^2 depth:

$$FWC = \frac{S_o - S}{S_o} \quad (3)$$

Where S_o is the reference salinity of 34.8 and S is the salinity at each depth interval, and the FWC at each depth were summed. The OHC relative to 0°C was calculated at each decibar depth interval of the column specified by the maximum N^2 depth:

$$OHC = c_{sw} \times \rho \times \Theta \quad (4)$$

Where c_{sw} is the specific heat capacity of seawater (set to 4 for the observed temperature and salinity ranges after Sharqawy et al., 2010), ρ is seawater density calculated using absolute salinity and conservative temperature, and Θ is conservative temperature. The OHC at each depth interval in the surface layer was then summed.

3 Results and Discussion

Air temperature, sea level pressure (SLP), wind, sea ice concentration and motion, surface solar radiation, and sea surface temperature results and discussion are presented by season with winter (January February, March), spring (April, May, June), and summer (July, August, September), summarizing key

processes and physical drivers prior to and during the BREA-MFP cruise (2 August-9 September 2014). Autumn (October, November, December) conditions are presented to provide the full annual perspective of temperature, SLP, sea ice, solar radiation, and SST.

3.1 Winter

Winter (January, February, and March) 2014 was warmest over the southern half of the Beaufort Sea and Amundsen Gulf, and cooler in the central Beaufort where the heaviest pack ice resides in winter (Figure 1). It was also cooler over the terrestrial environment, especially Banks and Victoria islands. The northern Beaufort Sea and Victoria Island in January 2014 were cooler than normal but winter 2014 was warmer than the climatological average by up to 6 °C (Figure 2). The SLP pattern in the study region contained the regionally significant Beaufort High in January 2014, but departed from the climatologically normal SLP pattern in February and March (Figure 3). The SLP in those months was lower than normal in the northern and eastern areas of the region in February, and lower than normal in the northwestern portion of the study region in March (Figure 4), with neither month containing the typical Beaufort High pressure center (Figure 3). Following on from the variability in the winter SLP pattern, winter winds in the study region were also variable in 2014 (Figure 5). January winds were light (Figure 5) and easterly in the southern half of the marine region, and northwesterly in the north half of the Beaufort Sea and M'Clure Strait (Figure 5). In February the 10-m winds were westerly (Figure 5) and much faster than the climatological standard normal (Figure 6), while in March the wind shifted again to a predominantly southerly direction (Figure 5) at slower than normal speeds in the southern Beaufort Sea and slightly faster than normal in the northern Beaufort Sea and along the continental coast in Amundsen Gulf (Figure 6).

Sea ice coverage in the study region in winter 2014 was complete, though sea ice in the Beaufort Sea and the whole of Amundsen Gulf was mobile for the duration of winter (Figure 7). Landfast sea ice presence was consistent in January, February, and March along the mainland coast, in Dolphin and Union Strait, Minto Inlet, Walker Bay, and Prince of Wales Strait, and in a thin band along the southwest and west coasts of Banks Island (Figure 7). Concentration of old, first-year, and new-plus-young sea ice stages of development that compose the total sea ice concentration in the region indicate variable dynamic forcing on the pack in winter 2014 (Figure 7). Linear features are obvious in the old and first-year sea ice concentration maps throughout the Beaufort Sea ice pack, indicating divergence within the old ice-dominated pack in the north. The mouth of M'Clure Strait also contained arched, reverse C-shape areas of new-plus-young sea ice indicating ice motion west away from M'Clure Strait and eastern Amundsen Gulf toward the west (Figure 7). Substantial (6+/10^{ths}) concentrations of new-plus-young sea ice occurred

in much of the Cape Bathurst flaw lead polynya complex across the continental coast in January (Figure 7), indicating that the Beaufort Sea pack was moving away from that area. The prevalence of these linear features of reduced old ice concentration coinciding with increased first-year sea ice concentration was diminished in February 2014 as the SLP pattern switched and the 10-m winds (Figure 5) became favorable to convergence, corroborated by eastward sea ice motion against the mouth of M'Clure Strait, the west coast of Banks Island, and in Amundsen Gulf (Figure 5), which closed January leads and reduced the regions' ability to generate new-plus-young sea ice concentration in the Cape Bathurst flaw lead polynya in February (Figure 7). In March, evidence of divergence in the sea ice pack of the study region returned. Southerly winds (Figure 5), though weak (Figure 6), dynamically forced sea ice away from the continental coast as indicated by the substantial width of new-plus-young sea ice concentration areas along the Mackenzie Shelf from the western limit of the study region to Cape Bathurst in March (Figure 7). The regional sea ice pack diverged slightly from the west coasts of Banks and Victoria Islands as indicated by flaw leads (new-plus-young sea ice) along the Mackenzie shelf, around the coast of Amundsen Gulf, and along the west coast of Banks Island in March 2014 (Figure 7). Winter sea ice concentration anomalies in the region (Figure 8) indicate that these linear features borne of divergence were unusual with respect to the climatological standard normal, and that they occurred in a 2014 Beaufort sea ice pack that was composed of more old ice than average (Figure 8). New-plus-young sea ice anomaly maps for winter 2014 also indicate that the flaw lead along the Mackenzie Shelf contained anomalously large concentrations of new-plus-young sea ice in January and March (Figure 8). Monthly average sea ice motion data corroborate the sea ice concentration and wind data; sea ice motion in January was anticyclonic, or clockwise, (Figure 15, 16) at anomalously high speed, likely due to the strength and position of high SLP in the region (Figure 3, 4). Sea ice motion slowed substantially in February and March (Figure 15).

3.2 Spring

Spring (April, May, June) 2014 began in April with a marked difference in 2-m air temperatures between the marine and terrestrial areas (Figure 1), though the entire region was colder than the climatological standard normal for April (Figure 2). In May, air temperatures in the study region warmed substantially (Figure 1), and were warmer than normal (Figure 2). Although the region continued to warm in June 2014, the air temperatures were below normal (Figures 1, 2), with much of the marine portion of the study region around freezing in June, and the terrestrial regions had become warmer (up to 12 °C) than the marine areas (around 0 °C).

The climatological standard normal SLP pattern for April is high pressure in the north and northeast and lower pressure in the southwest. In April 2014, that average pattern was nearly reversed (Figure 3) before returning to a pattern more similar to the climatological standard normal in May and June when the strength of the Beaufort High in the region was greater than climatological average (Figure 4). Anomalous SLP in April 2014 yielded westerly and northwesterly winds on average over the study region (Figure 5) which were opposite of the climatological mean wind direction, though slower than the climatological standard velocity (Figure 6). Winds in May and June 2014 were easterly, and then northerly respectively (Figure 5) at velocities greater than the climatological standard normal for May and June (Figure 6).

Sea ice coverage in the region in April 2014 was very similar to winter; September 2013-March 2014 exhibited multi-year sea ice recovery in the Arctic, which is indicated in part by the substantial spatial coverage (Figure 9) and positively anomalous concentrations of old ice in the region in spring (Figure 10). Sea ice in the northwestern quadrant of the study region was mostly composed of old ice, and moving from the northwest to the south and east, the total concentration became increasingly composed of first-year stages of development (Figure 9). Spring sea ice in Amundsen Gulf continued to be mobile, with the flaw lead polynya system existing at the interface between the offshore mobile sea ice and the thin band of landfast sea ice that surrounded it, as well as in central Amundsen Gulf between the southern tip of Banks Island and Cape Parry (Figure 9). Substantial new-plus-young sea ice concentrations in the flaw lead polynya system occurred in April, indicative of sea ice motion out of Amundsen Gulf to the west, and away from the Canadian Arctic Archipelago and the mainland coast west of Cape Bathurst (Figure 9). This is corroborated by anticyclonic (clockwise) sea ice motion in April (Figure 15), and further enabled by low concentrations in the Bering Sea through the autumn of 2013 and winter 2014 giving all this ice in the study region a place to move to. Subsequent early breakup of sea ice in the Bering Sea at the end of April allowed space for 'upstream' ice in the Beaufort to move clockwise, reducing internal stress in the western Arctic sea ice pack and creating divergence (Figure 9). In May 2014, Amundsen Gulf began to breakup dynamically (though ice motion was slower than the climatological average (Figure 16)), while below-freezing air temperatures over the region (Figure 1) continued to create substantial new-plus-young sea ice in the flaw lead system (Figure 9) highlighting the competing effects of dynamic breakup and thermodynamic ice growth under cold air temperatures. In June, the Beaufort sea ice pack continued to peel away *en masse* from the coast of the Archipelago, the west coast of Banks Island, Amundsen Gulf, and the continental coast west of Cape Bathurst (Figure 9) at above-average velocities (Figure 16), leaving open ocean that generated new-plus-young sea ice (Figure 9) under cooler than normal air temperatures

(Figure 1, 2). Anomalous new-plus-young ice production in June (Figure 10) lends further support to dynamic ice removal being the predominant breakup mechanism in spring 2014.

As a result of reduced sea ice concentration areas in spring 2014, there occurred some sea ice-adjusted surface solar radiation downward (SSRD, J m^{-2}) incident on open ocean surface in April, May, and especially June (Figures 17, 18). In June 2014, the sea ice-adjusted SSRD incident on open ocean surface was both substantial and positively anomalous in the flaw leads along the Mackenzie shelf west of Cape Bathurst, along the west coast of Banks Island, and in eastern Amundsen Gulf (Figure 17). The magnitude of the positive sea ice-adjusted SSRD anomalies in June (Figure 18) indicates that the ocean has climatologically (1983-2010) not received substantial surface solar radiation downward in June on average, largely because sea ice rarely broke up prior to July between 1983-2010. Further, this shows just how much solar radiation downward occurs in the physical system in June around the summer solstice. Mean sea surface temperatures in June indicated that much of the flaw lead polynya system was 2-4 °C (Figure 19), and positive SST anomalies occurred in the vicinity of the Mackenzie delta and eastern Amundsen Gulf in May and June (Figure 20). Conjecturally, it seems that warm water from the Mackenzie River may have played a role in the SST in the region in spring 2014 – warm air anomalies were very large on the continental landmass surrounding the Mackenzie River in May (Figure 1, 2). Positive SSRD anomalies (Figure 17) would not have warmed the sea surface in the presence of sea ice, creating a system akin to an ice bath working toward being isothermal around the freezing point.

3.3 Summer

Summer (July, August, September) began with cooler air temperatures predominantly over the marine environment and warmer air temperatures over the terrestrial environment in July and August (Figure 1). The 2-m air temperatures in July were cooler than normal over nearly the entire study region, while in August air temperatures over the marine areas were much warmer than normal (Figure 2). Positively anomalous warming continued over the entire study region in September (Figures 1, 2). The SLP pattern in summer 2014 was very consistent over July, August, and September, with the Beaufort High displaced farther north than its long term climatological standard position, which created zonal isobars over the marine region in all three summer months (Figure 3). This pressure pattern at the surface led to consistent positively anomalous wind speeds in an anticyclonic (clockwise) direction over the study region during summer (Figures 5, 6).

Summer 2014 sea ice concentrations (Figure 11), were generally negatively anomalous (Figure 12) in regions that were covered by first-year stages of development throughout 2014, except for M'Clure Strait where there was much more first-year sea ice than normal. Carrying on from winter and spring, there was still more old sea ice in the regional Beaufort pack than normal in summer 2014. The Beaufort sea ice pack rotated farther offshore of Banks Island than its climatological average summer position (Figures 11, 12) due to the position and strength of the Beaufort High over all three summer months and regional anticyclonic sea ice motion that resulted (Figure 15) at above-average velocities (Figure 16).

Following substantially increased sea ice-adjusted SSRD in June, sea ice-adjusted SSRD increased dramatically in summer 2014 following the summer solstice in late June (Figure 17), with a great deal of sea ice-adjusted SSRD reaching open ocean in July, and less so progressing through August and September as the system moved away from the solstice. Sea ice-adjusted SSRD was positively anomalous in much of the southern and eastern portion of the region in all three summer months, with the largest anomalies along southern and eastern edges of the summer sea ice pack (Figure 18). Sea ice-adjusted SSRD at the mouth of the Mackenzie River was near the climatological average over summer 2014 (Figure 18). Seasonal sea ice concentration reductions in the region in the southern Beaufort Sea and Amundsen Gulf in part created by large-scale anticyclonic sea ice motion westward out of the region allowed for substantial, consistently open ocean surface in summer 2014. As a result, sea ice-adjusted SSRD in summer 2014 was substantial in terms of total magnitude (Figure 17) and was positively anomalous (Figure 18) in July, August and September. Consistency in the position of the Beaufort Sea ice pack in 2014 might also be inferred from the accumulation of sea ice-adjusted SSRD in January to August 2014 (Figure 21a), which indicated that most of the ice-free southern reaches of the region and Amundsen Gulf received slightly more sea ice-adjusted SSRD than the climatological standard normal value for the eight-month annual period ending with August (Figure 21b). It is also notable that open water west of Banks Island and the mouth of M'Clure Strait accumulated more than average sea ice-adjusted SSRD in January to August 2014 (Figure 21) due to the packs' relatively consistent rotation away from the coast of the Archipelago (Figure 15) in 2014. Most striking is the positively anomalous accumulation of sea ice-adjusted SSRD at the open ocean surface in eastern Amundsen Gulf, the result of early dynamic sea ice removal in June (Figure 9, 17, 18). The SST in summer 2014 (Figure 19) was wildly anomalous, especially in July and August (Figure 20). Much of the Mackenzie Shelf and Amundsen Gulf were above 5 °C, with some SSTs above 8 °C (Figure 19), corresponding to positive anomalies as high as 6 °C (Figure 20). In both July and August 2014, the largest SSTs were observed at the mouth of the Mackenzie River (Figure 19). This result seems to follow on from the work of Wood et al. (2013) who showed that in 2011 and 2012, the Mackenzie

River plume was associated with surface layer stratification in the Beaufort Sea that was 6-8 m thick, and up to 12 °C. Ocean heat is being imported via river water warmed prior to reaching the ocean. These ocean temperatures would likely have a deleterious effect on arctic cod typically found under sea ice seeking refuge and/or feeding, or in cold (<4 °C) waters (Bluhm and Gradinger, 2008, Crawford and Jorgenson, 1993), which were shown to be all but absent from the region in 2014 (Niemi et al., 2019).

3.3.1 Summer Ocean Conditions

Between 2 August and 9 September 2014, CTD casts were conducted at 54 stations in the study region (Figure 23, Table 1). CTD cast data indicate the ocean surface temperature ranged from -0.19 °C in Prince of Wales Strait (PWS) to 9.05 °C at the southernmost station north of Kugmallit Bay on the Mackenzie Shelf (KUG01, Figure 24a); the mean surface temperature in 2014 using CTD casts was 5.52 °C. The minimum surface temperature in Prince of Wales Strait is somewhat misleading; the profile at that location shows the surface water temperature was below 0°C before increasing to > 1 °C around 10 m depth, likely indicating melting sea ice in the vicinity. Across the south end of Prince of Wales Strait near Alexander Milne Point (at the southeastern corner of Banks Island, ALX stations) the surface temperature was ~ 1 °C closest to Banks Island, before increasing to ~7 °C moving east toward Victoria Island (Figure 22a, Table 1). In Walker Bay and Minto Inlet, the surface temperature was ~7.5 °C. In Dolphin and Union Strait, the surface temperature was ~5 °C, save for the station nearest Victoria Island where the surface temperature was 0.6°C. The two stations offshore in eastern Amundsen Gulf were similarly warm (4.4 °C and 5.2 °C). In Franklin and Darnley Bays and near Cape Parry the surface temperature was between 5 and 8.5 °C (Figure 24a). The surface temperature at the NTC station was 5.2 °C, and moving north from there and west from Banks Island the surface temperatures decreased ranging between 0.3 °C and 5.2 °C (Figure 24a). Finally off the coast of the Tuktoyaktuk Peninsula along the Kugmallit Bay transect, the surface water was warmest in the south (9 °C), and decreased northward to 2.5 °C at the northernmost KUG station (Figure 24a, Table 1).

The mean surface salinity in the region in 2014 was 28.04 (standard deviation = 4.08), and the maximum surface salinity was 30.97 at the east end of Dolphin and Union Strait closest to Victoria Island. At the southernmost KUG01 station, the surface salinity was 0.2 due to the surface influence of terrestrial freshwater in that area (Figure 24b, Table 1). The surface salinity of the northern four stations on the Kugmallit Bay transect across the Mackenzie shelf was 28-29 (Figure 24b). There may be some uncertainty introduced here by the definition of “surface” because, despite selecting the topmost surface salinity in each cast, the profile at the southernmost station on the KUG transect where the surface salinity was

near-zero contained the very surface meter of data, while the other KUG stations, and indeed most of all the stations sampled in 2014, did not contain data in the surface meter (Table 1). As a result, the surface salinity at most of the stations in 2014 was selected from the 1.0 – 1.99 m, 2.0-2.99 m, or even the 3.0-3.99 m of data, potentially missing extremely fresh and warm terrestrial run-off that may have been on top of the seawater in an area. In the southern coastal bays, in Amundsen Gulf, and in Dolphin and Union Strait the surface salinity was greater (Figure 24b). In the northeast, specifically in Minto Inlet, Walker Bay, and Prince of Wales Strait, the surface was less saline, around 28 (Figure 24b); the innermost station in Minto Inlet which likely received run off from the Kuujjua River, and the Prince of Wales station that showed evidence of sea ice melt were even less saline (Figure 24b, Table 1).

The surface layer depth (depth of the N^2 maximum) of the ocean column in the study region at the end of summer 2014 varied between 1 and 34 dbar, (Table 1, mean = 13.9 dbar, standard deviation = 9.2). The surface layer depth was relatively deep across Dolphin and Union Strait (mean = 29.8 dbar) (Figure 25a) and was more variable but still relatively deep on average in Walker Bay, Minto Inlet, and Prince of Wales Strait (Figure 25a, Table 1). In Franklin and Darnley Bays, and at Cape Parry the surface layer depth was thinner, ranging from 1 to 23 dbar, with a mean of 9.4 dbar (standard deviation = 7.53). The surface layer depth was relatively thin closest to the west coast of Banks Island. The maximum N^2 value at the BNK stations was very near surface (due to rapidly increasing salinity with depth from the surface) which was not really indicative of the true surface layer, which was actually 25, 18, and 43 dbar upon visual inspection of the profiles at stations BNK01, BNK06, and BNK07 respectfully (values in parentheses in Table 1, profile plots in Appendix A). The rest of the Banks Island stations had an average surface layer depth value of 18 dbar using the N^2-maximum criterion (Figure 25a). Finally, along the Kugmallit Bay (KUG) transect, the most near-shore station had an N^2-derived surface layer depth of 0 dbar due to the freshwater sitting on top of saltwater at that location at that time resulting in the N^2-maximum at the surface. However, two other stations is the immediate vicinity (AGK01 and AGK02) had N^2-derived surface layer depths of 5 and 9 dbar, and the average surface layer depth over the remaining four more northerly KUG stations was 11.25 dbar (Figure 25a, Table 1).

The ocean heat content (OHC) in the N^2-derived surface layer, and the N^2-derived surface layer thickness were roughly linearly related in 2014. Exceptions with deep surface layers and very little OHC did occur, like DOL-5 on the east end of Dolphin and Union Strait closest to Victoria Island (28 m, 27.6 kJ), and ALX-01 at the mouth of Prince of Wales Strait closest to Banks Island (13 m, 58 kJ) (Table 1). In Dolphin and Union Strait, despite the low ocean heat content at one of the five stations, the average OHC was 449.53

kJ, and the maximum OHC was 675.54 kJ (Figure 25b, Table 1). In Minto Inlet, Walker Bay, and in Prince of Wales Strait the OHC was also high (average = 450.89 kJ, standard deviation = 296 kJ). The middle of Walker Bay had the highest OHC (792 kJ), and the station in the middle of Prince of Wales Strait had the lowest OHC (23.7 kJ)). In Franklin and Darnley Bays and north of Cape Parry, the OHC was lower (average = 254 kJ, standard deviation = 191 kJ). The maximum OHC in the surface layer in this area occurred in the middle of Franklin Bay (576.16 kJ) where surface layer depth was thick, and the minimum (20.34 kJ) also occurred in Franklin Bay, though the surface layer depth was very thin. The two stations offshore in eastern Amundsen Gulf contained 105.5 kJ and 256 kJ OHC (Figure 25a, b, Table 1). Stations along the Mackenzie shelf and Kugmallit Bay transect contained an average of 156.53 kJ of OHC (standard deviation = 80.6 kJ). The maximum OHC in this area was at ESC-03 close to the east end of the Tuktoyaktuk Peninsula (295.71 kJ); at this station the surface layer depth was only 11 dbar, but the entirety of the surface layer depth was greater than 7 °C (Appendix A). West of Banks Island, the OHC contained in the surface layer depended greatly on the depth of the surface layer; where the surface layer depth was deeper, the OHC was nearly 400 kJ, while areas with thin surface layers contained much less OHC (~10-45 kJ).

The N^2-derived surface layer depth and the freshwater content within the N^2-derived surface layer were roughly linearly related; where the surface layer depth is thicker, more freshwater is contained within it (Figure 25, Table 1). Consequently, the spatial pattern of freshwater content (FWC) in the study region in 2014 generally followed the ocean heat content (Table 1). The mean freshwater content (in meters) in Dolphin and Union Strait was 3.89 m (standard deviation= 0.90 m), and in Minto Inlet, Walker Bay, and Prince of Wales Strait the mean FWC was 3.37 m (standard deviation = 1.71 m). Despite containing little OHC, the station in the middle of Prince of Wales Strait (PWS-01) contained 3.03 m of freshwater. In the south, in Franklin and Darnley Bays and near Cape Parry, the mean freshwater content within the surface layer was only 1.27 m (standard deviation = 1.07 m). The two stations offshore in eastern Amundsen Gulf contained 0.82 m and 2.20 m FWC (Figure 25). The Kugmallit transect, combined with stations along the Mackenzie shelf west of Cape Bathurst contained a mean of 1.52 m of freshwater in the surface layer (standard deviation = 0.53 m). West of Banks Island, the stations closest to the coast contained the least freshwater content in the surface layer (BNK-01, BNK-06, BNK-07, average FWC = 0.33 m, standard deviation = 0.18 m). However, these values are low due to inaccurate surface layer thickness values created by very near-surface N^2 maxima; surface layer depths picked by eye using the N^2 profile for each of these three stations, as well as the OHC and FWC in the more accurate surface layer thickness picked by eye are presented in parentheses in Table 1. The five BNK stations farthest west of the coast averaged 2.66 m (standard deviation = 0.41 m).

Salinity and temperature section plots using five stations across Dolphin and Union Strait (DOL) from west to east are presented for the full cast depths in Figure 26 (a, c) and for the top 50 m (Figures 26b, d). In this section there was cooler, more saline water all the way to the surface on the east end of the section nearest Victoria Island. The predominant wind direction in this area of the region was easterly for July, August, and September (Figure 5) which may have pushed warmer, fresher water offshore of Victoria Island, accumulating it there (Figure 26). Conversely, in the west-to-east section of Minto Inlet (Figure 27), warm fresh water accumulated inland, due likely in part to terrestrial run off entering the Inlet from the Kuujjua River flowing off Victoria Island. The south-to-north section of Minto Inlet (Figure 28) indicates that fresher surface water is more prevalent on the south side of the Inlet than in the middle. In Walker Bay (WLK), the west-to-east section (Figure 29) is more ubiquitously warm and fresh throughout the surface layer, though that layer thins and is mixed at its bottom near the west end of Walker Bay. Across the south end of Prince of Wales Strait from Milne Point to Victoria Island (ALX stations, Figure 21) the temperature and salinity sections (Figure 30) show that the surface layer was deepest at the east end, and became thinner and more mixed towards Banks Island in the west. Substantial heat was contained in the eastern half of the section, but as discussed earlier, the presence of melting sea ice in the area affected the temperature profile more so than the salinity profile in the area. The ALX salinity section showed an accumulation of freshwater at the surface of the whole section that was mixed downward at the east end, and remained in the top 10-15 m in the west (Figure 28). Using the two stations offshore in central eastern Amundsen Gulf (AMN, Figure 23) to create temperature and salinity sections (Figure 31), it is observed that the north of the two stations was warmer at the surface but less well mixed vertically (Figure 31a). The salinity section also bears this out (Figure 31b). To the south of the two stations in central eastern Amundsen Gulf, it is cooler at the surface and more saline, but showed indications of vertical mixing (Figure 31).

In the south end of the study region, the Bennett Point section portrays a very stable, thin, fresh, and very warm surface layer that is consistent across Darnley Bay (Figure 32). However, moving from south to north from Cape Parry, there is cooler, saltier water at the surface nearest the Cape, which gives way to a thick warm and fresh surface layer that gets warmer and fresher moving northward (Figure 33). In Franklin Bay, the temperature and salinity sections indicate vertical mixing down to 50 m, especially in the temperature sections (Figure 34). From west to east, heat in the surface layer of Franklin Bay accumulated away from the coasts, with warm water only occurring in the top 5 m or so of the section at the west end. Saltier, cooler water was mixed from below at the east end of the section to within 10 m of the surface (Figure 34).

West of Banks Island, two sections were created using stations along similar latitudes (Figure 23). The northern of the two sections (BNK-N, Figure 35)) shows that heat was accumulated towards the coast of Banks Island in the surface layer, while farther offshore the temperature of the surface layer looks to have been cooled at the surface by ice melt in the vicinity (Figure 35b). The salinity of the section is relatively uniform, though more freshwater exists in the surface closer to the coast of Banks Island than offshore (Figure 35a). The BNK-N section shows evidence of vertical mixing throughout the top 55 m. On the BNK-S section (Figure 36) five stations were sampled (Figure 23), showing a surface layer affected by the presence of melting sea ice, and indicating vertical mixing down to at least 50 m (Figure 36). Still, substantial heat was contained in the upper 25-30 m in this section (Figure 36d), and relatively fresh surface water was observed near the coast of Banks Island and farthest off shore (Figure 36b) where evidence of sea ice melt existed in the temperature section (Figure 36d).

Finally, the last section sampled in 2014 was the KUG section north of Kugmallit Bay spanning roughly 70 nautical miles (125 km) from station KUG-01 on the Mackenzie shelf through four more stations (KUG-02 to KUG-05) on the shelf break in 80-500 m of water (Figure 23, 37). At the south end, the temperature and salinity section indicate that the water column was very warm, and was almost fresh due to its proximity to the Mackenzie River; the upper ocean was greater than 5 °C to about 13 m depth from KUG-01 (Figure 37d). On the shelf break, the temperature section showed a warm surface layer that had been cooled from the top down, likely due to sea ice melt in the vicinity (Figure 37d), while the salinity increased gradually with depth from the surface to 10 m (Figure 37b), also indicating sea ice melt in the immediate area.

3.4 Autumn

Autumn (October, November, and December) 2014 proceeded with below-zero air temperatures over the marine area of the study region in October (Figure 1), though positive 2-m air temperature anomalies were present in October over much of the Beaufort Sea, M'Clure Strait, and western Amundsen Gulf (Figure 2) as a result of the ocean losing large amounts of heat stored over summer (Figure 17-20). In November 2014, the 2-m air temperatures ranged from -16 °C in the southern parts of the Beaufort Sea and Amundsen Gulf to about -25 °C in the northwest quadrant of the study region (Figure 1). November 2014 air temperatures were very similar to the climatological standard normal values (Figure 2). The 2-m air temperatures continued to cool in December 2014; colder temperatures than the standard normal occurred across Victoria and Banks islands, and in the northwest quadrant of the region (Figure 2). The SLP pattern in all three autumn months in 2014 (Figure 3) was very similar to the climatological standard

normal for the study region, though the actual sea level pressure over the whole region was marginally lower than the long term mean (Figure 4). As a result, the wind direction in the study region (Figure 5) was anticyclonic in the whole of the Beaufort and easterly in Amundsen Gulf, very typical of the climatological standard normal wind direction. The wind speed was slightly greater than the standard normal in October 2014, slightly slower than the standard normal in November 2014, and nearly the same as the long term climatological wind speed in December 2014 (Figure 6).

In October, at the beginning of autumn 2014, the total sea ice concentration in the region occurred primarily in the northwest quadrant of the region and in M'Clure Strait and was made up of almost entirely old ice (Figure 13). From this regional old ice core, new-plus-young sea ice formed along the southeastern periphery of the old ice pack, growing southward. New-plus-young sea ice also formed in the mouth of the Mackenzie River and along the mainland coast all the way to Coronation Gulf, and encircled the eastern side of Amundsen Gulf including Dolphin and Union Strait and the west coast of Victoria Island and its embayments (Figure 13). October sea ice anomaly maps (Figure 14) indicate that the extent of total sea ice (composed of old ice) was spatially limited compared to the climatological standard normal, and that much of the new-plus-young sea ice that formed in October 2014 was positively anomalous (Figure 14). Sustained winds from the north in October (Figure 15) likely blew newly formed sea ice into coastal areas across the Mackenzie shelf and slope. Freeze up continued in the region under climatologically normal air temperatures, SLP, and wind speed and direction in November, resulting in near-complete sea ice coverage of the study region (Figure 13). However, the predominant stages of development in the region were old ice in the northwest, and highly positive concentration new-plus-young sea ice anomalies in the south and in Amundsen Gulf (Figure 13, 14). This prevalence of new-plus-young sea ice in November was counterbalanced by a complete and anomalous lack of first-year sea ice in the region (Figures 13, 14). Although the spatial extent of regional sea ice was nearly complete by the end of November as is typical for the region, it was mainly new-plus-young sea ice rather than thicker first-year sea ice. Relatively thin sea ice was present in the region because it was continuously formed and advected out of the area and replaced by new sea ice growth. The mean sea ice motion direction in October and November 2014 (Figure 15) was extremely conducive to western sea ice export from of the region, and the sea ice motion velocity was nearly double the climatological average for those months (Figure 16). Large positive new-plus-young sea ice anomalies and large negative first-year sea ice anomalies in autumn 2014 were the result of continual sea ice formation and near-immediate advection out of the region.

In Autumn 2014, and in October specifically, there occurred a small (Figure 17) but positively anomalous (Figure 18) amount of sea ice-adjusted SSRD that reached open ocean surface. This sea ice-adjusted SSRD at the open ocean surface was likely the result of negatively anomalous sea ice concentration in that area in October (Figures 13, 14). Following on from the mean accumulated sea ice-adjusted SSRD in the region between January and August 2014 (inclusive, Figure 21), the mean accumulated sea ice-adjusted SSRD in the region for the whole of 2014 (Figure 22a) showed that the Mackenzie Shelf along the mainland coast, and the southern and eastern parts of Amundsen Gulf accumulated some additional sea ice-adjusted SSRD at open ocean surface in autumn 2014, though not enough to appreciably change the annual accumulated sea ice-adjusted SSRD anomaly map for the region (Figure 22b).

4 Conclusion

This report provides monthly averaged 2-m air temperature, sea level pressure, 10-m winds, sea surface temperature, sea ice concentration and motion, and surface solar radiation downward adjusted for sea ice concentration in Canada's western marine Arctic in 2014. Monthly anomalies in these variables have also been presented in order to help compare these 2014 data to the climatological average period (1983-2010). Basic oceanographic information from 54 stations sampled in August and September within the study region have been presented, including surface salinity, surface temperature, surface layer depth, ocean heat content and freshwater content in the surface layer, and oceanographic sections of temperature and salinity. This report serves as contextual information on the physical environment of the region in 2014 in the pursuit of further understanding unique ecological phenomena in the study region in that year.

Winter 2014 was substantially warmer than normal, and the sea level pressure pattern in the region was atypical. Winter winds in the region were much faster than normal in February from the east, and faster than normal in March from the south. Sea ice motion was anomalously fast in winter. Sea ice remained mobile in the region including Amundsen Gulf throughout the winter months, and the Beaufort Sea pack exhibited features of divergence, which were unique and significant evidence of that mobility. Specifically, anomalous linear features in the northwest, and positively anomalous new-plus-young ice in much of the Cape Bathurst flaw lead polynya complex occurred in winter 2014.

Spring 2014 was a colder than average, though warm air occurred over the continental coast in May. Due to the anomalous SLP patterns in April the wind direction was also atypical, blowing predominantly from the west. Winds were faster than normal in May and June, but their direction was more anticyclonic as is

climatologically typical. Sea ice motion was relatively disconnected from the winds in the study region in 2014, maintaining its typical anticyclonic movement through the region even in April. This may signify that hemispheric rather than regional processes dominated the sea ice motion in 2014. Positive old ice concentration anomalies in all three summer months indicate import from the north as a result of hemispheric rather than regional processes. Early breakup in the downstream Chukchi Sea reduced internal stress in the pack, allowing for consistent new-plus-young sea ice formation in spring 2014 throughout the Cape Bathurst flaw lead polynya complex. Reduction in ice concentration in spring, especially in June around the summer solstice, allowed for positively anomalous SSRD incident on the open ocean. Sea surface temperatures in the flaw lead and eastern Amundsen Gulf were positively anomalous, as were SSTs in the Mackenzie Delta and air temperatures over the continental landmass surrounding the Mackenzie River.

Summer air temperatures in 2014 were much warmer than normal in all three months, especially in August and September. SLP was very consistent in summer 2014 with the Beaufort High farther north and west than its climatological average position, leading to anomalous zonal isobars in the region. Wind speed and direction were also consistent and similar to the climatological summer normal. Old ice replenishment in the region that began in late 2013 is still apparent in summer 2014, resulting from consistent anticyclonic sea ice motion over summer that also rotated the Beaufort Pack away from the west coast of Banks Island, and kept the shallower southern Beaufort Sea, shelf and Amundsen Gulf free of sea ice all summer via export westward combined with melt. These ice-free areas were collocated with positive sea ice adjusted-SSRD anomalies through summer, as well as being areas of sea ice adjusted-SSRD accumulation at open ocean surface from January to August 2014. Following on from June, the monthly SSTs in the region were extreme in July and August, and remained positively anomalous in September.

In autumn, large positive air temperature and SST anomalies continued from summer into October 2014, before they converged to the long-term normal in November and December. The SLP pattern and the wind speed and direction in autumn 2014 were similar to their climatological averages. Following consistent and substantial summer sea ice export, sea ice export from the southern reaches of the region continued in earnest in autumn 2014, creating substantial positive new-plus-young sea ice anomalies in October and November, which replaced what was typically old ice in October and old and first-year sea ice in November on average. Sea ice was exported from the region westward before it could grow thick enough to be classified as first-year sea ice until much later in the year than usual in December 2014.

5 Acknowledgements

We thank the Inuvialuit Game Council and the Fisheries Joint Management Committee for supporting this work and providing valuable input into study objectives. Funding was provided by the Beaufort Regional Environmental Assessment administered by Aboriginal Affairs and Northern Development Canada, the Environmental Studies Research Fund administered by Natural Resources Canada, Fisheries and Oceans Canada's International Governance Strategy and National Conservation Plan as well as other DFO funds. Finally, thanks to the crew and management team of the F/V Frosti for their tireless service and professionalism.

6 References

Aagaard, K., Carmack, E. C. 1989. The role of sea ice and other fresh water in the arctic circulation. Journal of Geophysical Research, 94, C10, 14485-14498.

Arteaga, L. A., Rousseaux, C. S. 2023. Impact of Pacific Ocean heatwaves on phytoplankton community composition. Communications Biology, 6:263, doi: 10.1038/s42003-023-04645-0

Belkin, I. M., Short, J. W. 2023. Echoes of the 2013-2015 marine heat wave in the eastern Bering Sea and consequent biological responses. Journal of Marine Science and Engineering, 11, doi: 10.3390/jmse11050958.

Bond, N. A., Cronin, M. F., Freeland, H., Mantua, N. 2015. Causes and impacts of the 2014 warm anomaly in the NE Pacific. Geophys. Res. Lett., 42, doi: 10.1002/2015GL063306.

B.A. Bluhm, R. Gradinger, 2008. Regional variability in food availability for Arctic marine mammals. Ecological Applications, 18 (Suppl. 2), pp. S77-S96

Cavole, L. M., Demko, A. M., Diner, R. E., Giddings, A., Koester, I., Pagniello, C. M. L. S., Paulsen, M.-L., Ramirez-Valdez, A., Schwenck, S.M., Yen, N. K., Zill, M. E., and Franks, P. J. S. 2016. Biological impacts of the 2013–2015 warm-water anomaly in the Northeast Pacific: Winners, losers, and the future. Oceanography 29(2):273–285, http://dx.doi.org/10.5670/oceanog.2016.32.

Chandler, P.C., King, S.A., and Perry, R.I. (Eds.). 2015. State of the physical, biological and selected fishery resources of Pacific Canadian marine ecosystems in 2014. Can. Tech. Rep. Fish. Aquat. Sci. 3131: vi + 211 p.

Choy, E. S., Rosenberg, B., Roth, J. D., and Loseto, L. L. 2017. Inter-annual variation in environmental factors affect the prey and body condition of beluga whales in the eastern Beaufort Sea. Mar. Ecol. Prog. Ser. 579: 213–225. doi: 10.3354/meps12256.

R.E. Crawford, J.K. Jorgenson, 1993. Schooling behaviour of Arctic cod, *Boreogadus saida*, in relation to drifting pack ice.Environmental Biology of Fishes, 36, pp. 345-357

Danielson, S. L., Ahkinga, O., Ashjian, C., Basyuk, E., Cooper, L. W., Eisner, L., Farley, E., Iken, K. B., Grebmeier, J. M., Juranek, L., Khen, G., Jayne, S. R., Kikuchi, T., Ladd, C., Lu, K., McCabe, R. M., Moore, G. W. K., Nishino, S., Ozenna, F., Pickart, R. S., Polyakov, I., Stabeno, P. J., Thoman, R., Williams, W. J., Wood, K., Weingartner, T. J. 2020. Manifestation and consequences of warming and altered heat fluxes over the Bering and Chukchi Sea continental shelves. Deep-Sea Research, Part II, doi: 10.1016/j.dsr2.2020.104781.

DFO. 2010. Monitoring indicators for the Tarium Niryutait Marine Protected Area (TNMPA). DFO Can. Sci. Advis. Sec. Sci. Advis. Rep. 2010/059.

DFO. 2014. Re-evaluation of Ecologically and Biologically Significant Areas (EBSAs) in the Beaufort Sea. DFO Can. Sci. Advis. Sec. Sci. Advis. Rep. 2014/052.

Freeland, H. 2014. Something odd in the Gulf of Alaska. CMOS Bull. SCMO, 42, 57–59.

Freeland, H. 2015. The “Blob” or Argo and other views of a large anomaly in the Gulf of Alaska in 2014/15. In State of the Physical, Biological and Selected Fishery Resources of Pacific in 2014; Canadian Technical Report of Fisheries and Aquatic Sciences; Chandler, P.C., King, S.A., Perry, R.I., Eds.; Fisheries & Oceans Canada Institute of Ocean Sciences: Sidney, BC, Canada, 2015; pp. 25–29.

Freeland, H., Ross, T. 2019. ‘The Blob’ – or, how unusual were ocean temperatures in the northeast Pacific during 2014-2018? Deep Sea Researchh Part I: Oceanographic Research Papers, 150, 103061, doi: 10.1016/j.dsr.2019.06.007

Geoffroy, M., Majewski, A., LeBlanc, M., Gauthier, S., Walkusz, W., Reist, J. D., and Fortier, L. 2016. Vertical segregation of age-0 and age-1+ polar cod (Boreogadus saida) over the annual cycle in the Beaufort Sea. Polar Biology, 39(6), doi: 10.1007/s00300-015-1811-z.

Häkkinen, S., and A. Proshutinsky, 2004. Freshwater content variability in the Arctic Ocean, Journal of Geophysical Research, 109, C3, doi: 10.1029/2003JC001940.

Hersbach, H., Bell, B., Berrisford, P., Biavati, G., Horányi, A., Muñoz Sabater, J., Nicolas, J., Peubey, C., Radu, R., Rozum, I., Schepers, D., Simmons, A., Soci, C., Dee, D., Thépaut, J-N. 2018. ERA5 hourly data on single levels from 1959 to present. Copernicus Climate Change Service (C3S) Climate Data Store (CDS). (Accessed June 2022), 10.24381/cds.adbb2d47

Iwahara, Y., Fujiwara, A., Ito, K., Miyashita, K., Mitani, Y. 2016. Gray whale sightings in the Canadian Beaufort Sea, September 2014.

Jeffries, M. O., Richter-Menge, J., Overland, J. E. 2014. Executive Summary [in Arctic Report Card 2014], http://www.arctic.noaa.gov/reportcard.

Jones, T., Parrish, J. K., Peterson, W. T., Bjorkstedt, E. P., Bond, N. A., Ballance, L. T., Bowes, V., Hipfner, J. M., Burgess, H K., Dulliver, J. E., Lindquist, K., Lindsey, J., Nevins, H. M., Robertson, R. R., Roletto, J., Wilson, L., Joyce, T., Harvey, J. 2018. Massive mortality of a planktivorous seabird in response to a marine heatwave. Geophysical Research Letters, 45, 3193–3202, doi: 10.1002/2017GL076164

Kelley, D. E. 2018. Oceanographic analysis with R. Springer, New York, NY. ISBN: 978-1-4939-8844-0, doi: 10.1007/978-1-4939-8844-0, 290pp+xxi.

Loseto, L. L., Brewster, J. D., Ostertag, S. K., Snow, K., MacPhee, S. A., McNicholl, D. G., Choy, E. S., Giraldo, C., and Hornby, C. A. 2018. Diet and feeding observations from an unusual beluga harvest in 2014 near Ulukhaktok, Northwest Territories, Canada. Arctic Science 4: 421–431. doi: 10.1139/as-2017-0046.

Majewski, A. R., Atchison S. P., Suchy, K. D., Henry, J., MacPhee S. A., Walkusz, W, Eert, J., Dempsey, M., Niemi, A., de Montety, L., Geoffroy, M., Giraldo, C., Michel, C., Archambault, P., Williams, W.J., Fortier, L., and Reist, J. D. 2016. Beaufort Sea Marine Fishes Project - Update for Stakeholders. Fisheries and Oceans Canada, Ottawa. viii+57pp.

McLaughlin, F. A., Carmack, E. C., Macdonald, R. W., and Bishop, J. K. B. 1996. Physical and geochemical properties across the Atlantic/Pacificwater mass front in the southern Canadian basin. J. Geophys. Res., 101(C1), 1183–1197, doi:10.1029/95JC02634

Mueter, F., Nahrgang, J., Nelson, R. J., and Berge, J. 2016. The ecology of gadid fishes in the circumpolar Arctic with a special emphasis on the polar cod (Boreogadus saida). Polar Biology, 39: 961–967. doi: 10.1007/s00300-016-1965-3.

Niemi, A., Ferguson, S., Hedges, K., Melling, H., Michel, C., Ayles, B., Azetsu-Scott, K., Coupel, P., Deslauriers, D., Devred, E., Doniol-Valcroze, T., Dunmall, K., Eert, J., Galbraith, P., Geoffroy, M., Gilchrist, G., Hennin, H., Howland, K., Kendall, M., Kohlbach, D., Lea, E., Loseto, L., Majewski, A., Marcoux, M., Matthews, C., McNicholl, D., Mosnier, A., Mundy, C.J., Ogloff, W., Perrie, W., Richards, C., Richardson, E., Reist, R., Roy, V., Sawatzky, C., Scharffenberg, K., Tallman, R., Tremblay, J-É., Tufts, T., Watt, C., Williams, W., Worden, E., Yurkowski, D., Zimmerman, S. 2019. State of Canada's Arctic Seas. Can. Tech. Rep. Fish. Aquat. Sci. 3344: xv + 189 p

Niemi, A., Majewski, A., Eert, J., Ehrman, A., Michel, C., Archambault, P., Atchison, S., Cypihot, V., Dempsey, M., de Montety, L., Dunn, M., Geoffroy, M., Hussherr, R., MacPhee, S., Mehdipour, N., Power, M., Swanson, H., Treau de Coeli, L., Walkusz, W., Williams, W., Woodard, K., Zimmerman, S., Reist, J. 2020. Data from the BREA-MFP and CBS-MEA research programs describing the Anguniaqvia niqiqyuam Marine Protected Area (ANMPA) ecosystem. Can. Data Rep. Fish. Aquat. Sci. 1316: ix + 90 p.

Overland, J., Hanna, E., Hanssen-Bauer, I., Kim, S.-J., Walsh, J., Wang, M., Bhatt, U. S. 2014. Air temperature [in Arctic Report Card 2014], http://www.arctic.noaa.gov/reportcard.

Peterson, W., Bond, N., Robert, M. 2016. The blob (part three): Going, going, gone? PICES Press, 24, 46–48.

Piatt, J. F., Parrish, J. K., Renner, H. M., Schoen, S. K., Jones, T. T., Arimitsu, M. L., Kuletz, K. J., Bodenstein, B., Garcia-Reyes, M., Duerr, R. S., Corcoran, R. M., Kaier, R. S. A., McChesney, G. J., Golightly, R. T., Coletti, H. A., Suryan, R. M., Burgess, H. K., Lindsey, J., Lindquist, K., Warzybok, P. M., Jahncke, J., Roletto, J., Sydeman, W. J. 2020. Extreme mortality and reproductive failure of common murres resulting from the northeast Pacific marine heatwave of 2014-2016. PLoS ONE, 15(1): e0226087.

R Core Team, 2022. R: A language and environment for statistical computing. R Foundation for Statistical Computing, Vienna, Austria. https://ww.R-project.org/

Renner, H.. M., Piatt, J. F., Renner, M., Dummond, B. A., Laufenberg, J. S., Parrish, J. K. 2024. Catastrophic and persistent loss of common murres after a marine heatwave. Science, 386, 1272-1276.

Rice, D. W., Wolman, A. A. 1971. The life history and ecology of the gray whale (*Eschrichtius robustus*). American Society of Mammalogists, Oklahoma.

Rugh, D. J., Shelden, K. E. W., Schulman-Janiger, A. 2001. Timing of the gray whale southbound migration, J. Cetacean Res. Manag. 3, 31-39.

Savage K. 2017. Alaska and British Columbia large whale unusual mortality event summary report. NOAA Fish Report, Juneau, August: 1–42.

Serreze, M. C., Barrett, A. P., Slater, A. G., Woodgate, R. A., Aagaard, K., Lammers, R. B., Steele, M., Moritz, R., Meredith, M., Lee, C. M. 2006.The large-scale freshwater cycle of the Arctic. J. Geophys. Res., 111,C11010, doi:10.1029/2005JC003424.

Sharqawy, M. H., Lienhard V, J.. H., Zubair, S. M. 2010. Thermophysical properties of seawater: a review of existing correlations and data, Desalination and Water Treatment, 16: 354-380, doi: 10.5004/dwt.2010.1079.

Stabeno, P. J., Kachel, N. B., Moore, S. E., Napp, J. M., Sigler, M., Yamaguchi, A., Zerbini, A. N. 2012. Comparison of warm and cold years on the southeastern Bering Sea shelf and some implications for the ecosystem. Deep-Sea Research Part II, 65-70: 31-45, doi: 10.1016/j.dsr2.2012.02.020.

Stabeno, P. J., Duffy-Anderson, J. T., Eisner, L. B., Farley, E. V., Hientz, R. A., Mordy, C. W. 2017. Return of warm conditions in the southeastern Beaufort Sea: Physics to fluorescence. PLoS ONE 12(9): e018464, doi: 10.1371/journal.pone.0185464.

Stevenson, D.E., Lauth, R.R., 2019. Bottom trawl surveys in the northern Bering Sea indicate recent shifts in the distribution of marine species. Polar Biol. 42, 407–421, doi: 10.1007/s00300-018-2431-1.

Stirling, I. 1980. The biological importance of Polynyas in the Canadian Arctic. Arctic, 33(2), 303-315.

Swanson, D. K., Sousanes, P. J., Hill, K. 2021. Increased mean annual temperatures in 2014-2019 indicate permafrost thaw in Alaskan national parks. Arctic, Antarctic, and Alpine Research, 53(1): 1-19.

Thorson, J. T. 2019. Measuring the impact of oceanographic indices on species distribution shifts: The spatially varying effect of cold-pool extent in the eastern Bering Sea. Limnol. Oceanogr., 64, 2632–2645.

Timmermans, M.-L., Proshutinsky, A. 2014. Arctic ocean sea surface temperature [in Arctic Report Card 2014], http://www.arctic.noaa.gov/reportcard.

Tschudi, M., Meier, W. N., Stewart, J. S., Fowler, C., Maslanik, J. 2019. *Polar Pathfinder Daily 25 km EASE-Grid Sea Ice Motion Vectors, Version 4.* [1983-2021]. Boulder, Colorado USA. NASA National Snow and Ice Data Center Distributed Active Archive Center. doi: https://doi.org/10.5067/INAWUWO7QH7B. [June 2022].

Tivy, A., Howell, S. E. L., Alt, B., McCourt, S., Chagnon, R., Crocker, G., Carrieres, T., Yackel, J. J. 2011. Trends and variability in summer sea ice cover in the Canadian Arctic based on the Canadian Ice Service Digital Archive, 1960-2008, and 1968-2008. Journal of Geophysical Research, Oceans, 116(C3), doi: 10.1029/2009JC005855.

Whitney FA. 2015. Anomalous winter winds decrease 2014 transition zone productivity in the NE Pacific. Geophysical Research Letters, 42: 428-431.

Wood, K. R., Overland, J. E., Salo, S. A., Bond, N. A., Williams, W. J., Dong, X. 2013. Is there a 'new normal' climate in the Beaufort Sea? Polar Research, 32, 19552, doi: 10.3402/polar.v3210.19552.

Woodgate R. A., Weingartner, T., Lindsay, R. 2010. The 2007 Bering Strait oceanic heat flux and anomalous Arctic sea-ice retreat. Geophysical Research Letters, 37, L01602, doi: 10.1029/2009GL041621.

von Biela, V.R., Arimitsu, M.L., Piatt, J.F., Heflin, B., Schoen, S.K., Trowbridge, J.L.,Clawson, C.M., 2019. Extreme reduction in nutritional value of a key forage fish during the Pacific marine heatwave of 2014–2016. Mar. Ecol. Prog. Ser. 613,171–182. https://doi.org/10.3354/meps12891.

Woodgate R. A., Weingartner, T., Lindsay, R. 2012. Observed increases in Bering Strait oceanic fluxes from the Pacific to the Arctic from 2001 to 2011 and their impacts on the Arctic Ocean water column. Geophysical Research Letters, L24603, doi: 10.1029/2012GL054092.

Woodgate, R. A. 2018. Increased in the Pacific inflow to the Arctic from 1990 to 2015, and insights into the seasonal trends and driving mechanism from year-round Bering Strait mooring data. Progress in Oceanography, doi: 10.1016/j.pocean.2017.12.007.

7 Figures

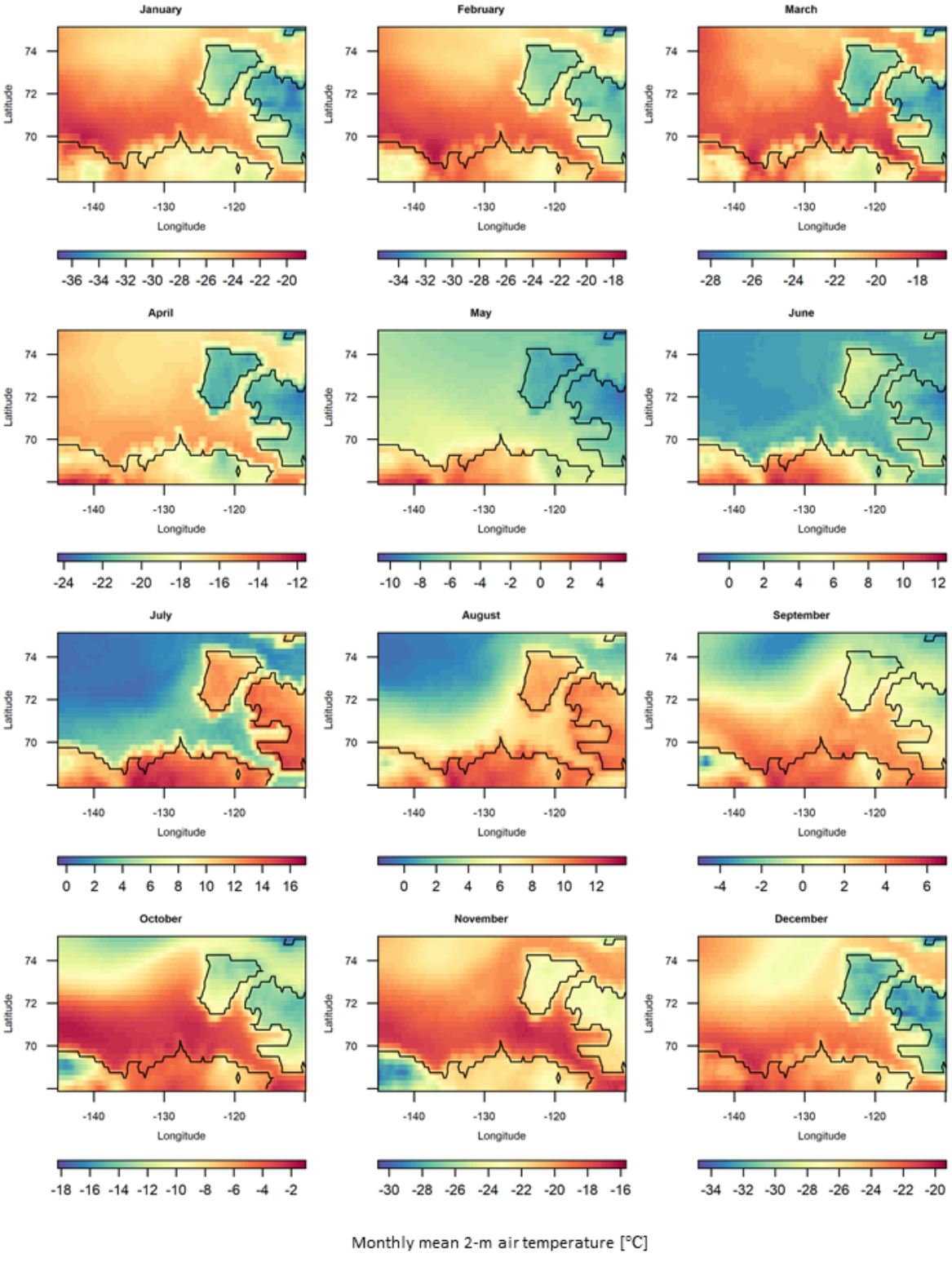


Figure 1. Monthly mean 2-m air temperature (°C) in 2014 over the Beaufort Sea and Amundsen Gulf.

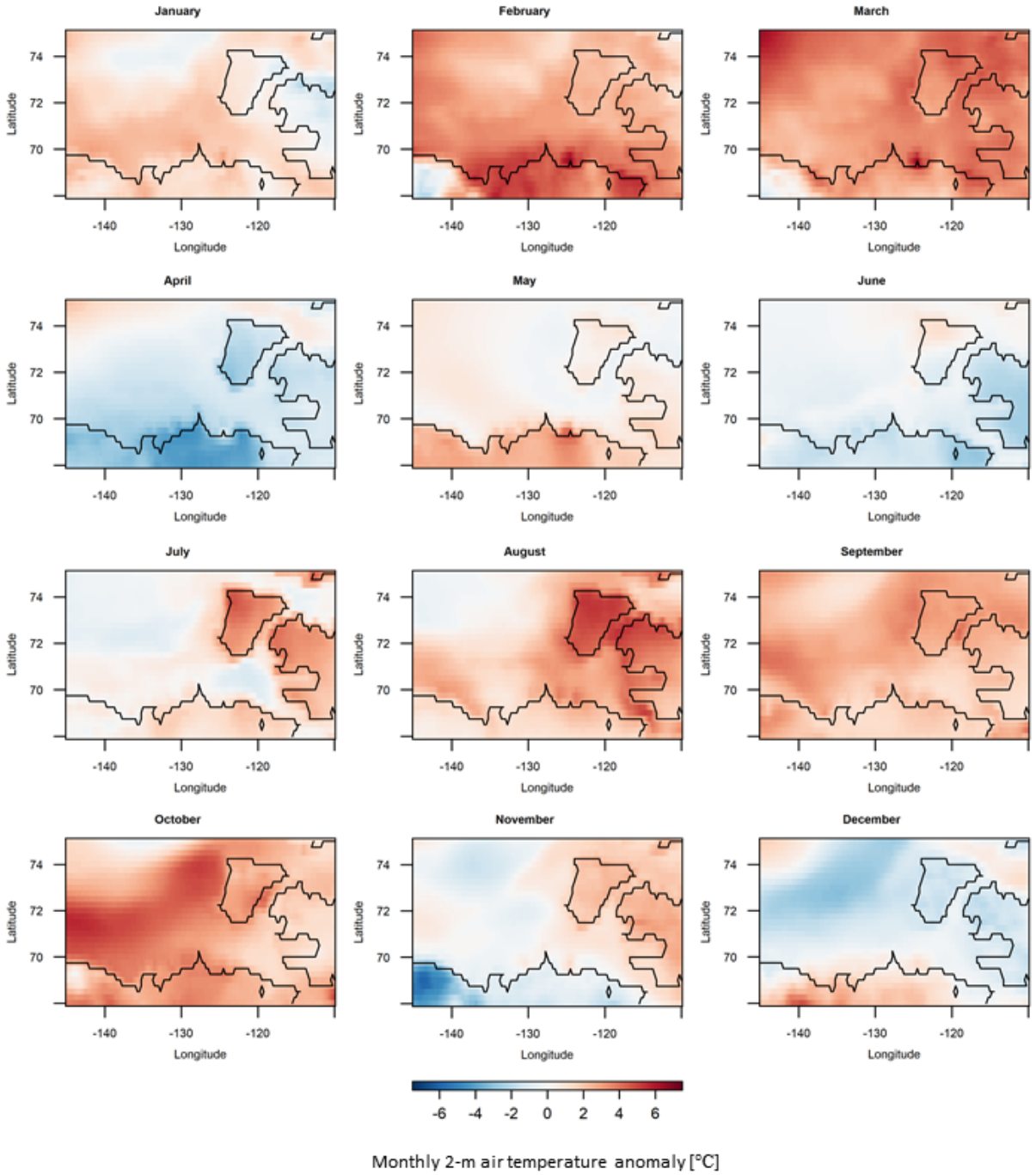


Figure 2. Monthly mean 2-m air temperature anomalies (°C) in 2014 from the climatological average period 1983-2010 in the Beaufort Sea and Amundsen Gulf.

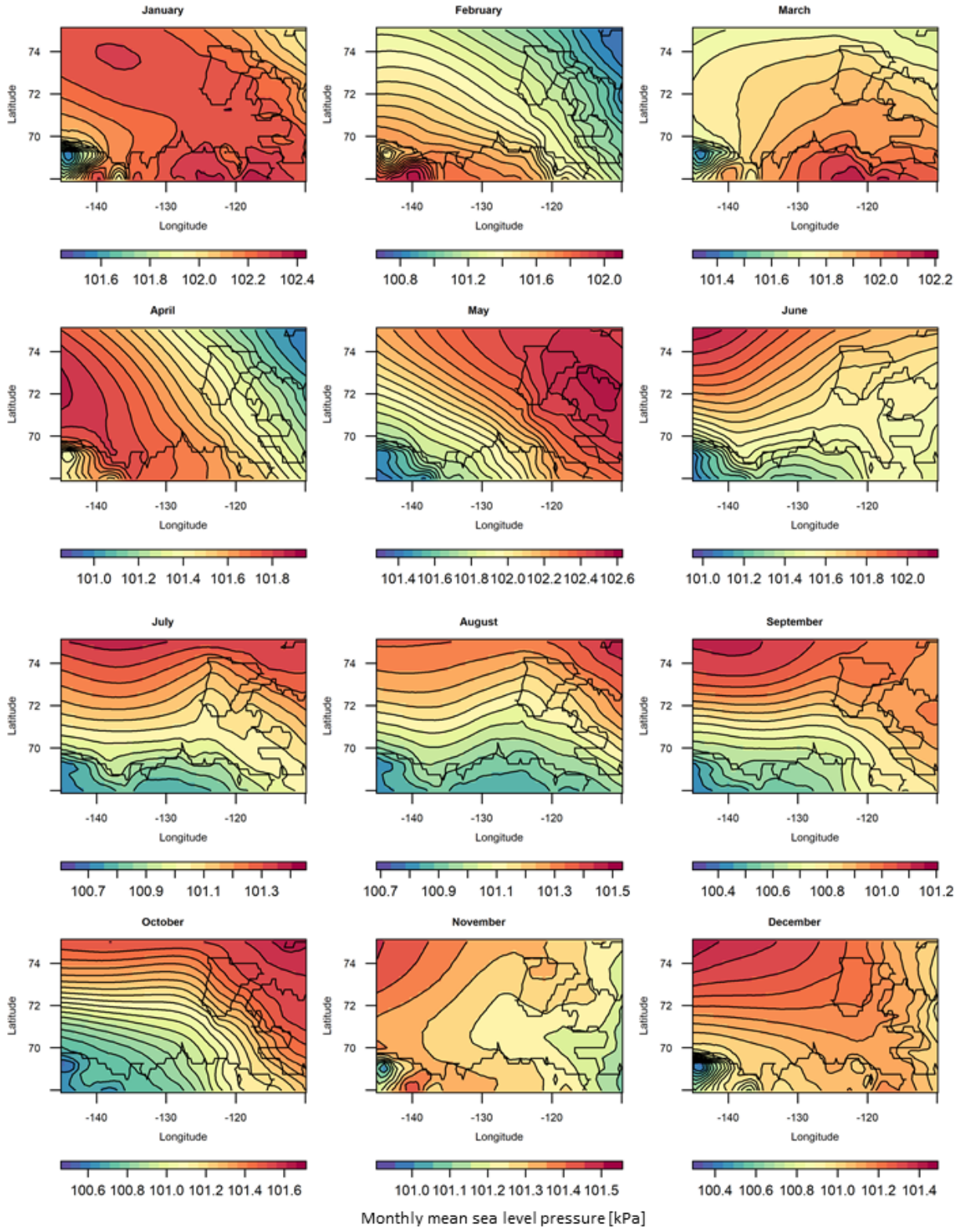


Figure 3. Monthly mean sea level pressure (kPa) over the Beaufort Sea and Amundsen Gulf in 2014.

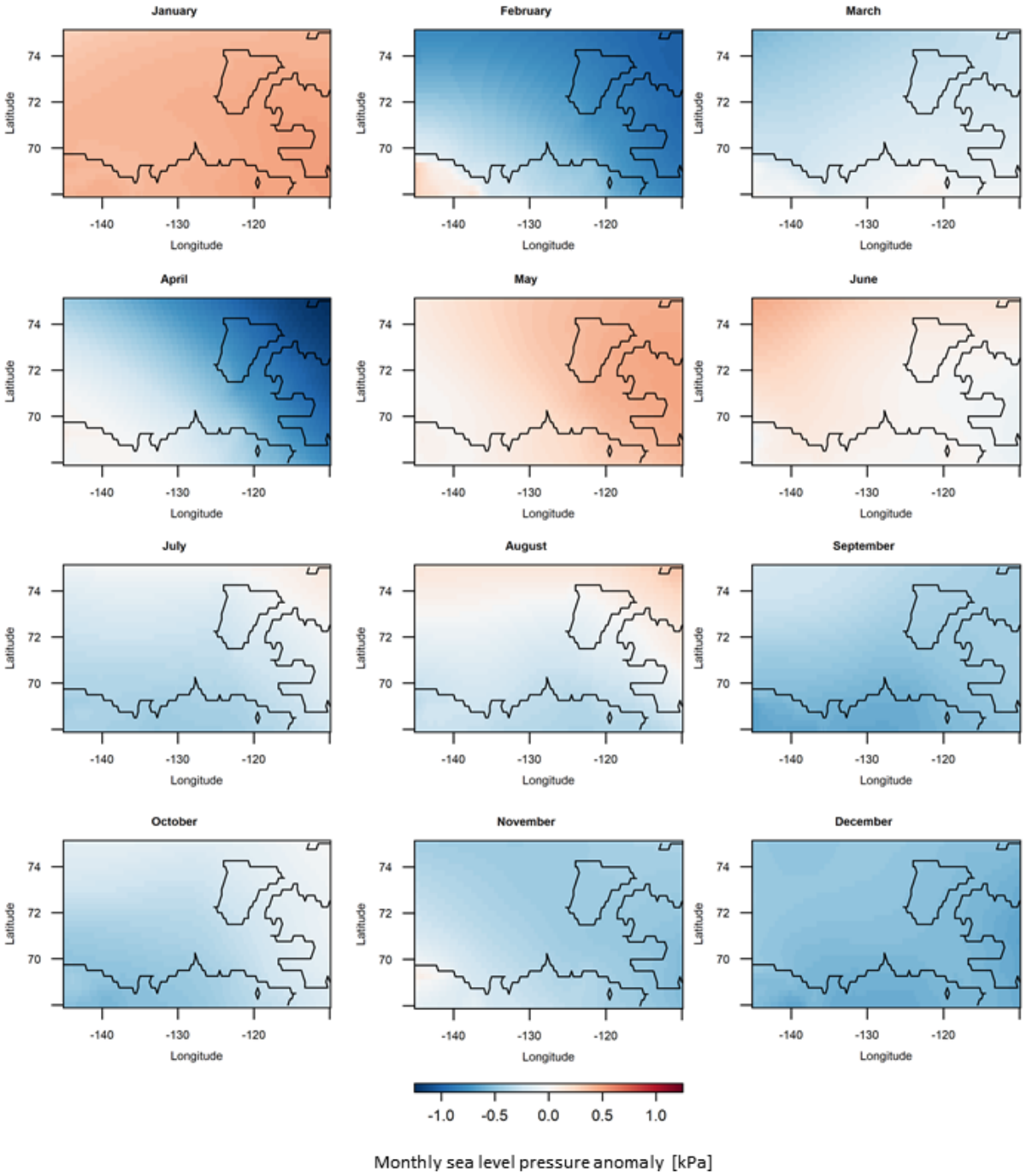


Figure 4. Monthly mean sea level pressure anomalies (kPa) in 2014 from the climatological average period 1983-2010 in the Beaufort Sea and Amundsen Gulf.

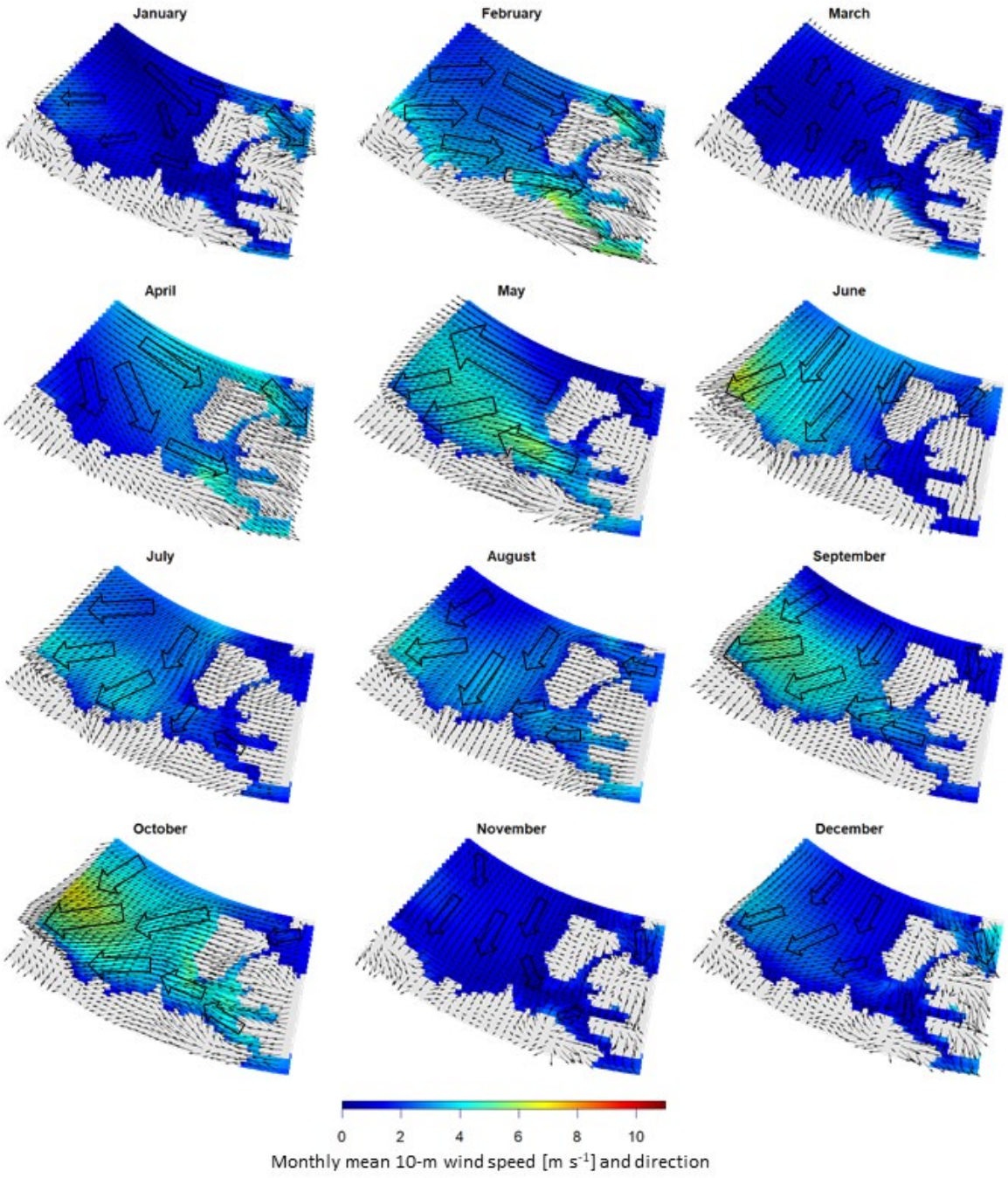


Figure 5. Monthly mean 10-m wind speed (m s^{-1}) and direction in 2014 in the Beaufort Sea and Amundsen Gulf.

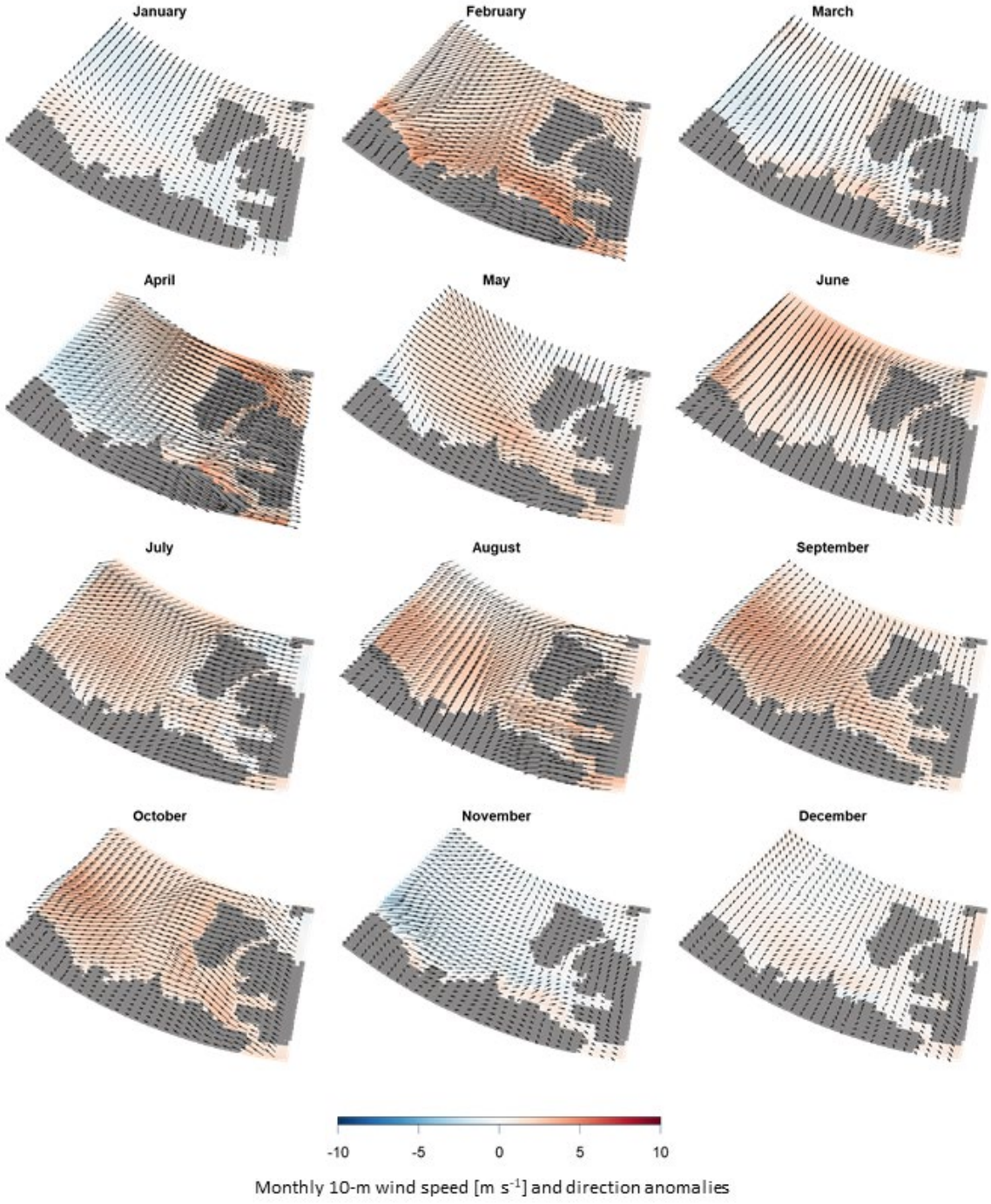


Figure 6. Monthly mean 10-m wind speed (m s^{-1}) and direction anomalies from the climatological average period 1983-2010 in the Beaufort Sea and Amundsen Gulf in 2014.

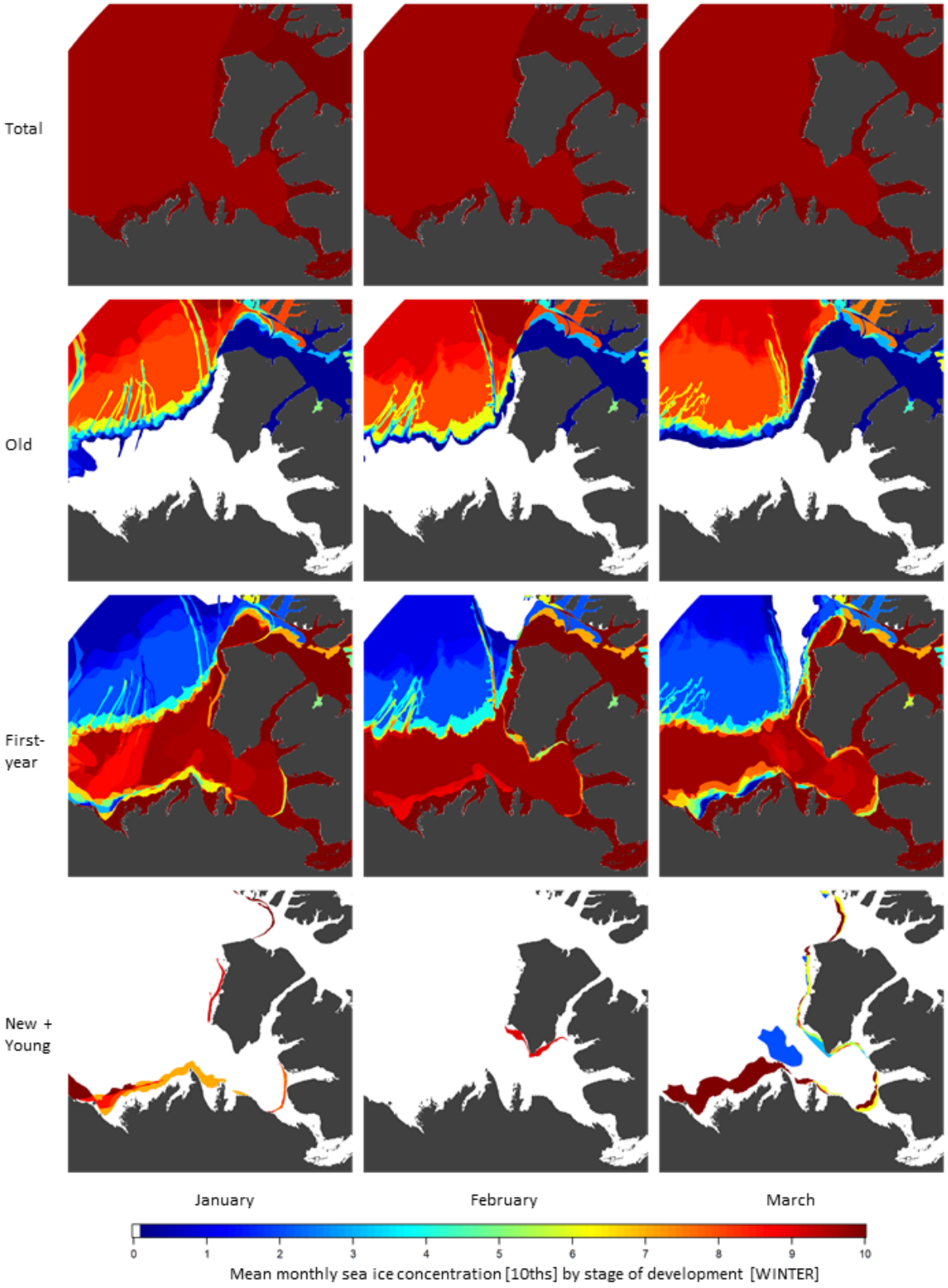


Figure 7. Monthly mean sea ice concentration (10^{ths}) for total sea ice and three stages of development (old, first-year, and young + new ice) for January, February, and March [winter] 2014.

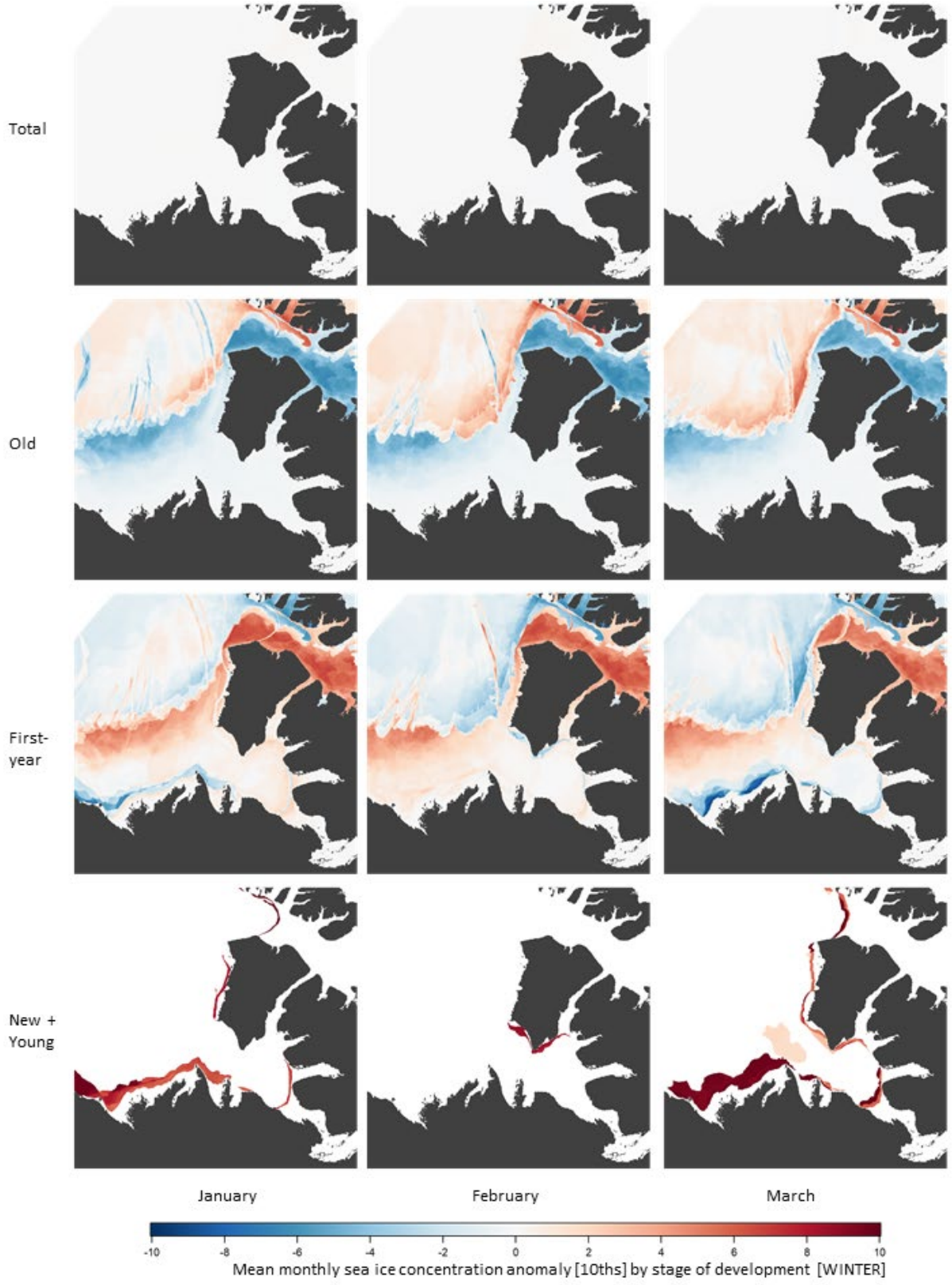


Figure 8. Monthly mean sea ice concentration anomalies (10^{ths}) for total sea ice and three stages of development (old, first-year, and young + new ice) for January, February, and March [winter] 2014.

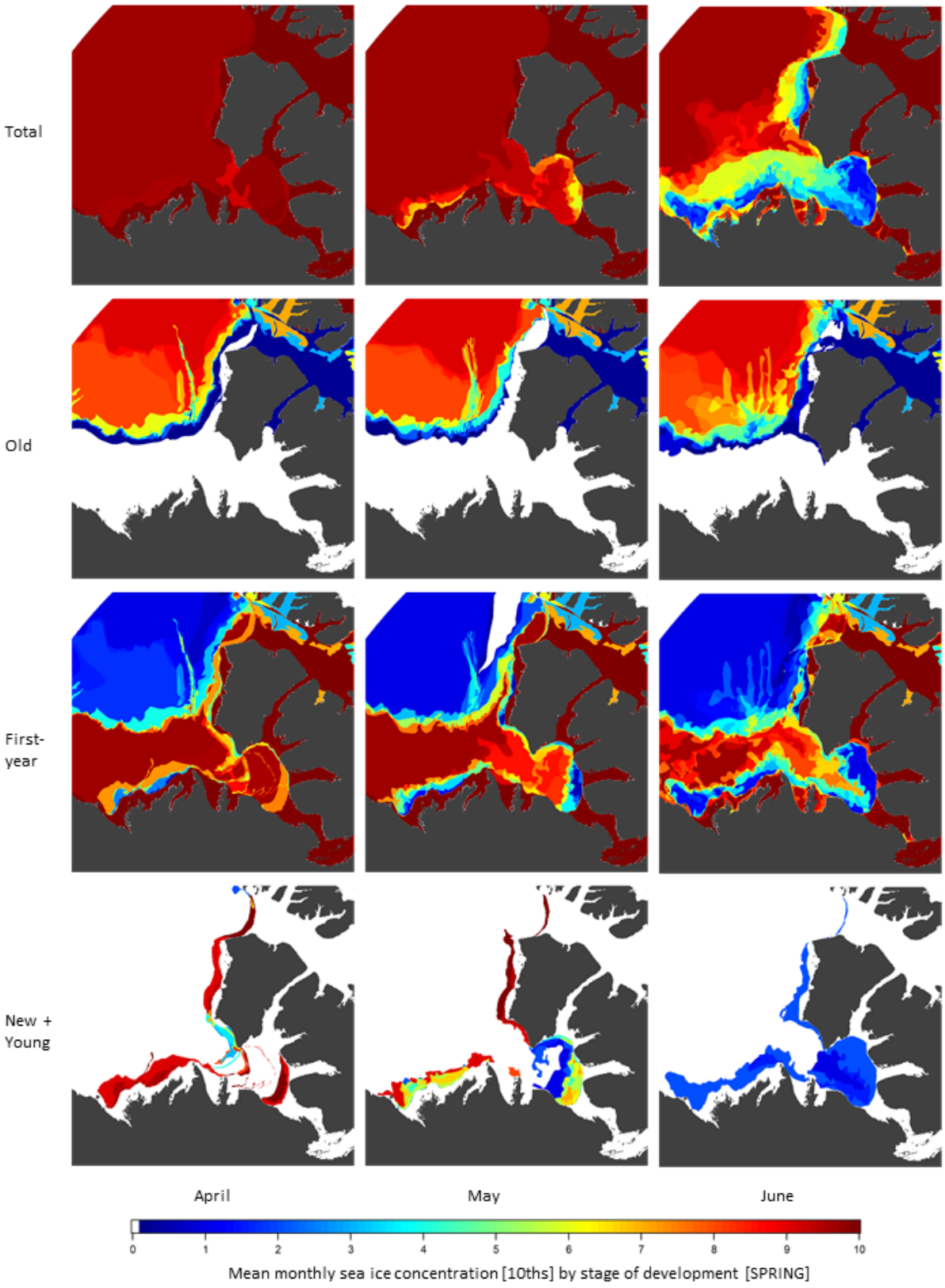


Figure 9. Monthly mean sea ice concentration (10^{ths}) for total sea ice and three stages of development (old, first-year, and young + new ice) for April, May, and June [spring] 2014.

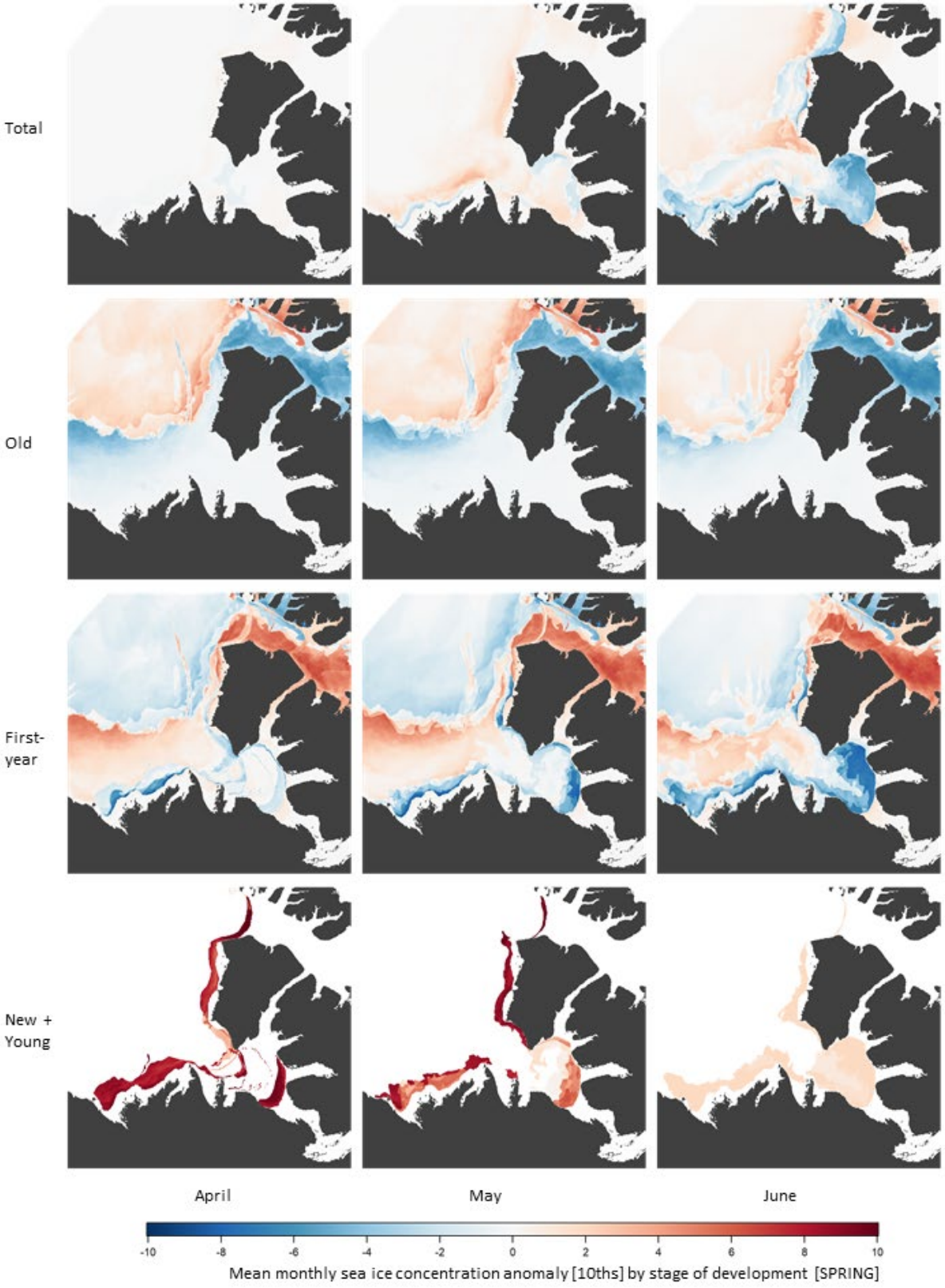


Figure 10. Monthly mean sea ice concentration anomalies (10^{ths}) for total sea ice and three stages of development (old, first-year, and young + new ice) for April, May, and June [spring] 2014.

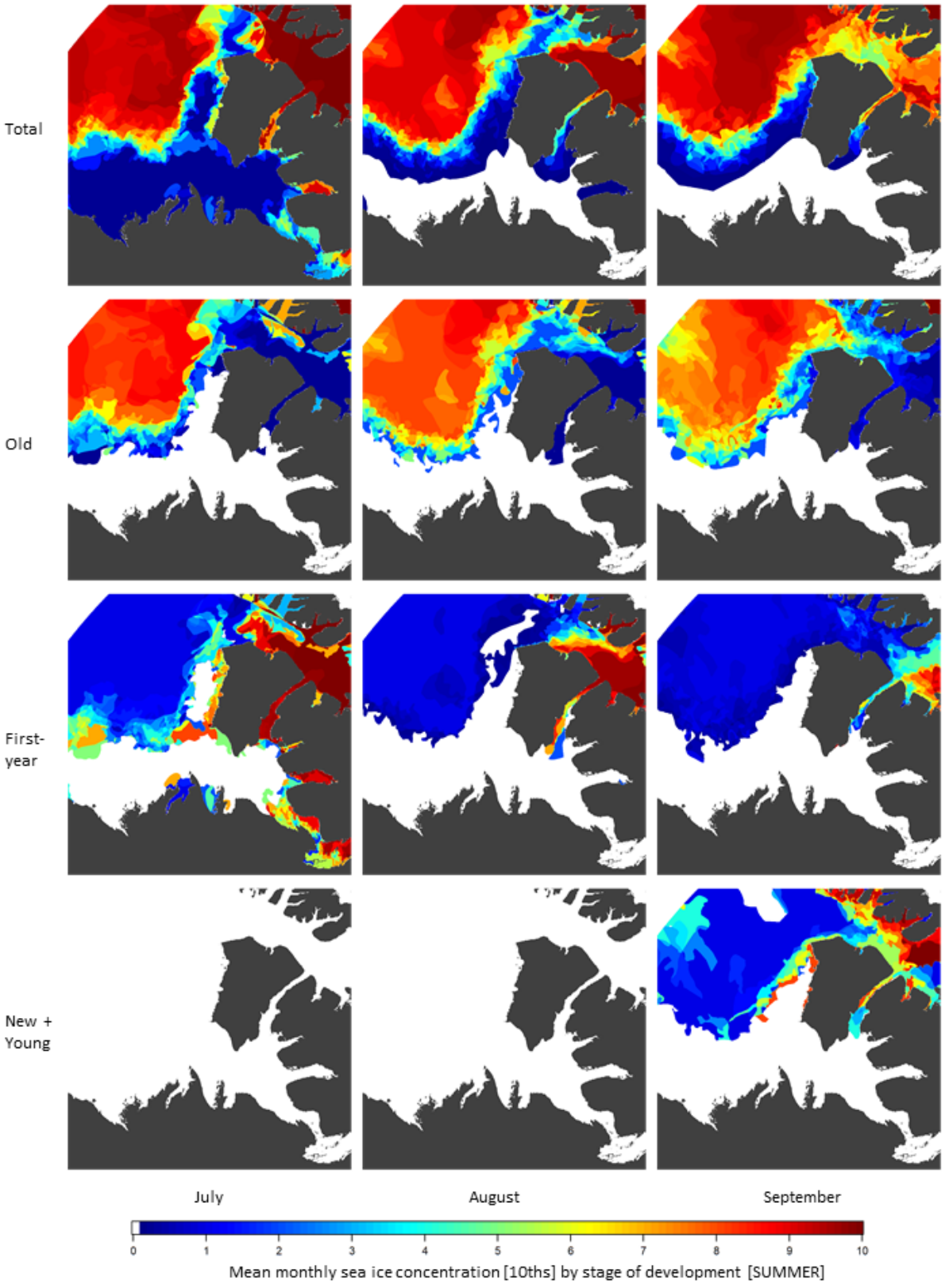


Figure 11. Monthly mean sea ice concentration (10^{ths}) for total sea ice and three stages of development (old, first-year, and young + new ice) for July, August, and September [summer] 2014.

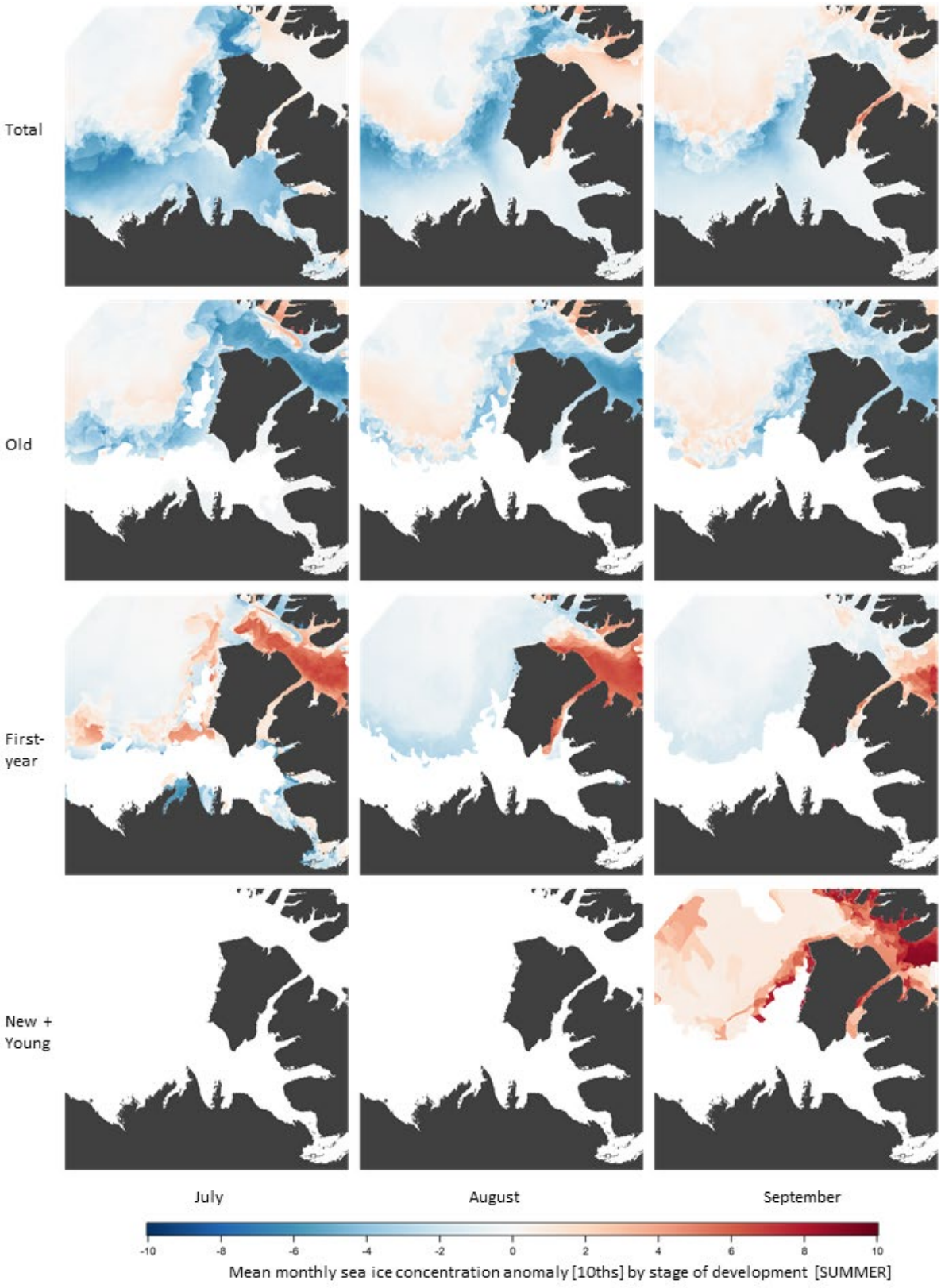


Figure 12. Monthly mean sea ice concentration anomalies (10^{ths}) for total sea ice and three stages of development (old, first-year, and young + new ice) for July, August, and September [summer] 2014.

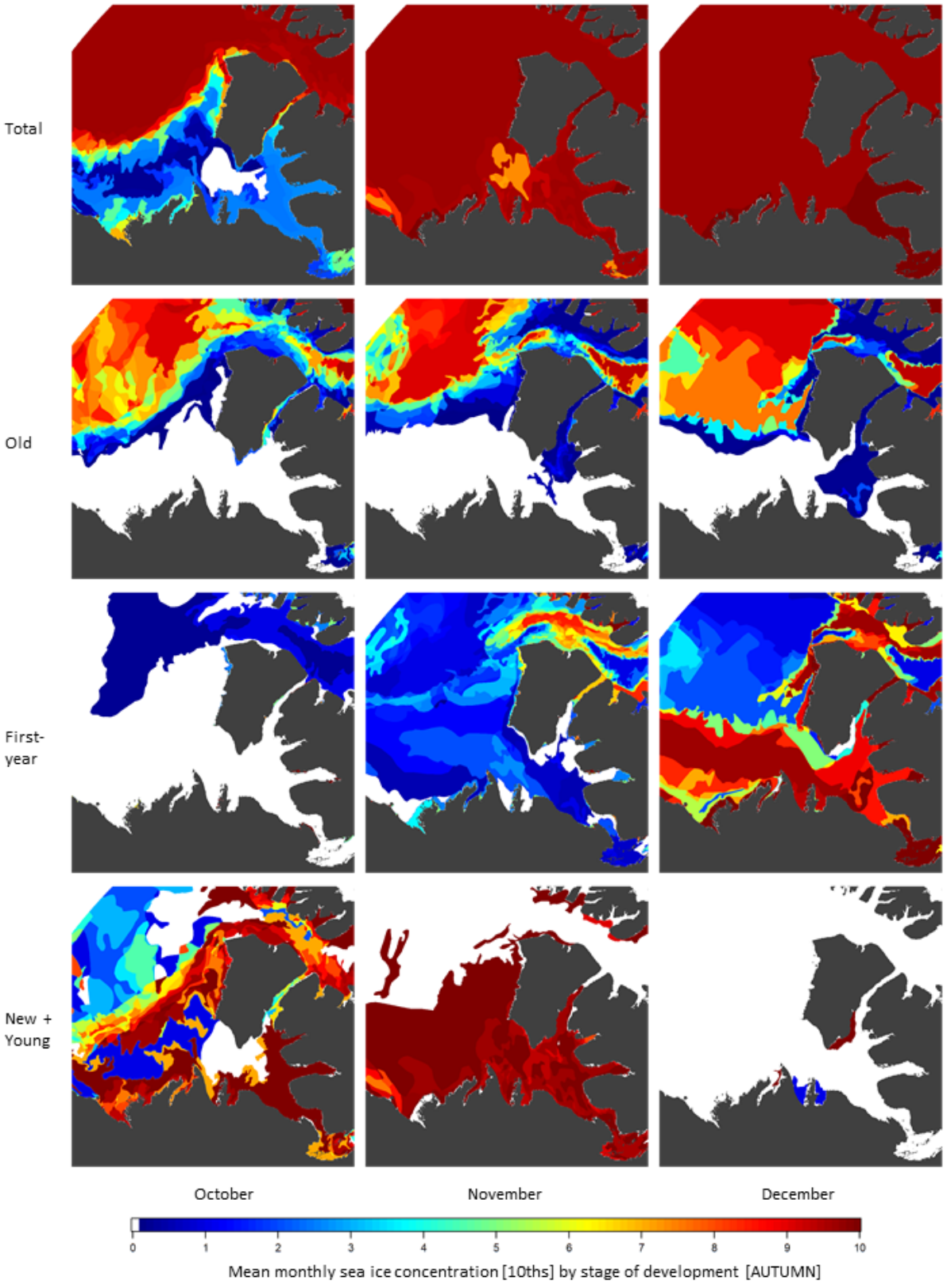


Figure 13. Monthly mean sea ice concentration (10^{ths}) for total sea ice and three stages of development (old, first-year, and young + new ice) for October, November, and December [autumn] 2014.

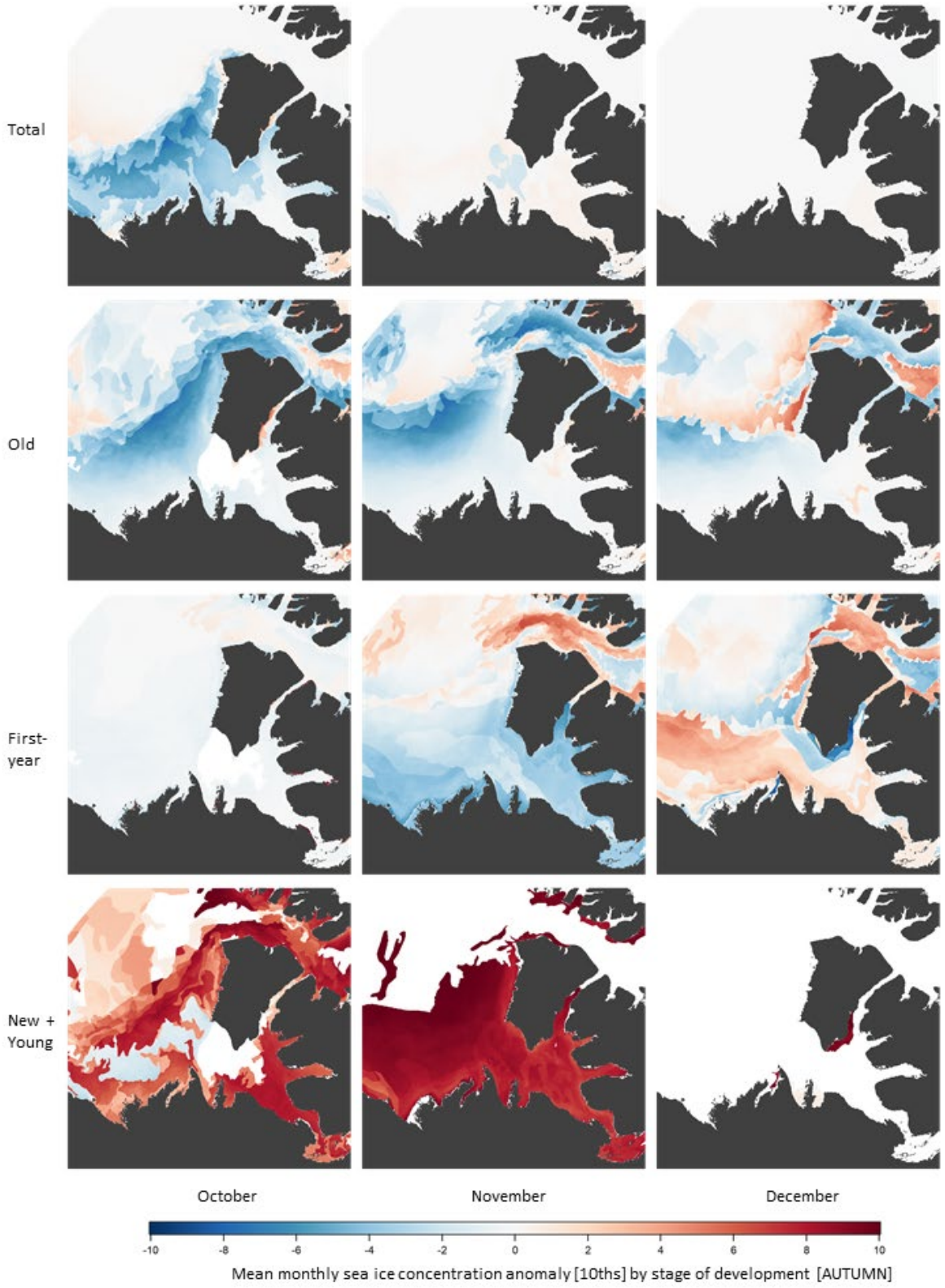


Figure 14. Monthly mean sea ice concentration anomalies (10^{ths}) for total sea ice and three stages of development (old, first-year, and young + new ice) for October, November, and December [autumn] 2014.

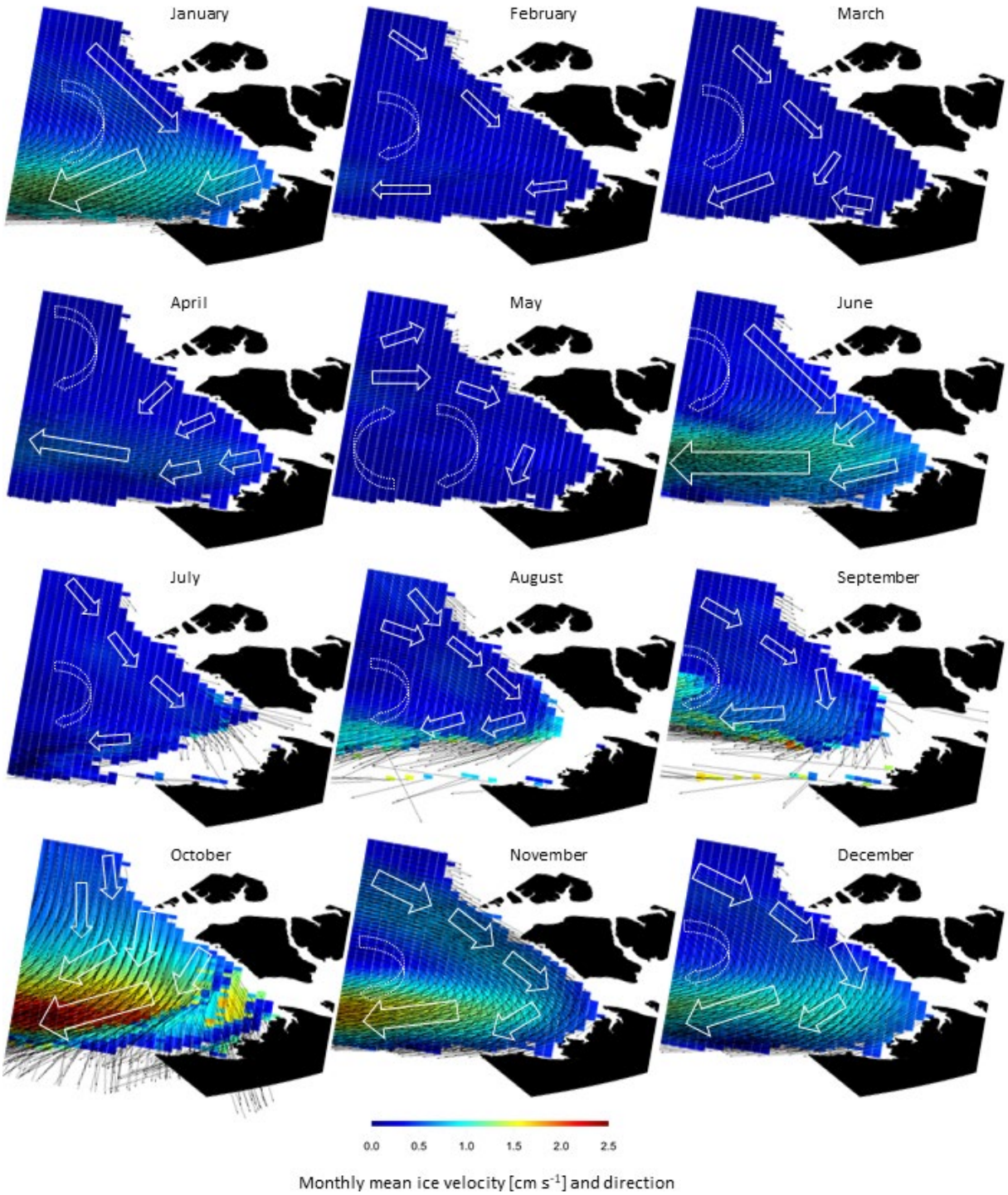


Figure 15. Monthly mean sea ice velocity (cm s^{-1}) and direction in 2014 in the Beaufort Sea and Amundsen Gulf.

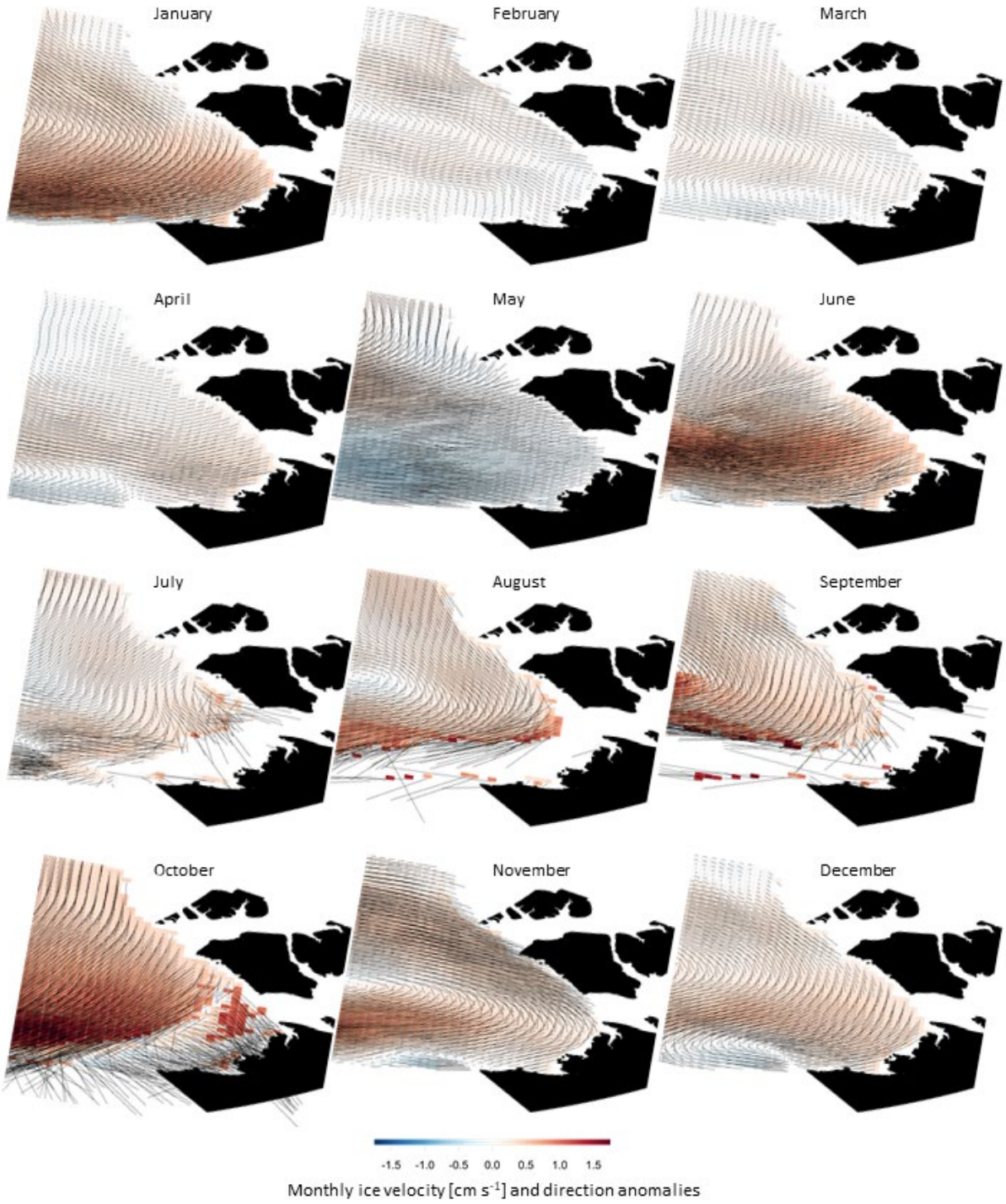


Figure 16. Monthly mean sea ice velocity (cm s^{-1}) and direction anomalies in 2014 from the climatological mean period 1983-2010 in the Beaufort Sea and Amundsen Gulf.

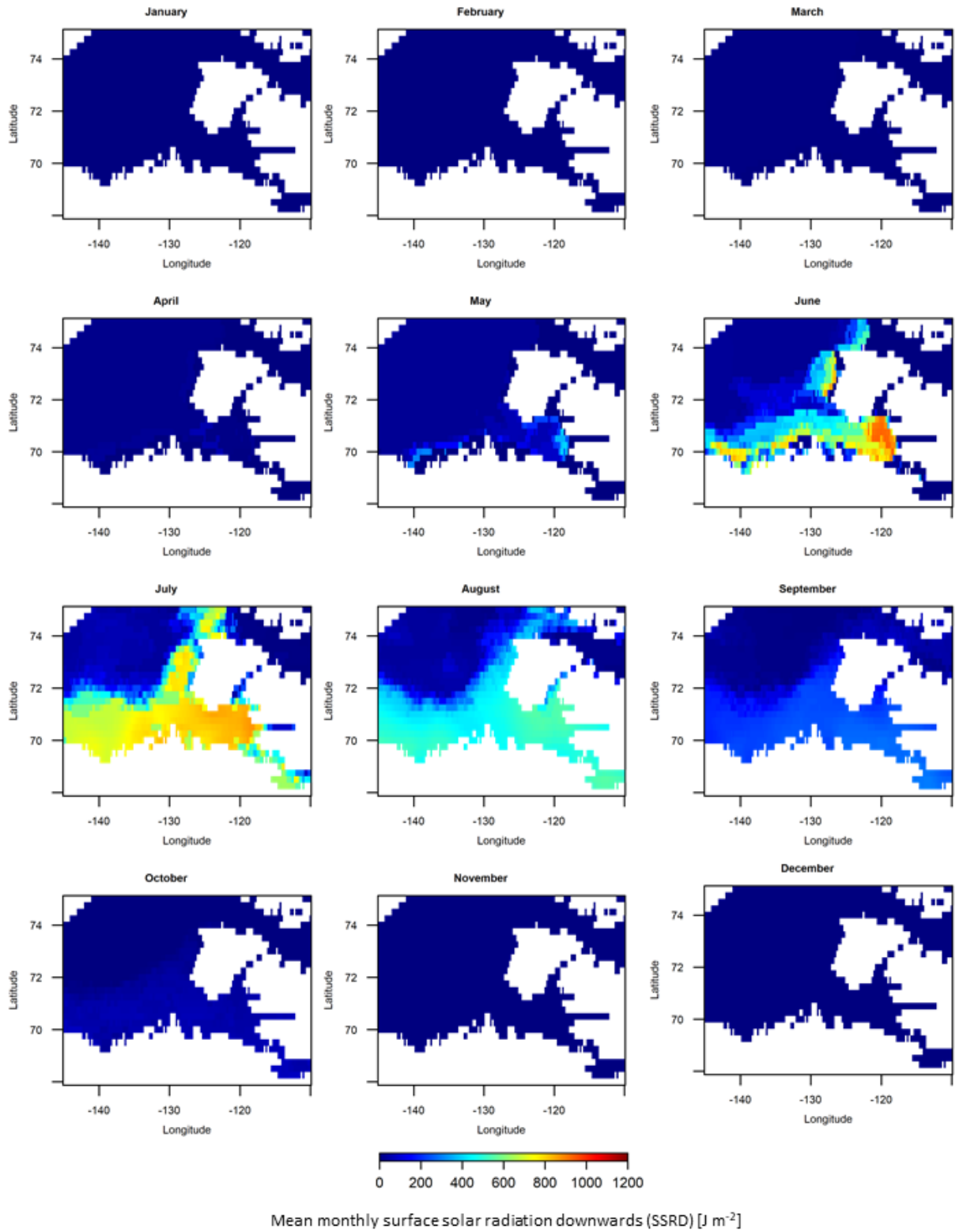


Figure 17. Monthly mean sea ice-adjusted surface solar radiation downwards (J m^{-2}) in 2014 in the Beaufort Sea and Amundsen Gulf.

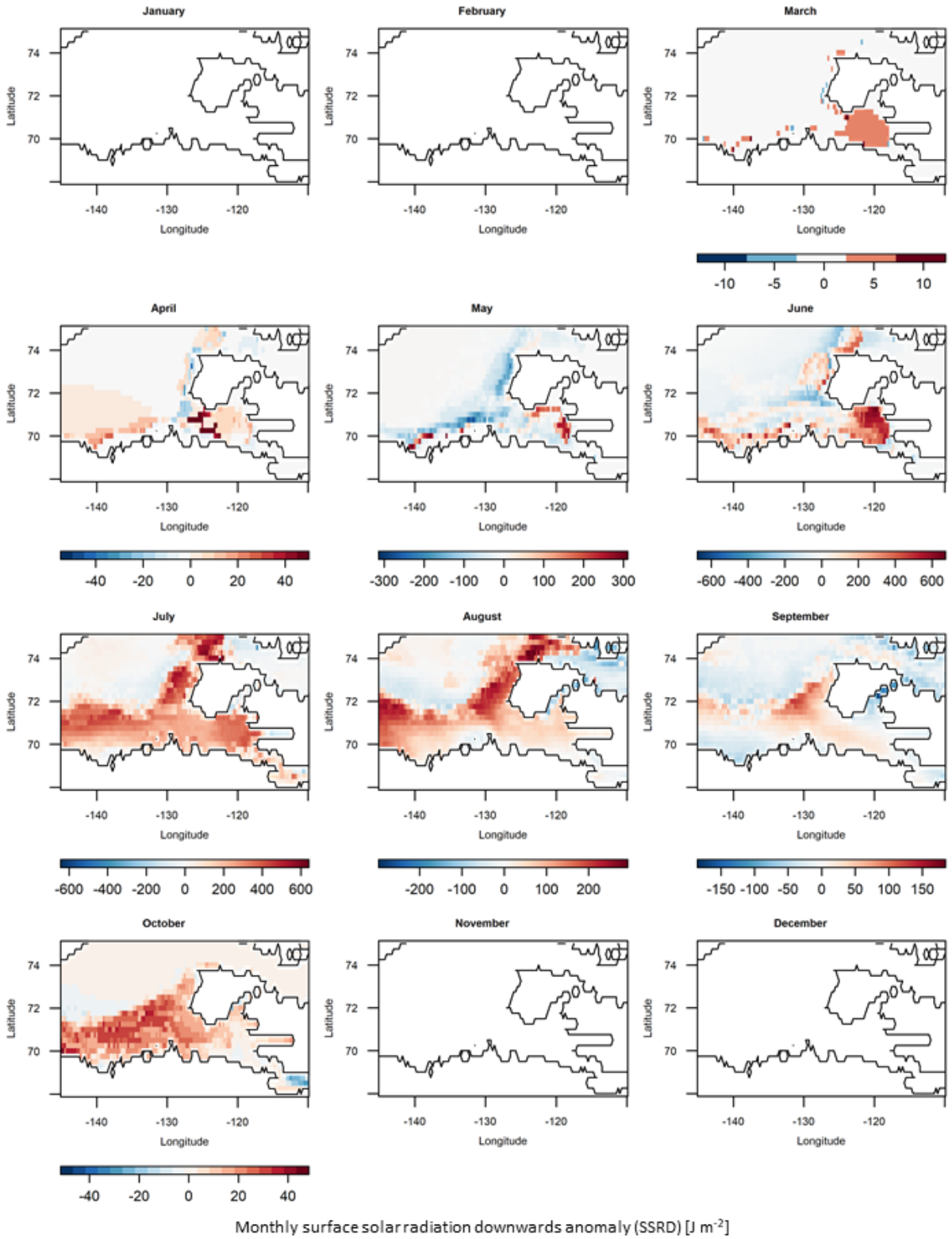


Figure 18. Monthly mean sea ice-adjusted surface solar radiation downwards anomalies (J m^{-2}) in 2014 compared to the climatological average period 1983-2010 in the Beaufort Sea and Amundsen Gulf.

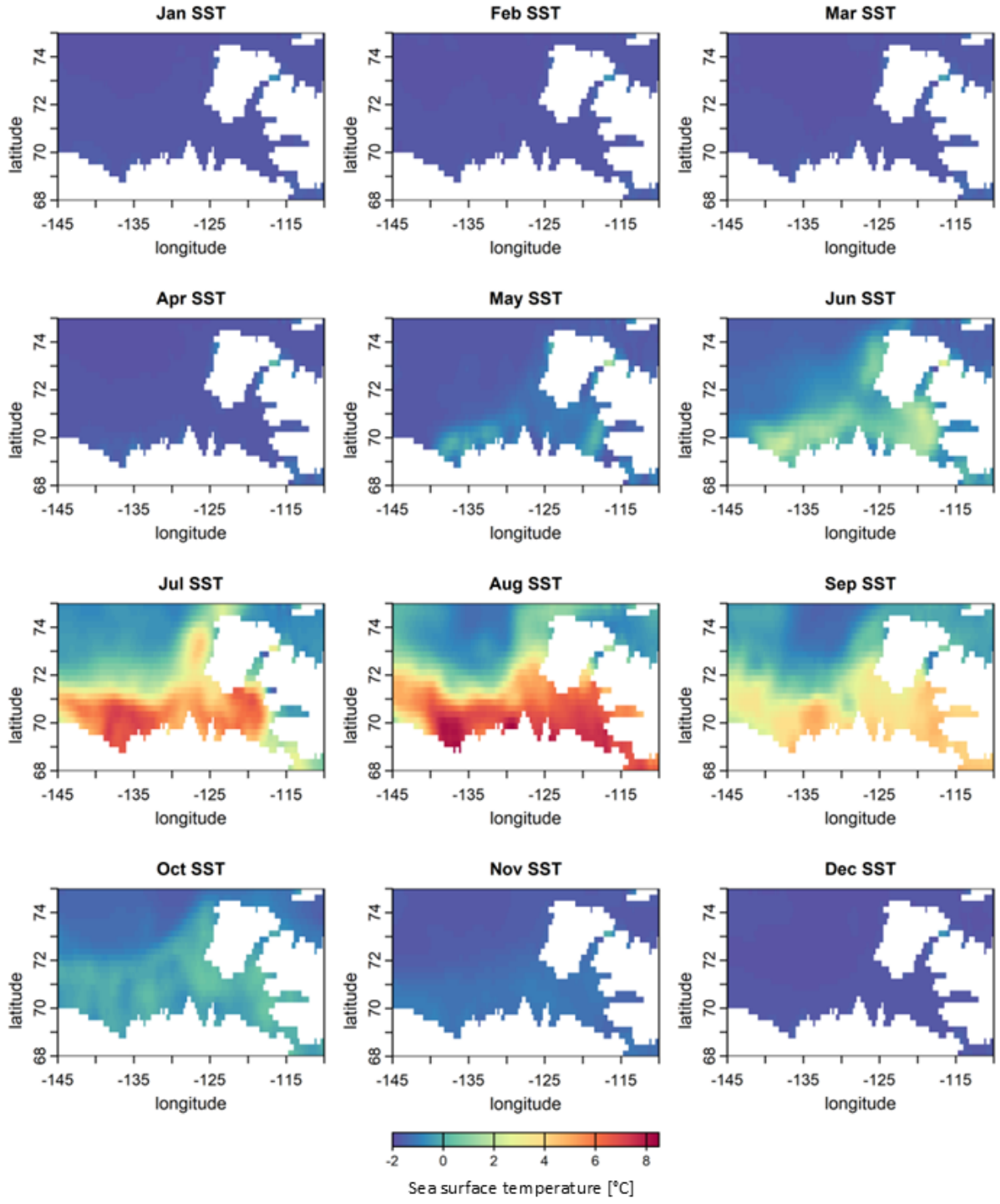


Figure 19. Monthly mean sea surface temperature (°C) in 2014 in the Beaufort Sea and Amundsen Gulf.

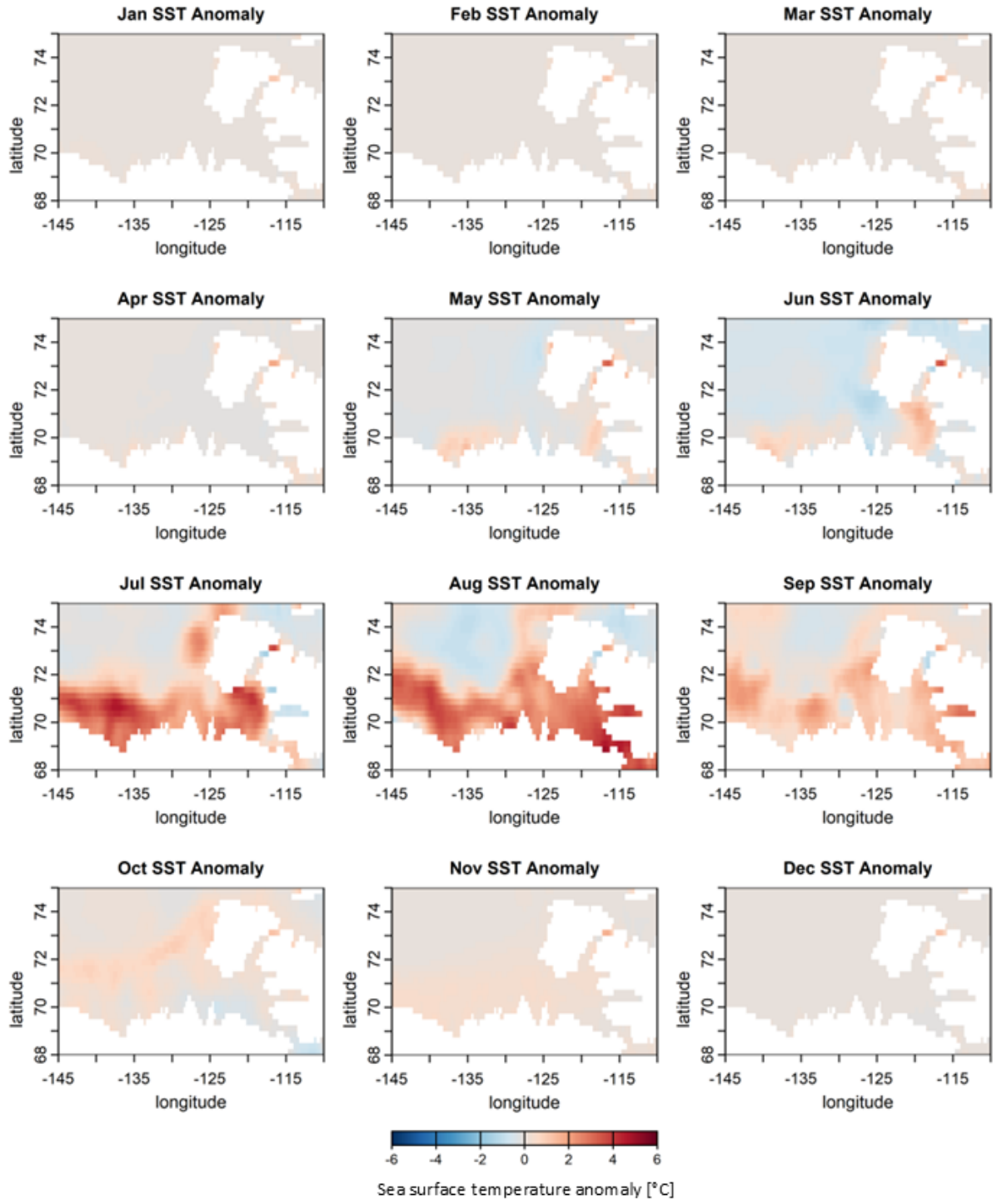


Figure 20. Monthly mean sea surface temperature anomalies (°C) in 2014 compared to the mean period 1983-2010 in the Beaufort Sea and Amundsen Gulf.

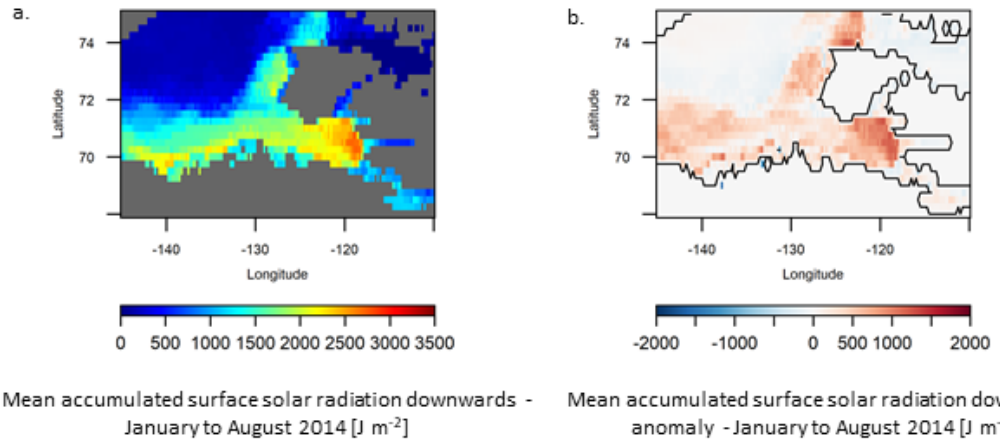


Figure 21. (a) Mean accumulated sea ice-adjusted surface solar radiation downwards (J m^{-2}) between January and August in 2014 (inclusive), and (b) accumulated sea ice-adjusted surface solar radiation downwards anomaly (J m^{-2}) between January and August 2019 (inclusive) compared to the climatological average over the period 1983-2010.

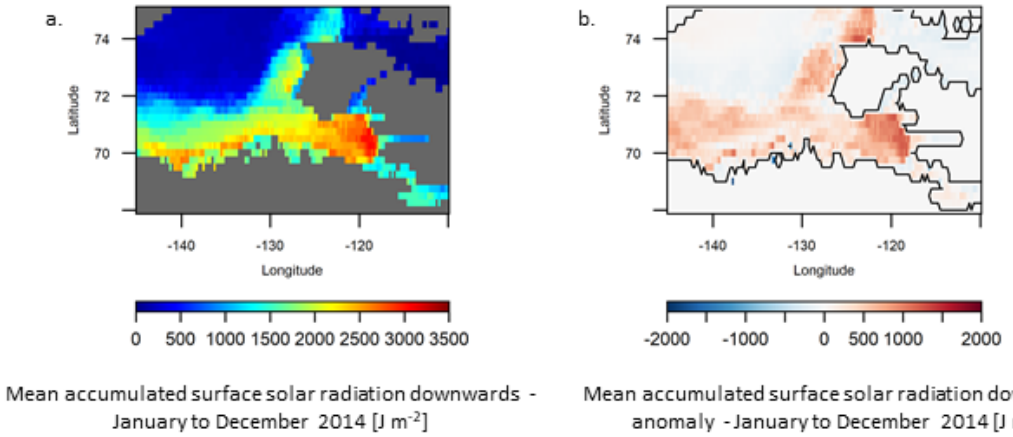


Figure 22. (a) Mean accumulated sea ice-adjusted surface solar radiation downwards (J m^{-2}) between January and December in 2014 (inclusive), and (b) accumulated sea ice-adjusted surface solar radiation downwards anomaly (J m^{-2}) between January and December 2019 (inclusive) compared to the climatological average over the period 1983-2010.

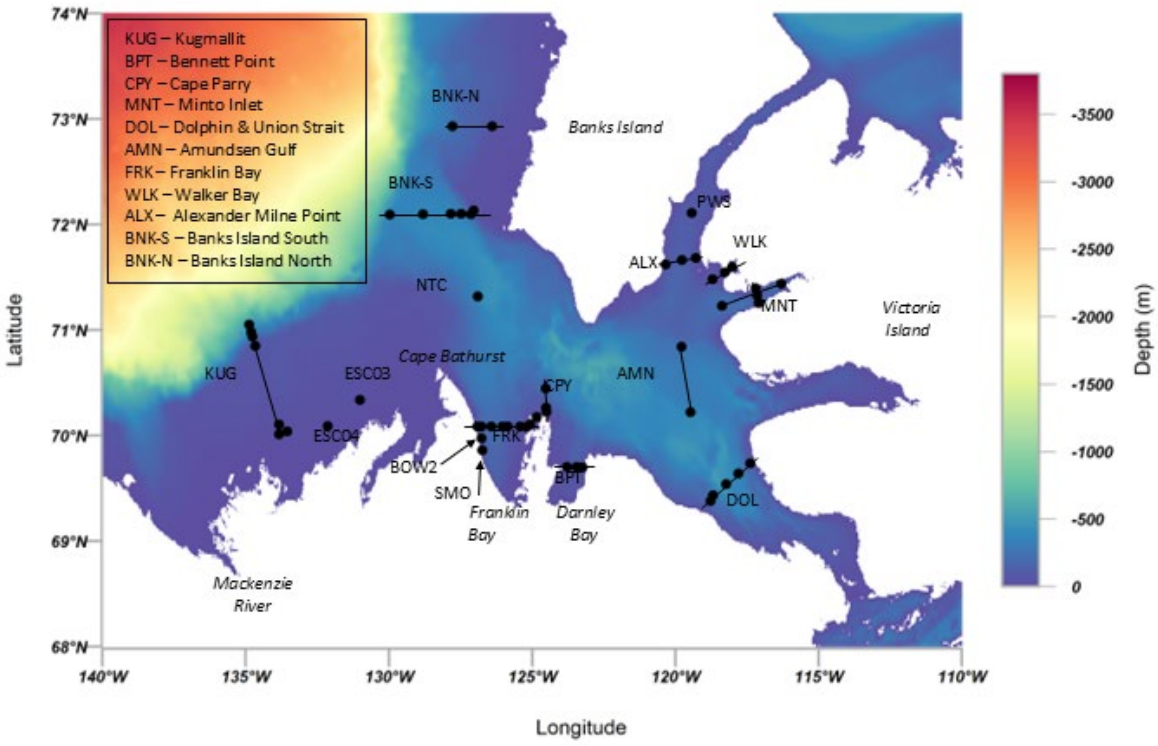


Figure 23. CTD station and section locations in the Amundsen Gulf region in 2014, overlain on ETOPO1 bathymetry data.

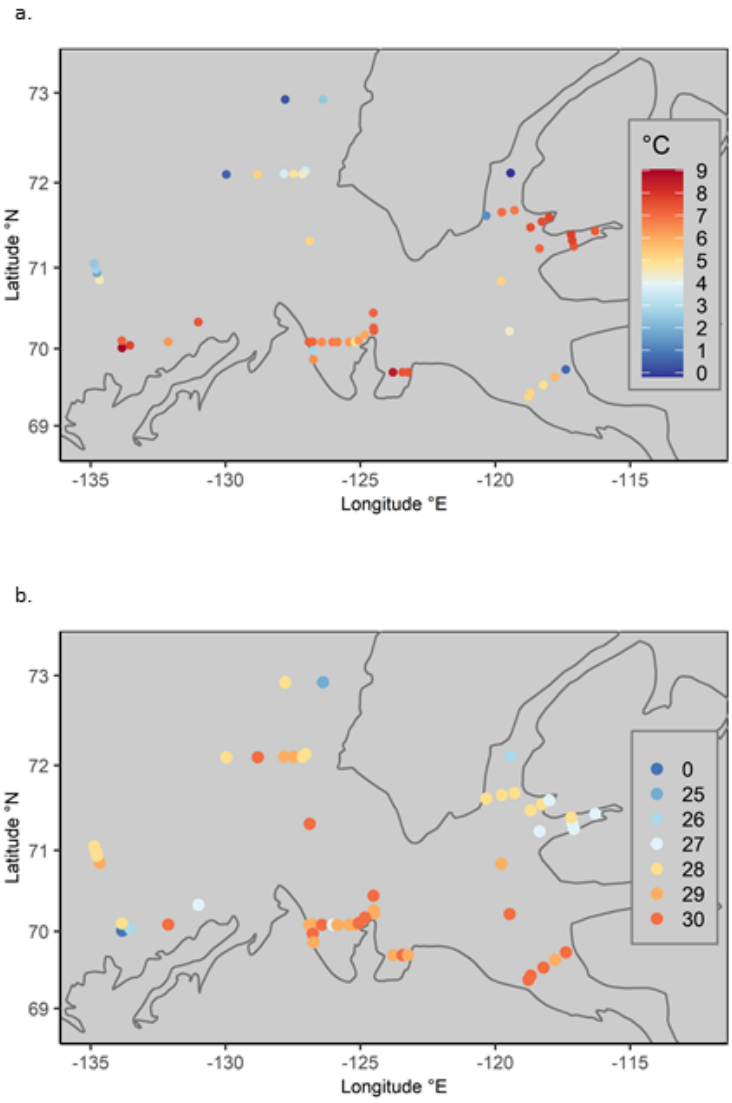


Figure 24. (a) Surface temperature (°C), and (b) surface salinity at each station in the Amundsen Gulf region in 2014.

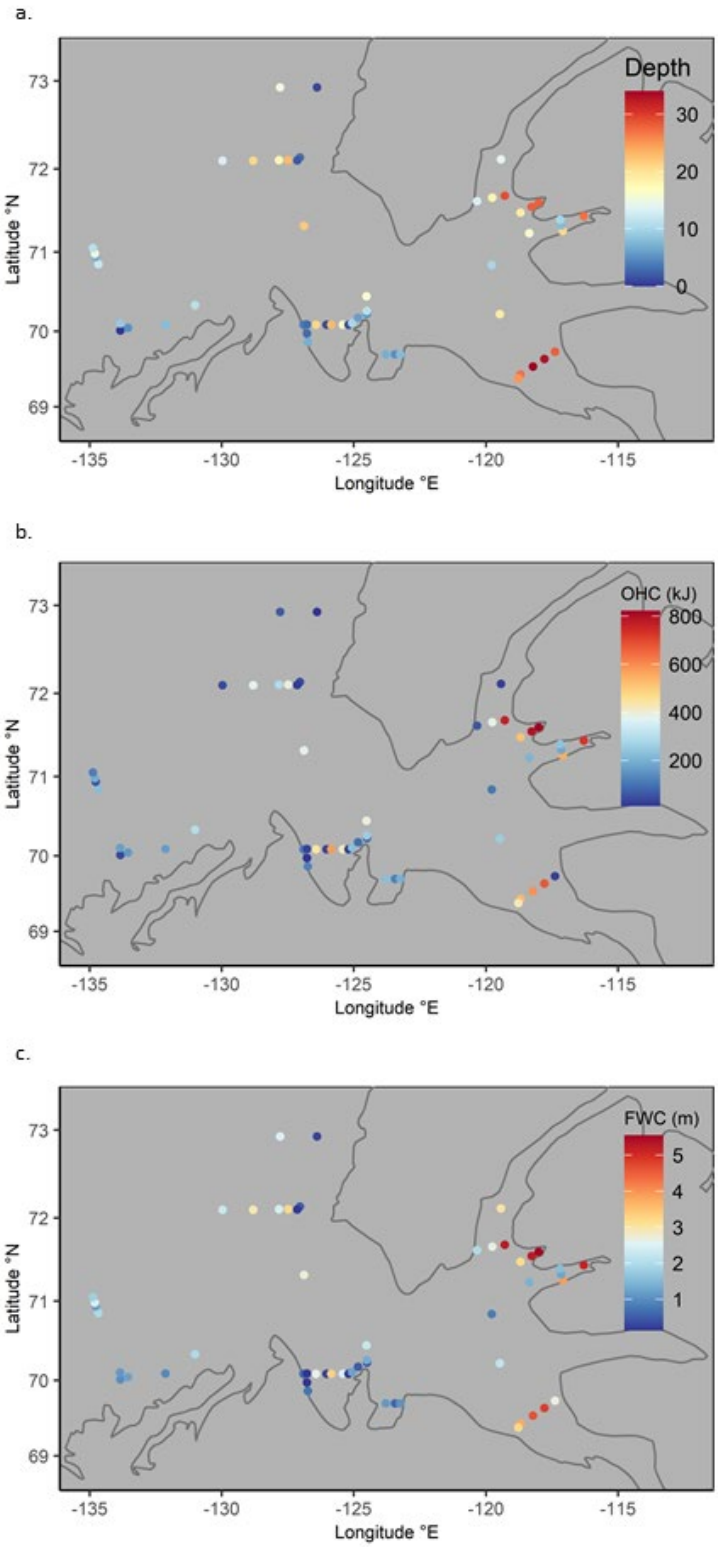


Figure 25. (a) Depth of the maximum N^2 in meters (b) Ocean heat content (kJ in a $1m^2$ column to a depth of the N^2 max), and (c) Freshwater anomaly relative to S = 34.8 (meters in a $1m^2$ column to the depth of the N^2 max) at each station in the Amundsen Gulf region in 2014.

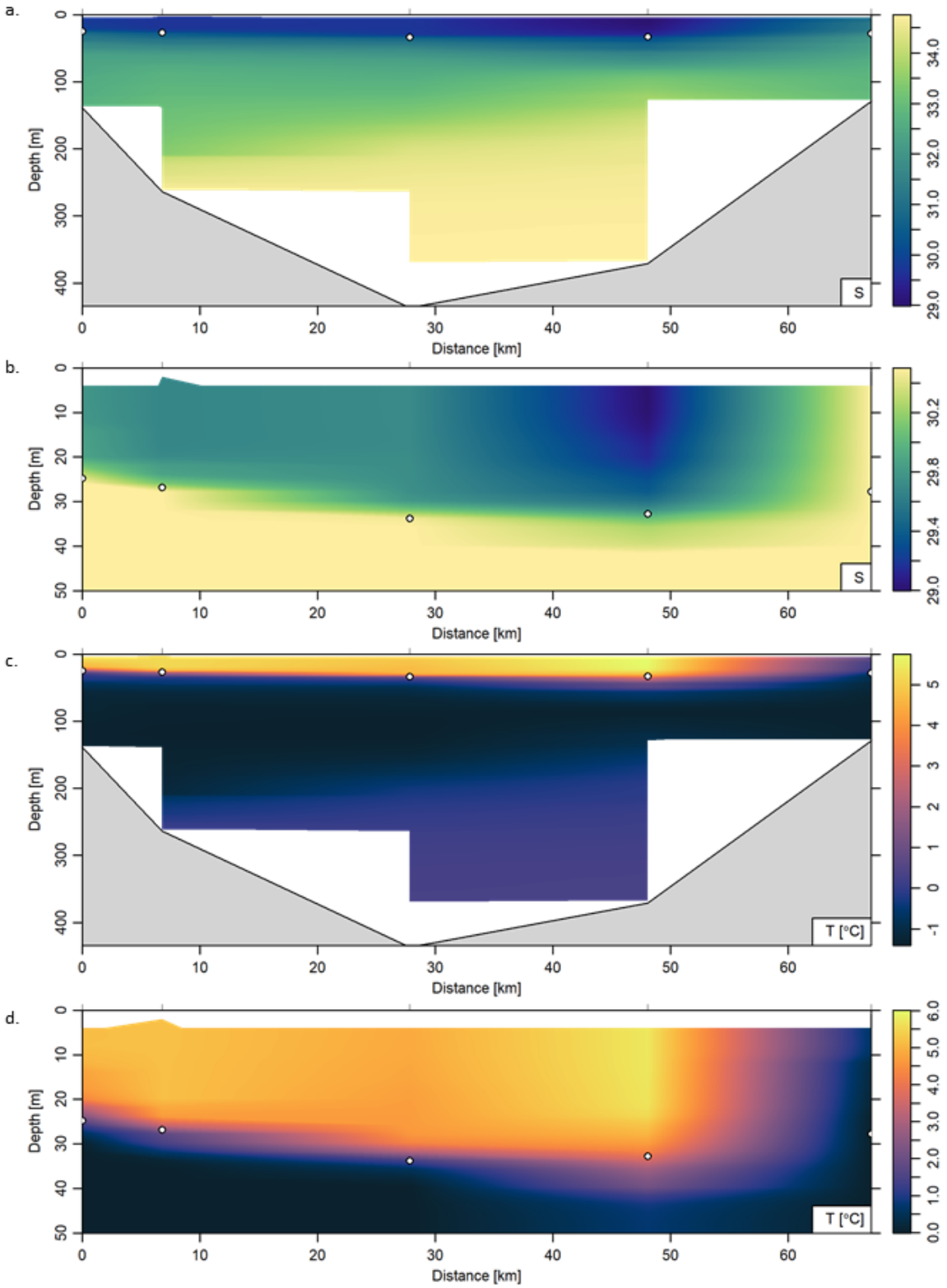


Figure 26. Sections from west to east across Dolphin and Union Strait (DOL) in 2014: salinity (a, b) and temperature (c, d). Full depth (a, c) and enlarged to show only the top 50m (b, d). N^2-derived surface layer depths at each station are connoted by white dots.

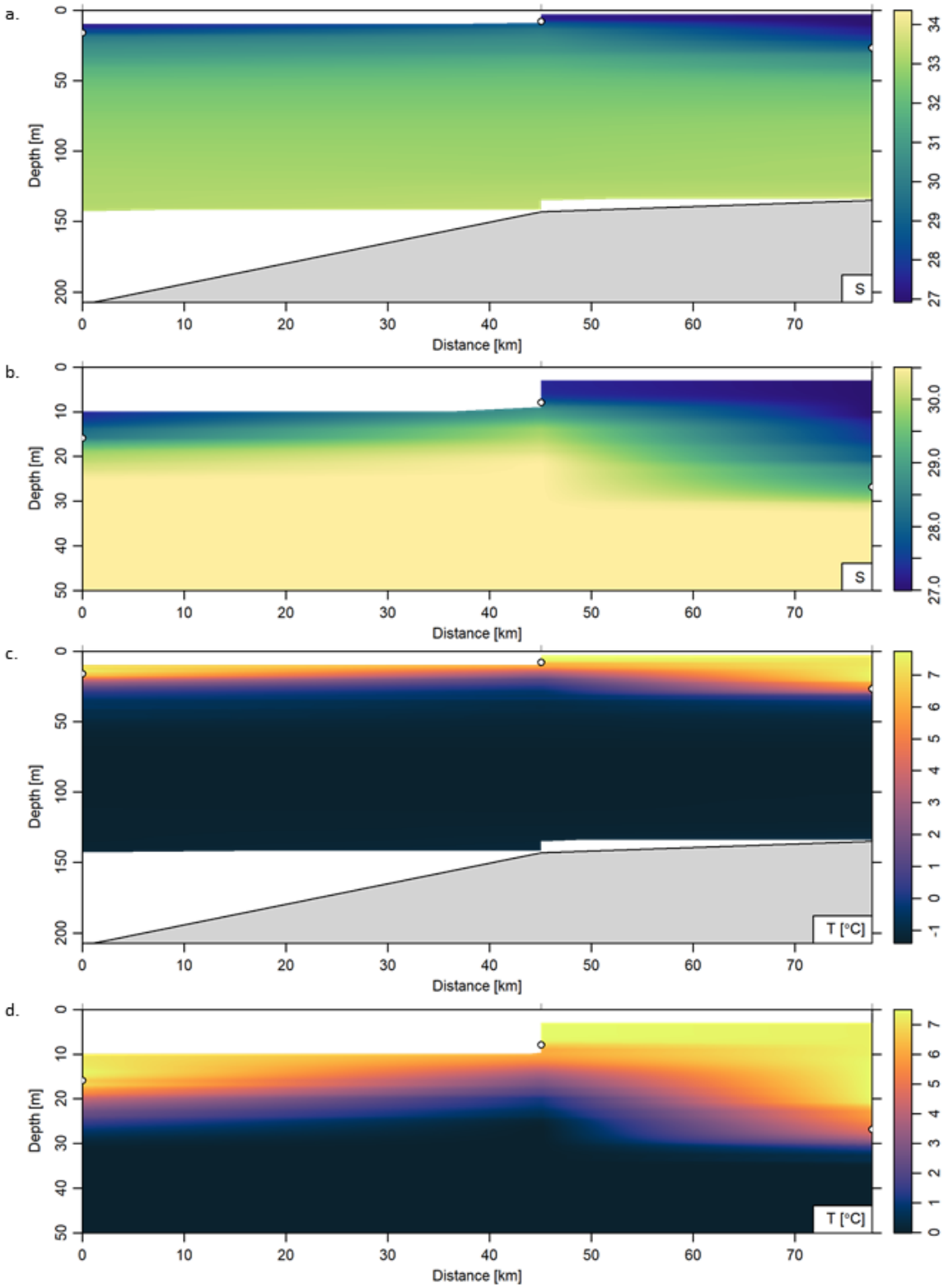


Figure 27. Sections from west to east across Minto Inlet in 2014: salinity (a, b) and temperature (c, d). Full depth (a, c) and enlarged to show only the top 50m (b, d). N^2-derived surface layer depths at each station are connoted by white dots.

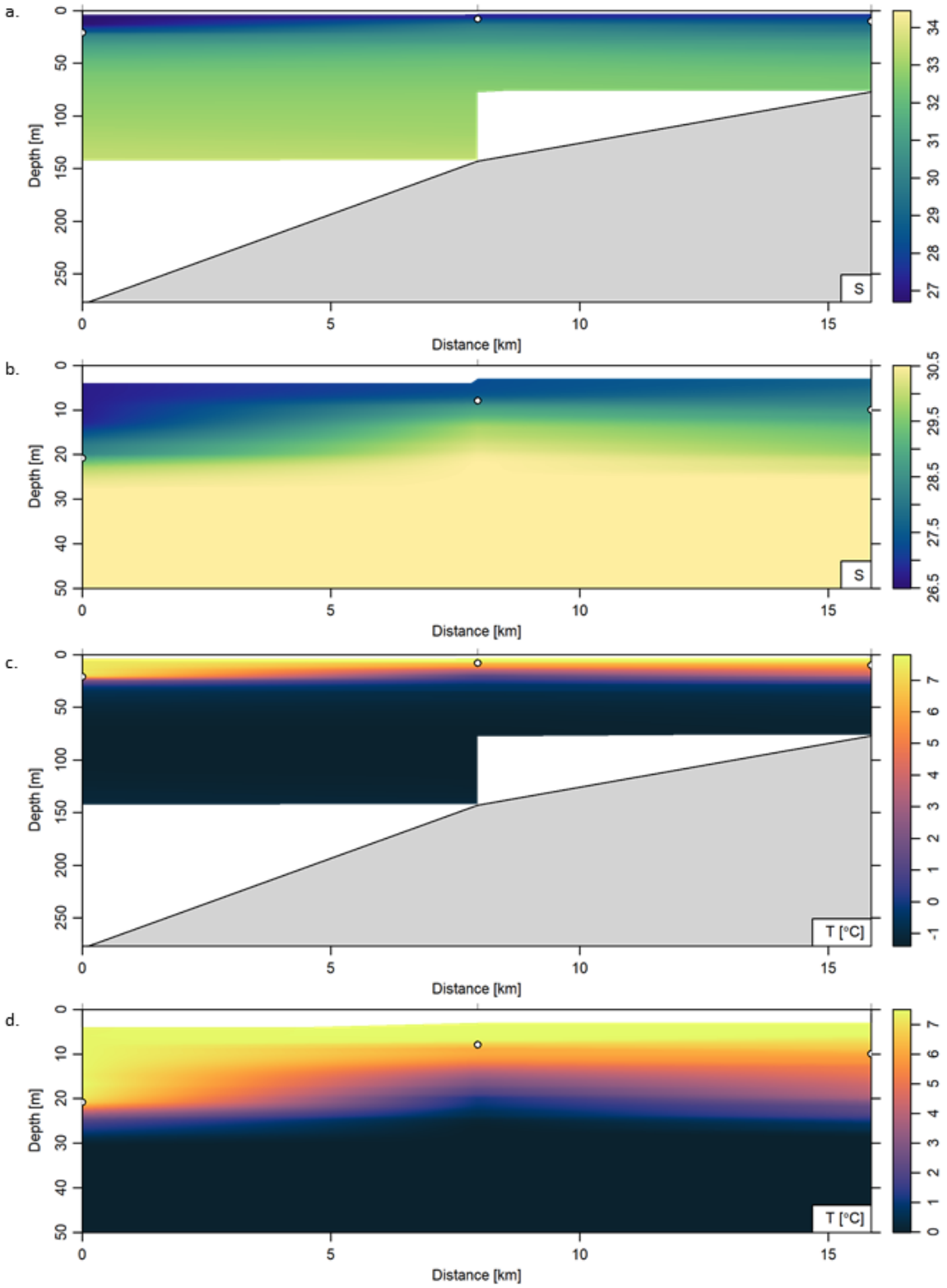


Figure 28. Sections from south to north across Minto Inlet (MNT) in 2014: salinity (a, b) and temperature (c, d). Full depth (a, c) and enlarged to show only the top 50m (b, d). N^2-derived surface layer depths at each station are connoted by white dots.

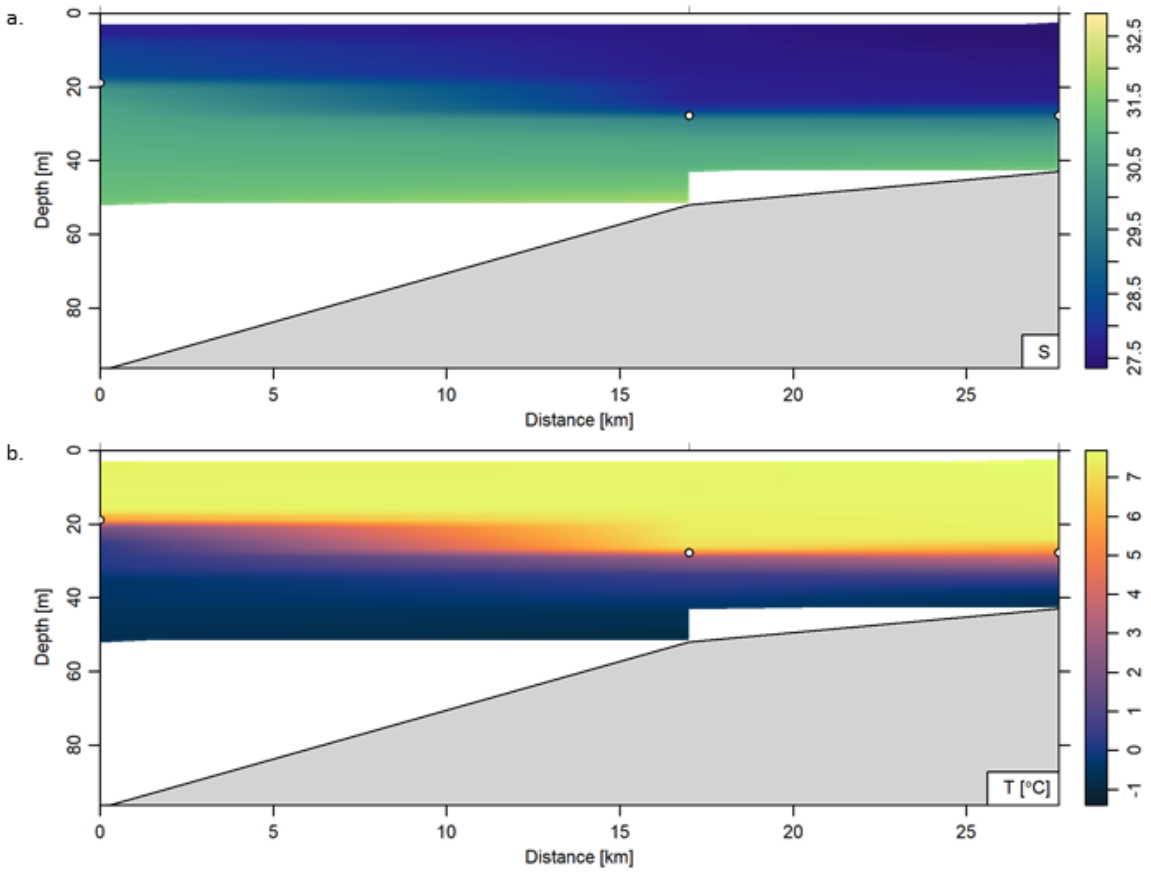


Figure 29. Sections from west to east across Walker Bay (WLK) in 2014: salinity (a) and temperature (b). N^2-derived surface layer depths at each station are connoted by white dots.

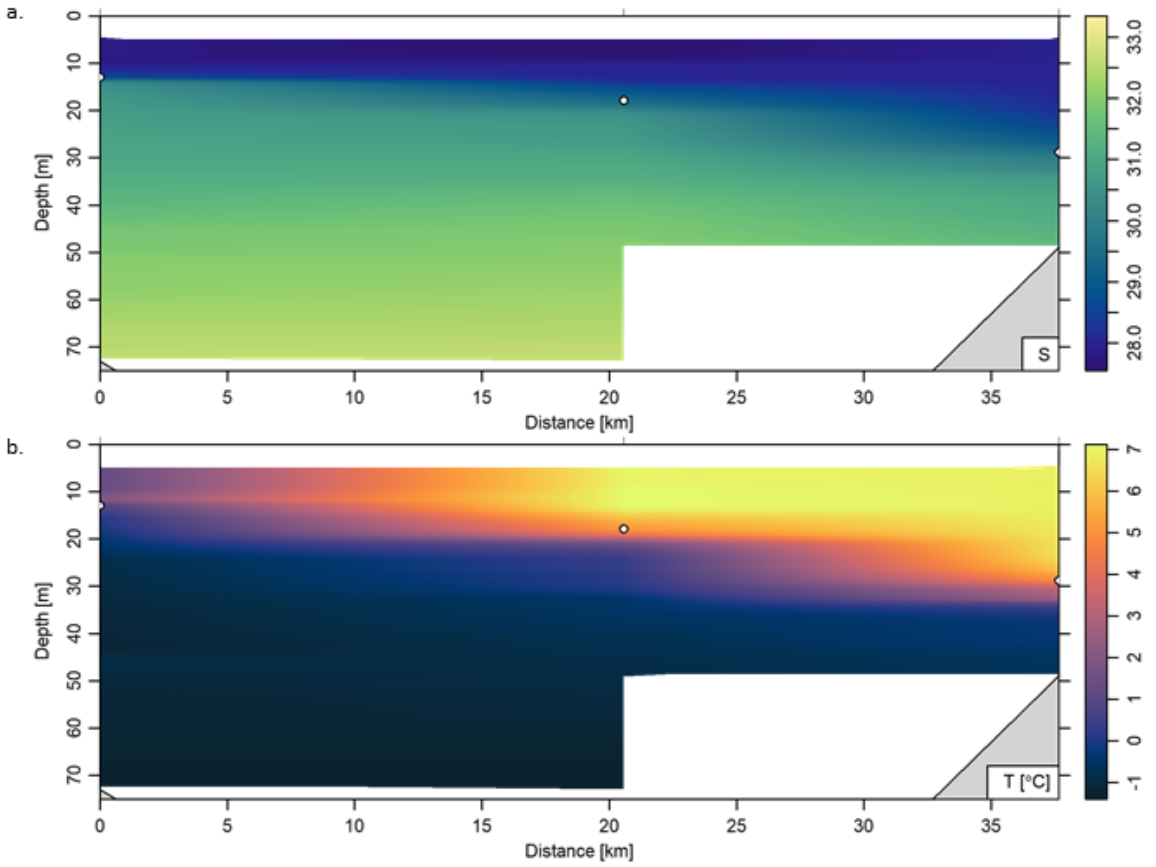


Figure 30. Sections from west to east across the south end of Prince of Wales Strait using the Alexander Milne Point (ALX) stations in 2014: salinity (a) and temperature (b). N^2-derived surface layer depths at each station are connoted by white dots.

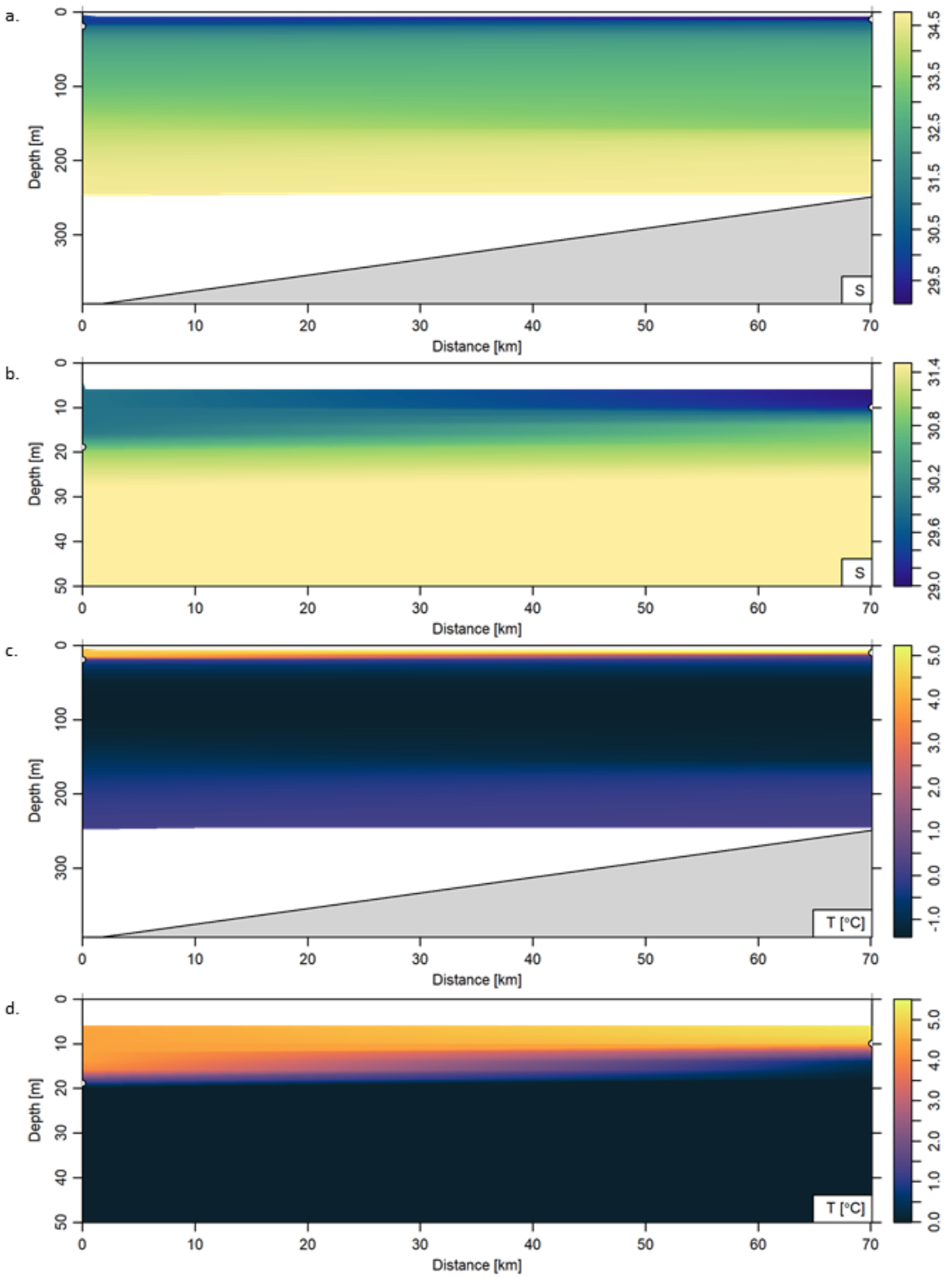


Figure 31. Sections from south to north in eastern Amundsen Gulf using the AMN stations in 2014: salinity (a, b) and temperature (c, d). Full depth (a, c) and enlarged to show only the top 50 m (b, d). N^2-derived surface layer depths at each station are denoted by white dots.

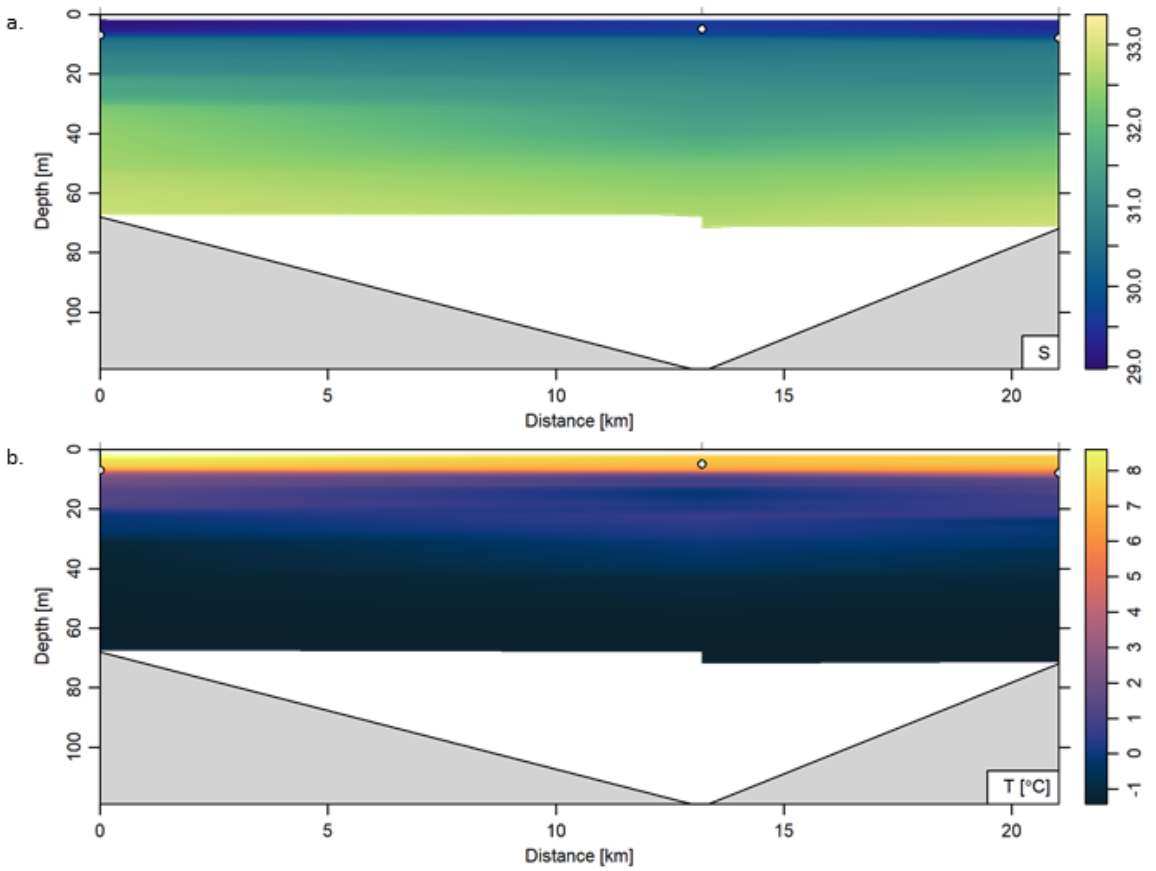


Figure 32. Sections from west to east across Darnley Bay using the Bennett Point (BPT) stations in 2014: salinity (a) and temperature (b). N^2-derived surface layer depths at each station are denoted by white dots.

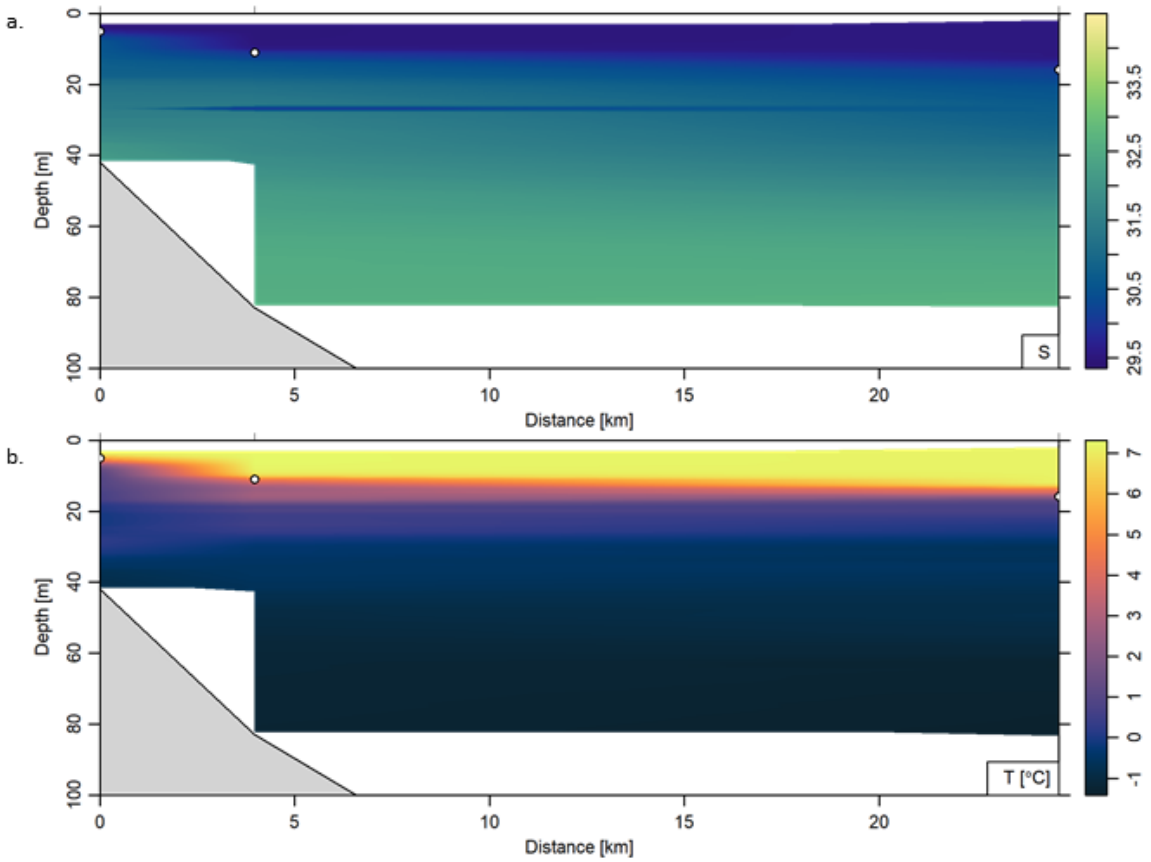


Figure 33. Sections from south to north along the Cape Parry (CPY) stations in 2014: salinity (a) and temperature (b). N^2-derived surface layer depths at each station are denoted by white dots.

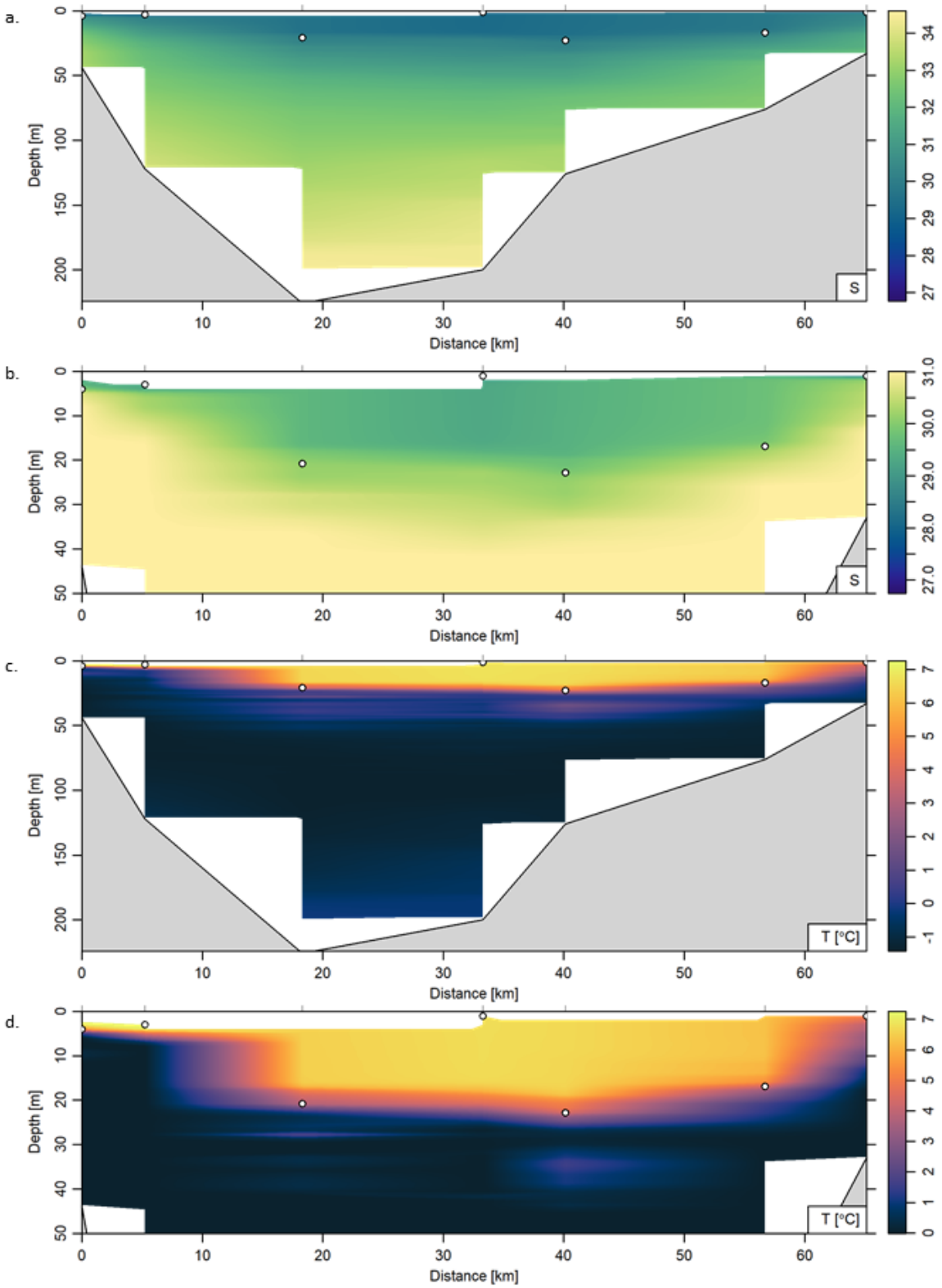


Figure 34. Sections from west to east across Franklin Bay (FRK) in 2014: salinity (a, b) and temperature (c, d). Full depth (a, c) and enlarged to show only the top 50 m (b, d). N^2-derived surface layer depths at each station are denoted by white dots.

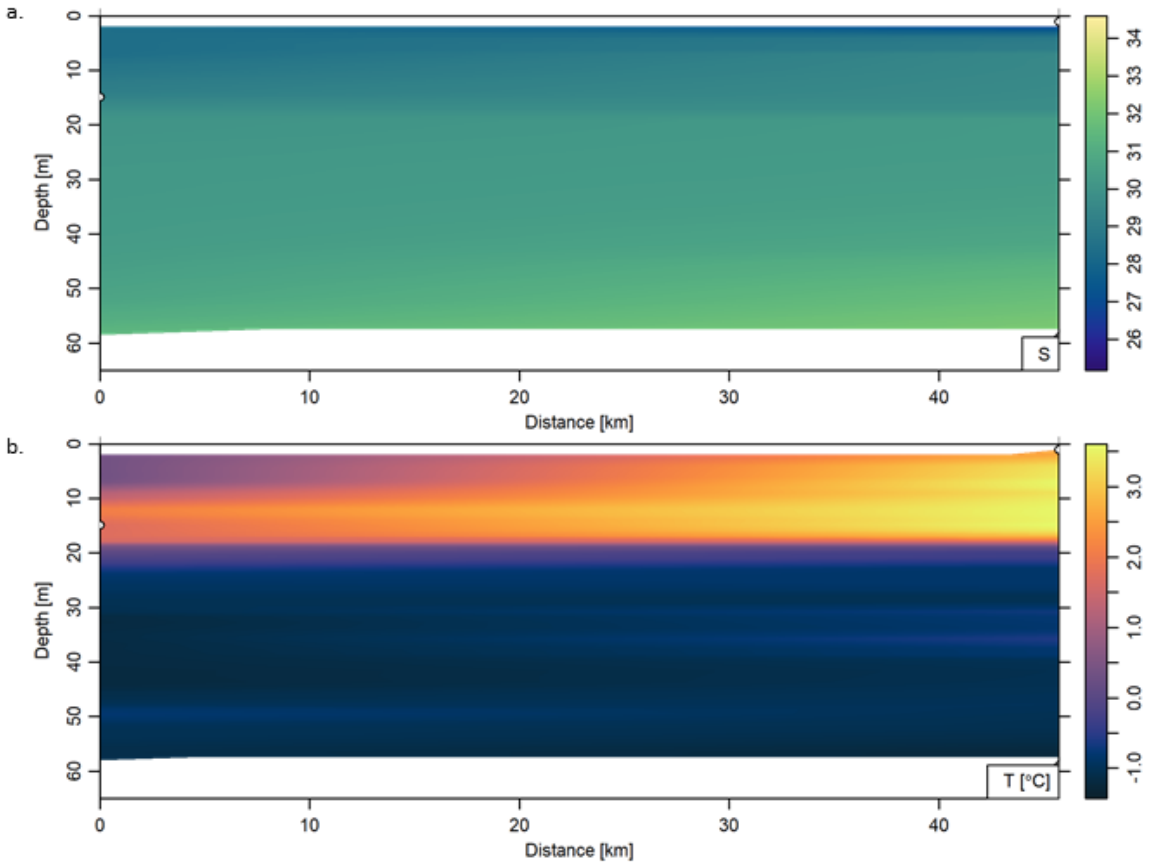


Figure 35. Sections from west to east along the Banks - North stations in 2014: salinity (a) and temperature (b). N^2-derived surface layer depths at each station are denoted by white dots.

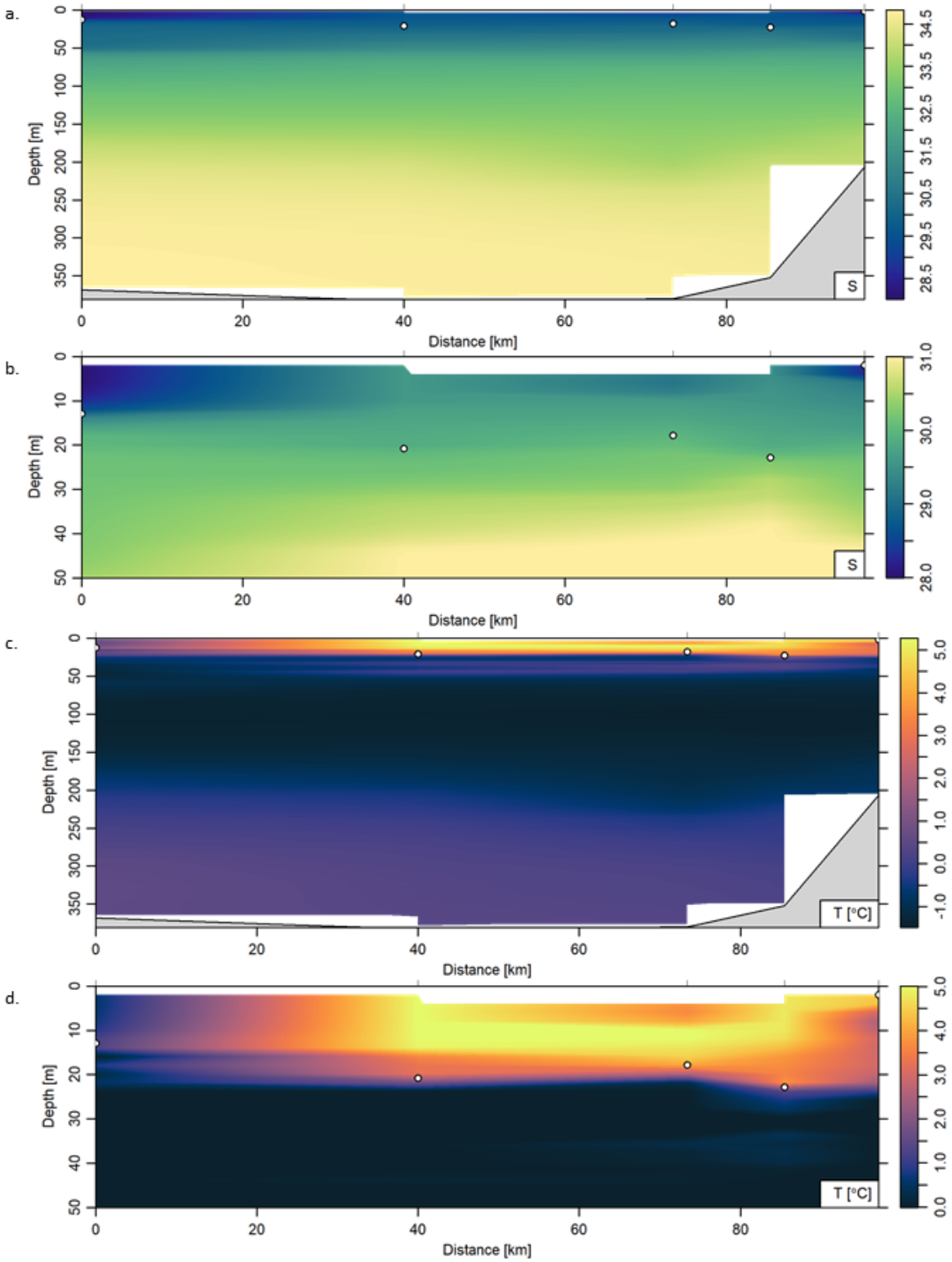


Figure 36. Sections from west to east along the Banks - South stations in 2014: salinity (a, b) and temperature (c, d). Full depth (a, c) and enlarged to show only the top 50 m (b, d). N^2-derived surface layer depths at each station are denoted by white dots.

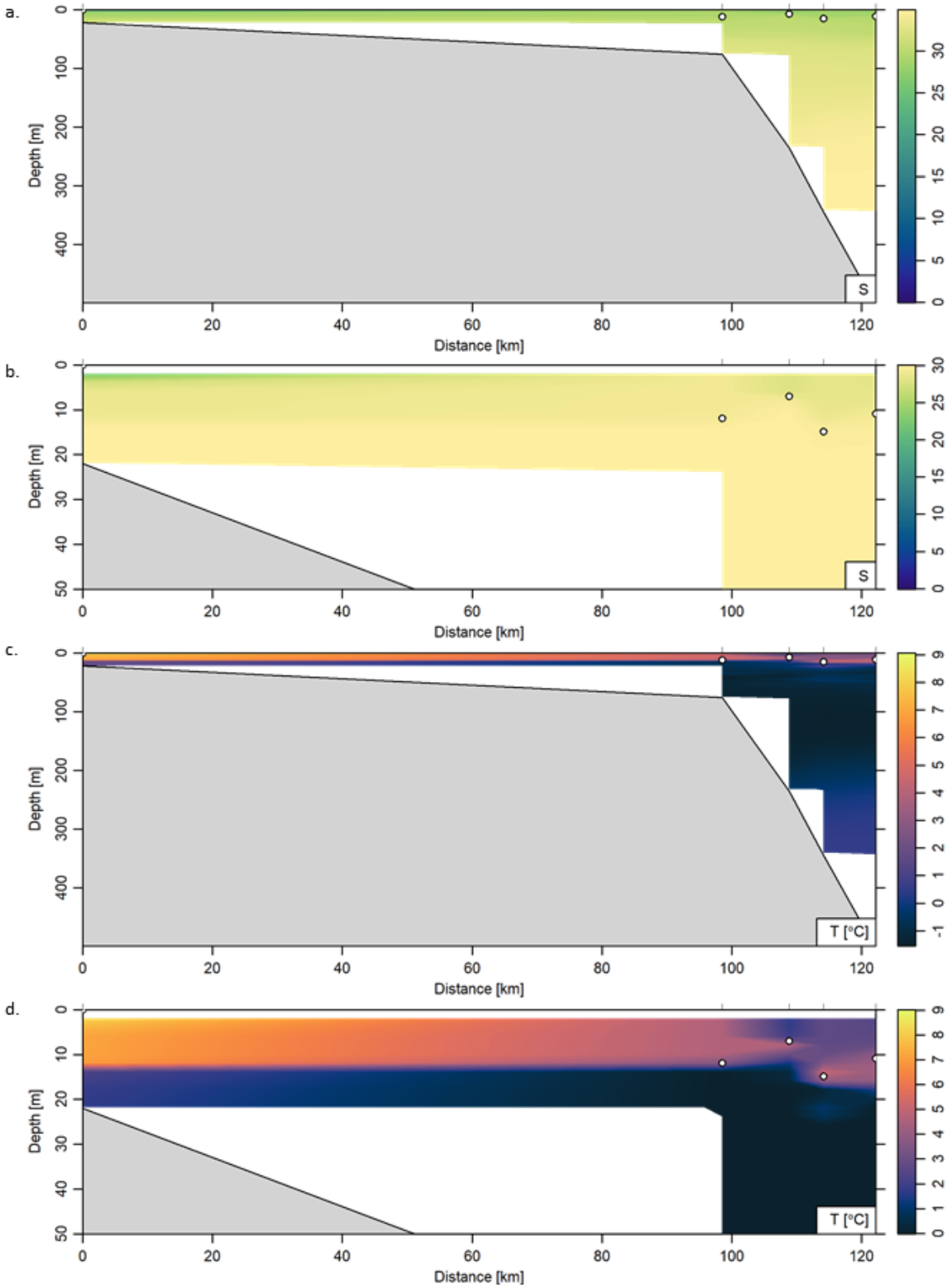


Figure 37. Sections from south to north along the Kugmallit (KUG) stations in 2014: salinity (a, b) and temperature (c, d). Full depth (a, c) and enlarged to show only the top 50 m (b, d). N^2-derived surface layer depths at each station are denoted by white dots.

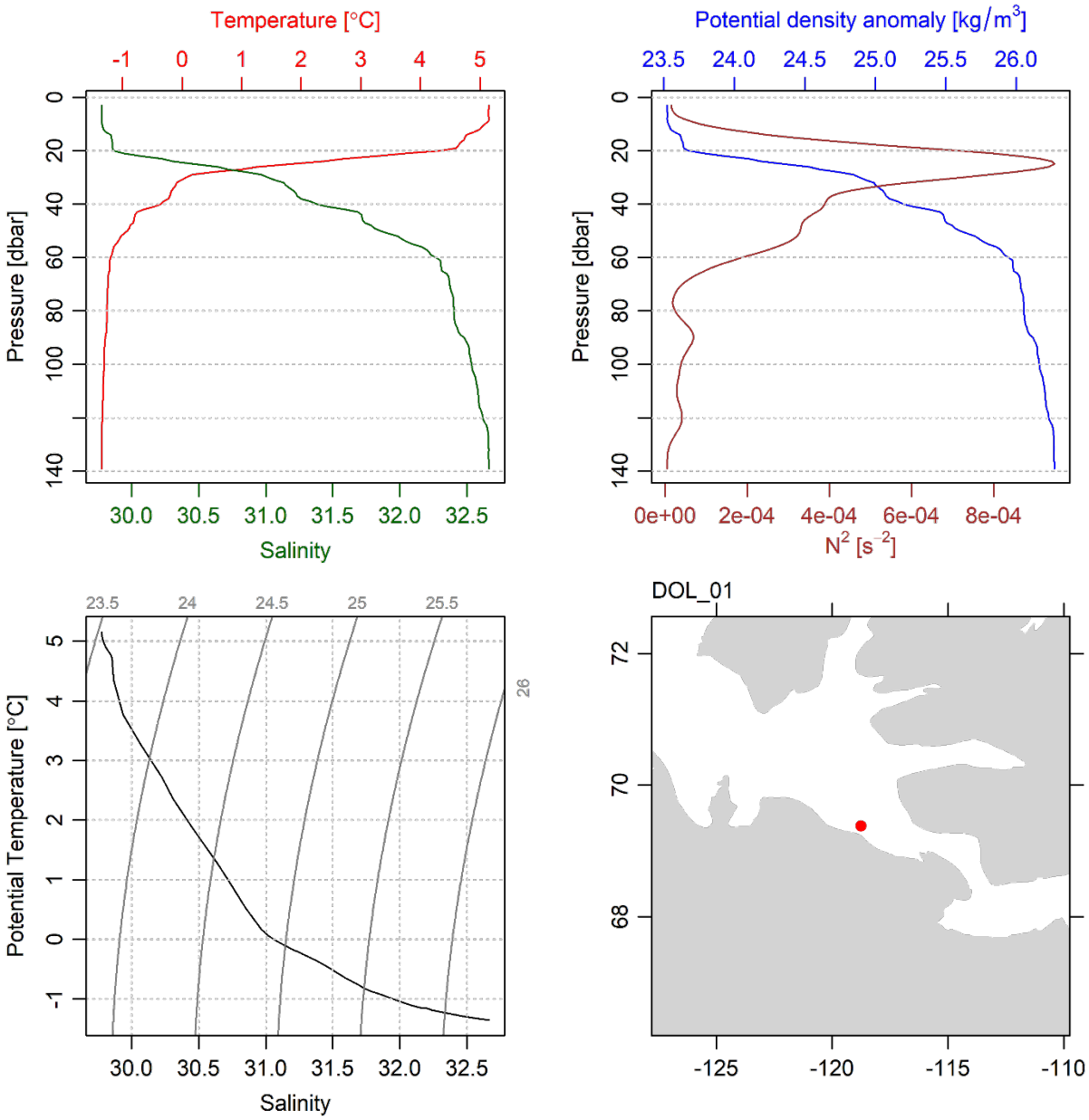
8 Tables

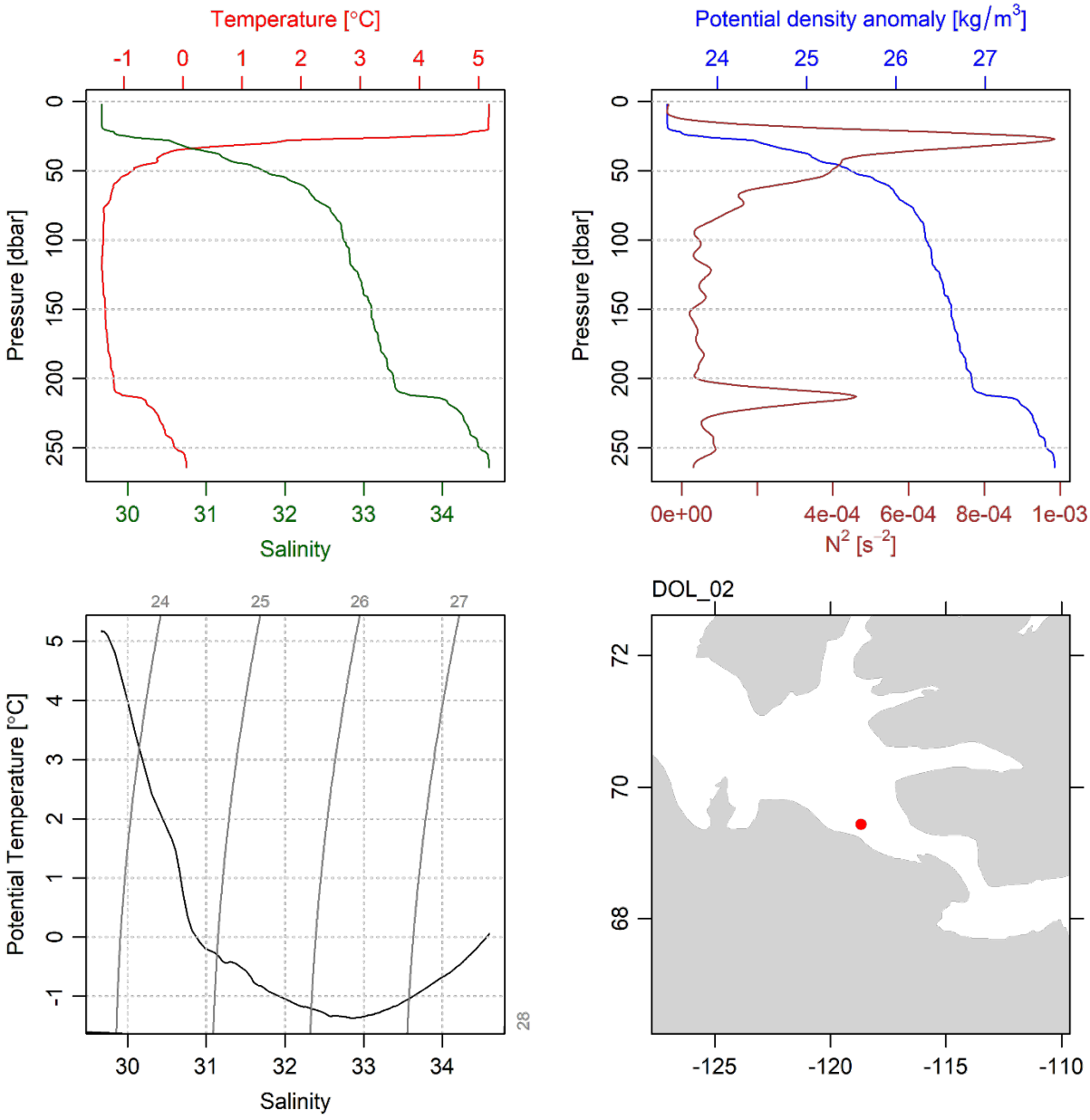
Table 1. Surface and surface layer oceanographic parameters at each BREA-MFP station, August-September 2014. Freshwater content (FWC) and ocean heat content (OHC) is integrated over the surface layer (dbar) depth.

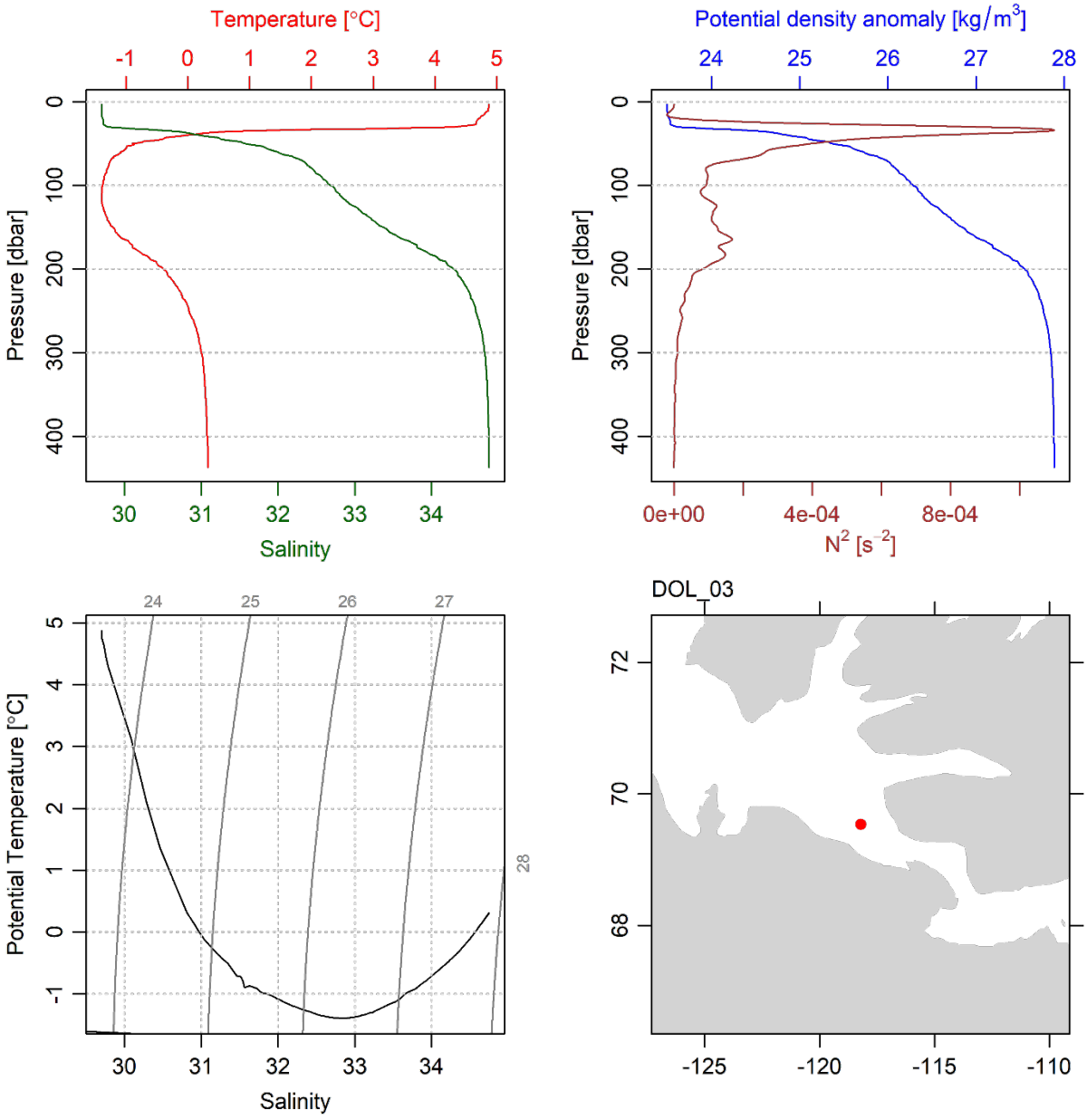
Station	Lat (°N)	Lon (°N)	Surface Temp (°C)	Surface Salinity	Surface depth (dbar)	Surface Layer (dbar)	OHC (kJ)	FWC (m)	Station Depth
DOL_05	69.73	-117.39	0.63	30.97	3	28	27.62	2.69	132
DOL_04	69.64	-117.79	5.74	29.00	4	33	675.54	4.83	373
DOL_03	69.54	-118.22	4.87	29.70	3	34	592.33	4.62	439
DOL_02	69.43	-118.69	5.18	29.67	2	27	528.08	3.77	269
DOL_01	69.38	-118.77	5.15	29.78	3	25	424.08	3.24	145
MNT_1	71.23	-118.37	7.11	27.27	10	16	207.48	1.41	214
MNT_2	71.26	-117.09	7.42	26.71	4	21	548.49	3.90	283
MNT_3	71.33	-117.15	7.73	27.29	3	8	186.45	1.27	146
MNT_4	71.40	-117.19	7.79	27.61	3	10	236.10	1.56	80
MNT_5	71.44	-116.30	7.34	26.94	3	27	726.47	5.14	139
WLK_01	71.48	-118.70	7.49	27.73	3	19	516.08	3.21	100
WLK_02	71.55	-118.27	7.56	27.58	3	28	792.08	5.26	60
WLK_03	71.60	-118.01	7.67	27.35	2	28	821.12	5.54	45
ALX_01	71.62	-120.34	1.29	27.77	3	13	57.96	1.98	76
ALX_02	71.66	-119.77	7.00	27.56	5	18	384.52	2.68	141
ALX_03	71.68	-119.28	6.81	27.88	2	29	765.63	5.26	46
BPT_2	69.70	-123.79	8.58	28.98	1	7	226.60	1.13	67
BPT_3	69.70	-123.45	7.45	29.56	2	5	120.54	0.60	121
BPT_4	69.70	-123.24	7.42	29.36	2	8	196.24	1.06	72
CPY-01	70.23	-124.50	7.30	29.36	3	5	81.76	0.45	44
CPY-02	70.26	-124.51	7.23	29.48	3	11	254.73	1.36	89
CPY-03	70.45	-124.52	7.14	29.53	2	16	395.79	2.24	212
FRK07	70.08	-126.91	7.25	29.32	1	4	111.98	0.60	42
FRK06	70.09	-126.77	7.12	29.30	3	3	29.42	0.16	125
FRK05	70.08	-126.43	6.54	29.58	4	21	447.79	2.65	228
FRK04	70.08	-126.03	6.75	26.79	1	1	27.96	0.23	202
FRK03	70.08	-125.85	6.69	29.46	2	23	576.16	3.33	128
FRK02	70.08	-125.42	6.29	29.42	1	17	425.72	2.46	79
FRK01	70.08	-125.20	4.91	28.60	1	1	20.34	0.18	36
BNK01	72.13	-127.04	3.67	28.49	1	3 (25)	44.41 (367.42)	0.53 (3.74)	56
BNK02	72.10	-127.48	4.78	29.46	2	23	391.81	3.24	351
BNK03	72.09	-129.97	0.58	28.02	2	13	41.14	2.26	367
BNK04	72.10	-128.81	5.23	29.59	2	21	378.87	2.93	388
BNK05	72.93	-127.79	0.35	28.36	2	15	62.50	2.47	249
BNK06	72.93	-126.39	2.50	25.20	1	1 (18)	10.46 (239.95)	0.28 (3.00)	61
BNK07	72.10	-127.14	4.41	28.26	2	2 (43)	18.30 (240.14)	0.19 (5.91)	209
BNKHC3	72.10	-127.83	3.69	29.14	3	18	290.64	2.42	379
KUG01	70.01	-133.83	9.05	0.02	0	0	38.18	1.00	22.4
KUG02	70.85	-134.67	4.58	29.17	1	12	223.70	1.93	77.2
KUG03	70.94	-134.77	1.75	27.76	2	7	49.46	1.19	234
KUG04	70.98	-134.80	2.72	28.47	2	15	189.78	2.43	345
KUG05	71.05	-134.87	2.46	28.23	2	11	120.51	1.80	505
AMN_01	70.84	-119.78	5.21	29.06	6	10	105.53	0.82	255
AMN_02	70.22	-119.47	4.36	29.91	4	19	256.11	2.20	397
ESC03	70.34	-131.01	7.42	26.85	2	11	295.71	1.97	20
ESC04	70.09	-132.13	6.33	29.70	2	8	163.37	0.95	20
AGK2	70.04	-133.55	7.70	25.95	1	5	157.94	1.23	30
AGK01	70.10	-133.84	7.17	27.97	4	9	170.15	1.13	32.2
NTC01	71.32	-126.89	5.19	29.64	4	22	381.31	2.75	354
BOW2	69.97	-126.77	2.82	30.01	3	3	11.71	0.14	43
SMO	69.86	-126.74	6.48	29.49	3	7	122.34	0.74	43
WIS-01	70.10	-125.06	6.27	29.98	2	10	226.24	1.24	49
WIS-02	70.17	-124.83	6.04	30.06	3	6	93.17	0.53	44
PWS_01	72.11	-119.43	-0.19	25.83	2	14	23.70	3.03	106

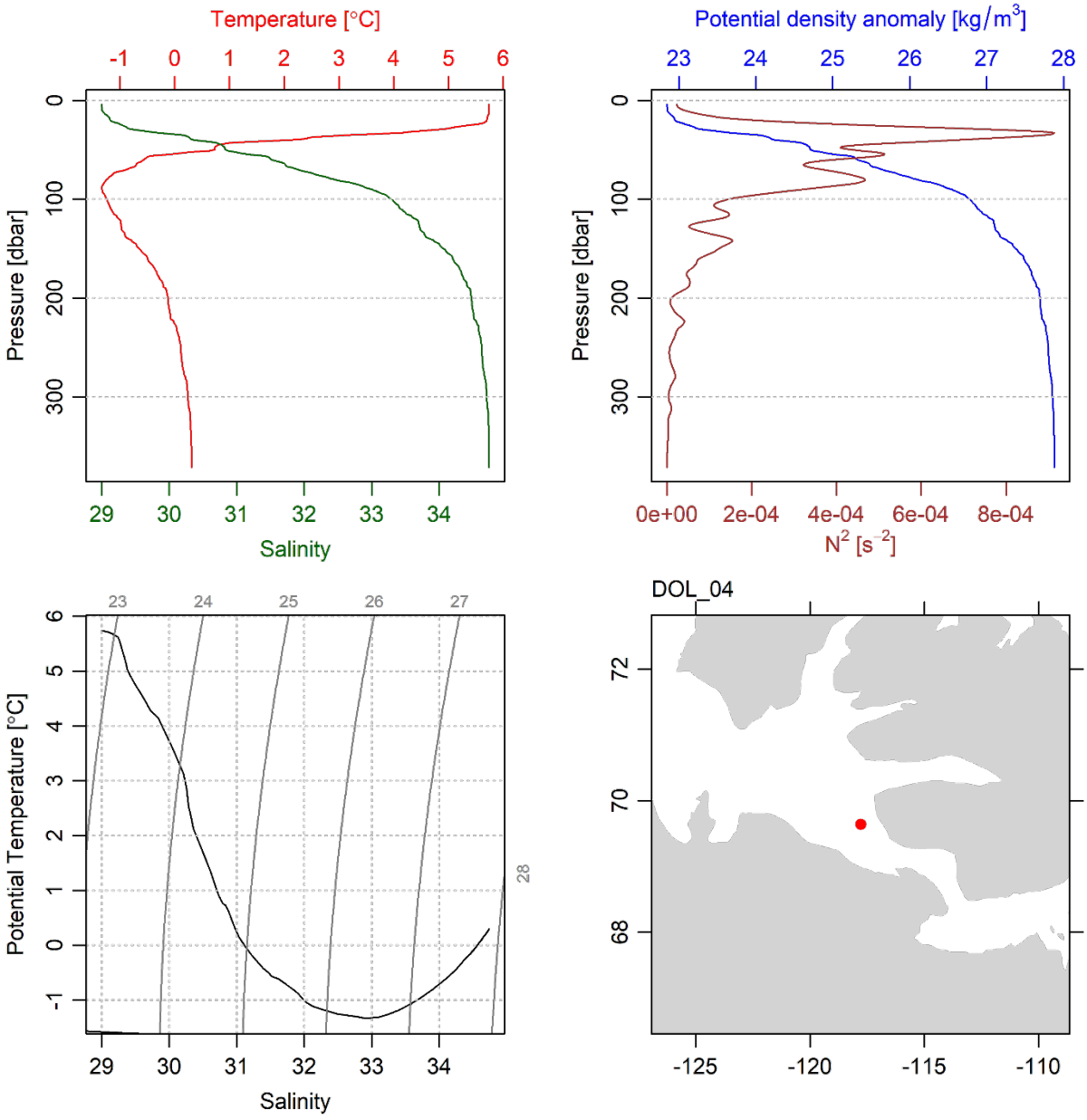
Appendix A – Profiles of salinity, temperature, potential density anomaly, and N^2, and T-S plots for each of the 59 stations sampled during BREA-MFP 2014.

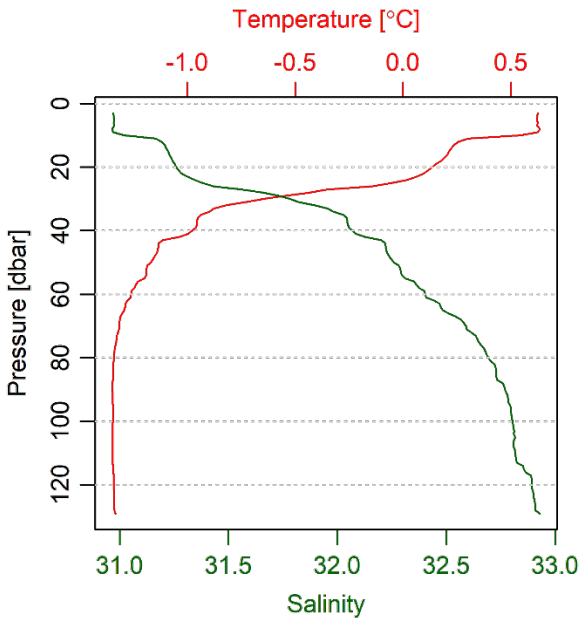
Station name is indicated on the map, showing the station location as described in Figure 23 and Table 1.

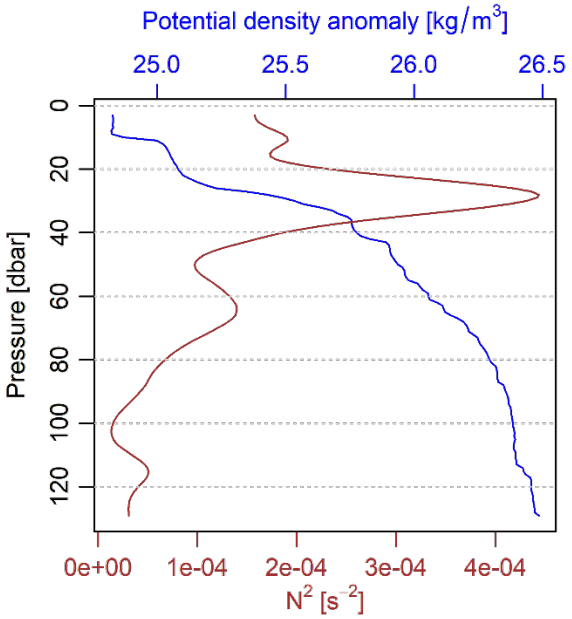


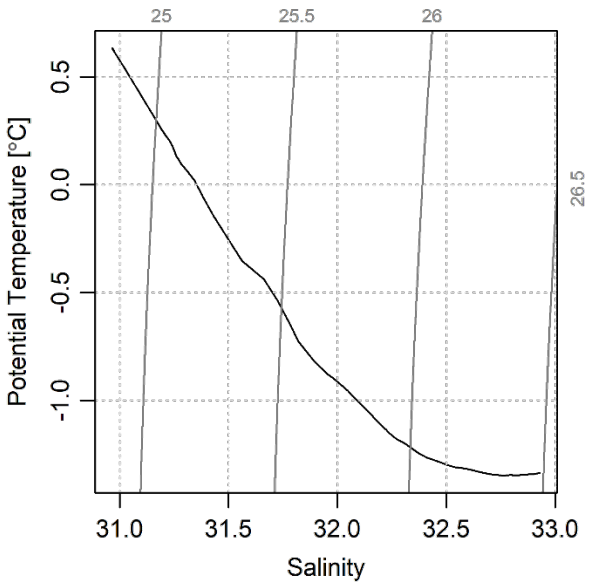

Temperature [°C]
-1 0 1 2 3 4 5
Pressure [dbar]
0 50 100 150 200 250
30 31 32 33 34
Salinity
Potential density anomaly [kg/m3]
24 25 26 27
0e+00 4e-04 6e-04 8e-04 1e-03
N2 [s-2]
Potential Temperature [°C]
24 25 26 27
-1 0 1 2 3 4 5
28
DOL_02
72 70 68
-125 -120 -115 -110

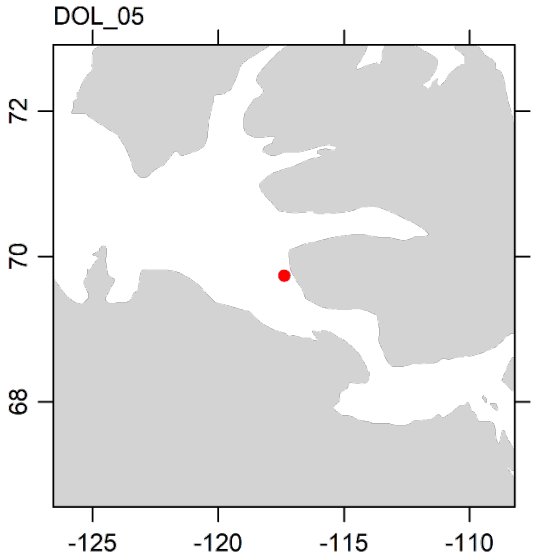

Temperature [°C]
-1 0 1 2 3 4 5
Pressure [dbar]
0 100 200 300 400
30 31 32 33 34
Salinity
Potential density anomaly [kg/m3]
24 25 26 27 28
0e+00 4e-04 8e-04
N2 [s-2]
Potential Temperature [°C]
24 25 26 27
28
DOL_03
72 70 68
-125 -120 -115 -110

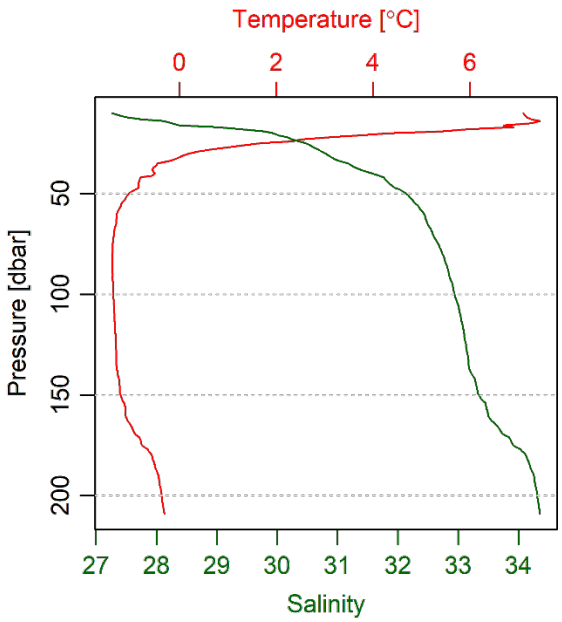

Temperature [°C]
-1 0 1 2 3 4 5 6
Pressure [dbar]
0 100 200 300
29 30 31 32 33 34
Salinity
Potential density anomaly [kg/m3]
23 24 25 26 27 28
Pressure [dbar]
0 100 200 300
0e+00 2e-04 4e-04 6e-04 8e-04
N2 [s−2]
Potential Temperature [°C]
-1 0 1 2 3 4 5 6
23 24 25 26 27
28
29 30 31 32 33 34
Salinity
DOL_04
72 70 68
-125 -120 -115 -110

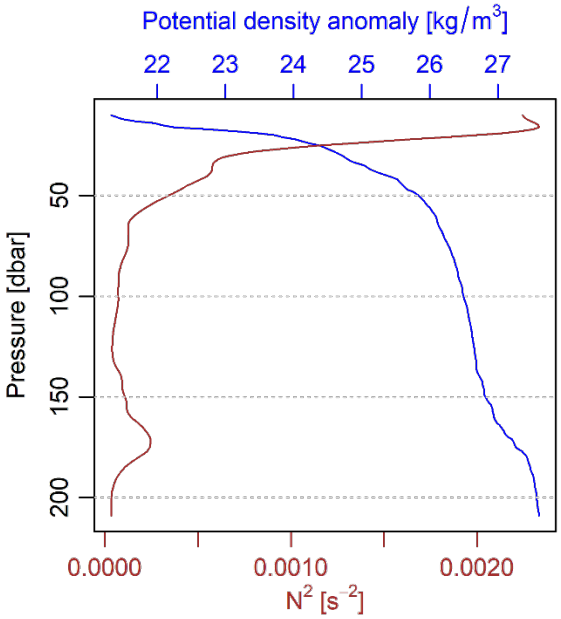

Temperature [°C]
-1.0
-0.5
0.0
0.5
Pressure [dbar]
0
20
40
60
80
100
120
31.0
31.5
32.0
32.5
33.0
Salinity

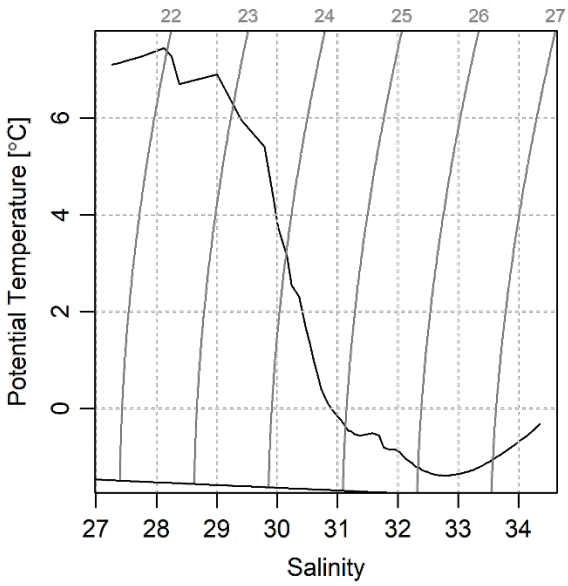

Potential density anomaly [kg/m3]
25.0
25.5
26.0
26.5
Pressure [dbar]
0
20
40
60
80
100
120
0e+00
1e-04
2e-04
3e-04
4e-04
N2 [s−2]

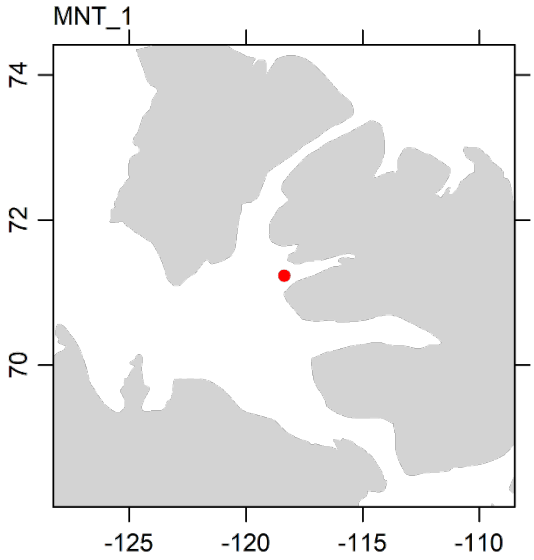

25
25.5
26
26.5
Potential Temperature [°C]
0.5
0.0
-0.5
-1.0
31.0
31.5
32.0
32.5
33.0
Salinity

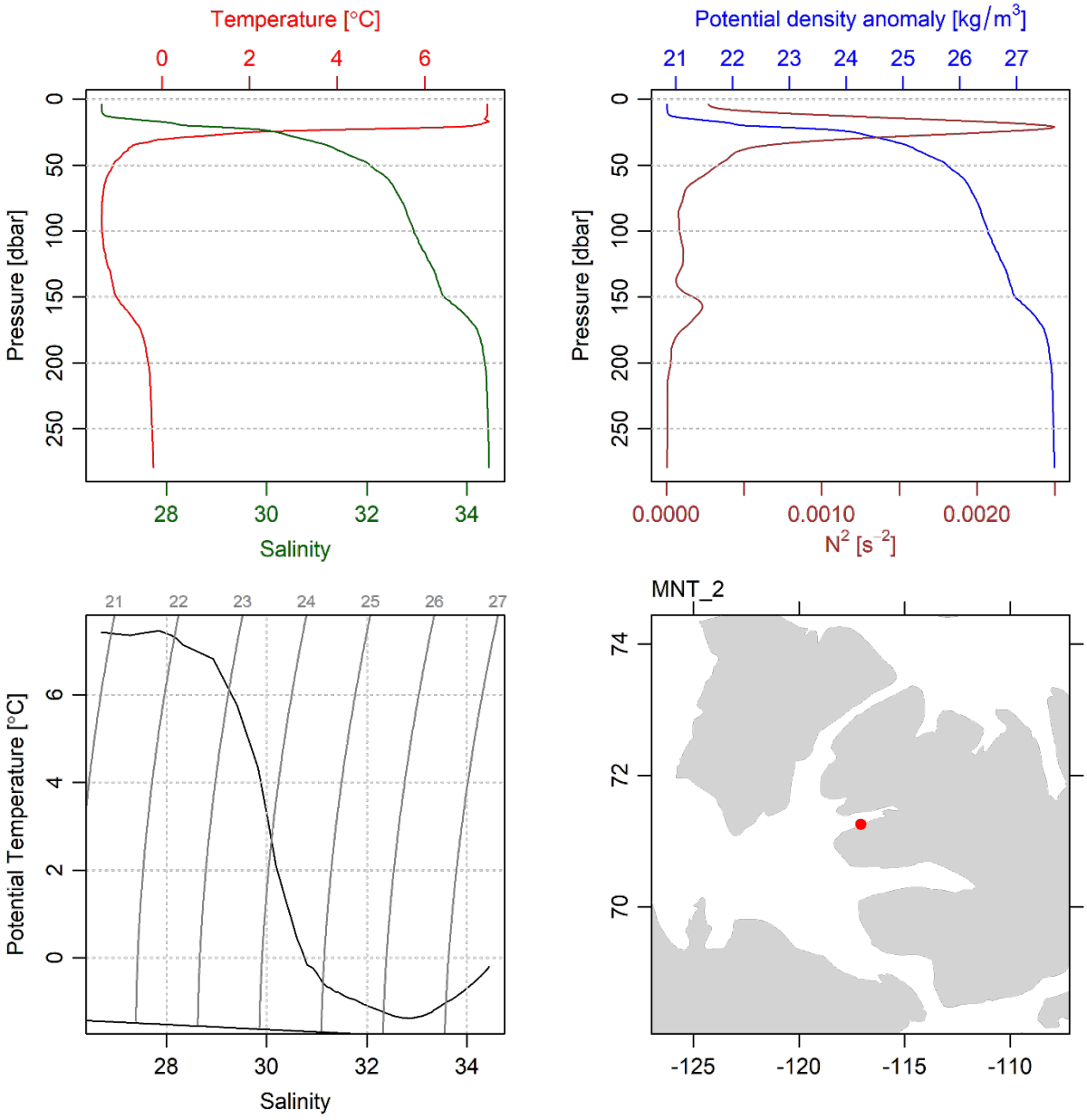

DOL_05
72
70
68
-125
-120
-115
-110

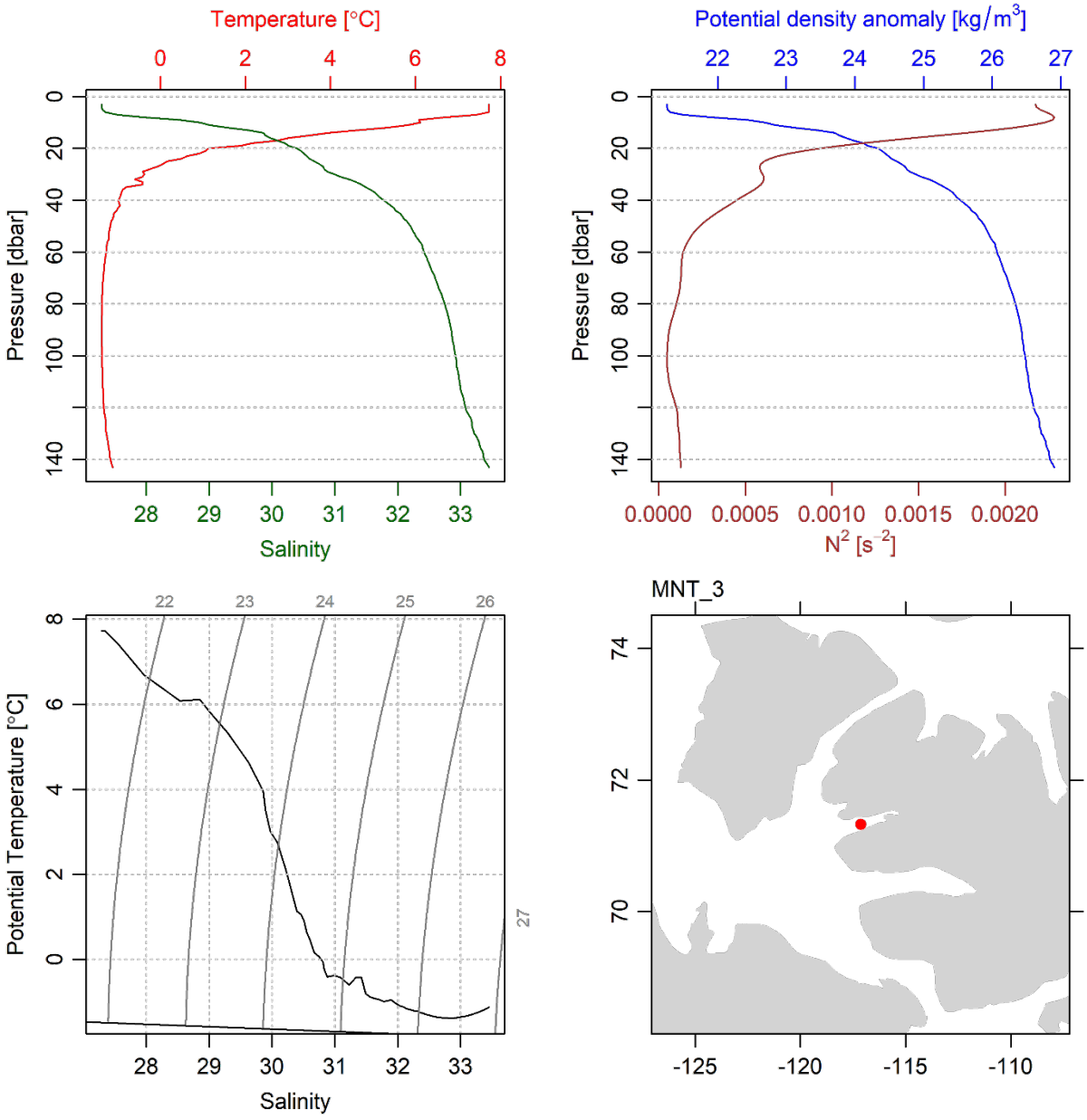

Temperature [°C]
0
2
4
6
Pressure [dbar]
50
100
150
200
27
28
29
30
31
32
33
34
Salinity

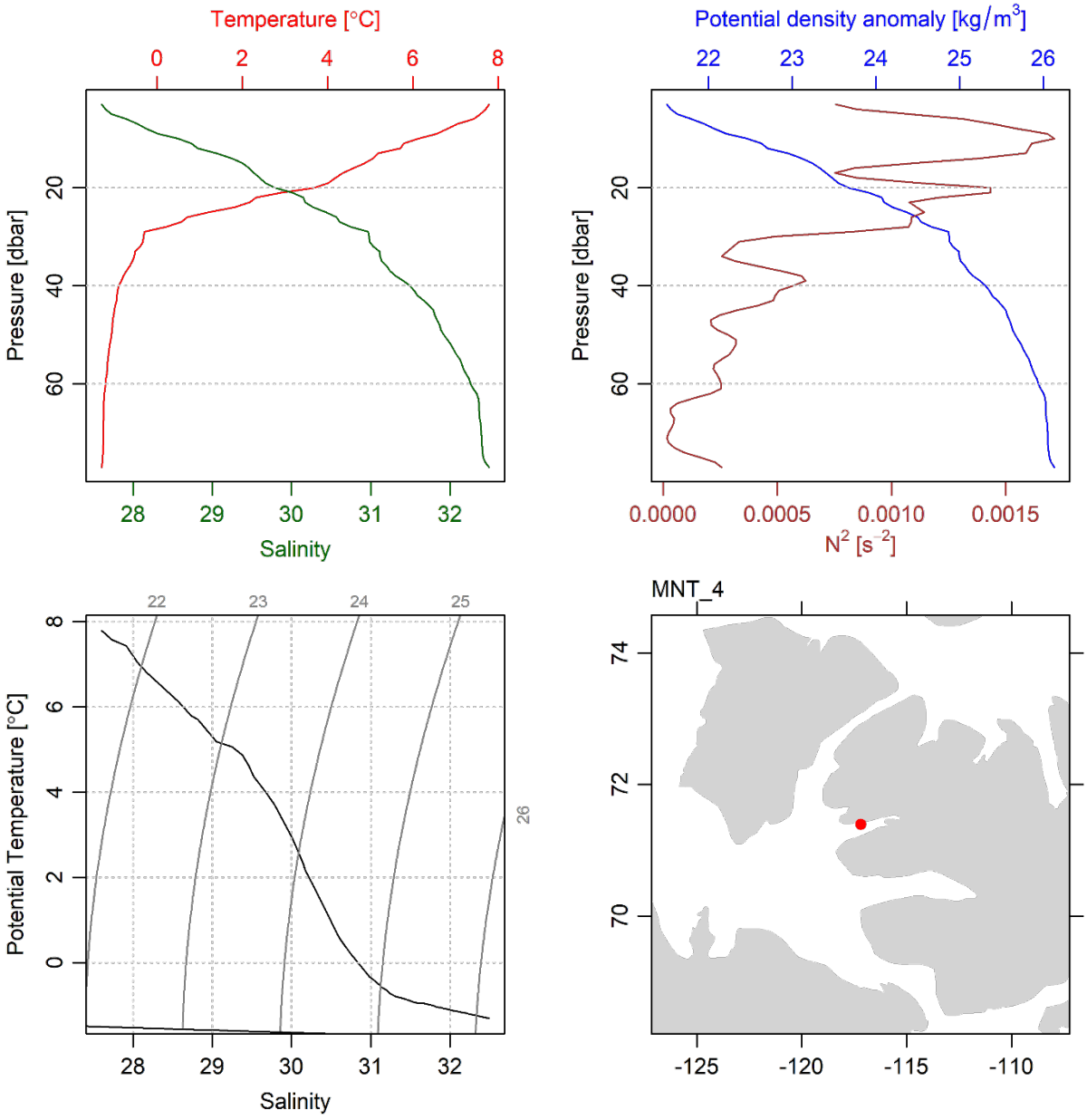

Potential density anomaly [kg/m3]
22
23
24
25
26
27
Pressure [dbar]
50
100
150
200
0.0000
0.0010
0.0020
N2 [s−2]

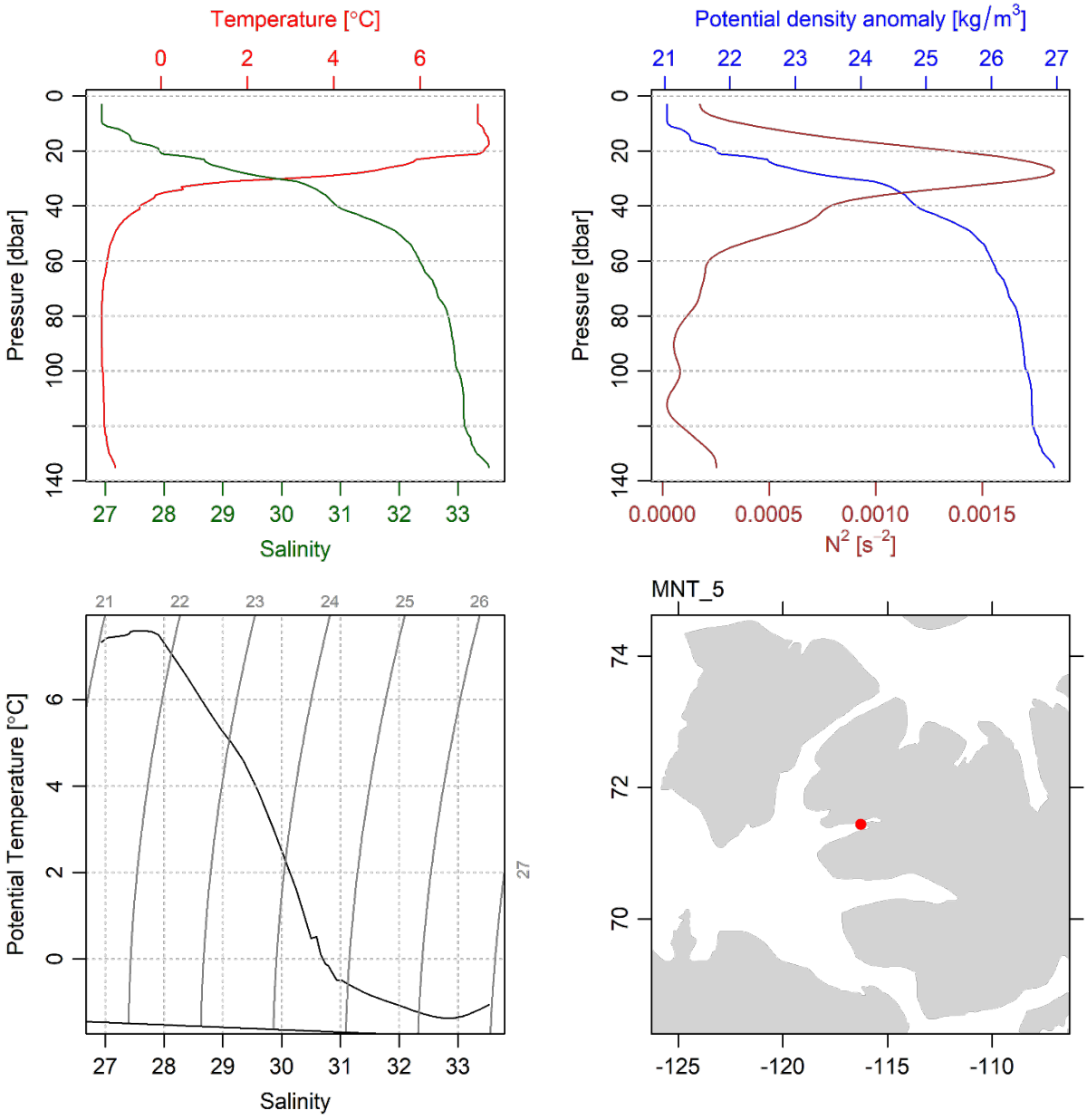

22
23
24
25
26
27
Potential Temperature [°C]
0
2
4
6
27
28
29
30
31
32
33
34
Salinity

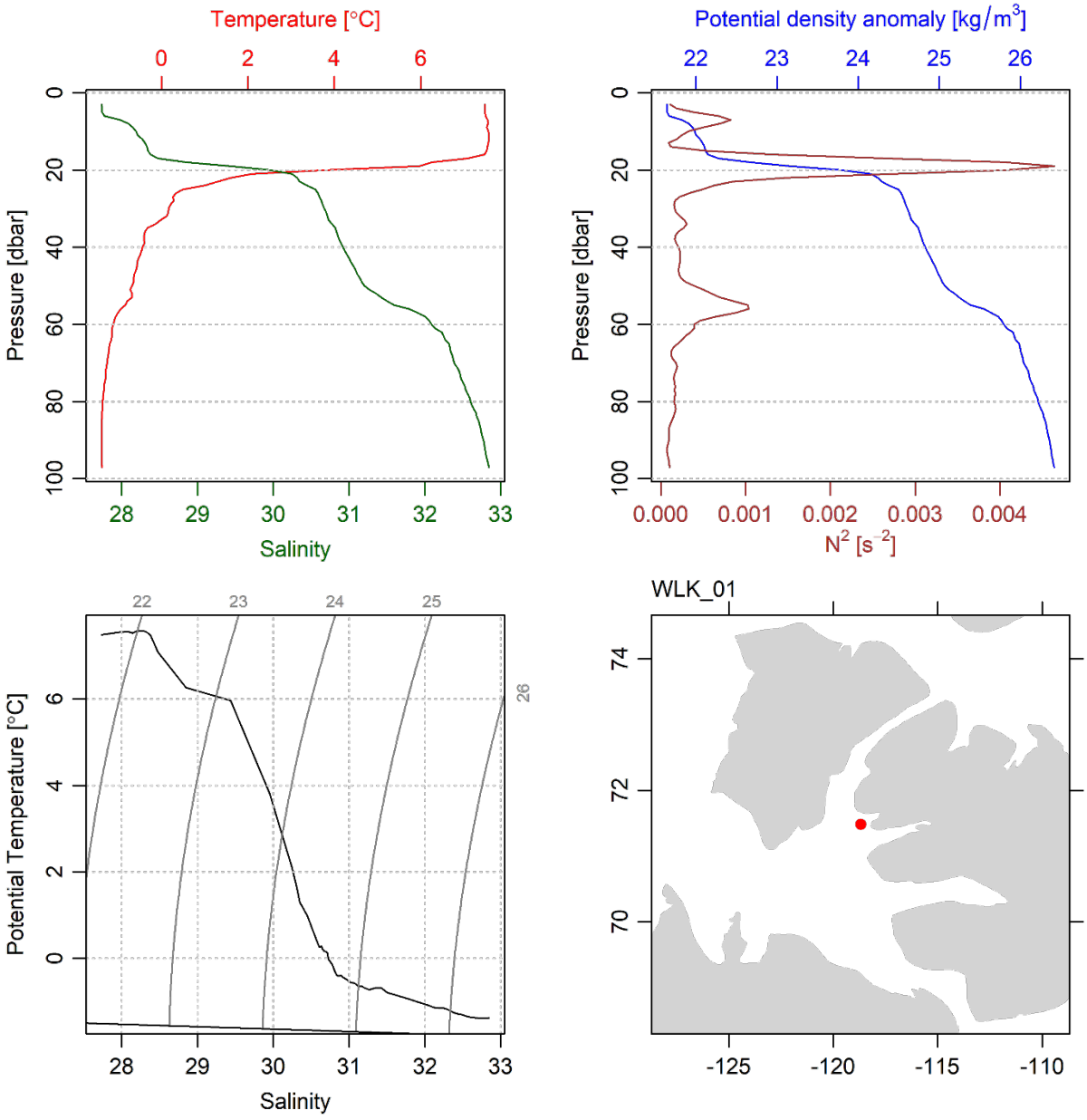

MNT_1
74
72
70
-125
-120
-115
-110

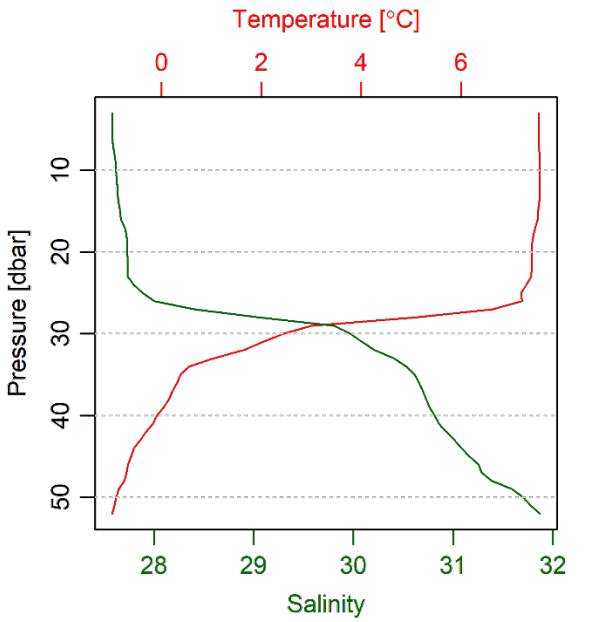

Temperature [°C]
0
2
4
6
Pressure [dbar]
0
50
100
150
200
250
28
30
32
34
Salinity
Potential density anomaly [kg/m3]
21
22
23
24
25
26
27
0.0000
0.0010
0.0020
N2 [s−2]
Potential Temperature [°C]
MNT_2
74
72
70
-125
-120
-115
-110

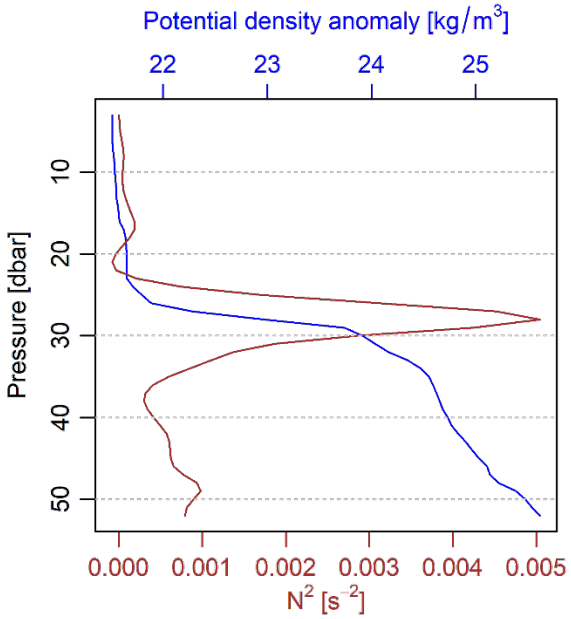

Temperature [°C]
0 2 4 6 8
Pressure [dbar]
0 20 40 60 80 100 140
28 29 30 31 32 33
Salinity
Potential density anomaly [kg/m3]
22 23 24 25 26 27
0.0000 0.0005 0.0010 0.0015 0.0020
N2 [s−2]
22 23 24 25 26
Potential Temperature [°C]
0 2 4 6 8
27
MNT_3
74 72 70
-125 -120 -115 -110

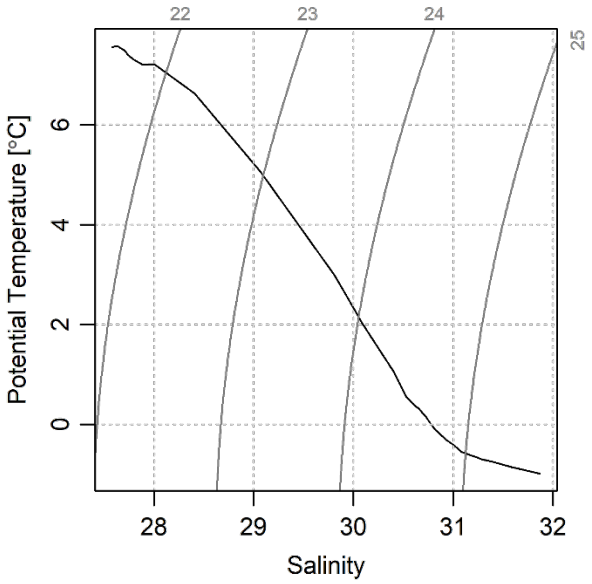

Temperature [°C]
0
2
4
6
8
Pressure [dbar]
20
40
60
28
29
30
31
32
Salinity
Potential density anomaly [kg/m3]
22
23
24
25
26
0.0000
0.0005
0.0010
0.0015
N2 [s−2]
Potential Temperature [°C]
22
23
24
25
26
MNT_4
74
72
70
-125
-120
-115
-110

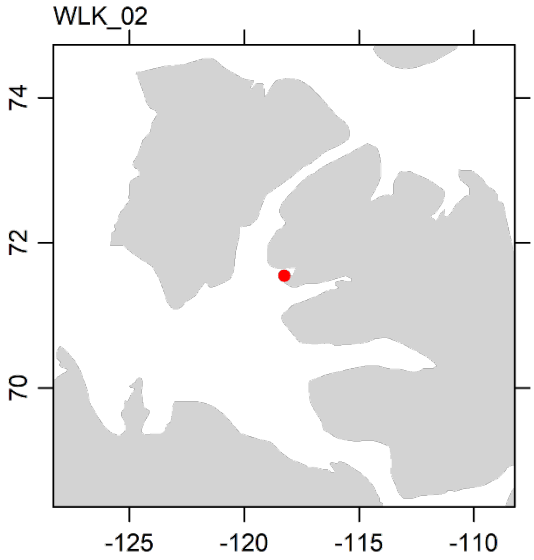

Temperature [°C]
0
2
4
6
Pressure [dbar]
0
20
40
60
80
100
140
27
28
29
30
31
32
33
Salinity
Potential density anomaly [kg/m3]
21
22
23
24
25
26
27
0.0000
0.0005
0.0010
0.0015
N2 [s−2]
Potential Temperature [°C]
MNT_5
74
72
70
-125
-120
-115
-110

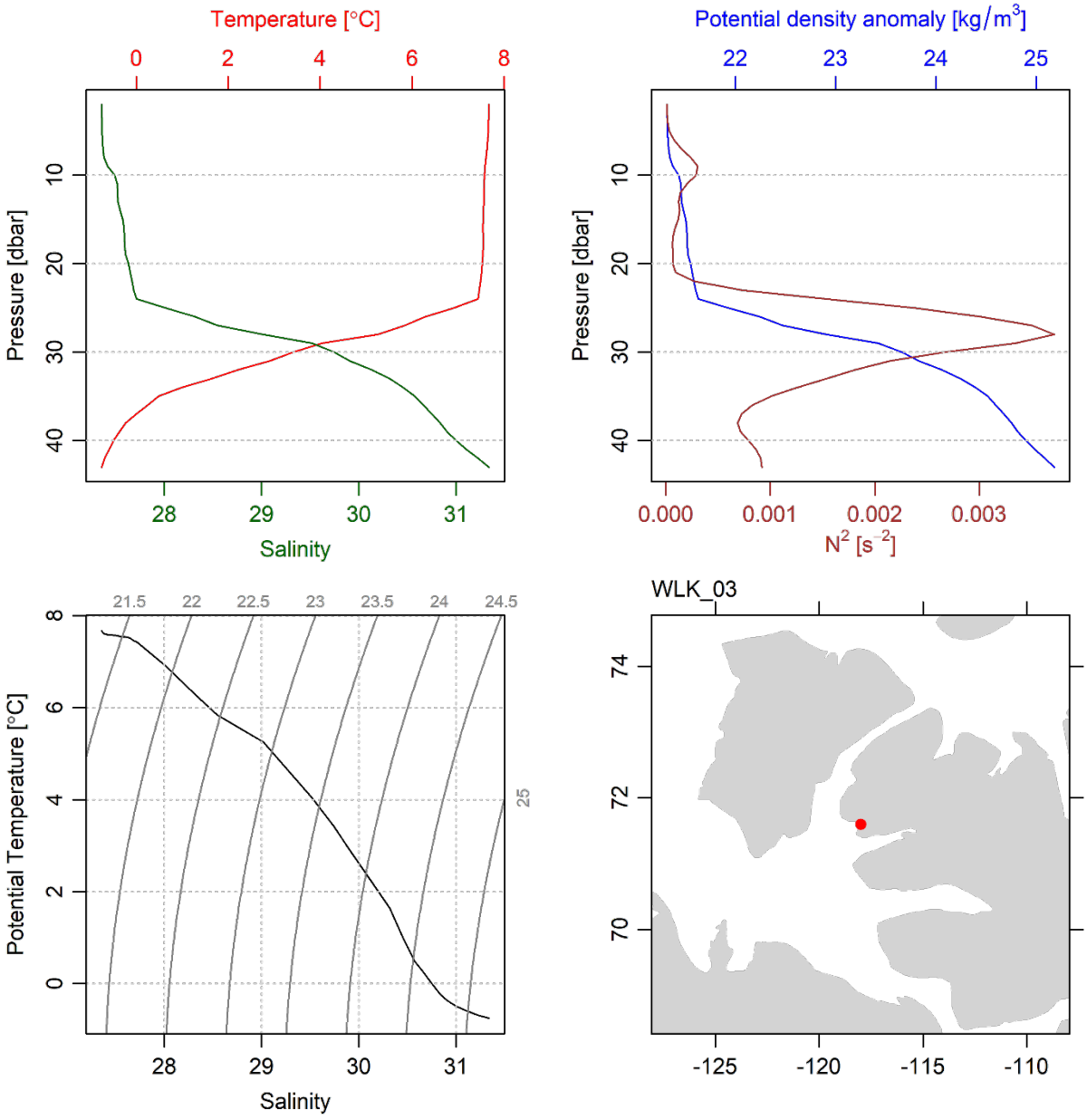

Temperature [°C]
0
2
4
6
Pressure [dbar]
0
20
40
60
80
100
28
29
30
31
32
33
Salinity
Potential density anomaly [kg/m3]
22
23
24
25
26
0.000
0.001
0.002
0.003
0.004
N2 [s−2]
Potential Temperature [°C]
22
23
24
25
26
WLK_01
74
72
70
-125
-120
-115
-110

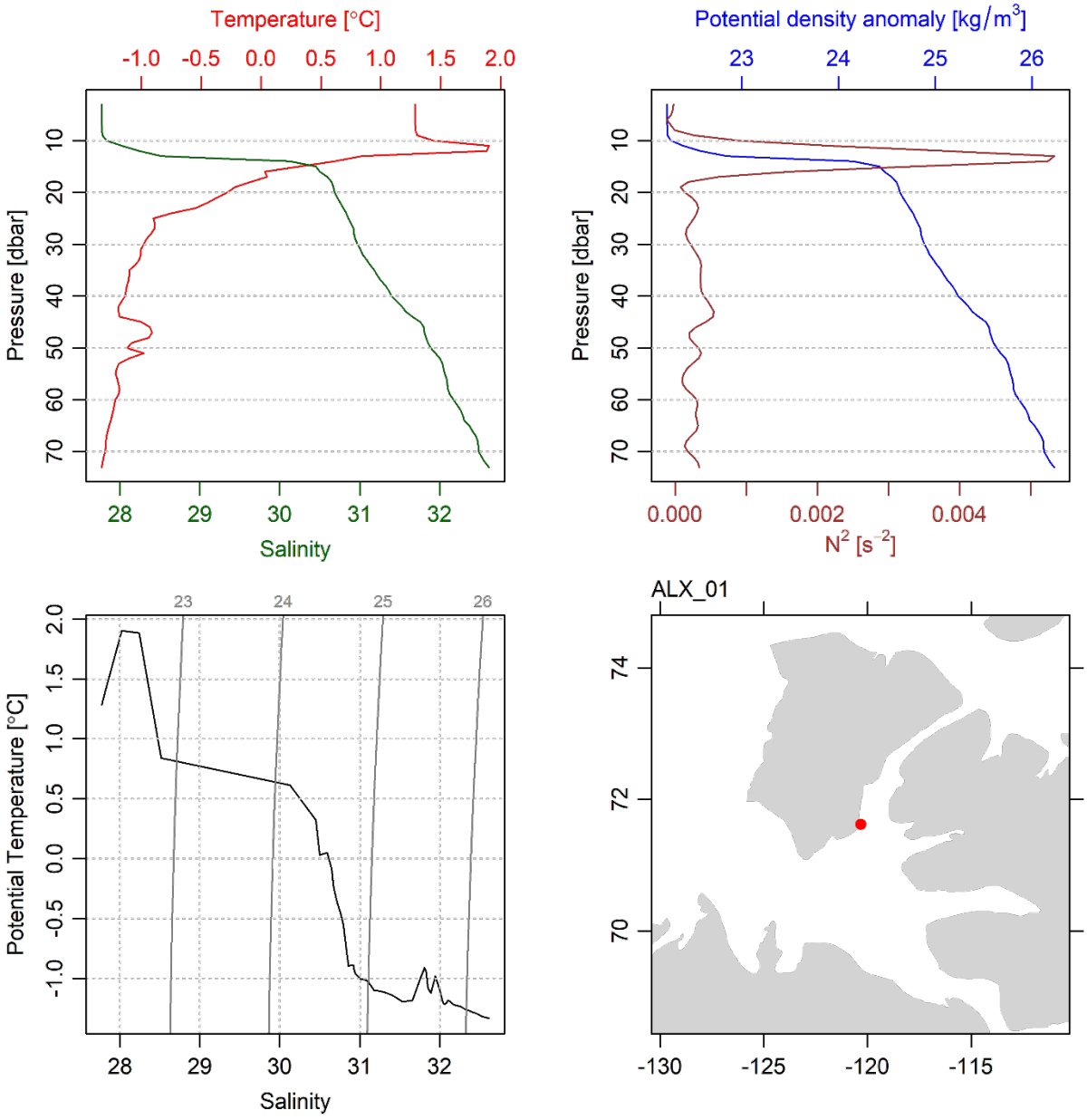

Temperature [°C]
0
2
4
6
Pressure [dbar]
10
20
30
40
50
28
29
30
31
32
Salinity

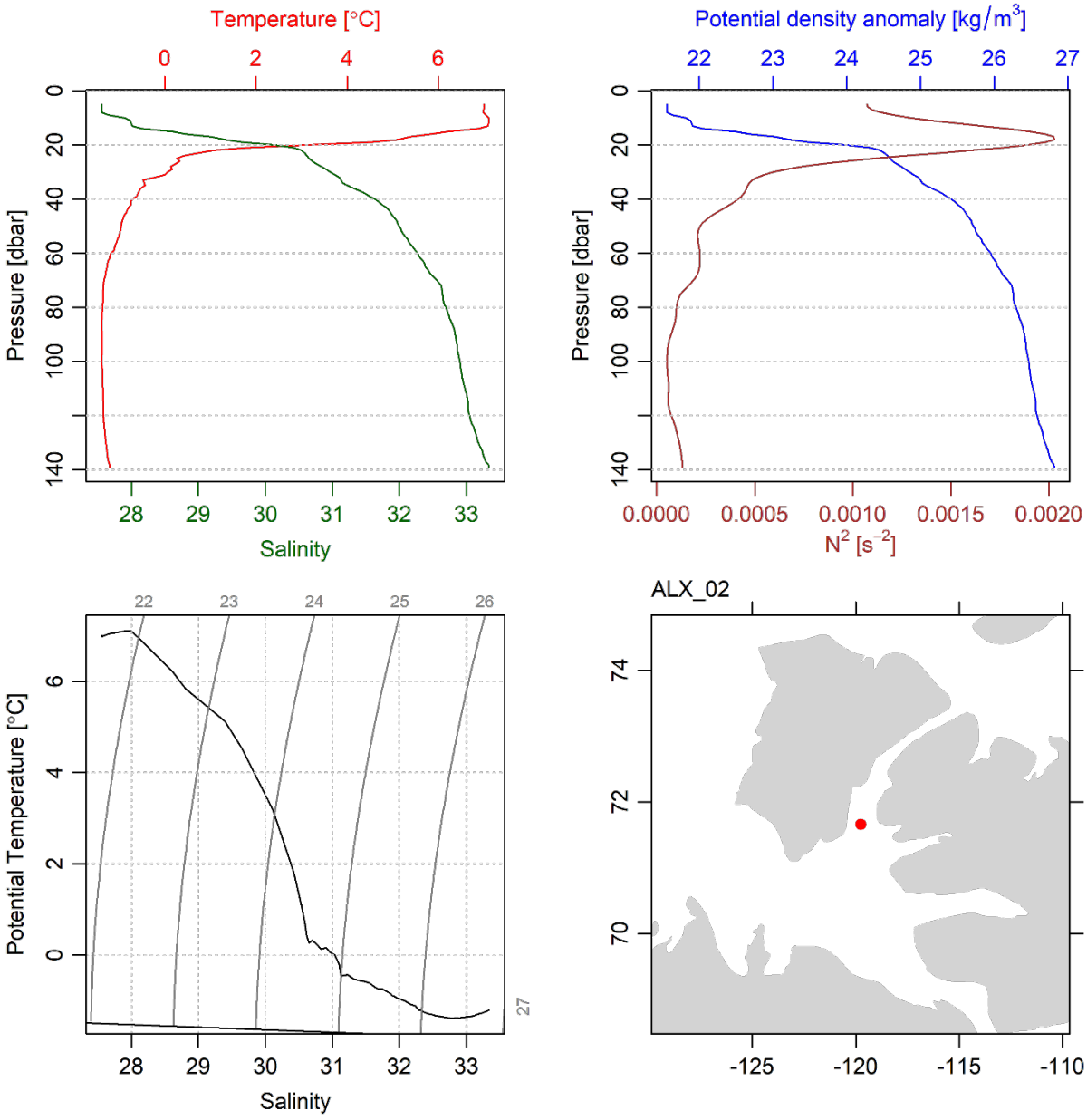

Potential density anomaly [kg/m3]
22
23
24
25
Pressure [dbar]
10
20
30
40
50
0.000
0.001
0.002
0.003
0.004
0.005
N2 [s−2]

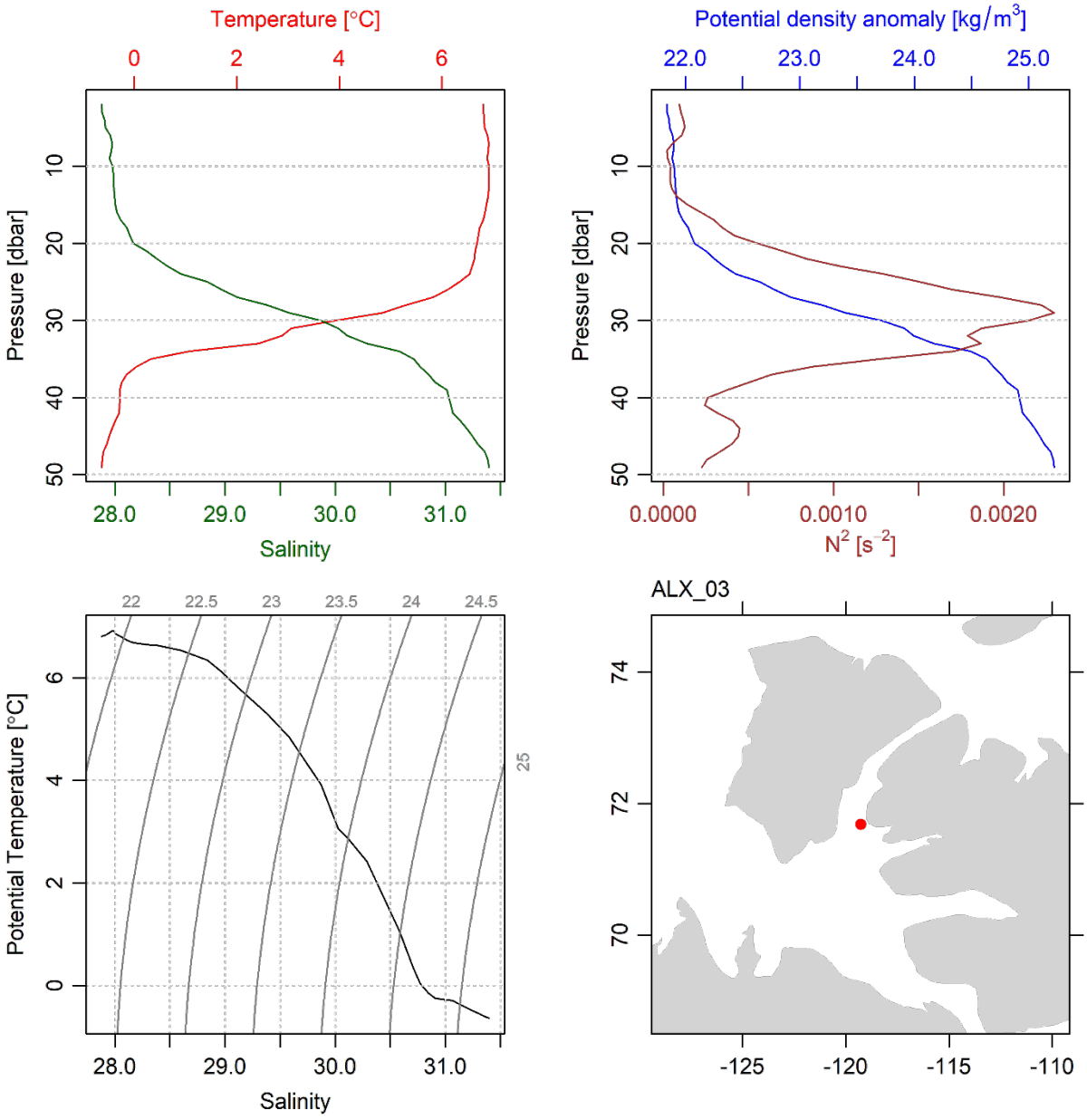

22
23
24
25
Potential Temperature [°C]
0
2
4
6
28
29
30
31
32
Salinity

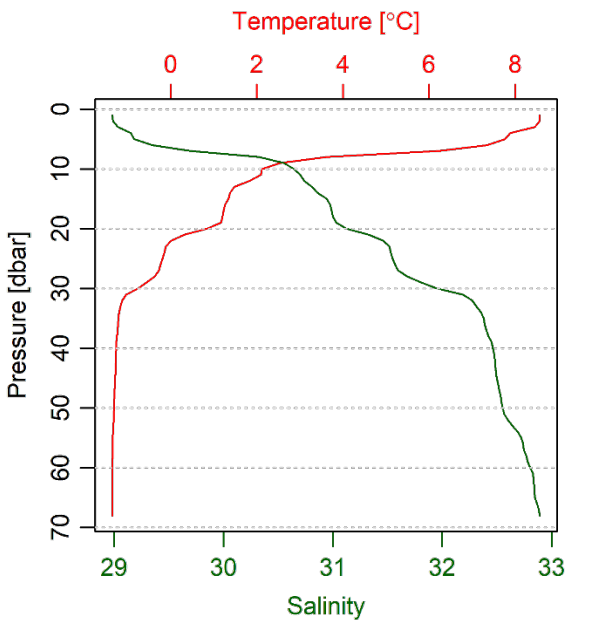

WLK_02
74
72
70
-125
-120
-115
-110

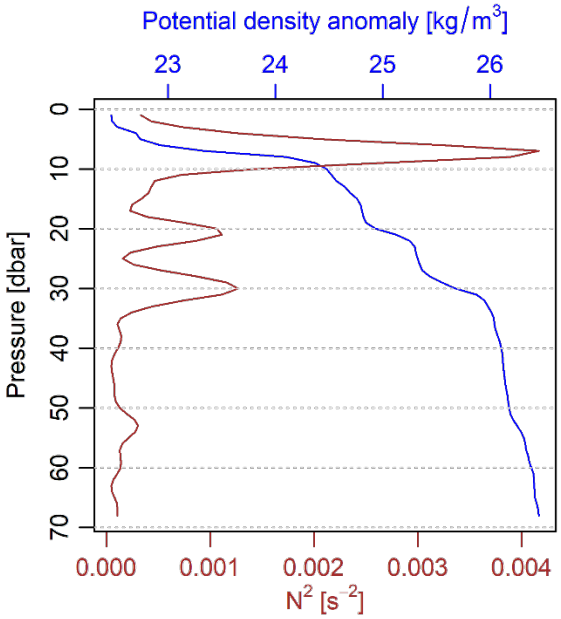

Temperature [°C]
0
2
4
6
8
Pressure [dbar]
10
20
30
40
28
29
30
31
Salinity
Potential density anomaly [kg/m3]
22
23
24
25
0.000
0.001
0.002
0.003
N2 [s−2]
21.5
22
22.5
23
23.5
24
24.5
25
Potential Temperature [°C]
0
2
4
6
8
WLK_03
74
72
70
-125
-120
-115
-110

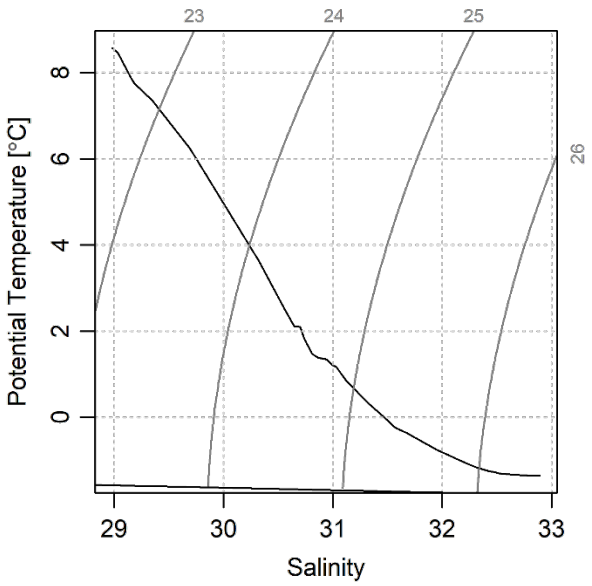

Temperature [°C]
-1.0 -0.5 0.0 0.5 1.0 1.5 2.0
Pressure [dbar]
10 20 30 40 50 60 70
28 29 30 31 32
Salinity
Potential density anomaly [kg/m3]
23 24 25 26
0.000 0.002 0.004
N2 [s-2]
23 24 25 26
Potential Temperature [°C]
2.0 1.5 1.0 0.5 0.0 -0.5 -1.0
ALX_01
74 72 70
-130 -125 -120 -115

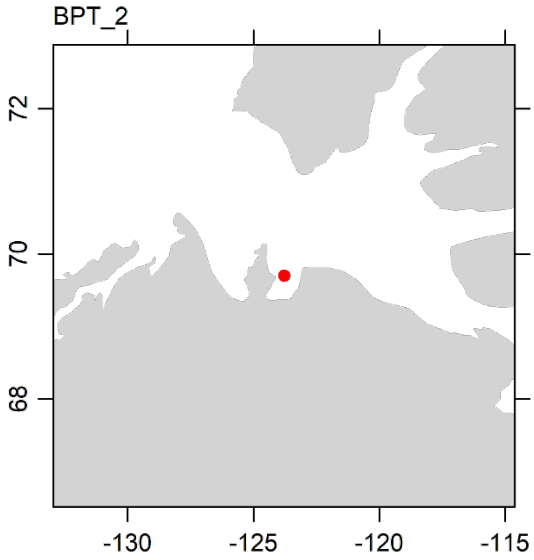

Temperature [°C]
0
2
4
6
Pressure [dbar]
0
20
40
60
80
100
140
28
29
30
31
32
33
Salinity
Potential density anomaly [kg/m3]
22
23
24
25
26
27
0.0000
0.0005
0.0010
0.0015
0.0020
N2 [s−2]
Potential Temperature [°C]
ALX_02
74
72
70
-125
-120
-115
-110

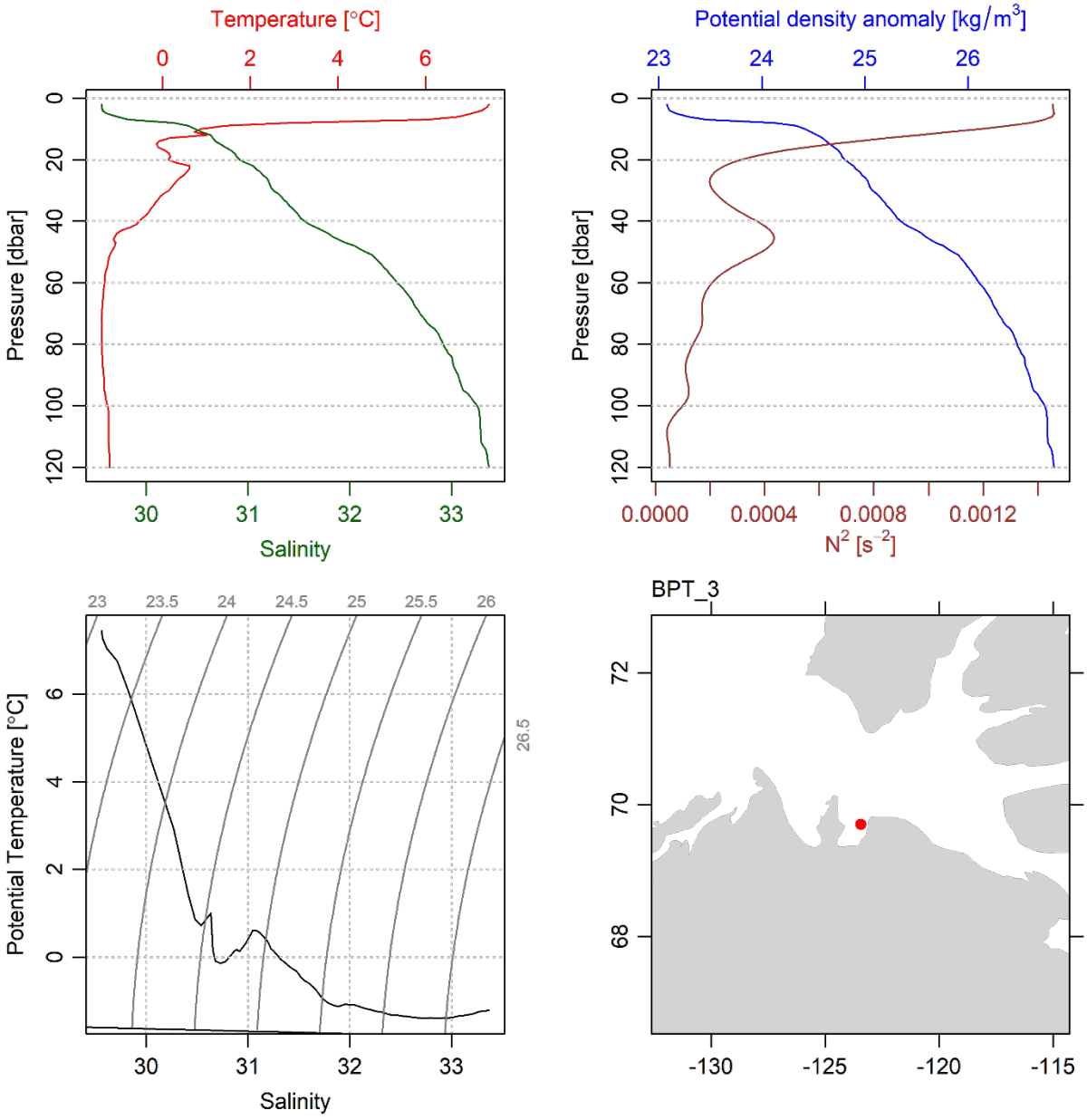

Temperature [°C]
0
2
4
6
Pressure [dbar]
10
20
30
40
50
28.0
29.0
30.0
31.0
Salinity
Potential density anomaly [kg/m3]
22.0
23.0
24.0
25.0
0.0000
0.0010
0.0020
N2 [s−2]
Potential Temperature [°C]
22
22.5
23
23.5
24
24.5
25
0
2
4
6
ALX_03
74
72
70
-125
-120
-115
-110

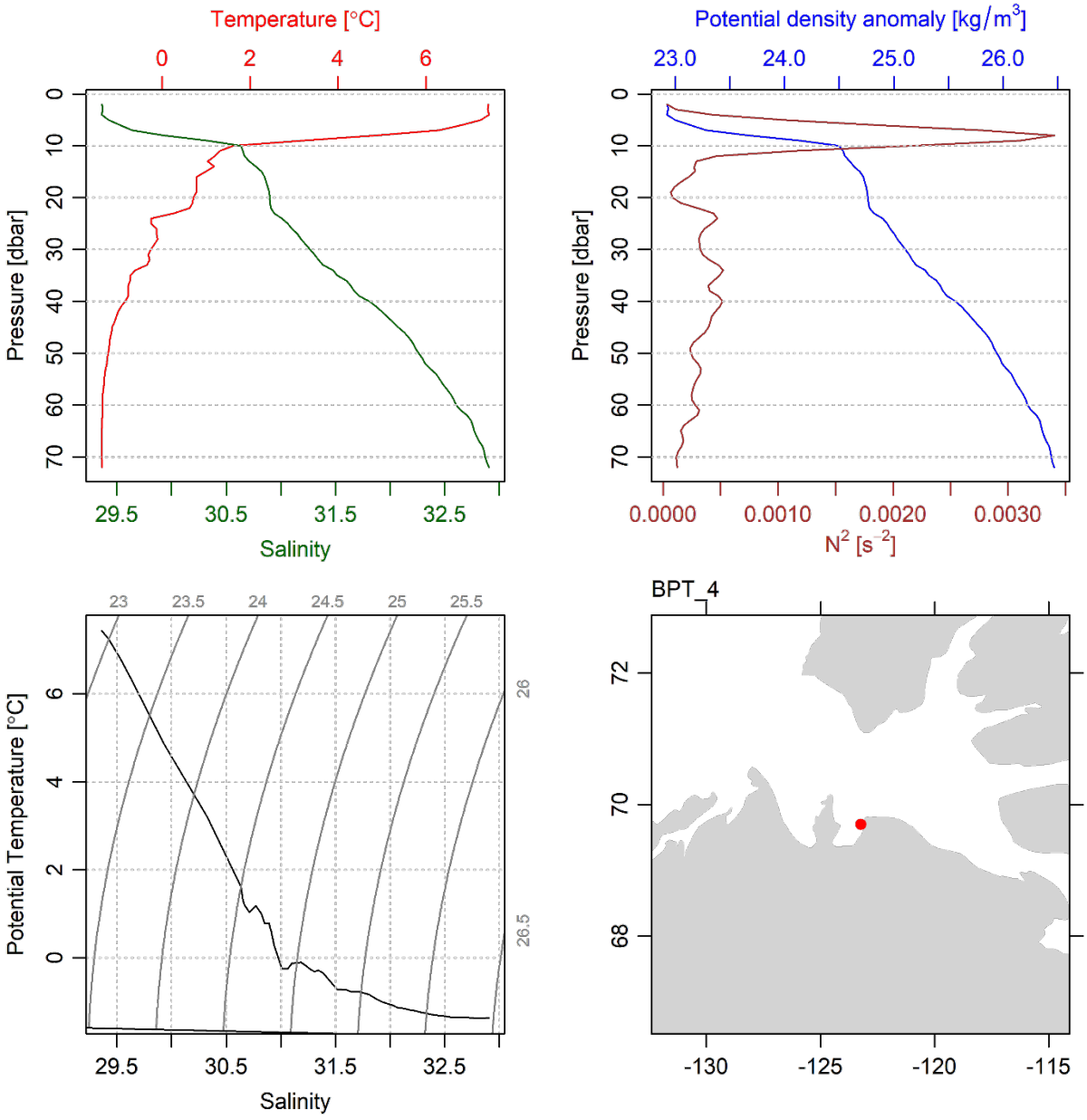

Temperature [°C]
0
2
4
6
8
Pressure [dbar]
0
10
20
30
40
50
60
70
29
30
31
32
33
Salinity

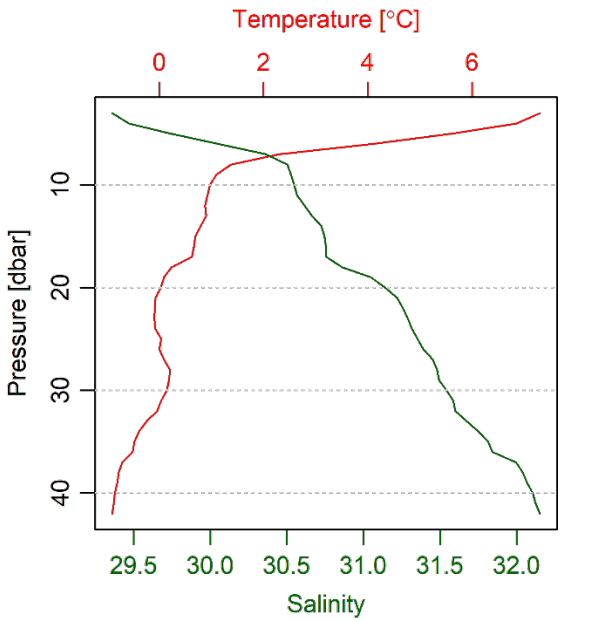

Potential density anomaly [kg/m3]
23
24
25
26
Pressure [dbar]
0
10
20
30
40
50
60
70
0.000
0.001
0.002
0.003
0.004
N2 [s−2]

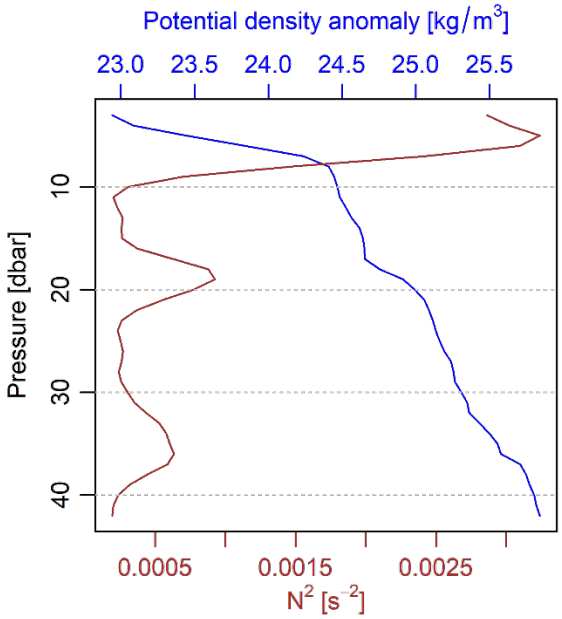

23
24
25
26
Potential Temperature [°C]
0
2
4
6
8
29
30
31
32
33
Salinity

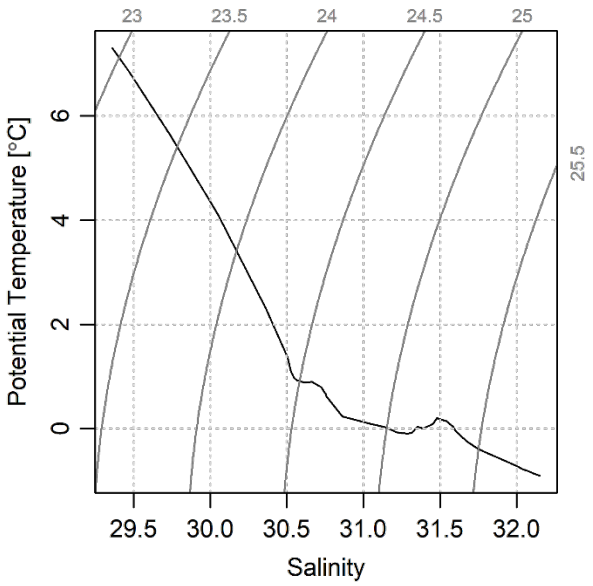

BPT_2
72
70
68
-130
-125
-120
-115

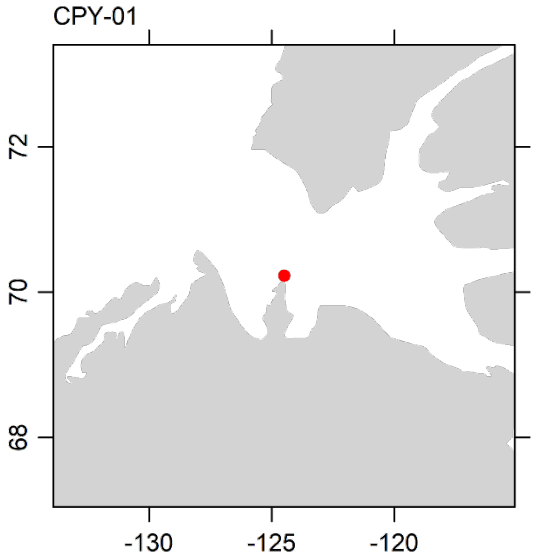

Temperature [°C]
0
2
4
6
Pressure [dbar]
0
20
40
60
80
100
120
30
31
32
33
Salinity
Potential density anomaly [kg/m3]
23
24
25
26
0.0000
0.0004
0.0008
0.0012
N2 [s−2]
Potential Temperature [°C]
23
23.5
24
24.5
25
25.5
26
26.5
BPT_3
72
70
68
-130
-125
-120
-115

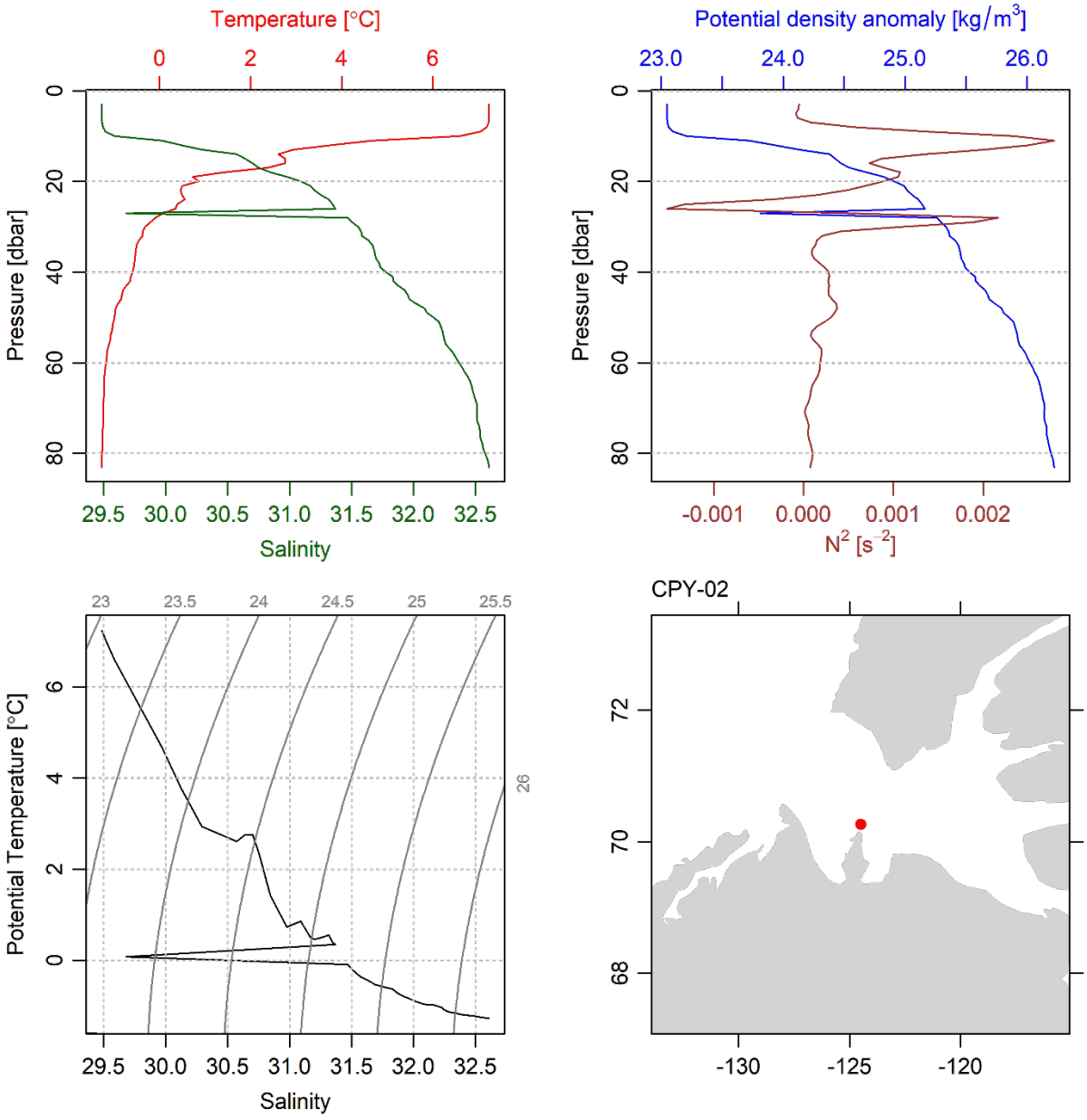

Temperature [°C]
0
2
4
6
Pressure [dbar]
0
10
20
30
40
50
60
70
29.5
30.5
31.5
32.5
Salinity
Potential density anomaly [kg/m3]
23.0
24.0
25.0
26.0
0.0000
0.0010
0.0020
0.0030
N2 [s−2]
23
23.5
24
24.5
25
25.5
Potential Temperature [°C]
26
26.5
BPT_4
72
70
68
-130
-125
-120
-115

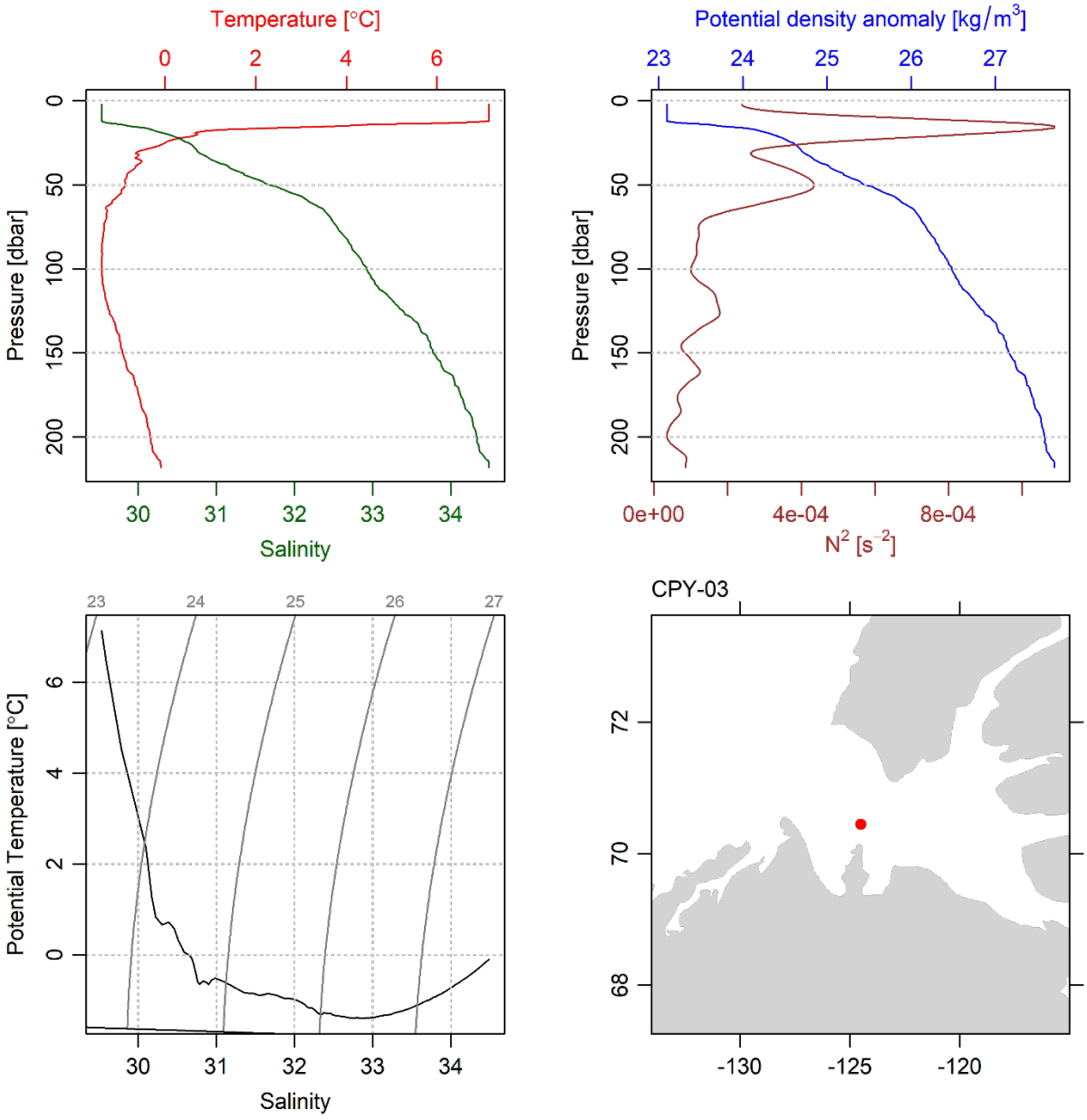

Temperature [°C]
0
2
4
6
Pressure [dbar]
10
20
30
40
29.5
30.0
30.5
31.0
31.5
32.0
Salinity

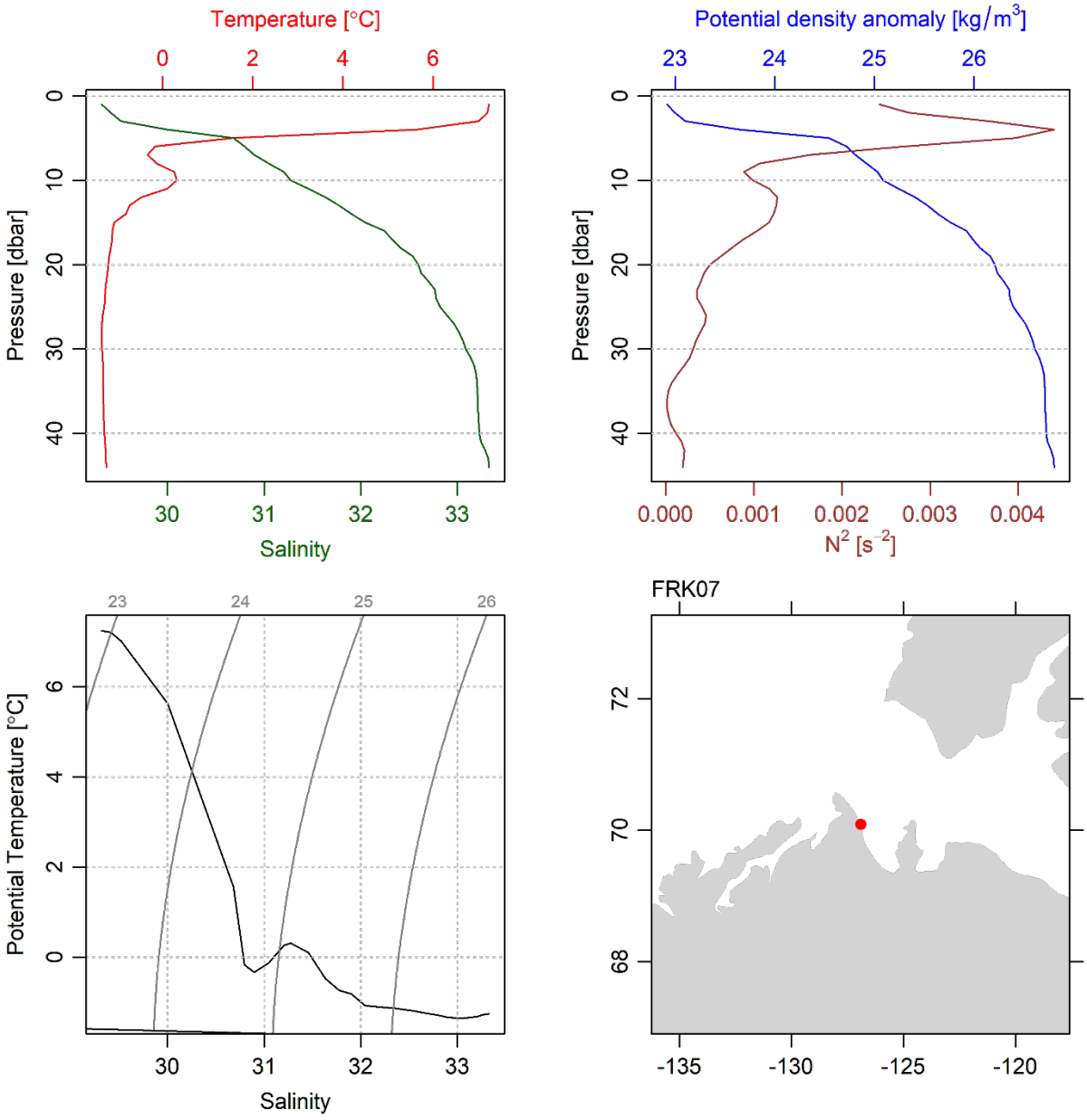

Potential density anomaly [kg/m3]
23.0
23.5
24.0
24.5
25.0
25.5
Pressure [dbar]
10
20
30
40
0.0005
0.0015
0.0025
N2 [s−2]

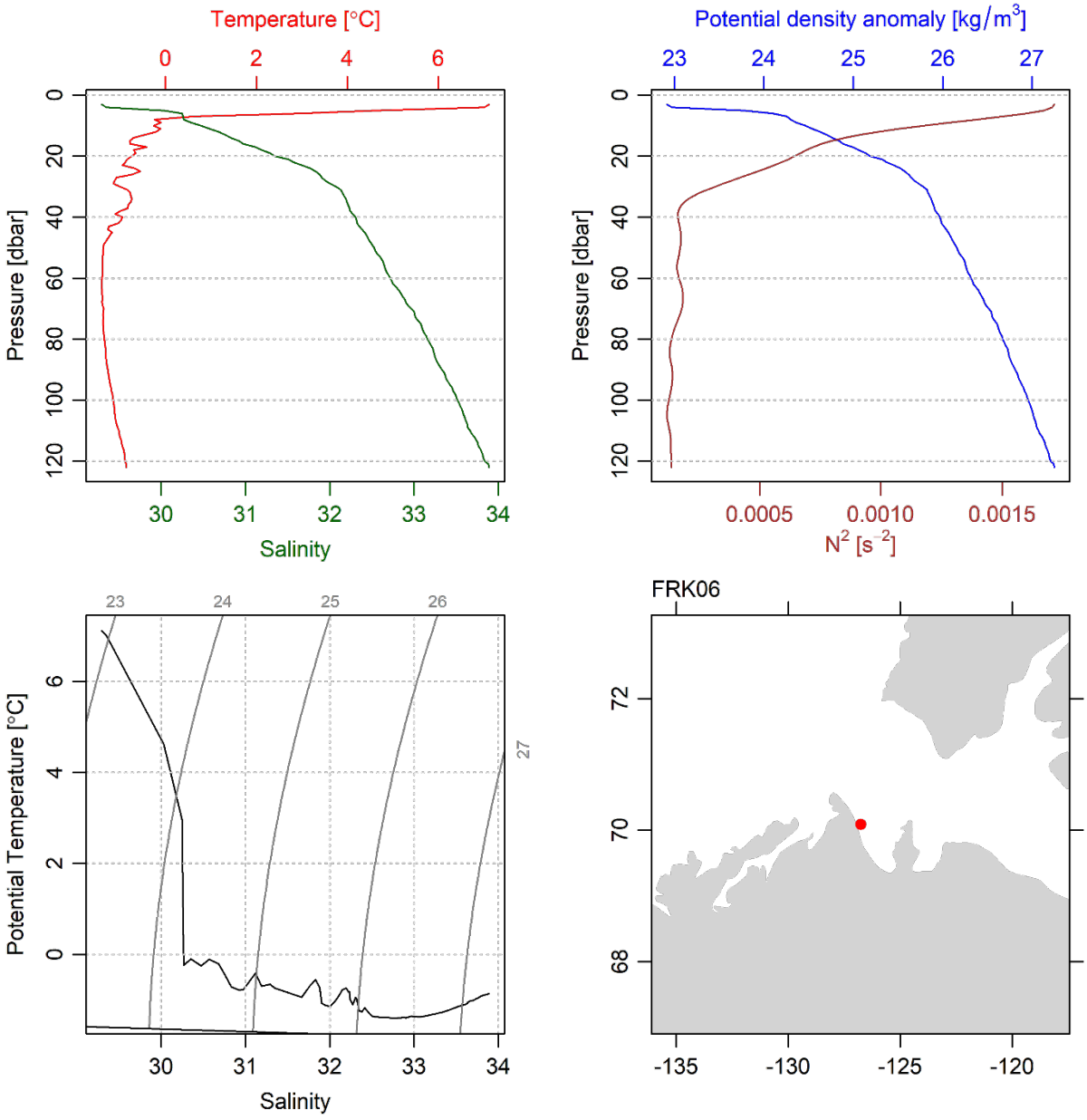

23
23.5
24
24.5
25
25.5
Potential Temperature [°C]
0
2
4
6
29.5
30.0
30.5
31.0
31.5
32.0
Salinity

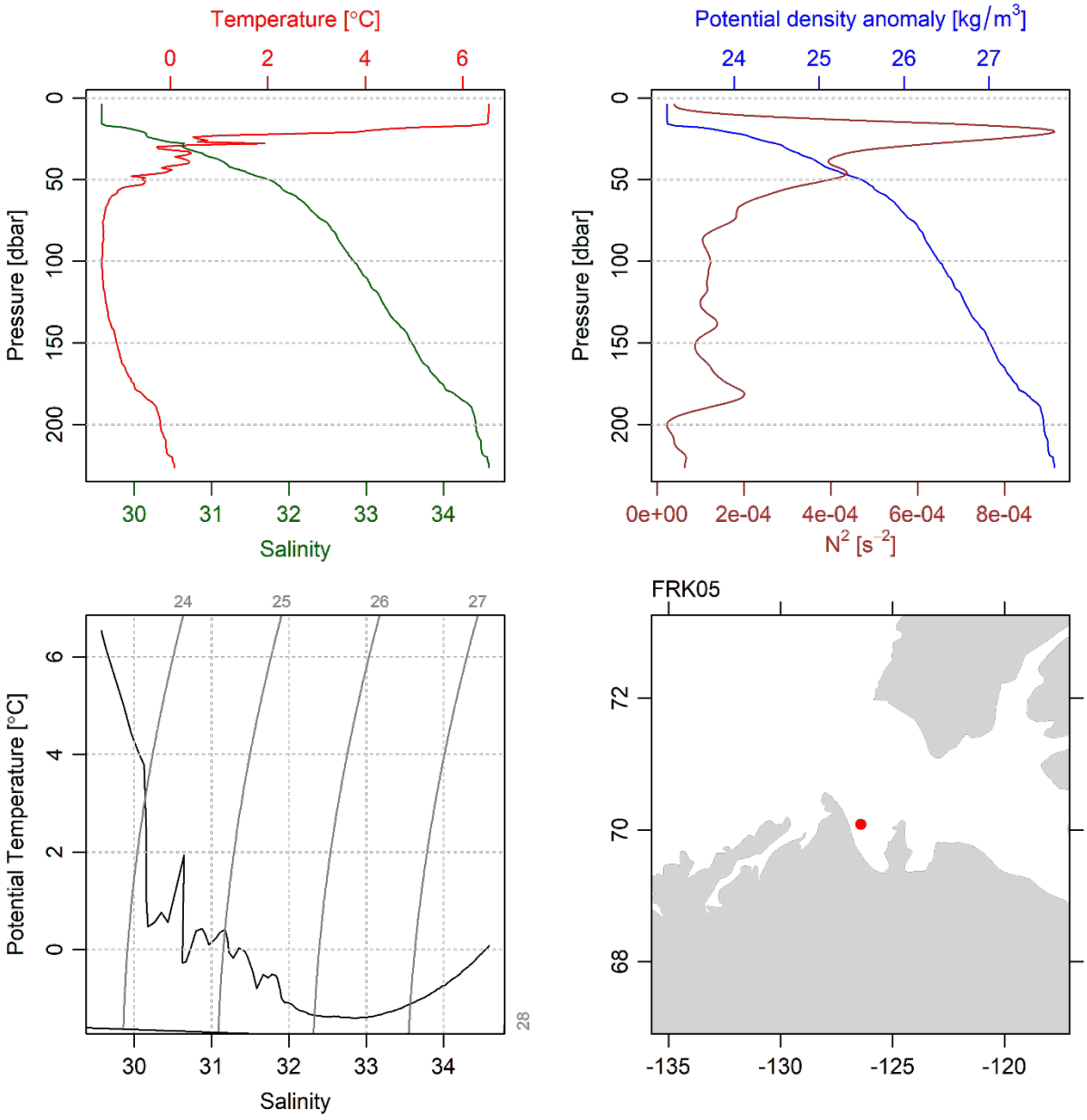

CPY-01
72
70
68
-130
-125
-120

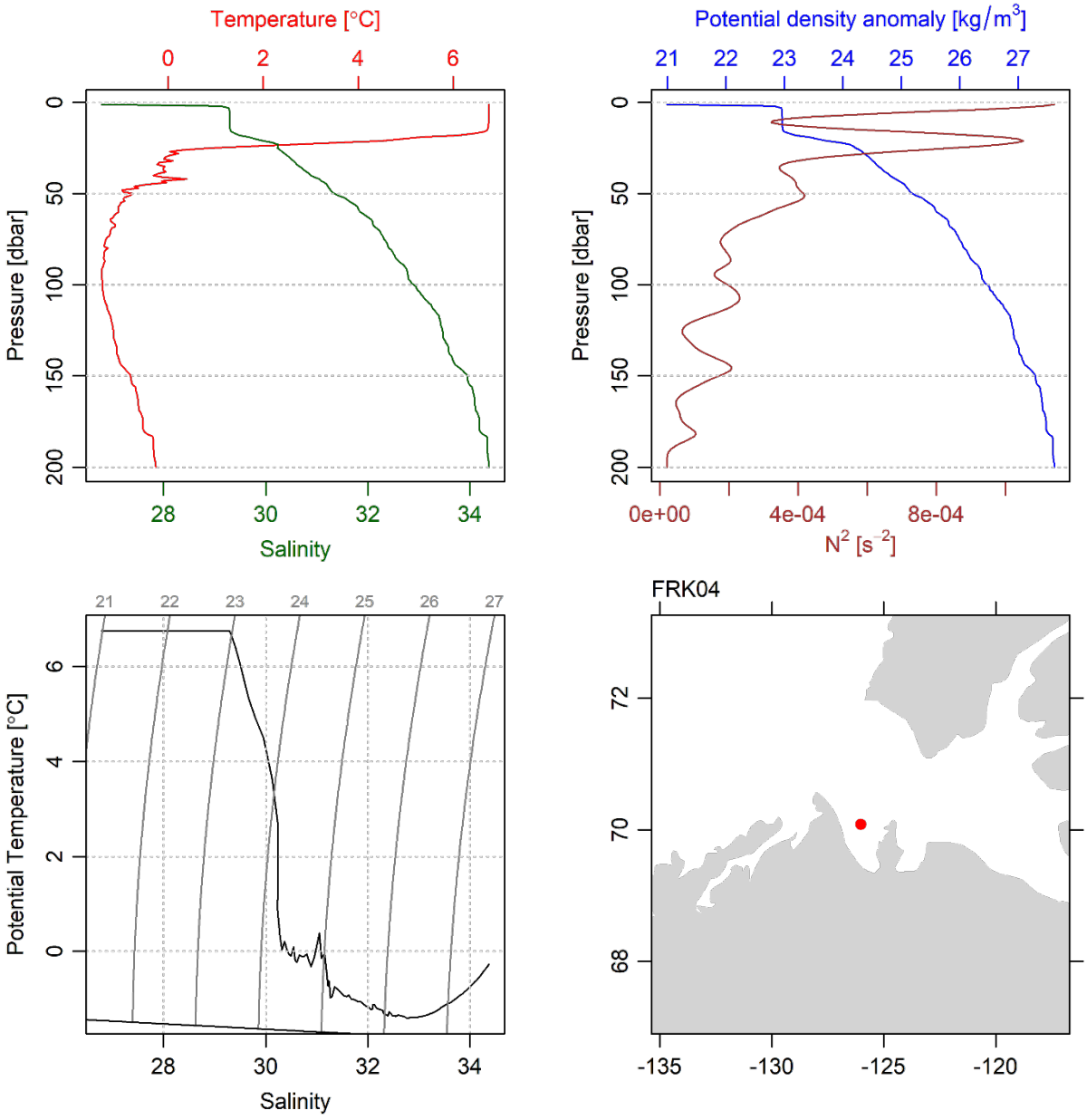

Temperature [°C]
0
2
4
6
Pressure [dbar]
0
20
40
60
80
29.5
30.0
30.5
31.0
31.5
32.0
32.5
Salinity
Potential density anomaly [kg/m3]
23.0
24.0
25.0
26.0
-0.001
0.000
0.001
0.002
N2 [s−2]
Potential Temperature [°C]
23
23.5
24
24.5
25
25.5
26
CPY-02
72
70
68
-130
-125
-120

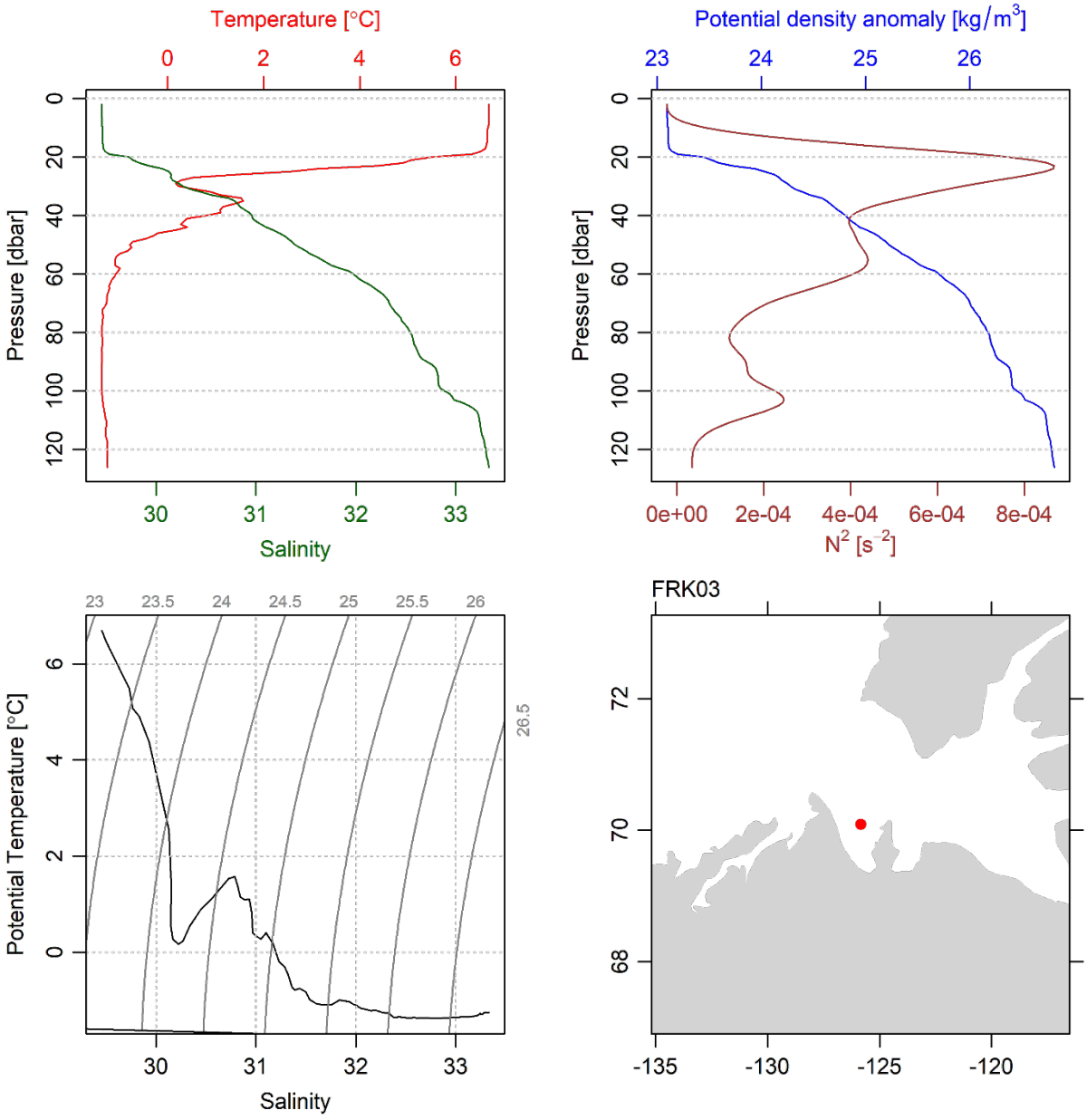

Temperature [°C]
0
2
4
6
Pressure [dbar]
0
50
100
150
200
30
31
32
33
34
Salinity
Potential density anomaly [kg/m3]
23
24
25
26
27
0e+00
4e-04
8e-04
N2 [s−2]
Potential Temperature [°C]
CPY-03
72
70
68
-130
-125
-120

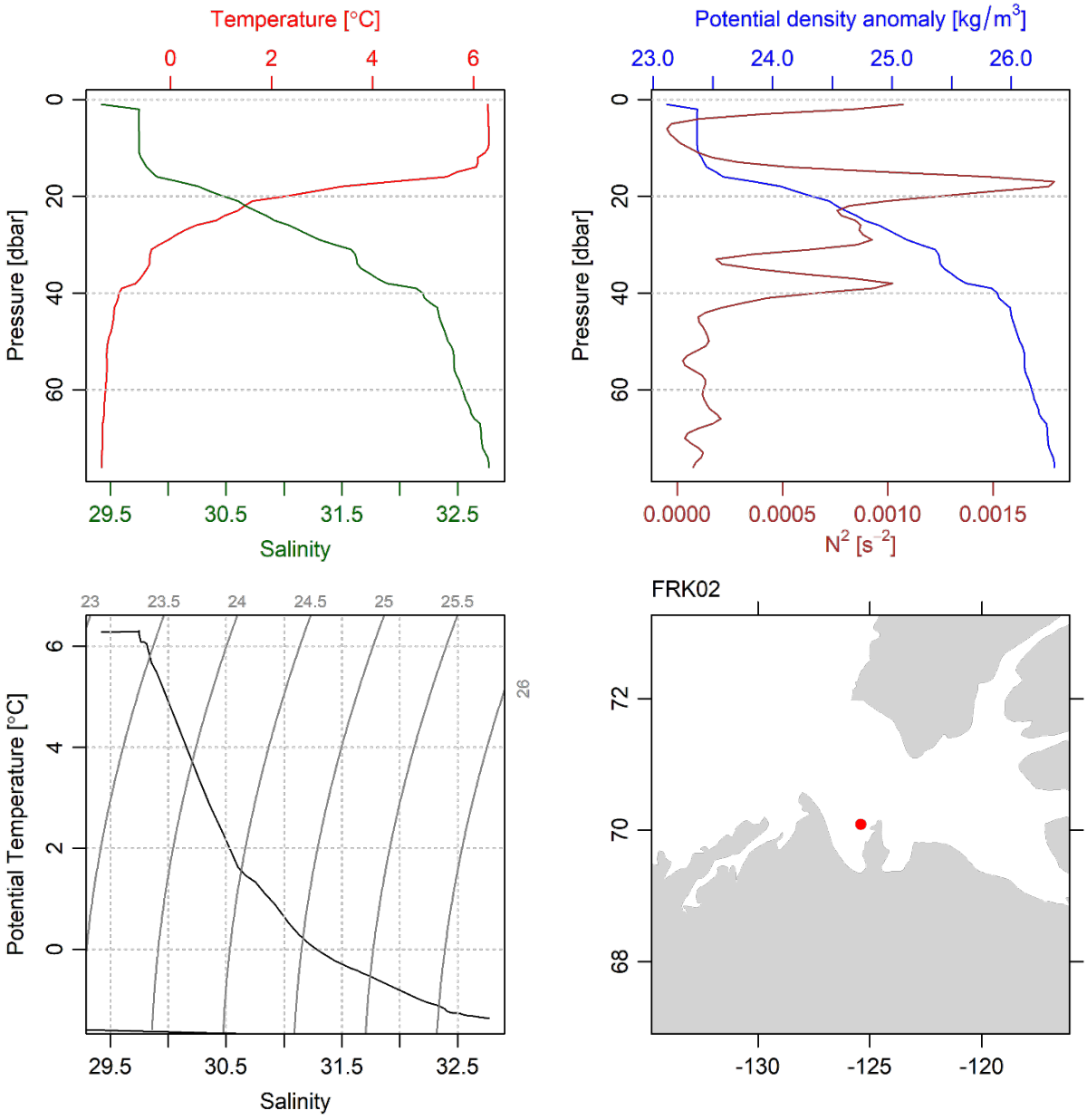

Temperature [°C]
0
2
4
6
Pressure [dbar]
0
10
20
30
40
30
31
32
33
Salinity
Potential density anomaly [kg/m3]
23
24
25
26
0.000
0.001
0.002
0.003
0.004
N2 [s−2]
Potential Temperature [°C]
FRK07
72
70
68
-135
-130
-125
-120

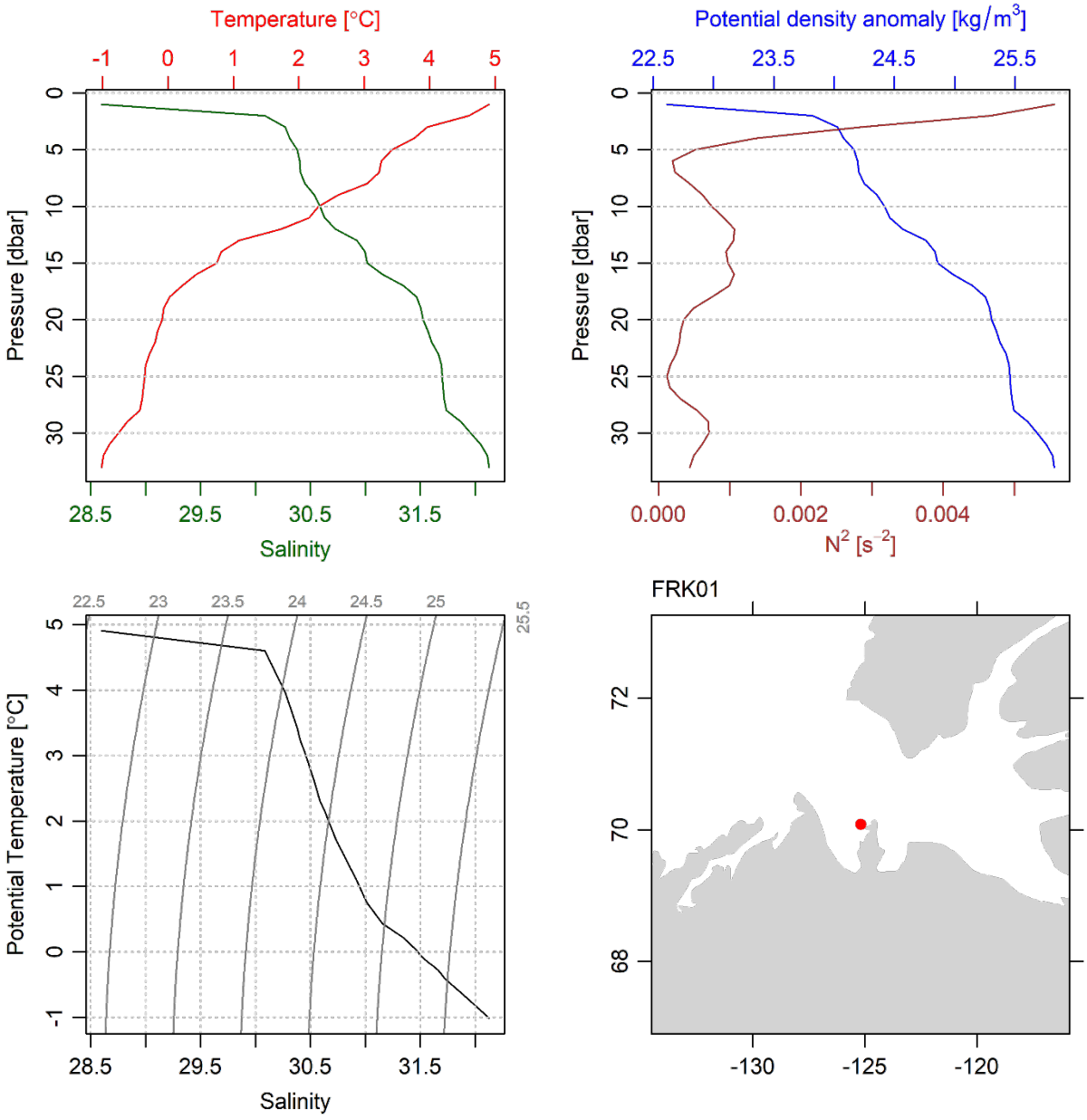

Temperature [°C]
0
2
4
6
Pressure [dbar]
0
20
40
60
80
100
120
30
31
32
33
34
Salinity
Potential density anomaly [kg/m3]
23
24
25
26
27
0.0005
0.0010
0.0015
N2 [s−2]
Potential Temperature [°C]
23
24
25
26
27
FRK06
72
70
68
-135
-130
-125
-120

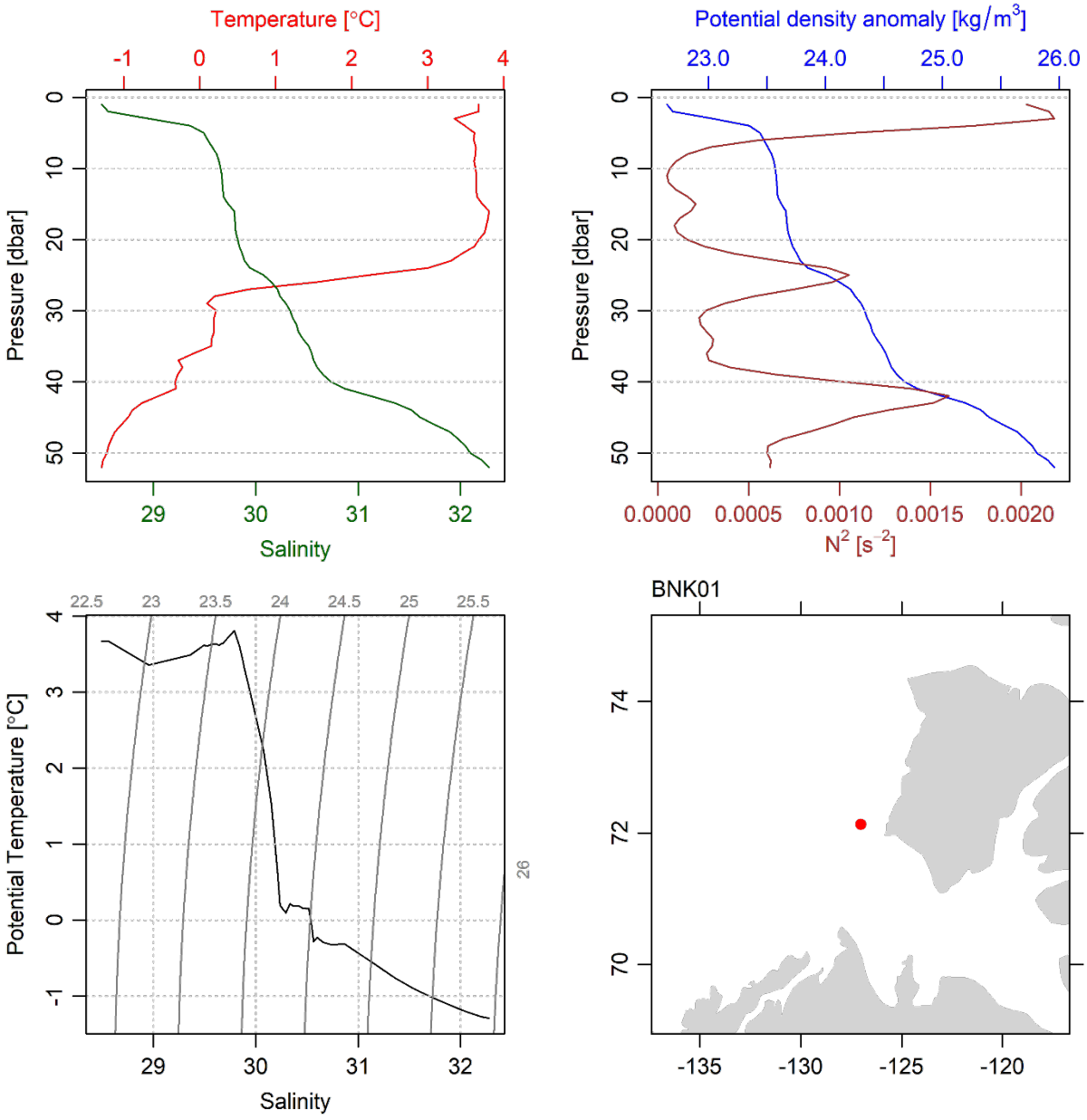

Temperature [°C]
0
2
4
6
Pressure [dbar]
0
50
100
150
200
30
31
32
33
34
Salinity
Potential density anomaly [kg/m3]
24
25
26
27
0e+00
2e-04
4e-04
6e-04
8e-04
N2 [s−2]
Potential Temperature [°C]
28
FRK05
72
70
68
-135
-130
-125
-120

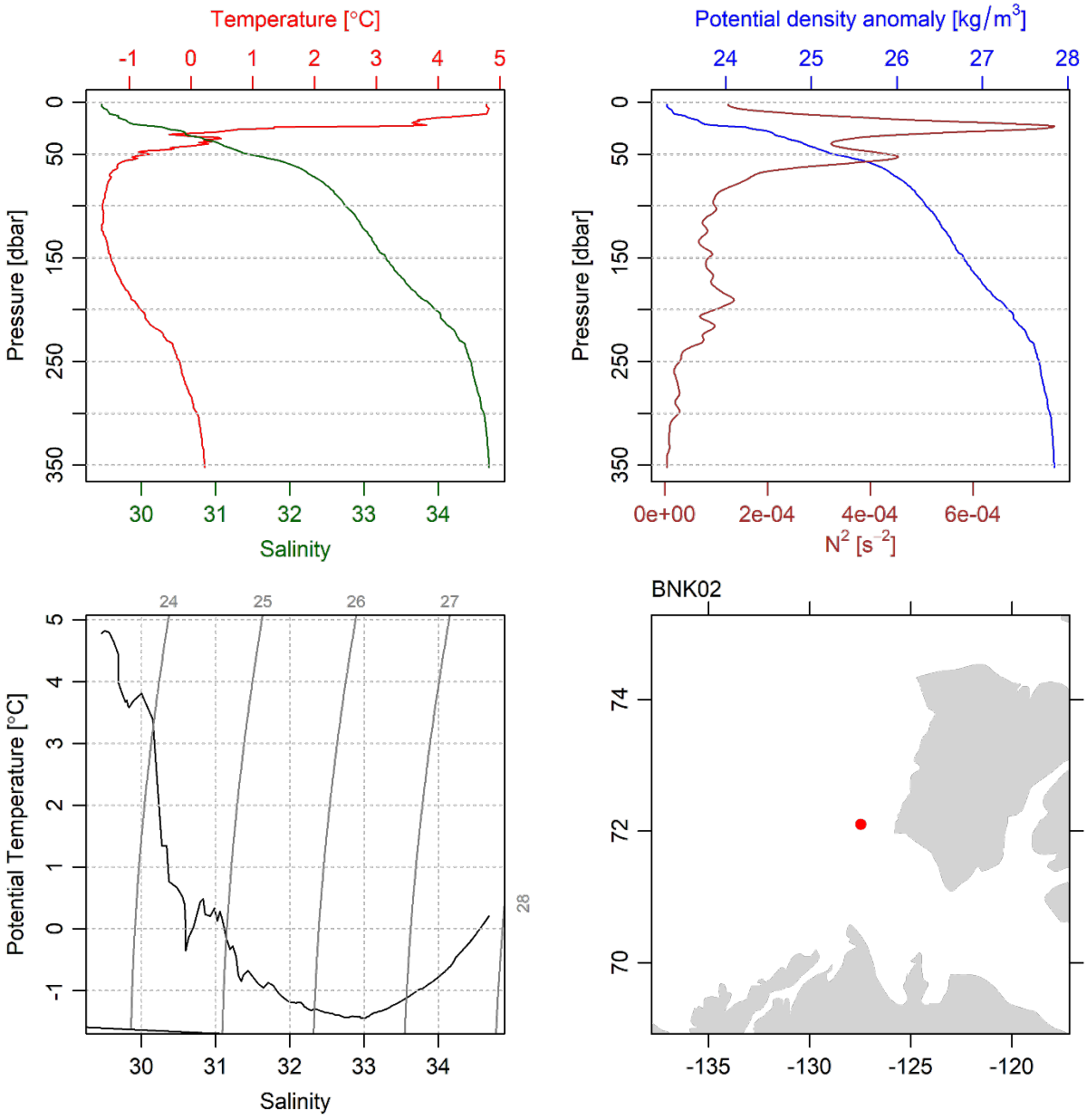

Temperature [°C]
0
2
4
6
Pressure [dbar]
0
50
100
150
200
28
30
32
34
Salinity
Potential density anomaly [kg/m3]
21
22
23
24
25
26
27
0e+00
4e-04
8e-04
N2 [s−2]
Potential Temperature [°C]
FRK04
72
70
68
-135
-130
-125
-120

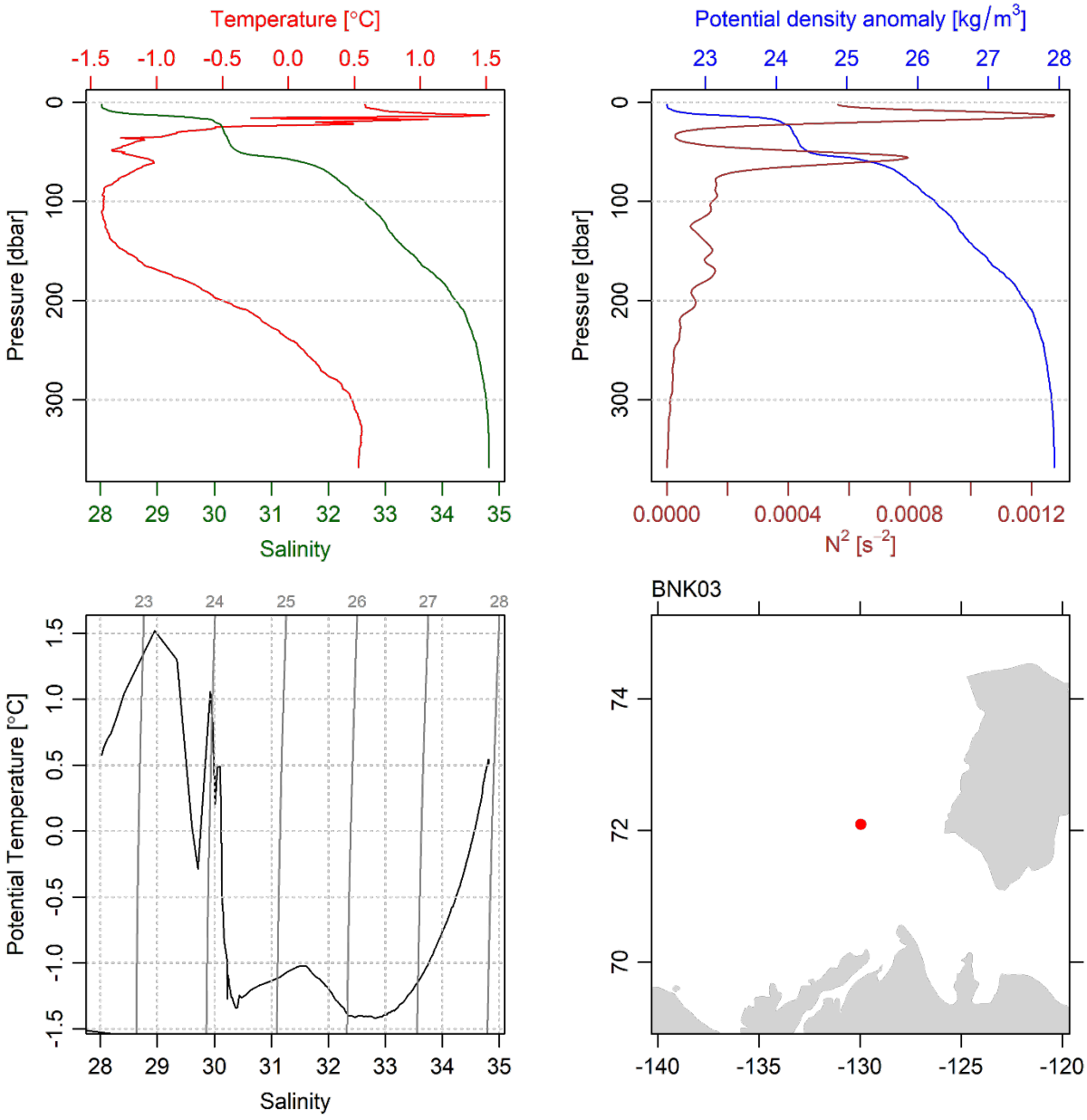

Temperature [°C]
0
2
4
6
Pressure [dbar]
0
20
40
60
80
100
120
30
31
32
33
Salinity
Potential density anomaly [kg/m3]
23
24
25
26
0e+00
2e-04
4e-04
6e-04
8e-04
N2 [s−2]
Potential Temperature [°C]
23
23.5
24
24.5
25
25.5
26
26.5
FRK03
72
70
68
-135
-130
-125
-120

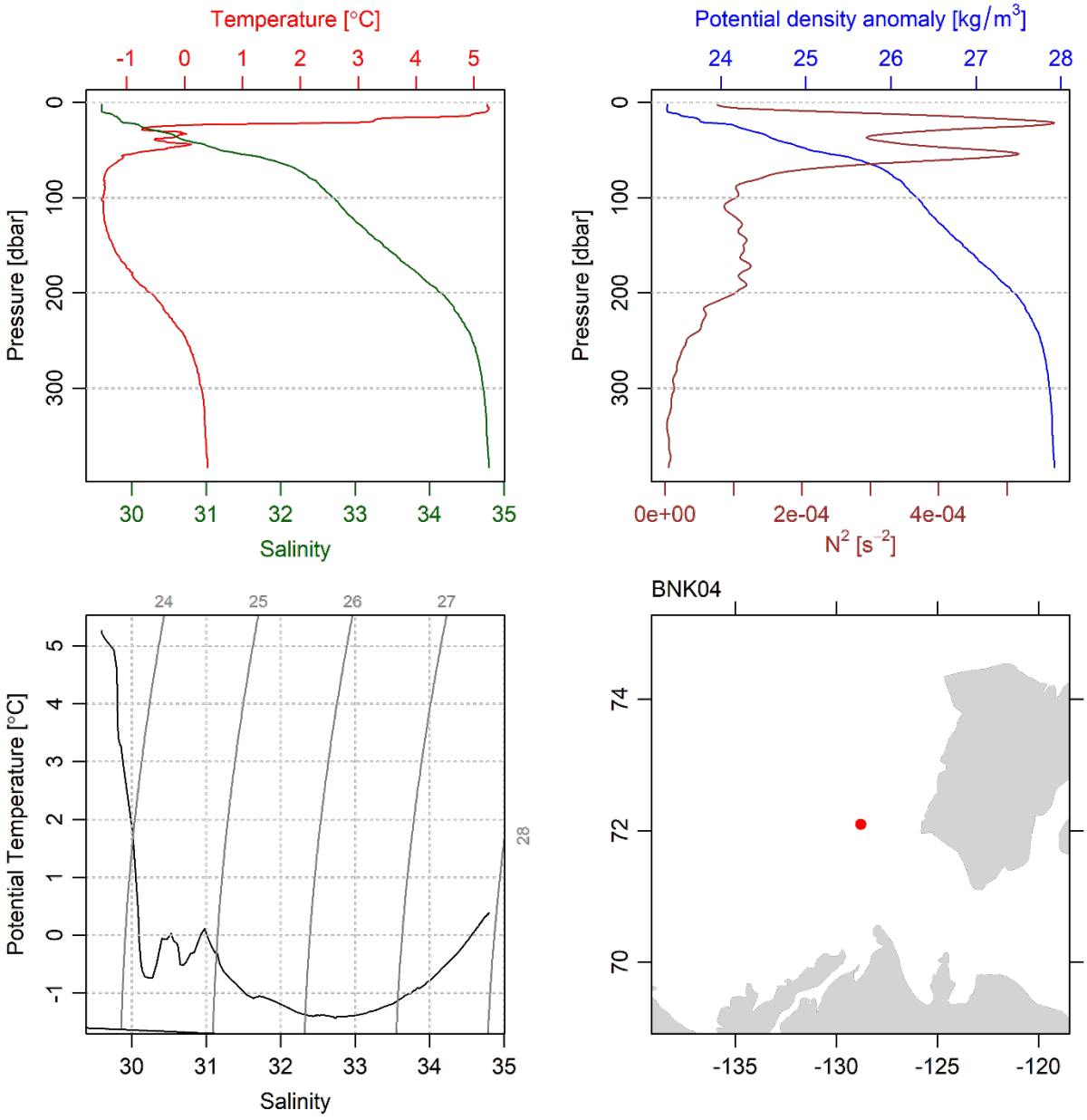

Temperature [°C]
0
2
4
6
Pressure [dbar]
0
20
40
60
29.5
30.5
31.5
32.5
Salinity
Potential density anomaly [kg/m3]
23.0
24.0
25.0
26.0
0.0000
0.0005
0.0010
0.0015
N2 [s−2]
23
23.5
24
24.5
25
25.5
26
Potential Temperature [°C]
FRK02
72
70
68
-130
-125
-120

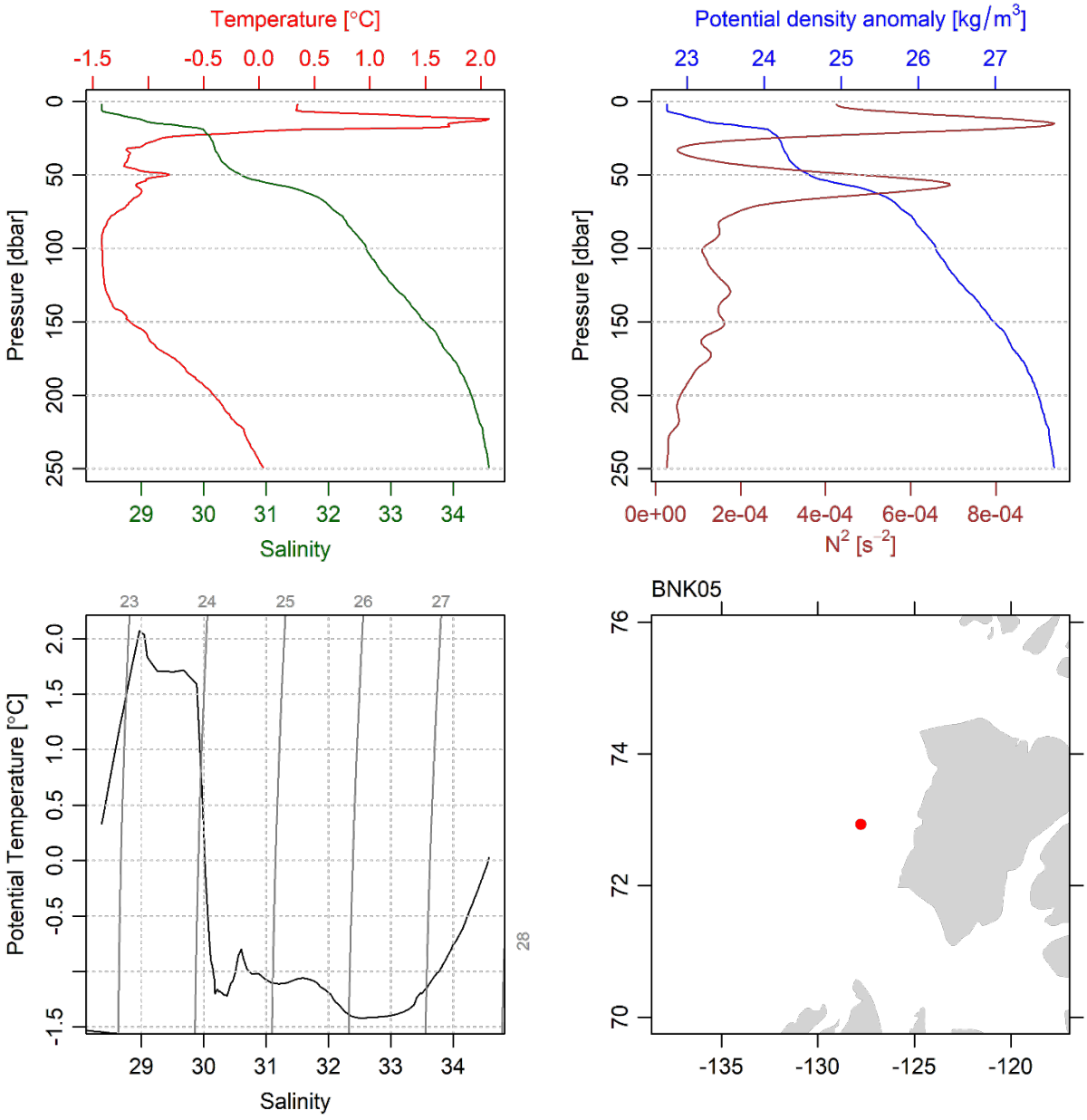

Temperature [°C]
-1
0
1
2
3
4
5
Pressure [dbar]
0
5
10
15
20
25
30
28.5
29.5
30.5
31.5
Salinity
Potential density anomaly [kg/m3]
22.5
23.5
24.5
25.5
0.000
0.002
0.004
N2 [s−2]
Potential Temperature [°C]
22.5
23
23.5
24
24.5
25
25.5
FRK01
72
70
68
-130
-125
-120

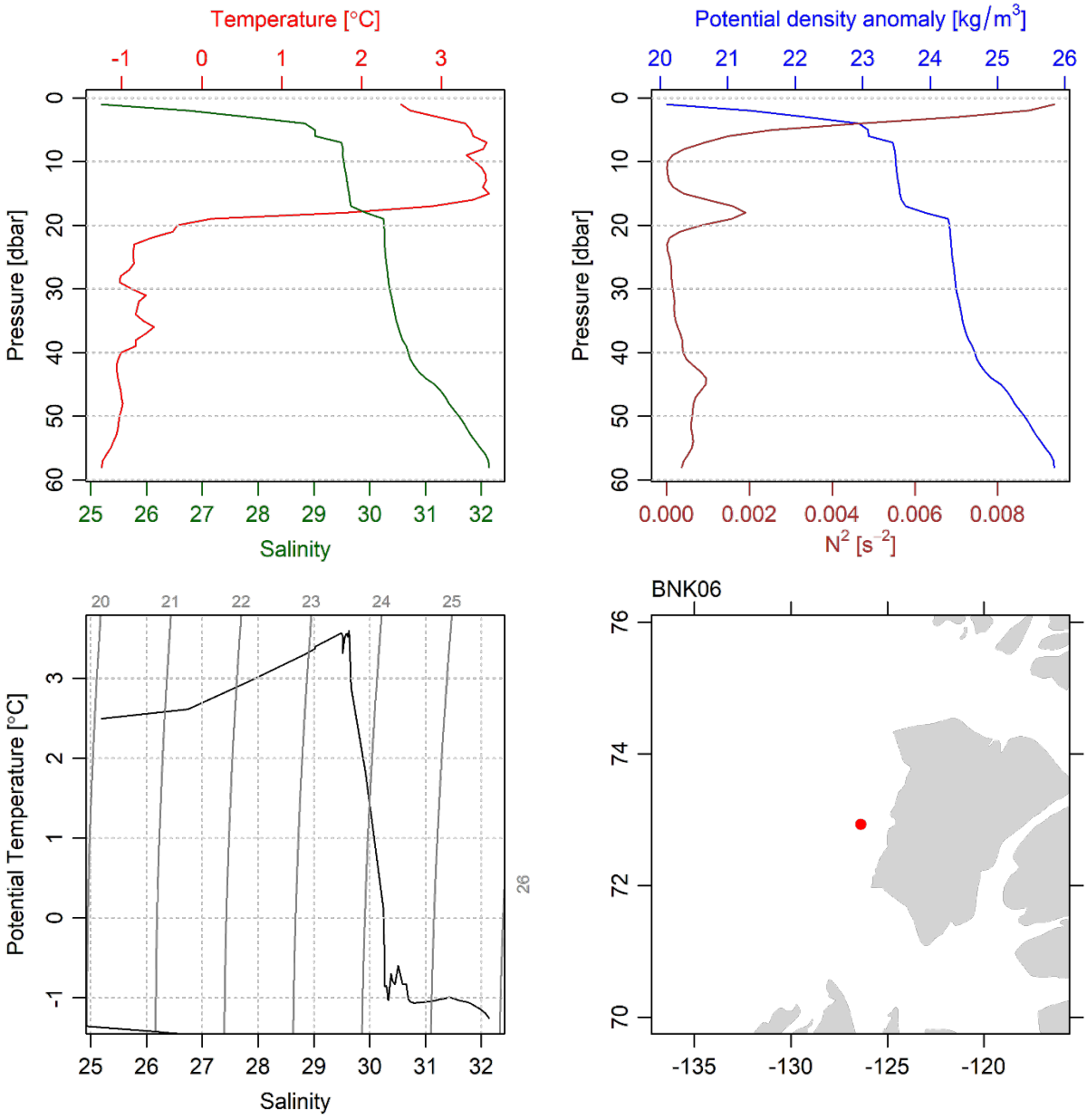

Temperature [°C]
-1
0
1
2
3
4
Pressure [dbar]
0
10
20
30
40
50
29
30
31
32
Salinity
Potential density anomaly [kg/m3]
23.0
24.0
25.0
26.0
0.0000
0.0005
0.0010
0.0015
0.0020
N2 [s−2]
22.5
23
23.5
24
24.5
25
25.5
Potential Temperature [°C]
26
BNK01
74
72
70
-135
-130
-125
-120

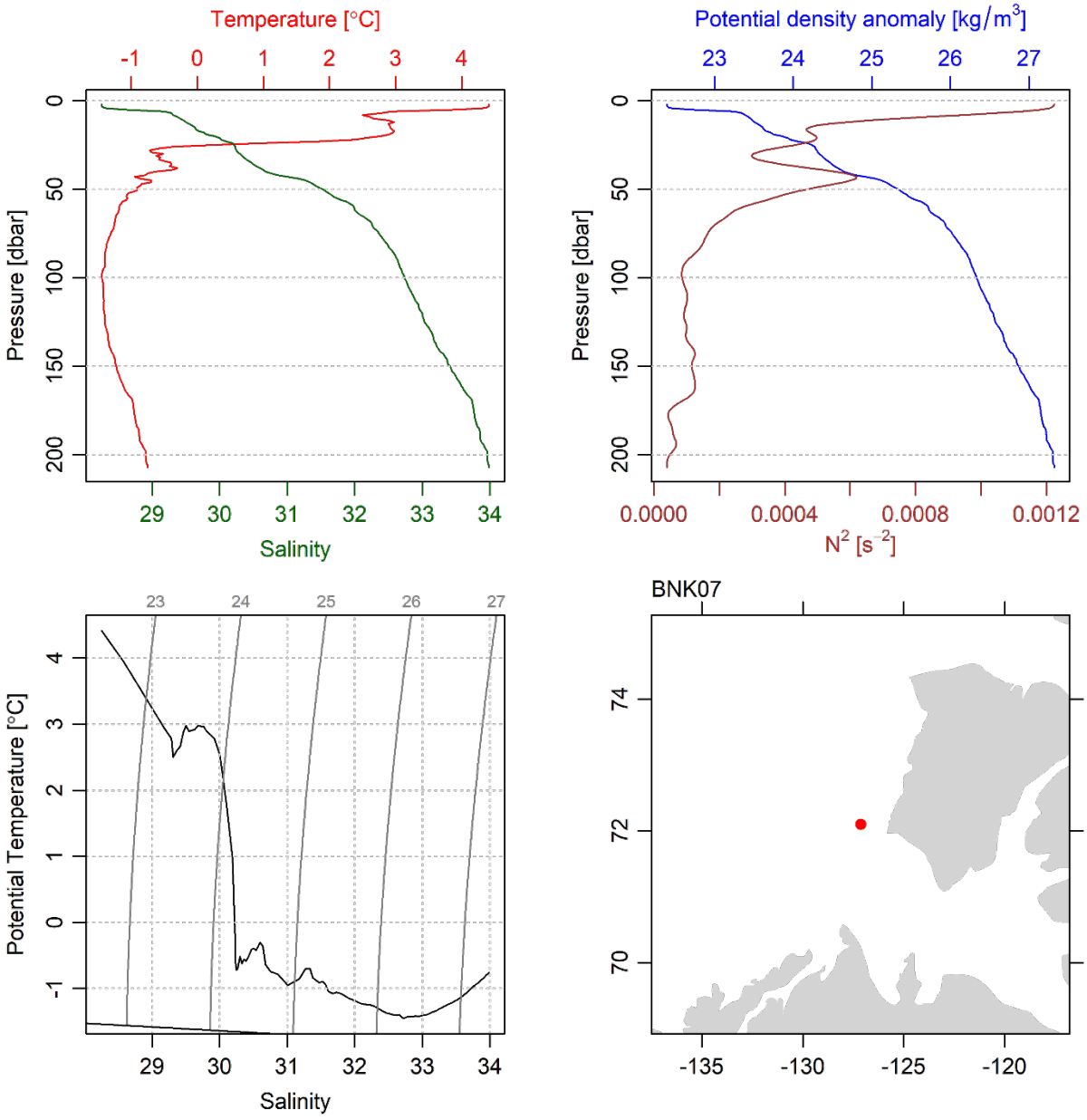

Temperature [°C]
-1 0 1 2 3 4 5
Pressure [dbar]
0 50 150 250 350
30 31 32 33 34
Salinity
Potential density anomaly [kg/m3]
24 25 26 27 28
0e+00 2e-04 4e-04 6e-04
N2 [s−2]
Potential Temperature [°C]
24 25 26 27
28
BNK02
74 72 70
-135 -130 -125 -120

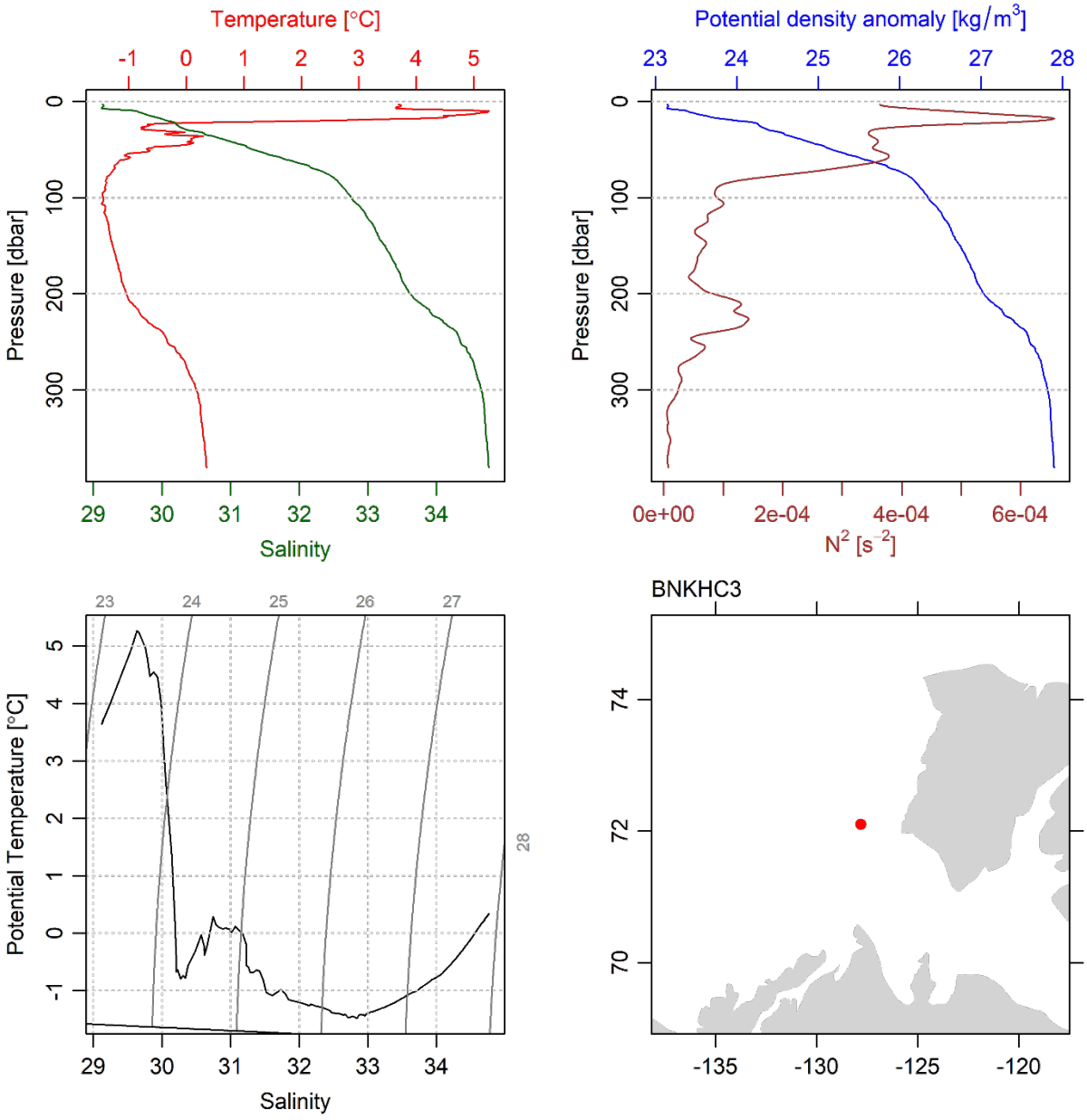

Temperature [°C]
-1.5 -1.0 -0.5 0.0 0.5 1.0 1.5
Pressure [dbar]
0 100 200 300
28 29 30 31 32 33 34 35
Salinity
Potential density anomaly [kg/m3]
23 24 25 26 27 28
0.0000 0.0004 0.0008 0.0012
N2 [s−2]
Potential Temperature [°C]
23 24 25 26 27 28
-1.5 -1.0 -0.5 0.0 0.5 1.0 1.5
BNK03
74 72 70
-140 -135 -130 -125 -120

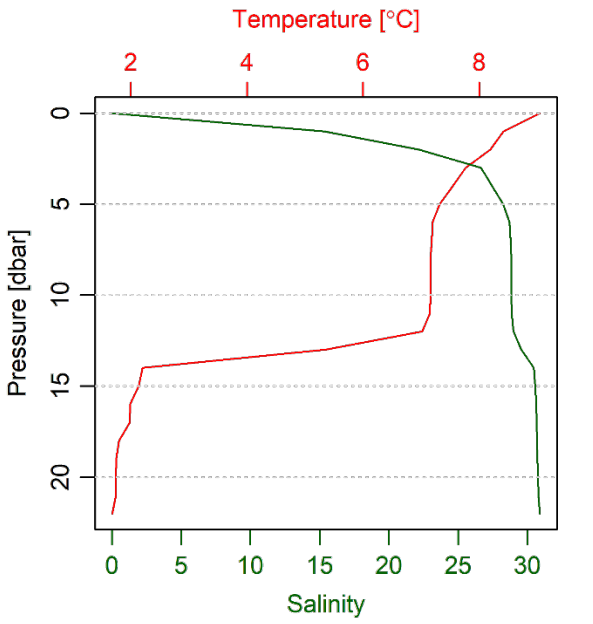

Temperature [°C]
-1 0 1 2 3 4 5
Pressure [dbar]
0 100 200 300
30 31 32 33 34 35
Salinity
Potential density anomaly [kg/m3]
24 25 26 27 28
0e+00 2e-04 4e-04
N2 [s-2]
24 25 26 27
28
Potential Temperature [°C]
-1 0 1 2 3 4 5
30 31 32 33 34 35
Salinity
BNK04
74 72 70
-135 -130 -125 -120

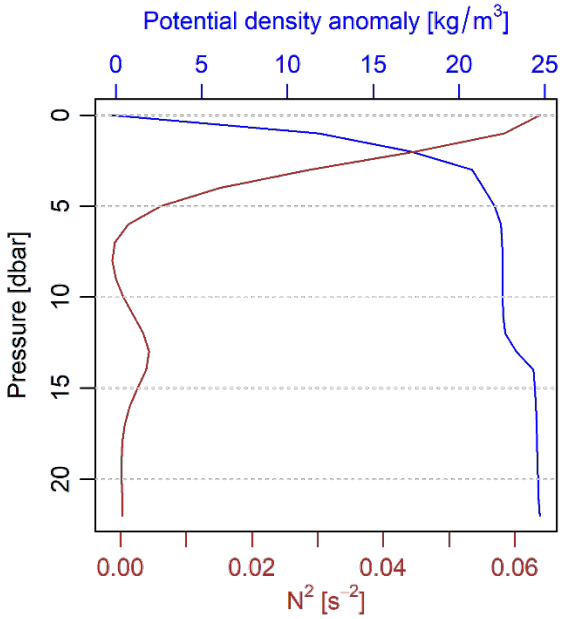

Temperature [°C]
-1.5
-0.5
0.0
0.5
1.0
1.5
2.0
Pressure [dbar]
0
50
100
150
200
250
29
30
31
32
33
34
Salinity
Potential density anomaly [kg/m3]
23
24
25
26
27
0e+00
2e-04
4e-04
6e-04
8e-04
N2 [s−2]
Potential Temperature [°C]
28
BNK05
76
74
72
70
-135
-130
-125
-120

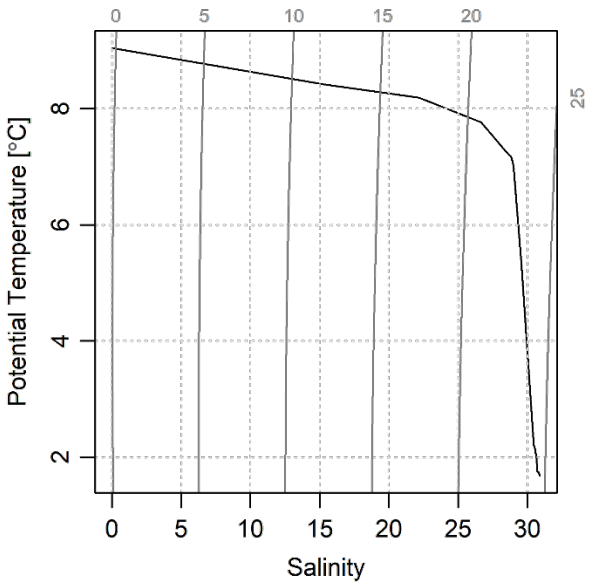

Temperature [°C]
-1
0
1
2
3
Pressure [dbar]
0
10
20
30
40
50
60
25
26
27
28
29
30
31
32
Salinity
Potential density anomaly [kg/m3]
20
21
22
23
24
25
26
0.000
0.002
0.004
0.006
0.008
N2 [s−2]
Potential Temperature [°C]
BNK06
76
74
72
70
-135
-130
-125
-120

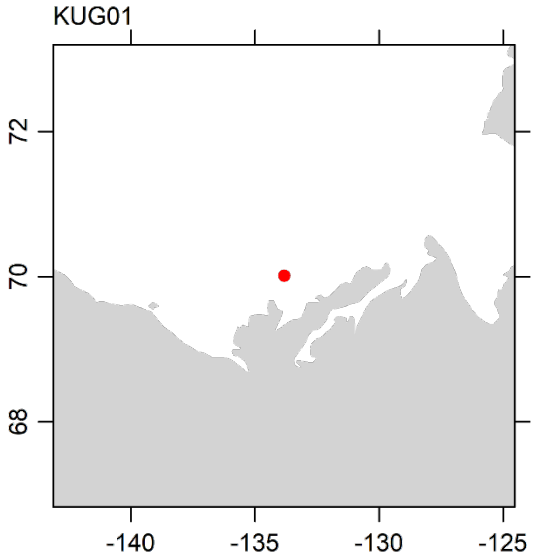

Temperature [°C]
-1
0
1
2
3
4
Pressure [dbar]
0
50
100
150
200
29
30
31
32
33
34
Salinity
Potential density anomaly [kg/m3]
23
24
25
26
27
0.0000
0.0004
0.0008
0.0012
N2 [s−2]
Potential Temperature [°C]
BNK07
74
72
70
-135
-130
-125
-120

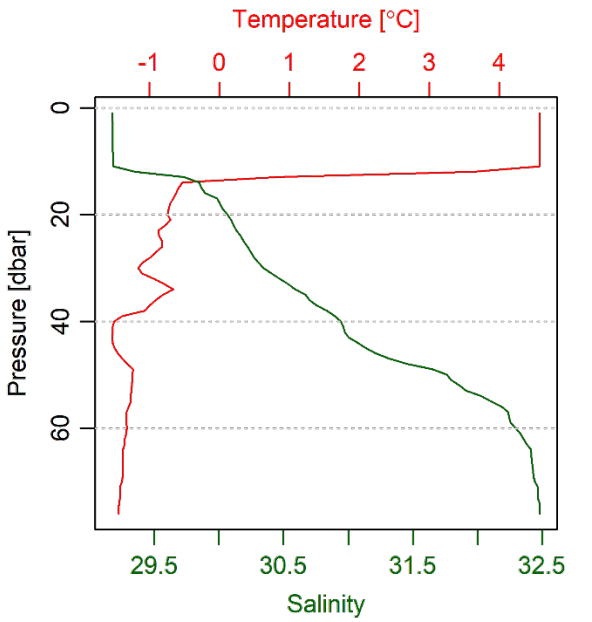

Temperature [°C]
-1 0 1 2 3 4 5
Pressure [dbar]
0 100 200 300
29 30 31 32 33 34
Salinity
Potential density anomaly [kg/m3]
23 24 25 26 27 28
0e+00 2e-04 4e-04 6e-04
N2 [s−2]
Potential Temperature [°C]
23 24 25 26 27
28
BNKHC3
74 72 70
-135 -130 -125 -120

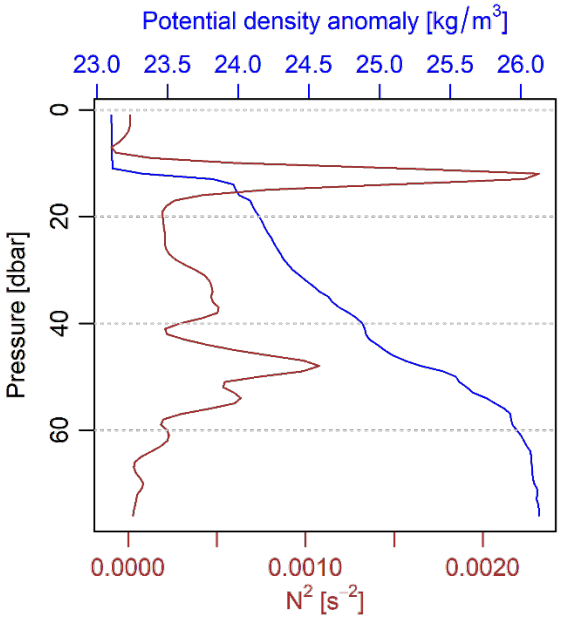

Temperature [°C]
2
4
6
8
Pressure [dbar]
0
5
10
15
20
0
5
10
15
20
25
30
Salinity

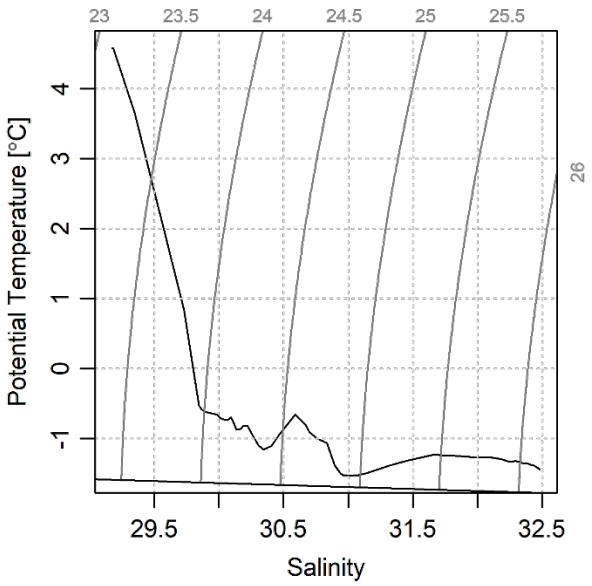

Potential density anomaly [kg/m3]
0
5
10
15
20
25
Pressure [dbar]
0
5
10
15
20
0.00
0.02
0.04
0.06
N2 [s−2]

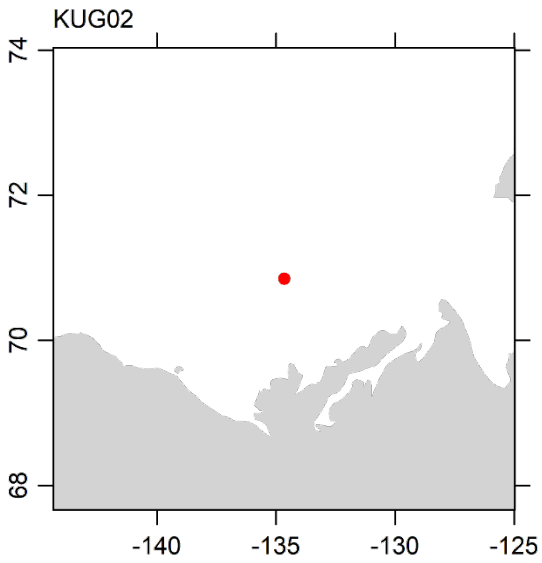

0
5
10
15
20
25
Potential Temperature [°C]
2
4
6
8
0
5
10
15
20
25
30
Salinity

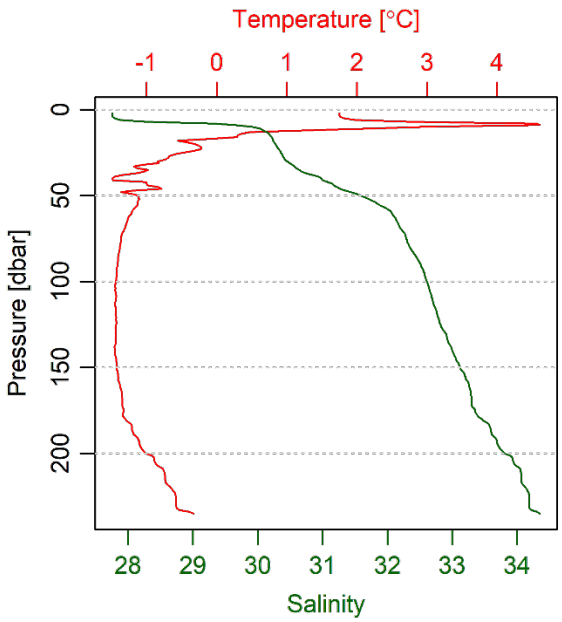

KUG01
72
70
68
-140
-135
-130
-125

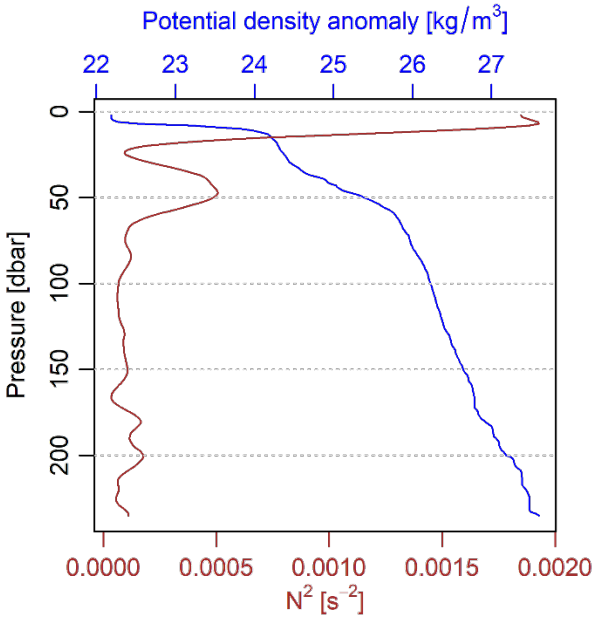

Temperature [°C]
-1
0
1
2
3
4
Pressure [dbar]
0
20
40
60
29.5
30.5
31.5
32.5
Salinity

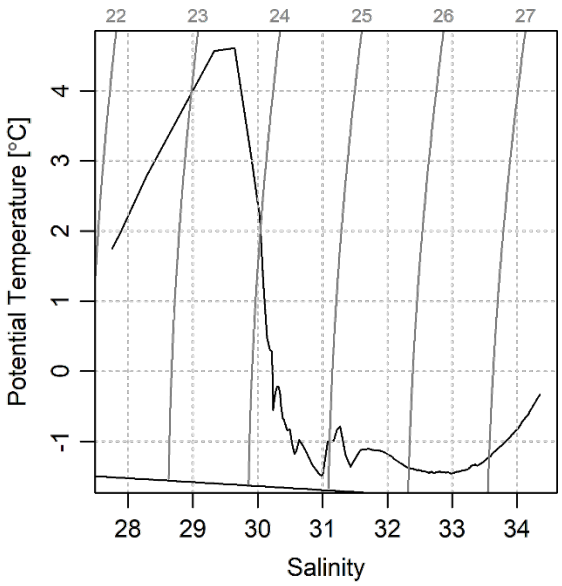

Potential density anomaly [kg/m3]
23.0
23.5
24.0
24.5
25.0
25.5
26.0
Pressure [dbar]
0
20
40
60
0.0000
0.0010
0.0020
N2 [s−2]

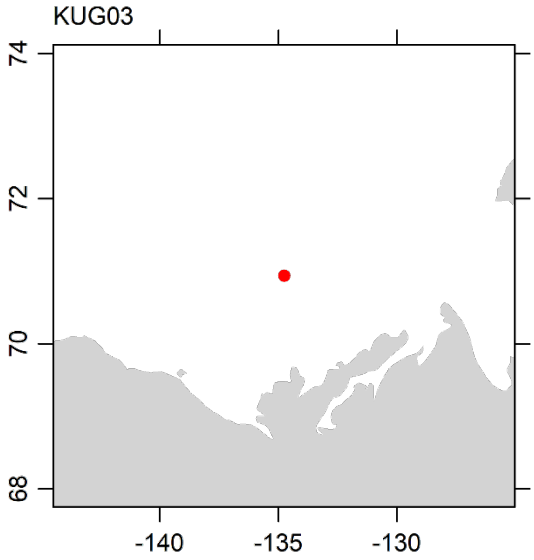

23
23.5
24
24.5
25
25.5
26
Potential Temperature [°C]
-1
0
1
2
3
4
29.5
30.5
31.5
32.5
Salinity

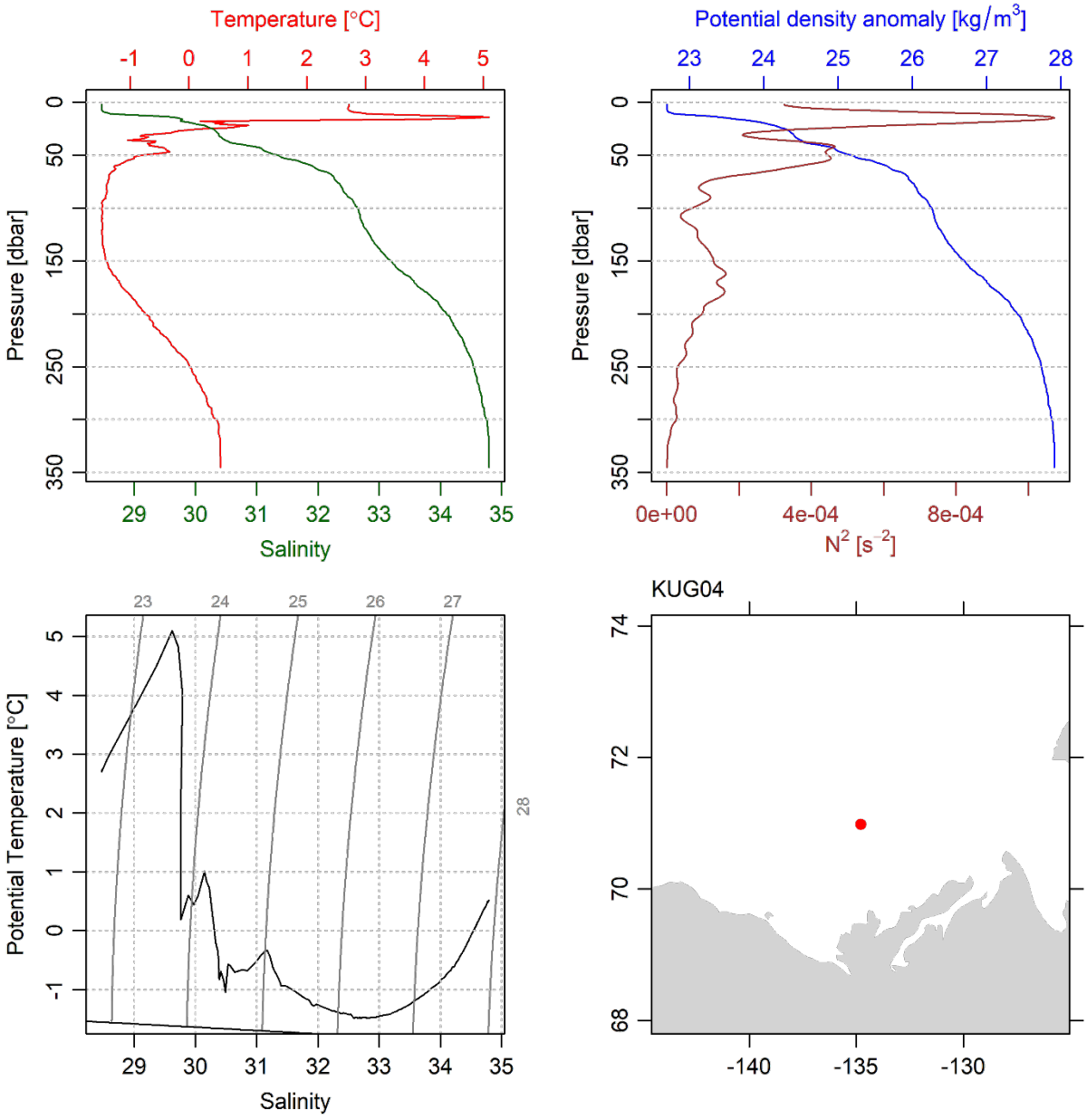

KUG02
74
72
70
68
-140
-135
-130
-125

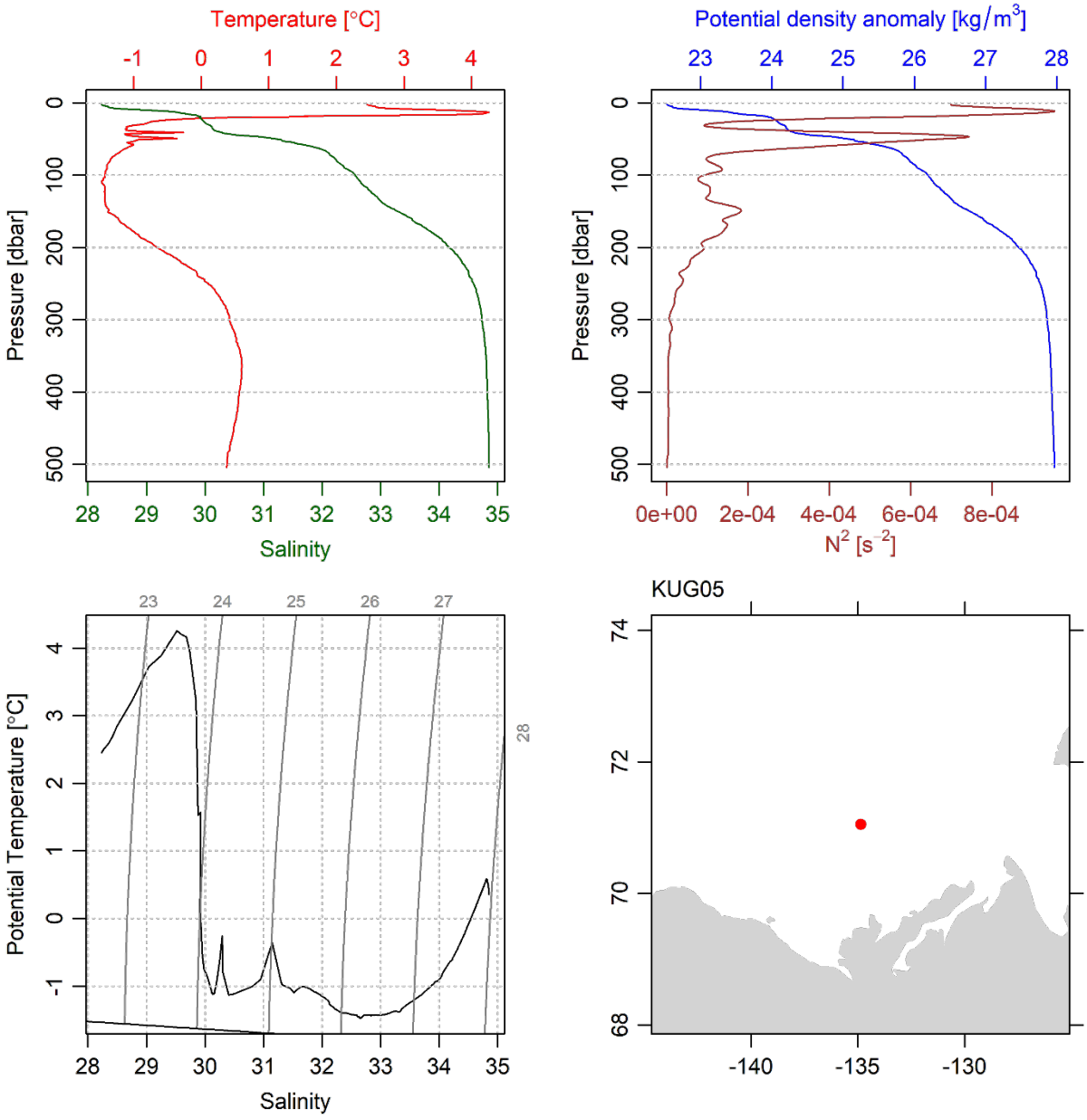

Temperature [°C]
-1
0
1
2
3
4
Pressure [dbar]
0
50
100
150
200
28
29
30
31
32
33
34
Salinity

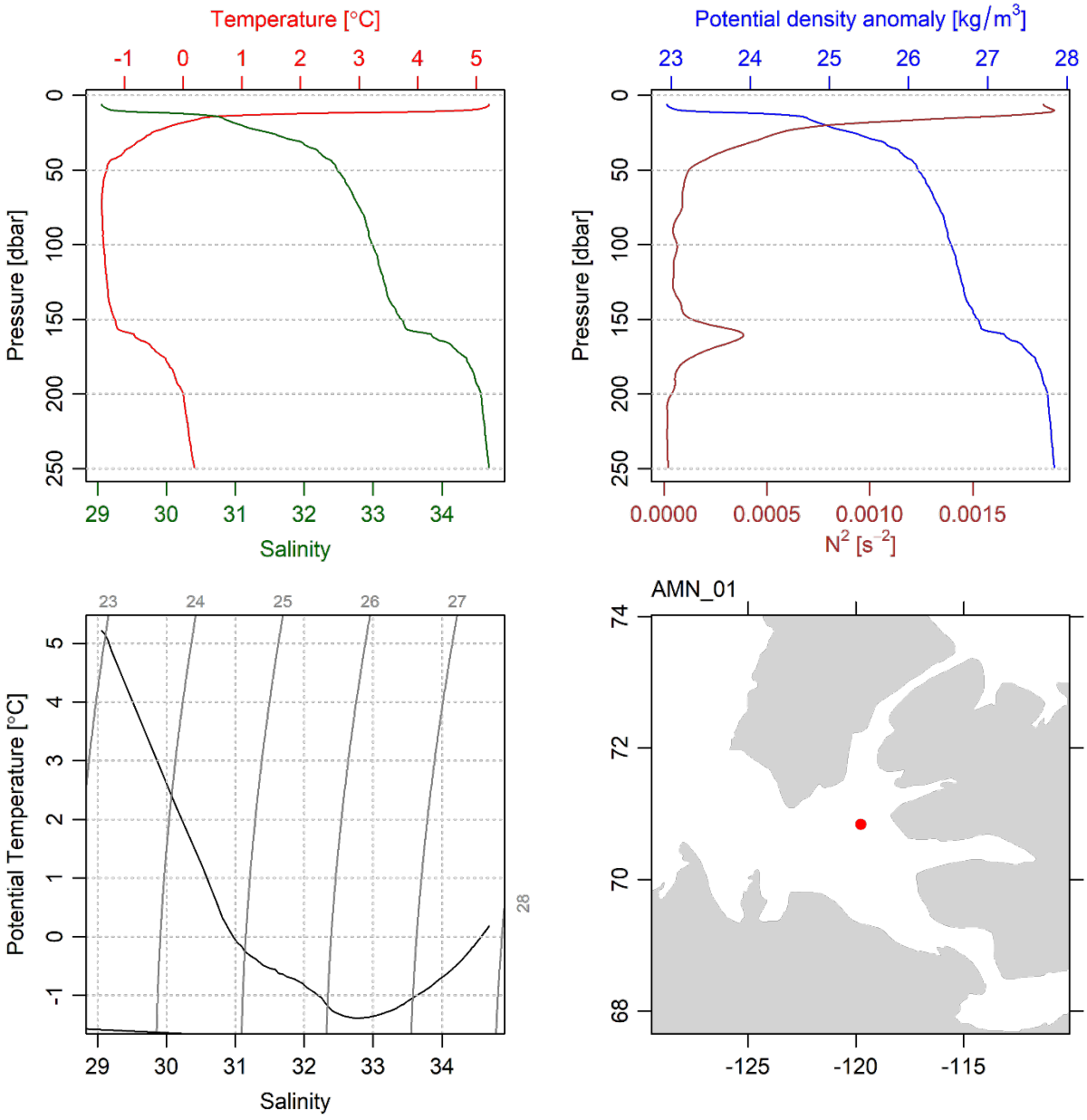

Potential density anomaly [kg/m3]
22
23
24
25
26
27
Pressure [dbar]
0
50
100
150
200
0.0000
0.0005
0.0010
0.0015
0.0020
N2 [s−2]

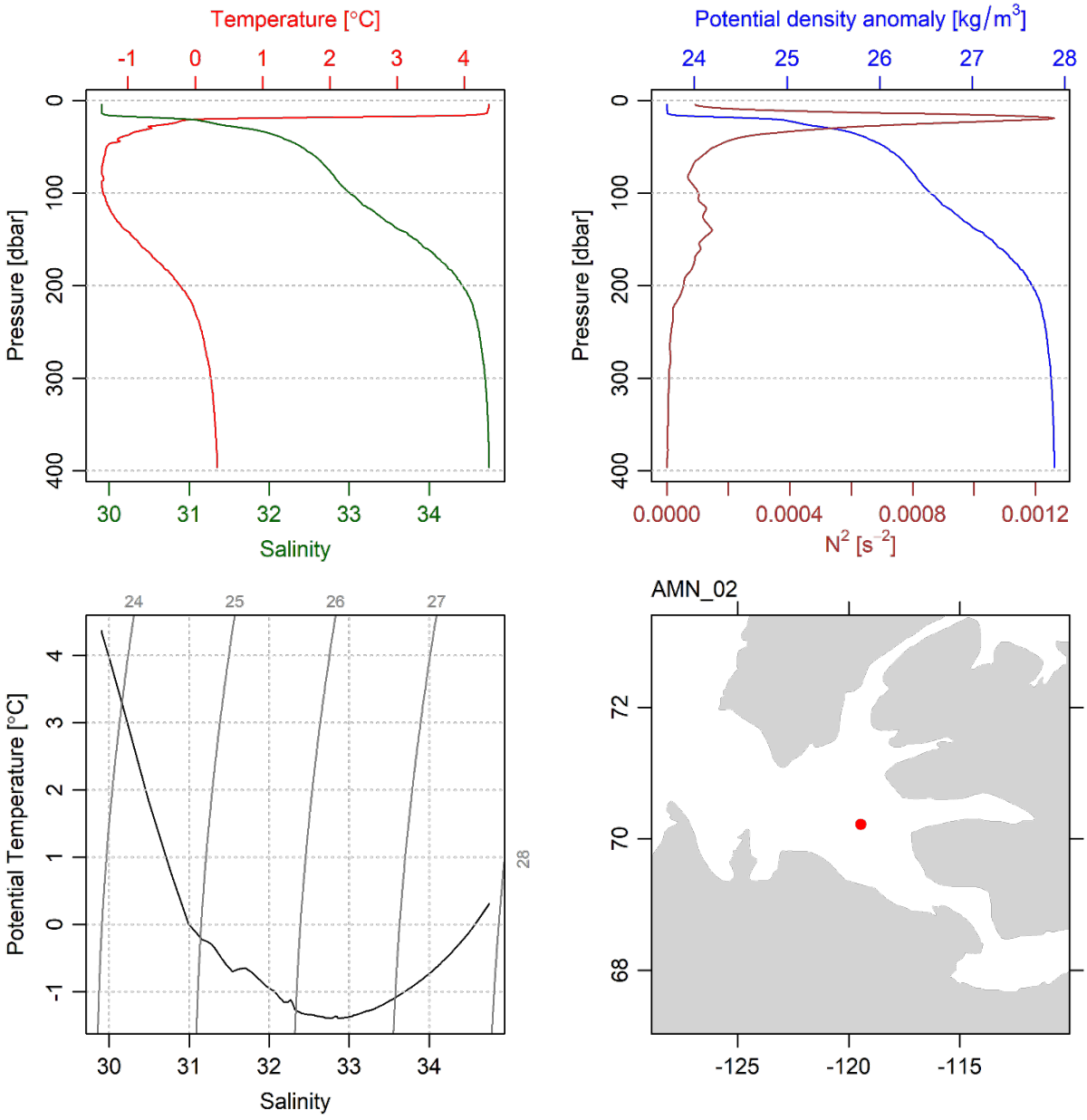

22
23
24
25
26
27
Potential Temperature [°C]
-1
0
1
2
3
4
28
29
30
31
32
33
34
Salinity

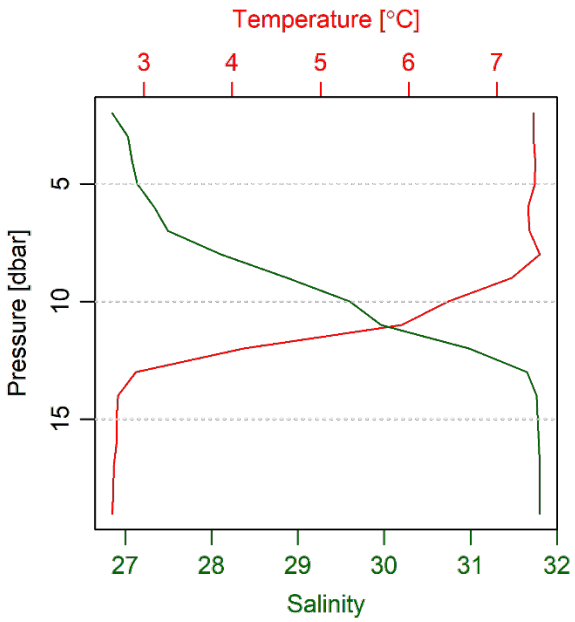

KUG03
74
72
70
68
-140
-135
-130

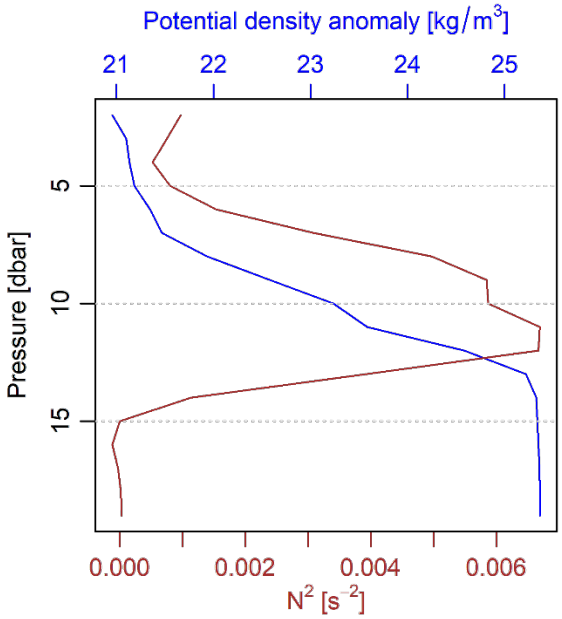

Temperature [°C]
-1 0 1 2 3 4 5
Pressure [dbar]
0 50 150 250 350
29 30 31 32 33 34 35
Salinity
Potential density anomaly [kg/m3]
23 24 25 26 27 28
0e+00 4e-04 8e-04
N2 [s-2]
Potential Temperature [°C]
23 24 25 26 27
28
KUG04
74 72 70 68
-140 -135 -130

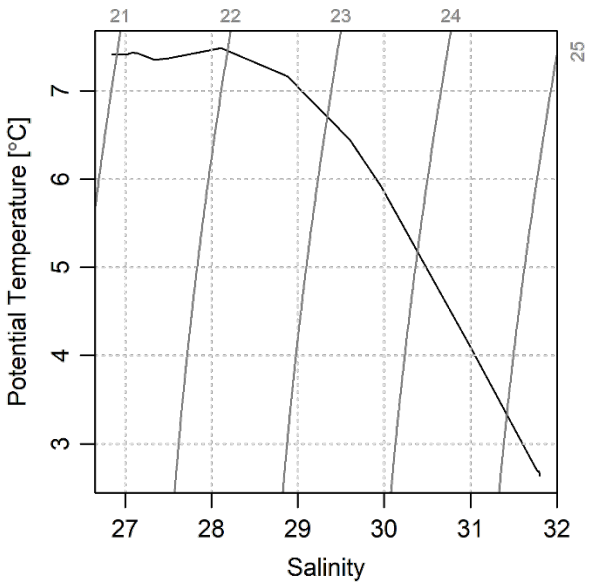

Temperature [°C]
-1
0
1
2
3
4
Pressure [dbar]
0
100
200
300
400
500
28
29
30
31
32
33
34
35
Salinity
Potential density anomaly [kg/m3]
23
24
25
26
27
28
0e+00
2e-04
4e-04
6e-04
8e-04
N2 [s−2]
Potential Temperature [°C]
23
24
25
26
27
28
KUG05
74
72
70
68
-140
-135
-130

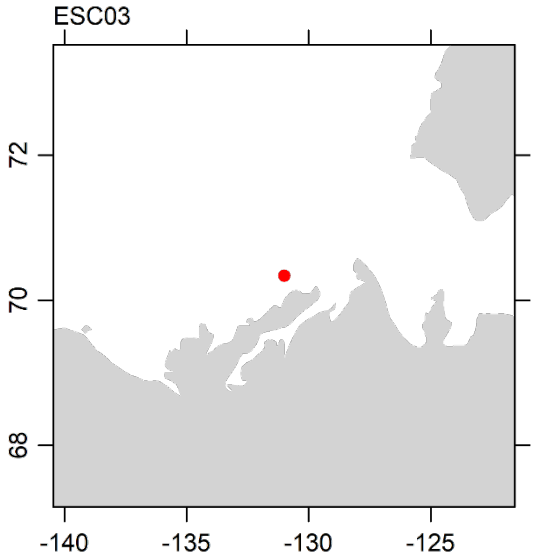

Temperature [°C]
-1 0 1 2 3 4 5
Pressure [dbar]
0 50 100 150 200 250
29 30 31 32 33 34
Salinity
Potential density anomaly [kg/m3]
23 24 25 26 27 28
Pressure [dbar]
0 50 100 150 200 250
0.0000 0.0005 0.0010 0.0015
N2 [s−2]
Potential Temperature [°C]
23 24 25 26 27
-1 0 1 2 3 4 5
28
29 30 31 32 33 34
Salinity
AMN_01
74 72 70 68
-125 -120 -115

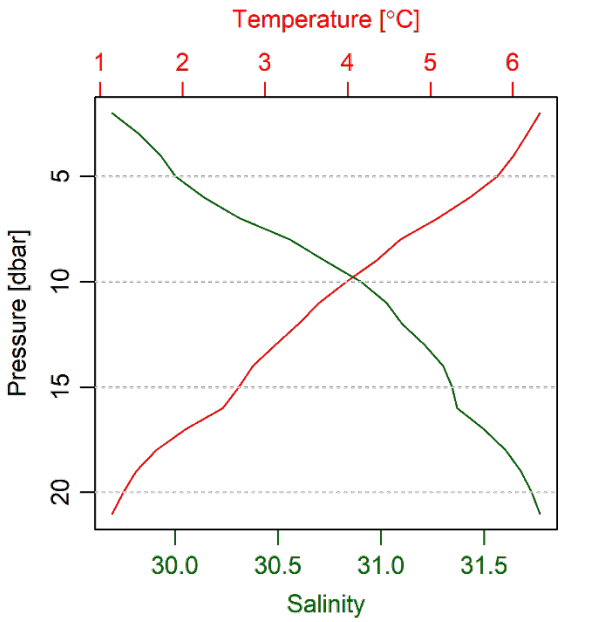

Temperature [°C]
-1
0
1
2
3
4
Pressure [dbar]
0
100
200
300
400
30
31
32
33
34
Salinity
Potential density anomaly [kg/m3]
24
25
26
27
28
0.0000
0.0004
0.0008
0.0012
N2 [s−2]
Potential Temperature [°C]
AMN_02
72
70
68
-125
-120
-115

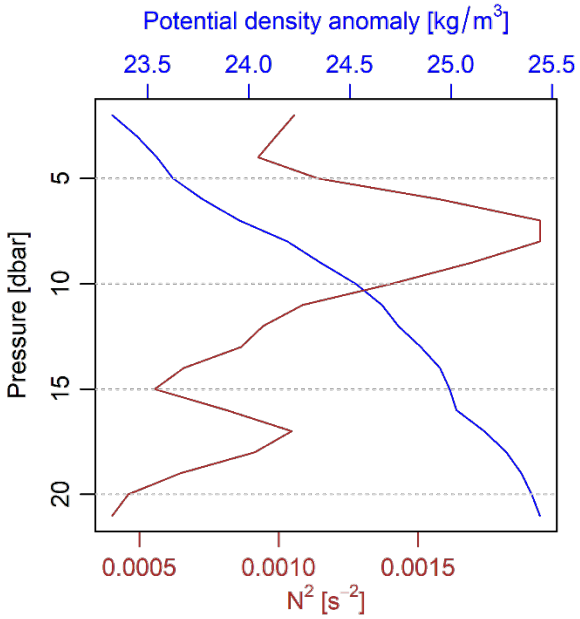

Temperature [°C]
3
4
5
6
7
Pressure [dbar]
5
10
15
27
28
29
30
31
32
Salinity

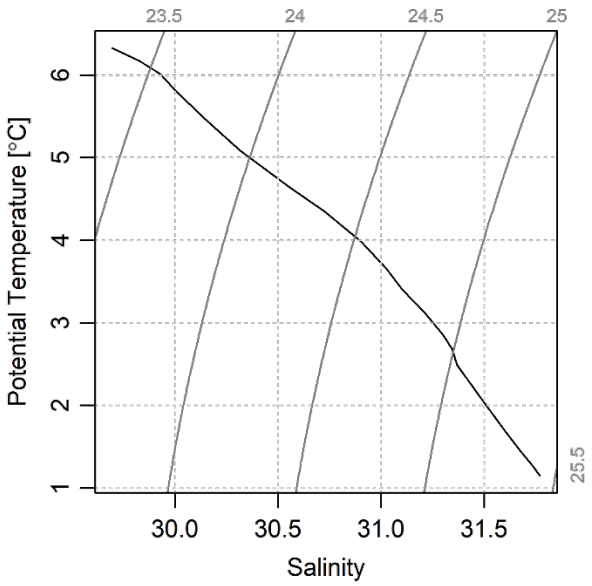

Potential density anomaly [kg/m3]
21
22
23
24
25
Pressure [dbar]
5
10
15
0.000
0.002
0.004
0.006
N2 [s−2]

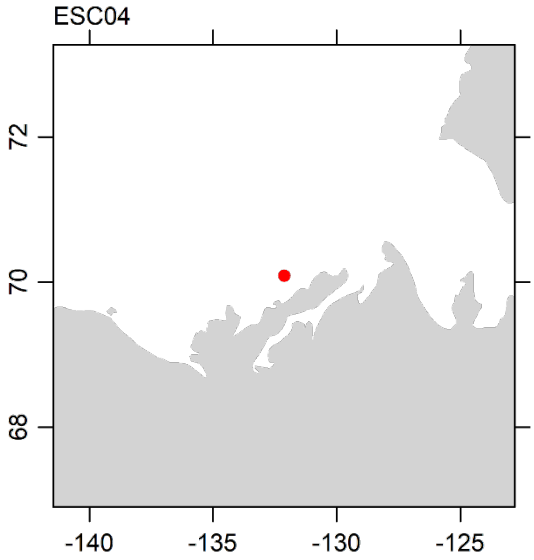

21
22
23
24
25
Potential Temperature [°C]
3
4
5
6
7
27
28
29
30
31
32
Salinity

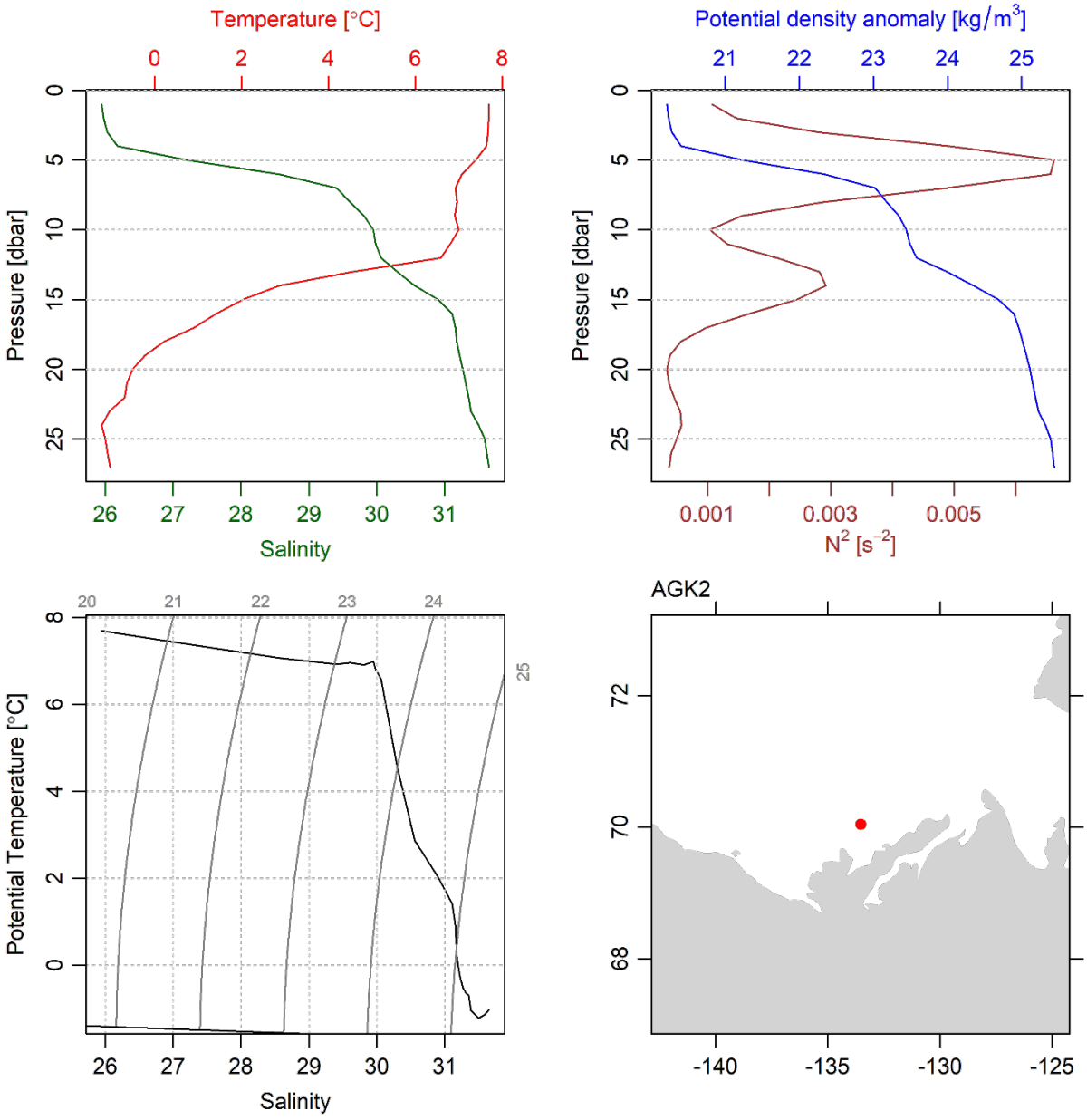

ESC03
72
70
68
-140
-135
-130
-125

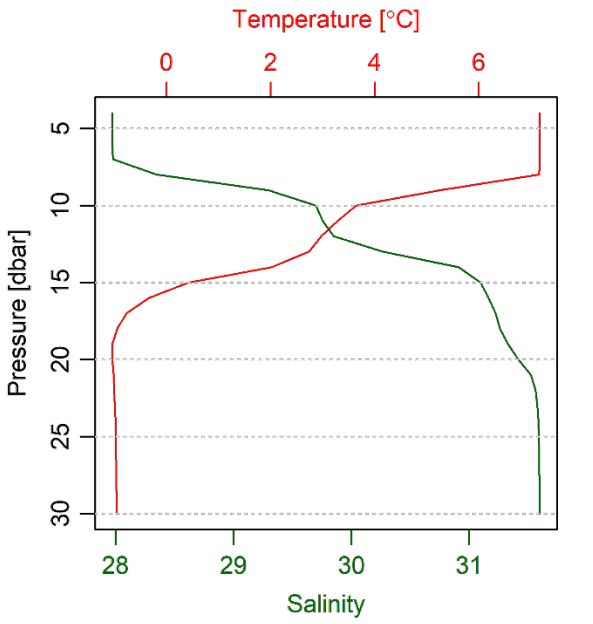

Temperature [°C]
1
2
3
4
5
6
Pressure [dbar]
5
10
15
20
30.0
30.5
31.0
31.5
Salinity

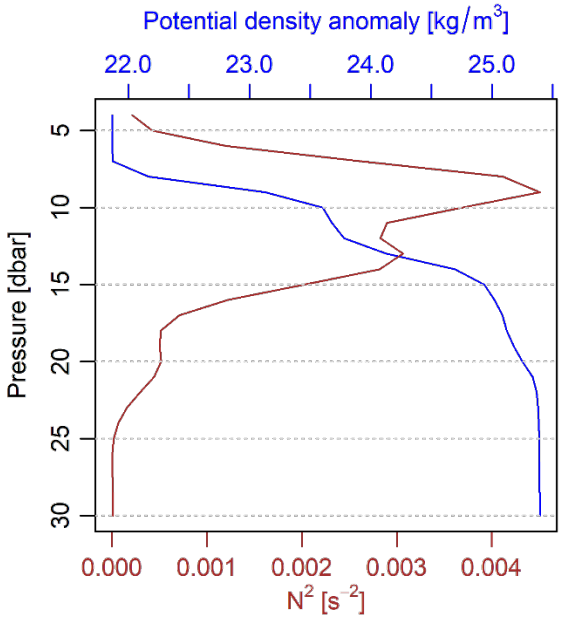

Potential density anomaly [kg/m3]
23.5
24.0
24.5
25.0
25.5
Pressure [dbar]
5
10
15
20
0.0005
0.0010
0.0015
N2 [s−2]

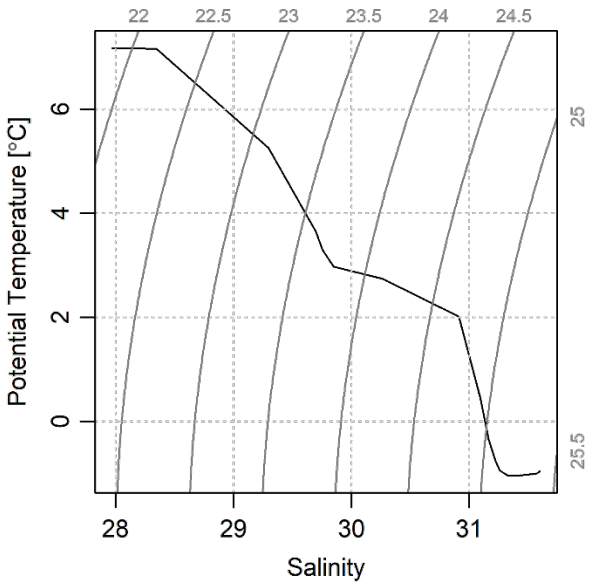

23.5
24
24.5
25
25.5
Potential Temperature [°C]
1
2
3
4
5
6
30.0
30.5
31.0
31.5
Salinity

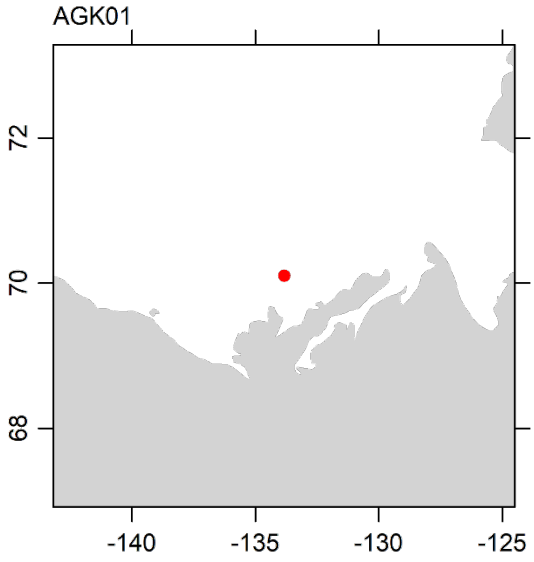

ESC04
72
70
68
-140
-135
-130
-125

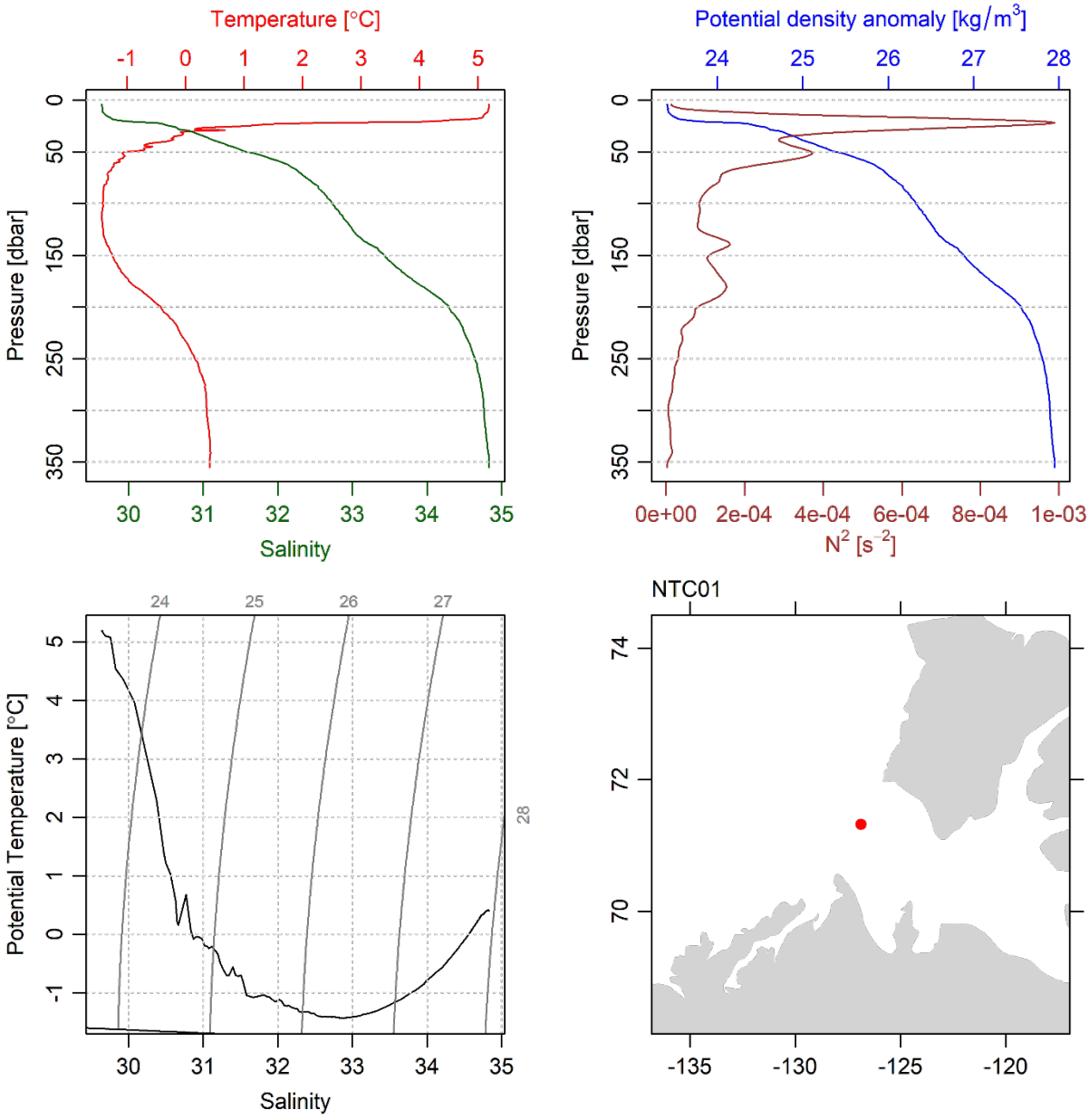

Temperature [°C]
0
2
4
6
8
Pressure [dbar]
0
5
10
15
20
25
26
27
28
29
30
31
Salinity
Potential density anomaly [kg/m3]
21
22
23
24
25
0.001
0.003
0.005
N2 [s−2]
Potential Temperature [°C]
20
21
22
23
24
25
AGK2
72
70
68
-140
-135
-130
-125

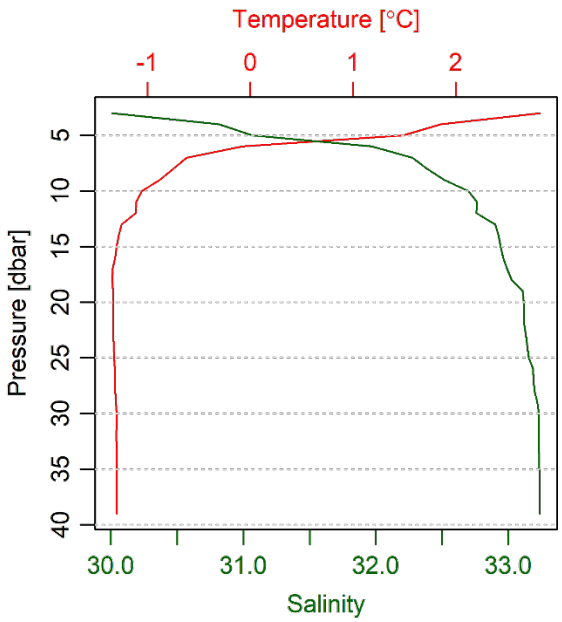

Temperature [°C]
0
2
4
6
Pressure [dbar]
5
10
15
20
25
30
28
29
30
31
Salinity

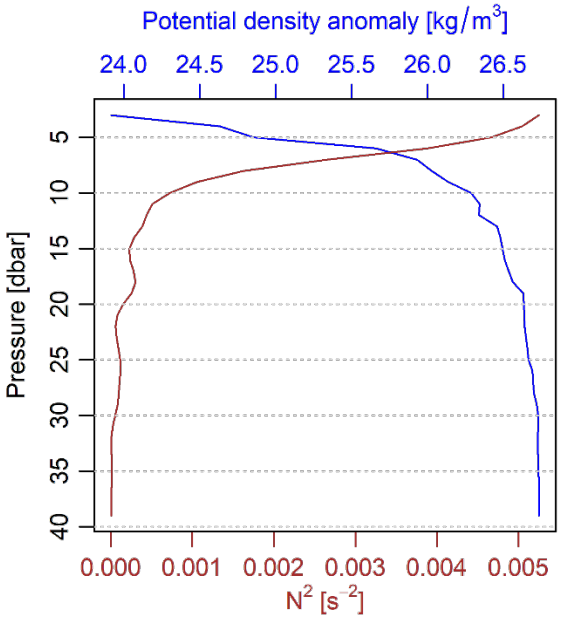

Potential density anomaly [kg/m3]
22.0
23.0
24.0
25.0
Pressure [dbar]
5
10
15
20
25
30
0.000
0.001
0.002
0.003
0.004
N2 [s−2]

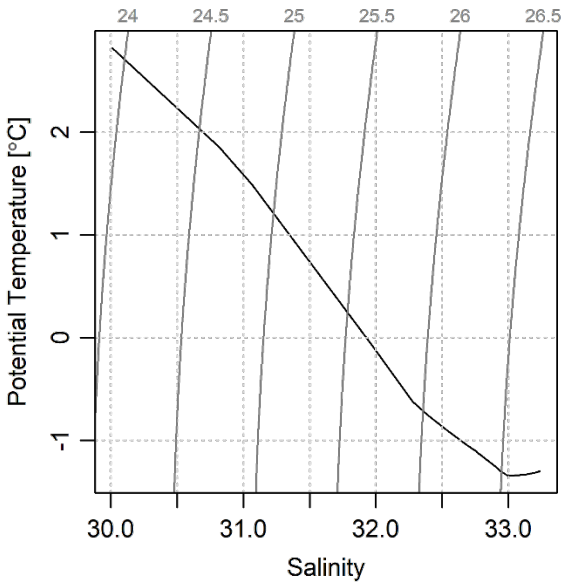

22
22.5
23
23.5
24
24.5
25
25.5
Potential Temperature [°C]
0
2
4
6
28
29
30
31
Salinity

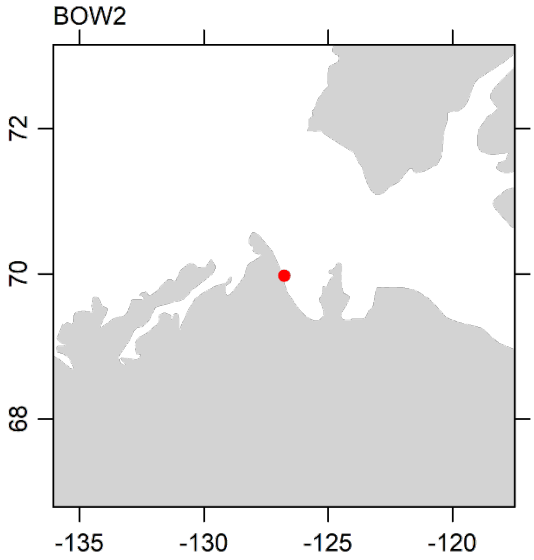

AGK01
72
70
68
-140
-135
-130
-125

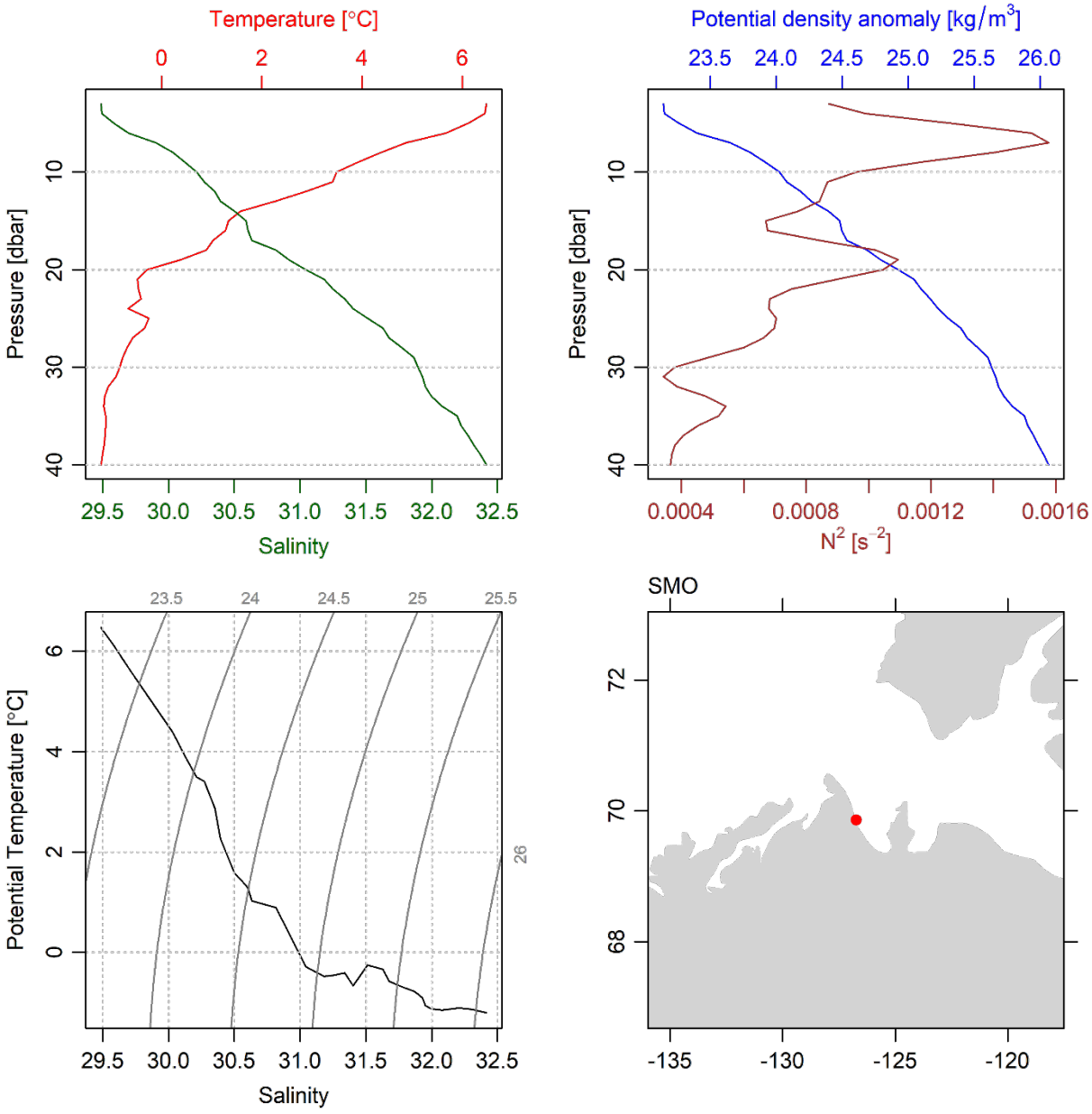

Temperature [°C]
-1 0 1 2 3 4 5
Pressure [dbar]
0 50 150 250 350
30 31 32 33 34 35
Salinity
Potential density anomaly [kg/m3]
24 25 26 27 28
0e+00 2e-04 4e-04 6e-04 8e-04 1e-03
N2 [s−2]
24 25 26 27
28
Potential Temperature [°C]
-1 0 1 2 3 4 5
30 31 32 33 34 35
Salinity
NTC01
74 72 70
-135 -130 -125 -120

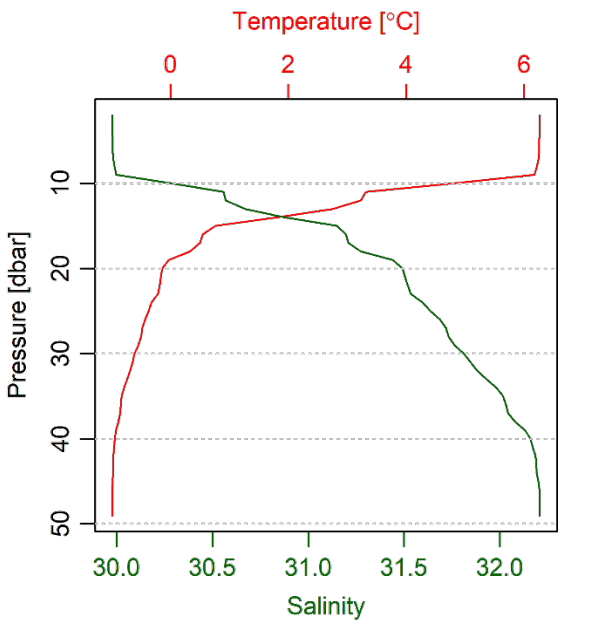

Temperature [°C]
-1
0
1
2
Pressure [dbar]
5
10
15
20
25
30
35
40
30.0
31.0
32.0
33.0
Salinity

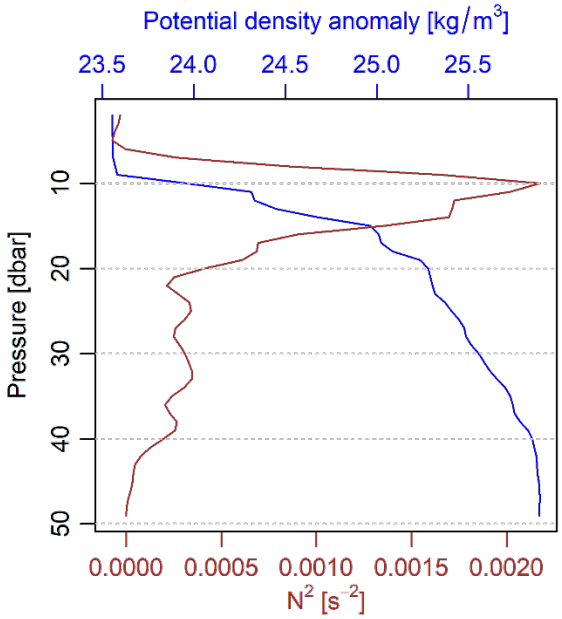

Potential density anomaly [kg/m3]
24.0
24.5
25.0
25.5
26.0
26.5
Pressure [dbar]
5
10
15
20
25
30
35
40
0.000
0.001
0.002
0.003
0.004
0.005
N2 [s−2]

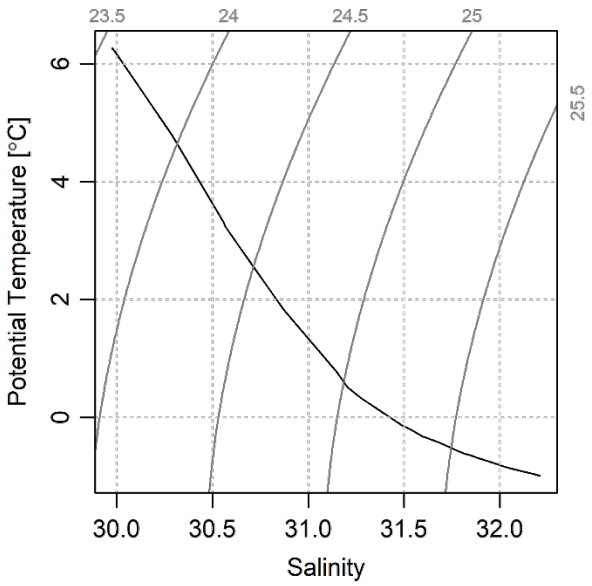

24
24.5
25
25.5
26
26.5
Potential Temperature [°C]
2
1
0
-1
30.0
31.0
32.0
33.0
Salinity

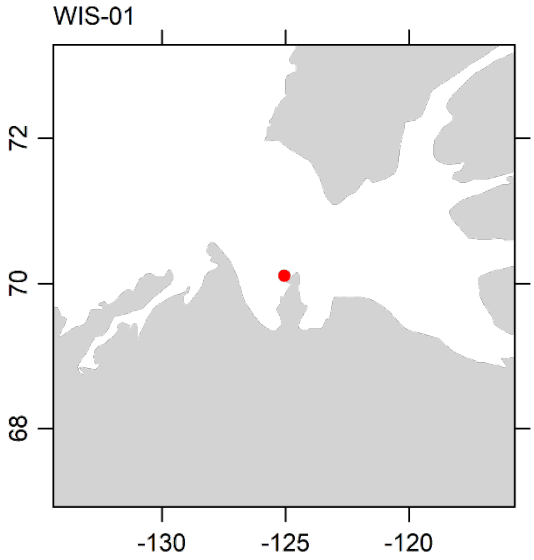

BOW2
72
70
68
-135
-130
-125
-120

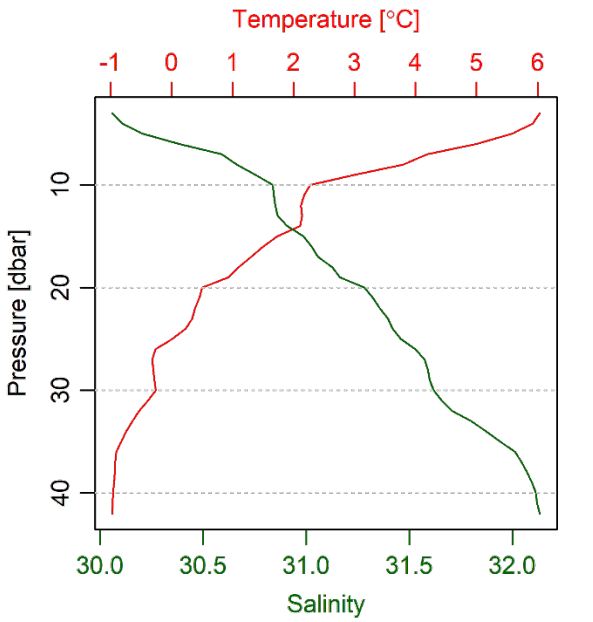

Temperature [°C]
0
2
4
6
Pressure [dbar]
10
20
30
40
29.5
30.0
30.5
31.0
31.5
32.0
32.5
Salinity
Potential density anomaly [kg/m3]
23.5
24.0
24.5
25.0
25.5
26.0
0.0004
0.0008
0.0012
0.0016
N2 [s−2]
Potential Temperature [°C]
23.5
24
24.5
25
25.5
26
SMO
72
70
68
-135
-130
-125
-120

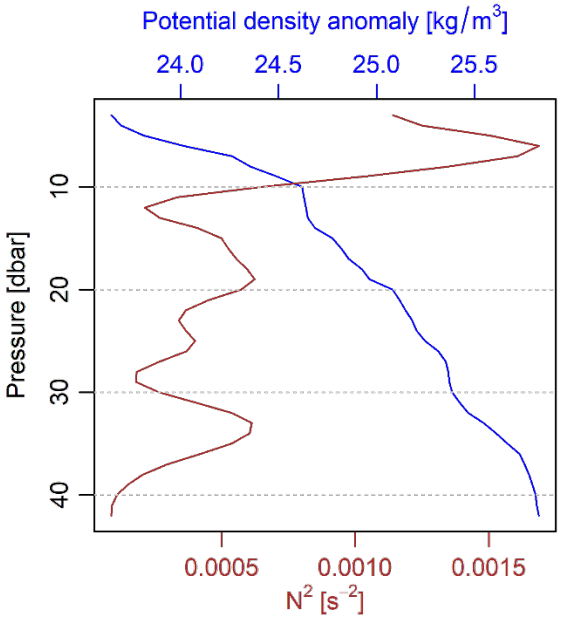

Temperature [°C]
0
2
4
6
Pressure [dbar]
10
20
30
40
50
30.0
30.5
31.0
31.5
32.0
Salinity

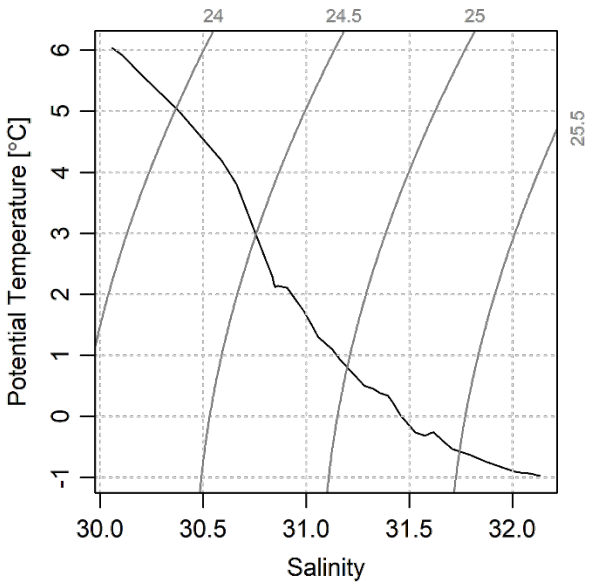

Potential density anomaly [kg/m3]
23.5
24.0
24.5
25.0
25.5
Pressure [dbar]
10
20
30
40
50
0.0000
0.0005
0.0010
0.0015
0.0020
N2 [s−2]

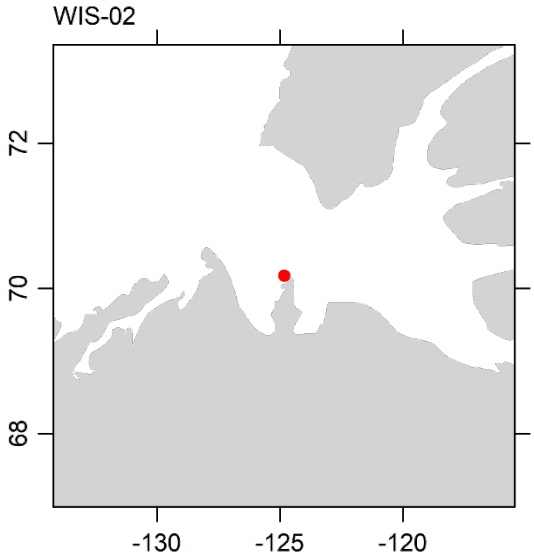

23.5
24
24.5
25
25.5
Potential Temperature [°C]
0
2
4
6
30.0
30.5
31.0
31.5
32.0
Salinity

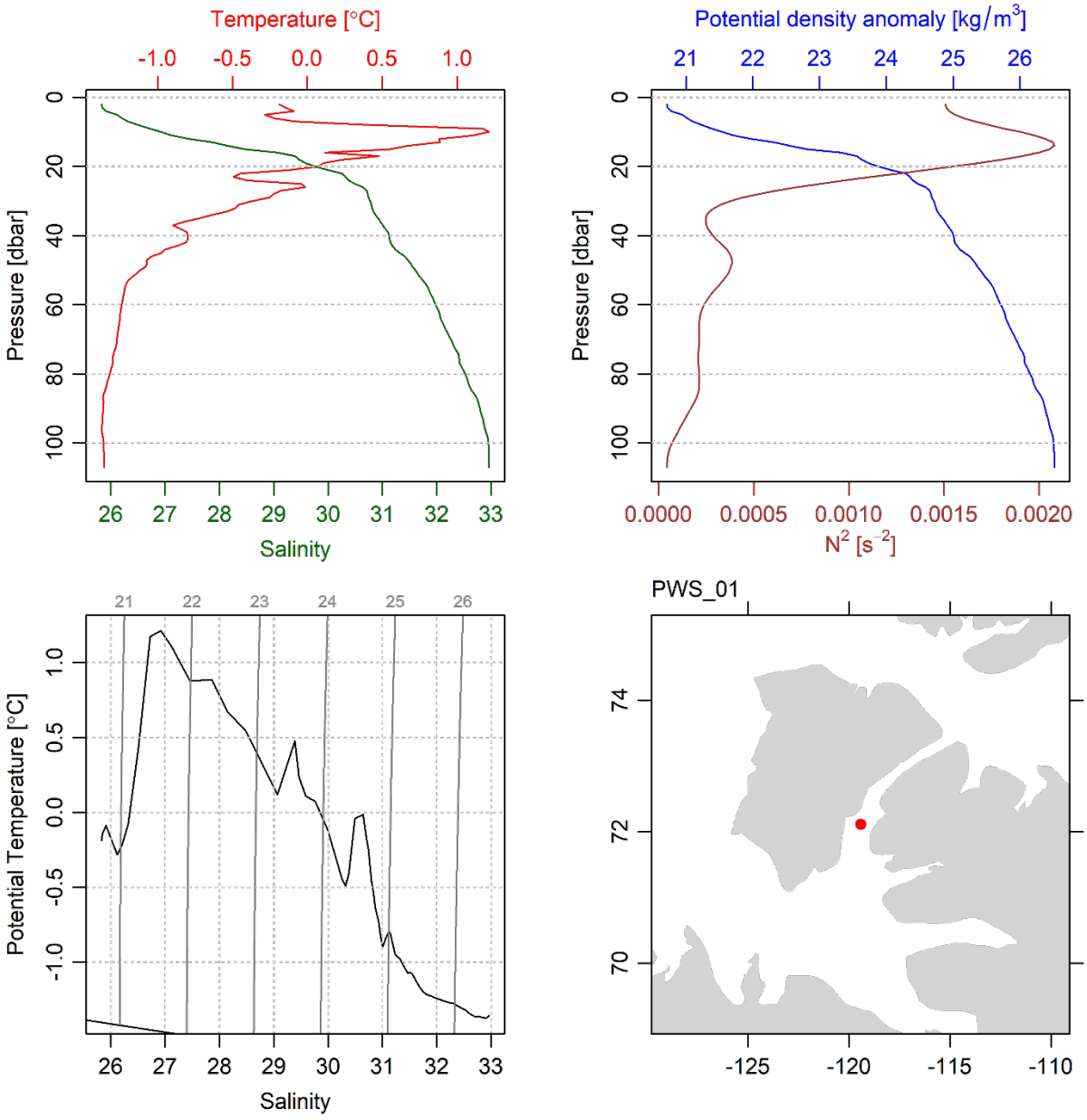

WIS-01
72
70
68
-130
-125
-120


Temperature [°C]
-1
0
1
2
3
4
5
6
Pressure [dbar]
10
20
30
40
30.0
30.5
31.0
31.5
32.0
Salinity


Potential density anomaly [kg/m3]
24.0
24.5
25.0
25.5
Pressure [dbar]
10
20
30
40
0.0005
0.0010
0.0015
N2 [s−2]


24
24.5
25
25.5
Potential Temperature [°C]
-1
0
1
2
3
4
5
6
30.0
30.5
31.0
31.5
32.0
Salinity


WIS-02
72
70
68
-130
-125
-120


Temperature [°C]
-1.0
-0.5
0.0
0.5
1.0
Pressure [dbar]
0
20
40
60
80
100
26
27
28
29
30
31
32
33
Salinity
Potential density anomaly [kg/m3]
21
22
23
24
25
26
0.0000
0.0005
0.0010
0.0015
0.0020
N2 [s−2]
Potential Temperature [°C]
PWS_01
74
72
70
-125
-120
-115
-110